McGill

Artificial Aging Treatments of 319-Type Aluminum Alloys

by:

Francisco Javier Tavitas-Medrano

Department of Mining, Metals
and Materials Engineering

McGill University, Montreal

February 2007

A thesis submitted to McGill University in partial fulfilment of the requirements of the degree of Doctor of Philosophy

Your file Votre référence
ISBN: 978-0-494-38652-1
Our file Notre référence
ISBN: 978-0-494-38652-1

ABSTRACT

Aluminum-silicon-copper cast alloys of the 319-type have attained a commercially important status because of their widespread use. Artificial aging treatments are routinely applied to these alloys in order to obtain precipitation hardening and improve their mechanical properties. Standard treatments may not always yield the optimum achievable properties, thus Mg and Sr are commonly added to improve the response of the alloy to aging and to modify the eutectic Si morphology from acicular to fibrous, respectively. The present study was carried out to investigate aging behavior of four 319-type alloys in regard to such mechanical properties as their ultimate tensile strength, yield strength, microhardness, percent elongation and impact toughness. Non-conventional aging cycles were applied so as to evaluate the degree of the improvement in strength obtainable. These treatments, labeled in this study as T6- and T7-type multi-temperature and interrupted aging treatments, involve several heating stages at different temperatures, as opposed to the single stage at constant temperature specifications of the standard T6 or T7 heat treatment regimes. Scanning electron microscopy was used to examine the fracture surfaces of selected tensile-tested samples to compare the fracture behavior. Transmission electron microscopy was used to reveal and identify the tiny precipitates which appear in the microstructure as a result of the precipitation-hardening process due to artificial aging. It was found that the main strengthening phase is θ-Al_2Cu in the form of needles; other phases were observed as minor constituents in this alloy, including the binary β-Mg_2Si, the ternary S-$CuAlMg_2$ and the quaternary Q-$Al_5Cu_2Mg_7Si_7$. The results show that while Mg and Sr additions improve the properties of the alloy, the standard T6 treatment may not be the best available option to produce optimum properties. In fact, when the peak-aged (T6) condition is desired, the optimum treatment consists of a continuous artificial treatment at 170°C for 8 h; when the overaged (T7) condition is desired, a T7-type multi-temperature treatment consisting of underaging at 170°C for 1 h, then at 190°C for 1 h, and finally overaging at 240°C for 2 h is the best option.

RÉSUMÉ

Les alliages de fonderie aluminium-silicium-cuivre de type 319 sont d'une grande importance pour l'industrie automobile. Les traitements thermiques par vieillissement artificiel sont couramment utilisés afin de produire un durcissement structural et de ce fait, améliorer les propriétés mécaniques. Les meilleures propriétés ne sont pas nécessairement atteintes avec les traitements standards, ainsi l'ajout de magnésium et de strontium est fait afin d'augmenter la réponse au vieillissement et de modifier la morphologie du silicium eutectique d'un aspect aciculaire à fibreux, respectivement. Cette étude porte sur l'analyse du comportement en vieillissement de quatre types d'alliages 319 en fonction des propriétés mécaniques telles que la résistance à la traction, la limite d'élasticité, la microdureté, la déformation maximale et la ténacité. Des cycles non conventionnels de vieillissement ont été effectués afin d'évaluer l'amélioration de la résistance mécanique. Ces traitements, identifiés dans cette étude comme T6 et T7, à températures multiples et à vieillissements interrompus, i.e. plusieurs étapes de chauffage à différents températures, contrairement aux spécifications des traitements T6 et T7 à étape simple et à température fixe. Un microscope électronique à balayage a été utilisé pour l'analyse comparative des surfaces de rupture des éprouvettes de traction. Un microscope électronique à transmission a été utilisé afin d'illustrer et d'identifier les minuscules précipités obtenus après le durcissement structural dû au vieillissement artificiel. Il a été remarqué que la phase binaire θ-Al_2Cu est celle qui participe principalement au durcissement. Par ailleurs, les phases suivantes apportent également une contribution minime au durcissement à savoir : la binaire β-Mg_2Si, la ternaire S-$CuAlMg_2$ et la quaternaire Q-$Al_5Cu_2Mg_7Si_7$. Les résultats démontrent que les ajouts de Mg et de Sr contribuent à l'amélioration des propriétés de l'alliage, mais que le traitement standard T6 n'est pas la meilleure option pour obtenir les propriétés optimales. En effet, quand les conditions optimales du traitement T6 sont désirées, un vieillissement artificiel continu de 8 heures à 170°C est requis. D'autre part, lorsqu'un survieillissement (T7) est désiré, la meilleure option est un traitement T7 à températures multiples qui consiste à un vieillissement de 1 heure à 170°C, une autre vieillissement de 1 heure à 190°C et finalement un survieillissement de 2 heures à 240°C.

ACKNOWLEDGEMENTS

The completion of this research would have not been possible without the assistance of several individuals and organizations. I would like to thank my supervisors, Prof. John E. Gruzleski and Prof. Fawzy H. Samuel, for their support, commitment, patience, guidance and valuable feedback during my research work at McGill University and L'Université du Québec à Chicoutimi (UQAC); I have learned many worthy lessons from their example. The financial support to conduct this research was provided by the following organizations: the Natural Sciences and Engineering Research Council of Canada (NSERC); special thanks to Dr. Herbert W. Doty of General Motors Powertrain Group (USA).

I am greatly indebted to Dr. Salvador Valtierra of Corporativo Nemak for his constant trust, encouragement, support and advice throughout the years. He has helped me shape my career; and if it was not for that talk we had about 10 years ago I would definitely not be here.

Many thanks to all the administrative staff and professors in the Department of Mining, Metals and Materials Engineering for their help; particularly Barbara

Hanley, Heather Holowathy, Nikki Middlemiss, Prof. Robin Drew, Prof. James Finch, and Dr. Florence Paray. Thanks also to my classmates and colleagues for creating a friendly atmosphere at McGill especially Chun Hui Zhang, Khaled Elalem, Sa'ed Musmar, Neivi Andrade, Li Hong Shang, and Hu Jun Zhao.

Special thanks go to Prof. Agnes Samuel from UQAC for her insightful suggestions, valuable discussions, and kind help and patience in the writing process of this thesis and several papers. I would also like to thank Ms. Marion Sinclair for proofreading and correcting the original manuscript and for putting up with my *chaotic* use of prepositions.

I would also like to acknowledge assistance I received in operating some of the equipment used in this research. Thanks to Alain Bérubé and Mathieu Paradis from UQAC (special thanks to Mathieu for translating the abstract); Dr. Rodrigo Gonzalez and Fernando Morales from Nemak; Jean-Philippe Masse and Philippe Plamondon from École Polytechnique and Ernesto Rincón from ITS. Without their help I would not have learned how to operate the simplest machine, such as a furnace, to even the most complex ones, such as a TEM.

I would have never gotten this far without the unwavering support and unconditional love of my family: my dad Javier, my mom Marta and my brother Gerardo. There are no words to describe my gratitude towards them and if I attempted to do so I would fill pages endlessly, which is why instead I dedicate this thesis, as modest as it may be, to them.

My *family by choice*, or friends, was very important in the completion of this work as well. Thanks to Mario for his tenacious friendship, to Lydia for those lengthy discussions about our respective projects, to Pablo, Diana, Monica and Izumi for all those great times we had discovering Montreal together, and to Jason for his encouragement in the last few months of the completion of this thesis. Thanks also to Pilar, Alan and Hugo for their patience and for providing me with online conversations in the breaks I took during the long hours in front of my computer screen.

TABLE OF CONTENTS

INDEX OF FIGURES

2. REVIEW OF THE LITERATURE

3. EXPERIMENTAL PROCEDURES

INDEX OF TABLES

1. INTRODUCTION

2. REVIEW OF THE LITERATURE

3. EXPERIMENTAL PROCEDURES

4. RESULTS AND DISCUSSION

5. SUMMARY OF RESULTS

Chapter 1

Introduction

Perplexity is the beginning of knowledge.

Kahlil Gibran

1.1 Background

Aluminum is the most abundant metallic element to be found in the Earth's crust, and as early as the 1820s Christian Oersted, a Danish chemist, was the first to isolate it; at a later date in 1845, Friedrich Wöhler improved on Oersted's process. A few decades further on, in 1886, Hall, in the United States, and Héroult, in France, discovered that aluminum oxide could dissolve in fused cryolite and then be decomposed by electrolysis into molten metal. This process is low-cost and is still used nowadays for the commercial production of aluminum.

Most commercial uses of aluminum require greater strength than the pure metal can provide. For this reason, the addition of other elements produces various useful alloys with improved mechanical properties. Many metallic elements may be alloyed with aluminum, but only a few are major alloying elements in commercial aluminum-based alloys. Aluminum alloys are classified in two main categories: wrought alloys and cast alloys.

The selection of an aluminum alloy should be made carefully in the light of the nature of each alloy and the variety of production processes available. This selection should take into consideration the particular application and the function for which the product is designed in order to meet the desired properties including good foundry characteristics, stability of mechanical properties over the required service life, machinability, pressure tightness, finishability, and so forth.

Wrought alloys are used mainly in the production of worked products such as sheets, plates, tubes, forgings, extrusions, foils and wires. Castings may be produced by a variety of processes such as: (i) high-pressure die casting, (ii) plaster casting, (iii) investment casting, (iv) permanent mold casting and (v) sand mold casting for certain chemical composition ranges, thereby replying to a number of useful engineering needs and applications as in the automotive, aerospace, and military industries.

There are several designations for aluminum cast alloys but the more commonly used system is that of the American Aluminum Association. This system has a 4 digit code to identify the alloy, where the first digit indicates the major alloying element in the group, the following two digits have no specific significance (except for the 1XX.X series, where they indicate the aluminum content – 170.x corresponding to a 99.70% grade purity aluminum) and the last digit indicating the form of the product as either casting (0) or ingot (1 or 2). This designation system is shown in Table 1.1.

Table 1.1: Designation System for Casting Alloys of the Aluminum Association

1XX.X	Unalloyed composition; aluminum 99.0% or greater
2XX.X	Copper
3XX.X	Silicon with magnesium and/or copper
4XX.X	Silicon
5XX.X	Magnesium
7XX.X	Zinc
8XX.X	Tin

Sometimes, a prefix letter is used to distinguish alloys that are of the same type, but which may differ in the percentage of minor alloying elements present. For example, one of the most common cast alloys, 356, has variations A356, B356, and C356; each of these alloys has identical major alloy contents, but has decreasing specification limits applicable to impurities, especially iron content.

The Aluminum-Silicon-Copper 319-type cast alloys are of commercial importance because of their applications in the automotive industry; this alloy offers a combination of a high degree of achievable strength, with excellent castability, light weight and good machinability in both, permanent mold and sand casting. The standard chemical composition of alloy 319 is shown in Table 1.2.

Table 1.2: Standard Composition of Aluminum Alloy 319

% Si	% Cu	% Fe	% Zn	% Mn	% Ni	% Ti	% Mg
5.5 – 6.5	3.0 – 4.0	<1.0	<1.0	<0.5	<0.35	<0.25	<0.10

The automotive products usually obtained from Alloy 319 are pistons, transmission housings, suspension components, engine blocks, and cylinder heads, among a number of other possible parts. This alloy system, however, is seldom used in its as-cast state since it yields relatively poor mechanical properties. This drawback may be explained by the presence of a coarse acicular silicon eutectic phase which, because of its morphology of sharp ends and edges, acts as a stress raiser for the material under an applied load.

Chemical and thermal treatments are thus applied to this alloy in order to achieve improved mechanical properties. The most common chemical treatment consists of modifying the morphology of the silicon eutectic phase from an acicular to a fibrous one, thereby improving mechanical properties, particularly elongation. Silicon modification is achieved by the addition of small amounts of sodium or strontium to the melt. Another common chemical treatment is the addition of Mg so as to increase the response of the alloy to artificial aging. As regards heat treatment, this process is used to obtain the desired combination of mechanical properties such as strength and ductility. The T6 treatment is the one which provides the best combination of mechanical properties.

The T6 treatment comprises three stages: solution heat treating, water quenching and artificial aging. The solution heat treatment is carried out at a relatively high temperature (~500°C) in order to (i) dissolve the solutes, mainly Cu, present in the alloy which are responsible for the hardening response; (ii) homogenize the casting, and (iii) spheroidize the eutectic silicon. The main purpose of the solution heat treatment is to obtain a supersaturated solid solution but in order to maintain this desired condition at low temperatures, water quenching is needed. The artificial aging stage consists of further heating the alloy at relatively low temperatures (155°C) and it is during this stage that the precipitation of dissolved elements occurs. These precipitates are responsible for the observed hardening of the material.

There is a certain amount of research available in the area of the heat treatment of wrought and cast aluminum alloys. This research applies experimental heat treatment cycles which involve varying the times and temperatures in the artificial aging stage of the treatment. Research on interrupted aging and secondary precipitation on aluminum alloys has been carried out [1, 2] with promising results, as an increase of up to 10% in strength is achieved. Unfortunately, there is no data relating to Alloy 319. In general, not much work has been accomplished on the aging behavior of this specific alloy, given its complexity and because of the phase transitions that occur during the aging treatment. Nor is there sufficiently detailed research available, to date, on the precipitation sequence or precipitate identification, since these precipitates are very small and over-similar in shape, all of them being needle-like and only identifiable with high-resolution electron microscopy techniques.

1.2 Objectives

Since heat treatment is one of the most common means of improving the mechanical properties of Alloy 319, and considering the limited data available thus far, the need for a study which assesses the aging behavior of the alloy becomes evident. The aim of the present work, therefore, is to study the aging behavior of the 319 cast alloy when it is subjected to several artificial aging cycles, including conventional aging as specified by the standard T6 artificial aging regime, and non-conventional aging which covers several stages at different temperatures.

The specific objectives are:

- To study the effect of artificial aging treatments on the properties of the 319 alloy under the following conditions: unmodified, modified, unmodified with the addition of Mg, and modified with the addition of Mg.

- To investigate attainable improvement of the properties of the alloy by using non-conventional aging cycles.

- To identify the precipitating phases observed in the alloy in order to explain the subsequent variation in mechanical properties.

- To provide a better understanding of the precipitation process and hardening mechanisms which occur in this alloy, with a view to optimizing heat treatment conditions.

- To obtain a more detailed understanding of the mechanisms that govern the improvement of alloy properties, and to design an optimum artificial aging treatment cycle which would yield the best combination of properties.

Chapter 2

Review of the Literature

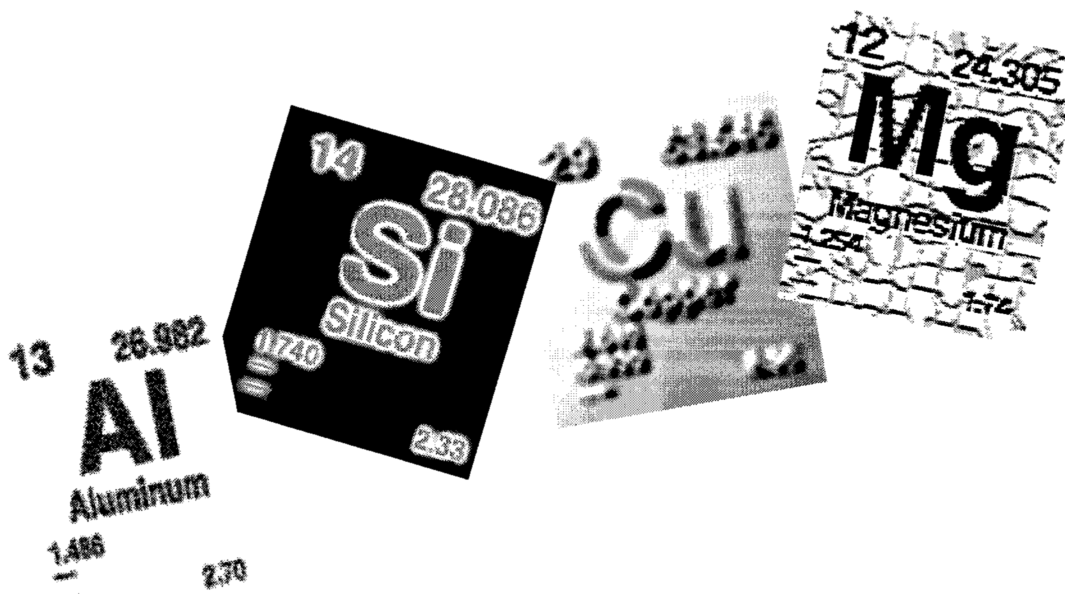

2.1 Aluminum-Silicon Alloys

Aluminum-silicon castings add up to 85 – 90% of the total aluminum cast parts produced. These alloys provide excellent castability, good corrosion resistance, and satisfactory machining and welding properties [3]. In addition to silicon, other elements are present in Al-Si alloys [4, 5] either as intentional additions for obtaining improved properties, or as impurities. These elements include the following:

- *Antimony, Strontium, Calcium* and *Sodium*, which are known to modify eutectic silicon from its habitual acicular platelike form into a lamellar or fibrous form;
- *Phosphorus*, which is considered as an impurity in casting alloys due to its interactions with common silicon modifiers (Na and Sr) thereby reducing their modifying power, although it is used in hypereutectic Al-Si alloys because it reduces the size of the primary silicon phase particles;
- *Titanium* and *Boron*, which are used for grain refining purposes;
- *Copper*, which is used to increase strength and hardness in heat-treatable alloys at the expense of a reduction in corrosion and hot tearing resistance, as well as adequate castability;

- *Magnesium*, which has potent hardening and strengthening effects since it forms the hardening phase Mg_2Si;
- *Iron*, which is considered an impurity, forms insoluble brittle intermetallics (Al_5FeSi) that have a direct impact on the ductility of the alloy;
- *Manganese,* which is used to neutralize the effect of the brittle Al_5FeSi intermetallic phase by converting it to a compact Chinese script form;
- *Beryllium*, which is used to prevent oxidation losses; it also modifies the morphology of iron-containing phases, but since it is listed as a carcinogen it should be used prudently;
- And lastly *Silver* and *Zinc*, which are used to increase the age-hardening response of the alloy.

Figure 2.1 shows the equilibrium binary Al-Si phase diagram. It will be observed from this diagram that silicon has a maximum 1.62% solid solubility in Aluminum at 577°C and that a simple eutectic is formed at a composition of 12.6% Si. Additions of silicon up to the eutectic composition reduce the solidification range and improve fluidity in the molten state. In the eutectic composition, a large volume fraction of eutectic is formed, thus improving fluidity and the feeding ability.

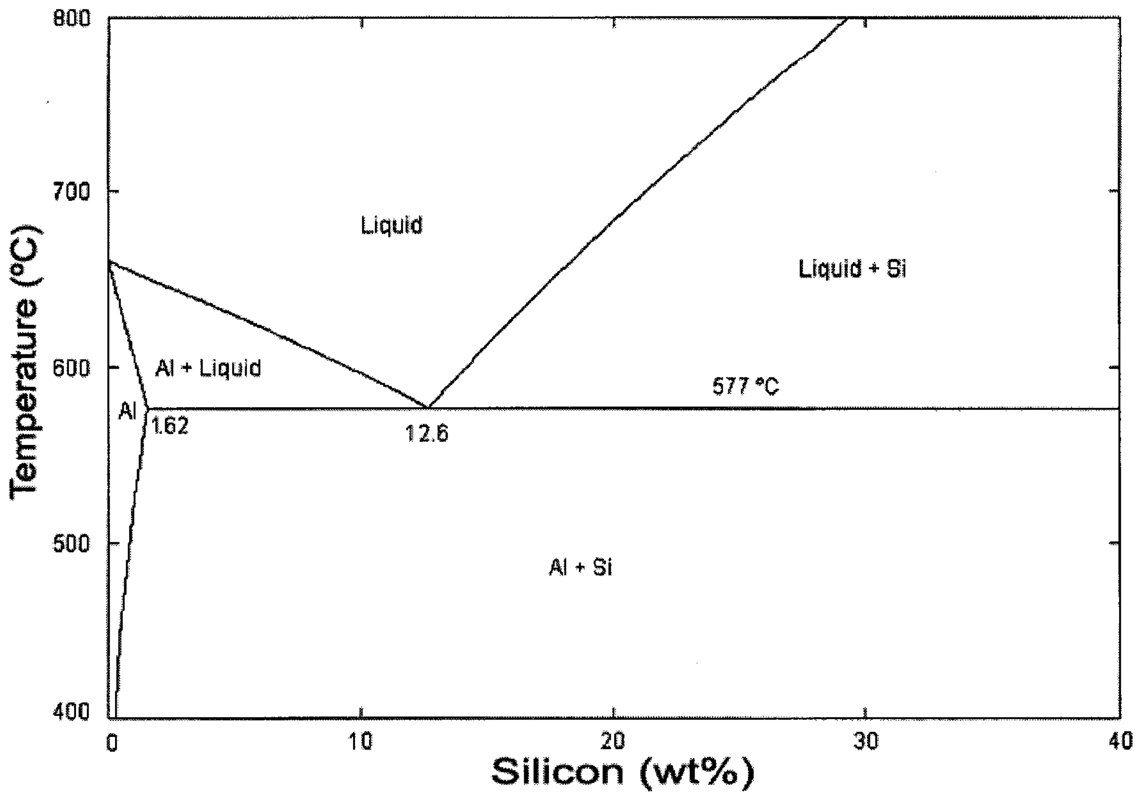

Figure 2.1 Equilibrium binary Al-Si phase diagram.

Al-Si cast alloys may be divided in three main groups [6]:

- hypoeutectic with silicon contents between 5% and 10%
- eutectic alloys with 11 – 13% Si
- hypereutectic with contents of more than 13% silicon

Hypereutectic alloys are used when excellent wear resistance, first rate casting characteristics and low thermal expansion are required, as in the case of alloy 390 [7]; the main drawback in the use of these alloys, however, is the presence of the extremely hard primary silicon phase which has a direct impact on machining properties, thus increasing production costs [8, 9]. Certain treatments have proved to produce finer and more evenly distributed primary silicon crystals in hypereutectic Al-Si alloys, thus improving their mechanical properties. These treatments include the addition of mischmetal, the control of the calcium content in the alloy and the addition of phosphorus. When phosphorus is added, however, any sodium present in the melt must be removed beforehand because sodium phosphide would otherwise form and the nucleating effect on silicon be lost [10, 11].

Hypoeutectic and near-eutectic Al-Si alloys are more commercially common than hypereutectic Al-Si alloys and the addition of copper, magnesium or nickel greatly improves the strength of this type of alloy and enhances its response to heat treatment. Heat-treated products manufactured with these alloys find a wide range of engineering applications. Nevertheless, the eutectic silicon phase which is present in the alloy consists of brittle acicular flakes and plates, producing a direct impact on the mechanical properties of the alloy, namely on its strength and ductility. In order to overcome such a disadvantage, a process of chemical modification of the silicon eutectic by small additions of Na or Sr may be carried out. Noticeable improvements in strength and significant increases in ductility will then be observed. These are well-documented facts [3, 12-18] which will be presented in further detail in the next section.

2.2 Eutectic Silicon Modification

The term modification refers to the transformation of the silicon phase from acicular to fibrous in aluminum-silicon alloys. This phenomenon was first discovered in the 1920's by Aladar Pacz and, since then, there have been numerous developments in the related science and technology, which have brought about the increased use of aluminum casting alloys [3].

Modification may be obtained by two different means:

- the addition of very low concentrations (typically 0.01% to 0.02%) of chemical agents, called modifiers, such as rare earths and elements from groups IA and IIA,

- rapid solidification (or quenching) of the melt.

Figure 2.2 shows typical changes which occur in the morphology of the silicon eutectic after modification. There is no noticeable difference between the optical microstructures of Al-Si alloys modified by each of the two methods mentioned above.

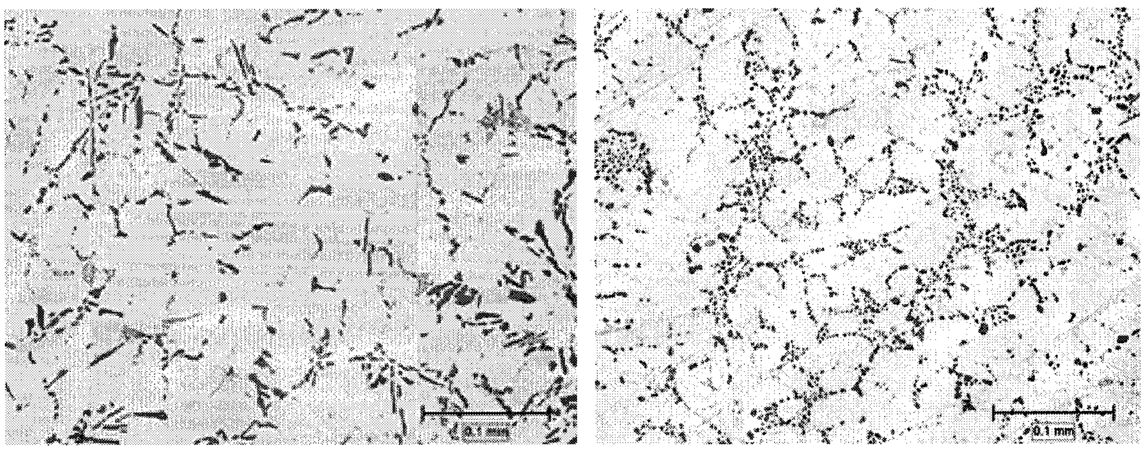

(a) unmodified (b) modified

Figure 2.2 Optical micropraphs of as-cast microstructures of hypoeutectic Al-Si alloys.

When the material is quenched, the eutectic silicon solidifies into an exceedingly fine form but with the same acicular morphology observed in the unmodified alloy, provided that the solidification takes place at high freezing rates. Commercial casting processes are not able to attain such modified conditions, thus chemical modification is usually applied. A combination of relatively high freezing rates, or chilling, and chemical modification is often conducive to modification since both processes act in cooperation to produce a modified structure. Modification depends on a wide variety of factors which include Si content, chemical composition of the alloy, type of modifier, holding time, and degassing conditions, to name but a few [3].

Among the elements which produce modification, only sodium and strontium impart a significant modifying effect at low concentrations [19, 20]. Sodium, however, has the disadvantage of being highly reactive in its pure state, of fading rapidly through evaporation, and of releasing pollutant fumes upon its addition to the melt. Strontium therefore, tends to be used more extensively nowadays.

Strontium is more soluble in aluminum than sodium, and consequently can be added to the melt in the form of master alloys such as Al-3.5%Sr, Al-10%Sr, Al-10%Sr-14%Si and Al-90% Sr. Occasionally, pure strontium may be added, but it is more difficult to dissolve in the melt than sodium because it forms strontium oxide, SrO, which is highly stable. This stability is what governs the fading effect of the strontium and not the evaporation which rules the fading in the case of sodium. Another advantage of strontium is that it is considered to be a semi-permanent modifier, with a lower rate of loss than sodium and high recoveries of over 90% of the original addition. The relative stability of strontium makes it possible for the modified material to be remelted and recast without appreciable loss.

2.2.1 Mechanisms of Eutectic Modification in Al-Si Alloys

The mechanisms which alter the morphology of the silicon eutectic phase have been the subject of extensive research over the years [21]. The theories proposed to explain eutectic modification deal with either restricted growth or restricted nucleation mechanisms [22].

Crosley and Mondolfo [23] proposed a theory where AlP (Aluminum Phosphide) particles play a key role in the nucleation of eutectic silicon, acting as an effective nucleant because of the similarity in crystal structures. When there is enough phosphorus in the melt, as in commercial Al-Si cast alloys, abundant AlP particles are present, and silicon forms acicular flakes at small undercoolings of less than 2°C. By adding a chemical modifier, a reaction between the phosphorus in the melt and the modifier occurs, thereby neutralizing the nucleating effect of phosphorus. An increase in the undercooling for nucleation of silicon by aluminum occurs and results in modified fibrous structures.

The main obstacle emerging from the theories based on restricted nucleation mechanisms, like that of Crosley and Mondolfo, is that they are founded on the assumption that the silicon eutectic phase is discontinuous and its formation depends on repeated nucleation. This assumption is not accurate since the restriction in nucleation would not affect the structure of the phase; also, it has been observed that the silicon eutectic phases present in unmodified and Sr-modified alloys are different, and that they are both continuous [3, 14, 15], thus a more suitable explanation is required here.

Growth of the Al-Si eutectic occurs in two ways, either coupled or uncoupled growth. Uncoupled growth means one phase grows into the liquid well before the other; this type of growth is characterized by a non-planar, non-isothermal solid-liquid interface which results in a flake or platelike structure. In coupled growth, both aluminum and silicon phases form from the liquid at a common interface, being almost planar and isothermal; thus, resulting in a lamellar or fibrous structure [22].

It is believed that the solid solution α-aluminum phase has a minor influence on the process of modification. Unmodified silicon solidifies in the form of crystals attached together by definite crystallographic planes (111) and grows in specific crystallographic directions <112>. This condition facilitates the formation of twin planes at the (111) planes which results in a self-perpetuating groove of 141° at the solid-liquid interface. This growth condition is called the *twin-plane re-entrant edge* mechanism (TPRE) [3, 22, 24-26] (see Figure 2.3). The crystallographic perfection of the silicon phase allows it to grow in a flake-like coarse acicular fashion, so when this perfection is disturbed, the silicon becomes modified.

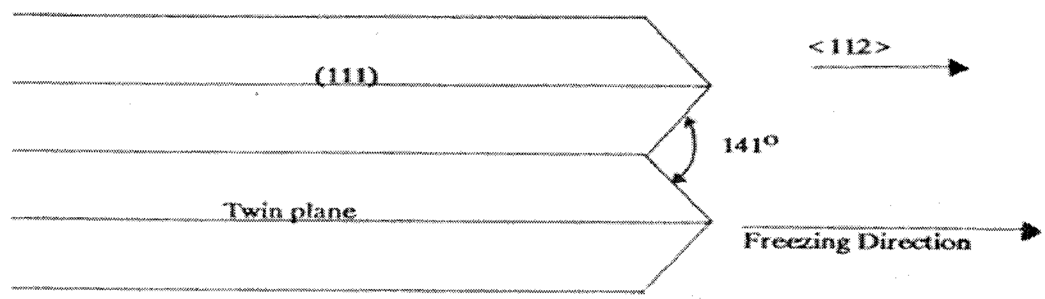

Figure 2.3 Schematic representation of an acicular Silicon crystal growth from the melt [3].

Shamsuzzoha and Hogan [25, 26] have proposed that twinning in the silicon phase is frequent during the slow cooling of Al-Si alloys, thereby promoting small angular distortions along the twinning planes which lead to branching as a consequence. When the solidification rate is increased, silicon atoms do not have sufficient time to fit into the growth ledges, thus, they generate more twin planes, and consequently more distortion and branching.

Makhlouf *et al.* [27] carried out research on unmodified hypoeutectic Al-Si alloys. They report that in alloys with relatively high iron contents, in excess of 0.0015%, the β-AlSiFe phase forms. During the solidification primary α-Al dendrites nucleate at the liquidus temperature, and the β-AlSiFe particles nucleate in the solute field ahead of these growing dendrites at a temperature that is at, or slightly above, the eutectic temperature of the alloy. Eutectic Si nucleates on these β-AlSiFe particles, resulting in platelike silicon morphology since it displays the freedom to grow. When a chemical modifier is added, towards the end of solidification of the mushy zone, the modifier concentration in the eutectic liquid within the interdendritic regions reaches relatively high levels. The modifier in solution changes the viscosity of the eutectic liquid ahead of the α-Al dendrites, thereby altering the interfacial characteristics between the eutectic liquid and the solid substrates, as β-AlSiFe particles, on which the eutectic phases nucleate. Hence, the eutectic phases do not nucleate on the solid substrates at the eutectic temperature, and significant undercooling of the melt occurs. Meanwhile, the α-Al dendrites continue to grow, causing the eutectic liquid to become supersaturated with silicon. This supersaturation and undercooling cause precipitation of primary, blocky silicon particles in front of the dendrites, thereby forming a boundary between the α-Al dendrites and the liquid. The liquid is not able to penetrate through this chain of blocky silicon particles to further the growth of the α-Al dendrites. However, numerous Al grains nucleate in the supercooled liquid. The eutectic silicon grows between the arrays of eutectic aluminum grains and is aided by the ability of silicon to twin easily, thus acquiring the fibrous morphology which is characteristic of chemically modified hypoeutectic Al-Si alloys rather than the flaky platelike morphology observed in unmodified alloys.

Lu and Hellawell [28-30] have proposed an alternate explanation for silicon modification. Their explanation states that there is a local enrichment of the atoms of the modifying element at the silicon-liquid interface, in such a way as to cause them to become absorbed. The absorption will distort the ledges formed during silicon growth and promote twinning and branching. This process, known as the *twin plane re-entrant edge (TPRE) poisoning mechanism*, impairs the crystallographic perfection of the silicon phase which is responsible for its flake-like structure, causing a modified fibrous structure to appear instead.

2.2.2 Strontium-Modification and Porosity

Strontium-modification has been associated with an increase in the amount of the porosity observed in castings for many years. A large amount of work has been carried out to investigate and explain this particular phenomenon. Early works by Argo and Gruzleski [31] on modified and unmodified A356 alloys concluded that in modified alloys a redistribution of porosity takes place. Instead of primary piping, microporosity is observed giving the impression of more pores [3, 32-36]. The first attempts to explain this phenomenon were based on the assumption that the addition of strontium as a modifier increased the hydrogen pickup rate of the melt. More recent investigations [37-40], however, have shown that Sr additions to the melt affect the eutectic solidification mode which is responsible for the redistribution in porosity, whereas the number of pores formed is dependent on a combination of casting design and feeding efficiency.

Other researchers [41] have found that the porosity observed in Al-Si castings, as well as its shape, is associated with the formation of strontium oxides in the melt (either as particles or films). Strontium possesses a high degree of affinity for oxygen and it is extremely difficult to remove these oxides from the melt through degassing, thus they have to be removed mechanically.

Studies of porosity related to Sr-modification in Al-Si-Cu alloys indicate that this effect is not considerable in melts with hydrogen contents lower than 0.1 mL/100g Al [42]. Strontium additions of 200 – 300 ppm in Al-Si-Cu alloys are optimum property-wise, in view of the fact that higher additions tend to overmodify the eutectic and give rise to an increase in porosity levels, which in turn, lower the mechanical properties [43].

Other factors are related to porosity formation in Al-Si casting alloys. Caceres *et al.* [44] studied the effect of adding copper to an Al-Si-Mg base alloy; their results indicate that additions of Cu exceeding 0.2% result in a noticeable increase in dispersed microporosity. This increase seems to correlate well with the formation of large amounts of interdendritic Cu-rich phases and is related to the formation of interdendritic ternary liquid which solidifies at a lower temperature than the Al-Si eutectic and is therefore difficult to feed with the liquid metal, thereby generating cavities.

A similar phenomenon was observed by Samuel *et al.* [45, 46] and Taylor *et al.* [47, 48] in Al-Si-Cu type alloys containing Fe. Iron forms the β-Al_5FeSi intermetallic phase in long, thick platelets which are often branched. When examined under an optical microscope, these platelets appear as needles because the observation is made on a two-dimensional surface. Large shrinkage pores are formed within the casting due to the difficulty of feeding the liquid metal into the spaces between the branches of the β-Al_5FeSi platelets. However, Sr-modification affects this intermetallic phase as well, breaking it down into small fragments, thus reducing the shrinkage-porosity associated with this phase.

2.3 Heat Treatment of Aluminum-Silicon Castings

"Heat-treatable" is the term used to describe aluminum castings which can be strengthened and hardened by means of heat treatment or the application of different heating/cooling cycles. Heat treatment of aluminum castings has further advantages of microstructural homogenization, residual stress relief, and of improved dimensional stability, machinability and corrosion resistance. In order to benefit from these improvements, the castings may be annealed, solution heat treated, quenched, precipitation hardened, overaged or treated in combinations of these practices [5].

The general methods for heating aluminum alloys include fluidized bed, air-chamber and induction furnaces [49, 50]. The choice of heating equipment depends on the alloy, the heat treatment and the configuration of the parts to be processed [51].

Air furnaces are the most common heat treating equipment used for aluminum castings because they permit greater flexibility in adjusting the operating temperature when a variety of alloys and/or treatments are used and they are more suitable for the treatment of large parts, since it is less expensive to hold the temperature of a large volume of air than the same volume of a salt bath used in fluidized bed furnaces. Fluidized bed technology has the advantages of heating the parts faster (see Figure 2.4), reducing the dimensional distortion during heat treatment due to the buoyant effect of the salt and better temperature control and uniformity [52]. The fact that the heating rate in a fluidized bed furnace is higher than in a conventional air furnace increases the kinetics of metallurgical phenomena such as Si fragmentation and spheroidization during solution heat treatment, as well as the precipitation rate of the hardening phases during aging [53-56]. However, disadvantages such as operation of the hazardous molten salt baths and the possibility of explosions resulting from chemical and physical reactions are the main drawbacks of this type of heating furnace. Figure 2.5 shows a schematic configuration of a typical fluidized bed conveyor belt with an idealized temperature profile of a part heat treated through the system.

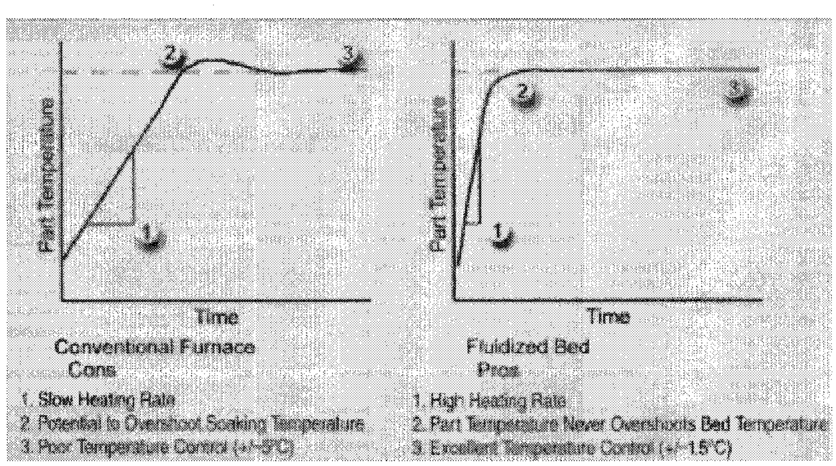

Figure 2.4 A comparison of temperature profiles for a part heated in a conventional furnace to that treated in a fluidized bed [52].

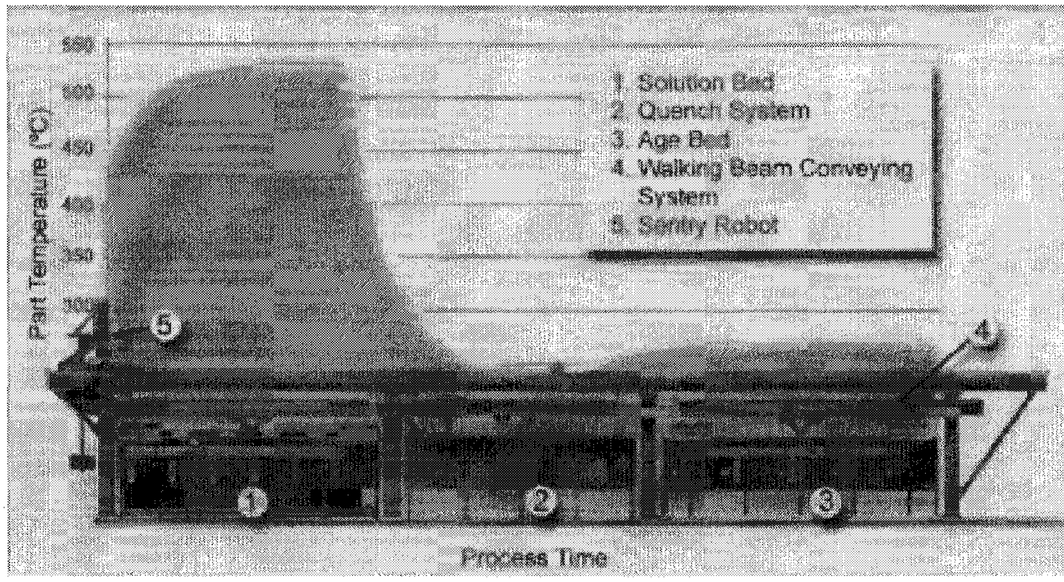

Figure 2.5 Schematic configuration of a typical fluidized bed conveyor belt with an idealized temperature profile of a part heat treated through the system [52].

The basic requirement for an alloy to be amenable to age-hardening is a decrease in the solid solubility of one or more of the alloying elements present with decreasing temperature [57]. Three basic operations are carried out when heat treating a product fabricated from aluminum castings: solution heat treating, quenching and aging [9, 57, 58]. This sequence comprises the most common heat treatment procedure applied to heat-treatable 319 alloy (Al-6.5%Si-3.5%Cu), in view of the fact that such a heat treatment regime is capable of yielding the best properties. This treatment is designated as the T6 treatment (or temper) by the Aluminum Association of America [19]. A detailed description of the stages of the T6 treatment is provided in the following sections.

2.3.1 Solution Heat Treatment

Solution heat treatment is carried out to maximize the dissolution of certain elements present in the alloy such as Cu and Mg in the α-aluminum solid solution. The dissolution of these elements will cause precipitation hardening during the artificial aging treatment. Also, spheroidization of the undissolved constituents and general homogenization of the microstructure occurs during this treatment.

Heat treating of cast alloys differs from that carried out in wrought alloys because of the presence of complex eutectic phases [4]. Extensive information is available on the heat treatment of commercial Al-Si-Mg alloys [59-63]. It should be noted here that the popular casting alloy 356 belongs to this family. The purpose of the solution heat treatment in this alloy is to obtain a maximum concentration of the age-hardening constituent Mg_2Si in solid solution, so as to homogenize the casting and to change the structural characteristics of the silicon particles through coarsening and spheroidization. The standard solution heat treatment for this alloy is carried out at 540°C for 4 – 12 h [58], this temperature is high enough to dissolve the Mg_2Si phase as may be observed in the pseudo binary phase diagram shown in Figure 2.4.

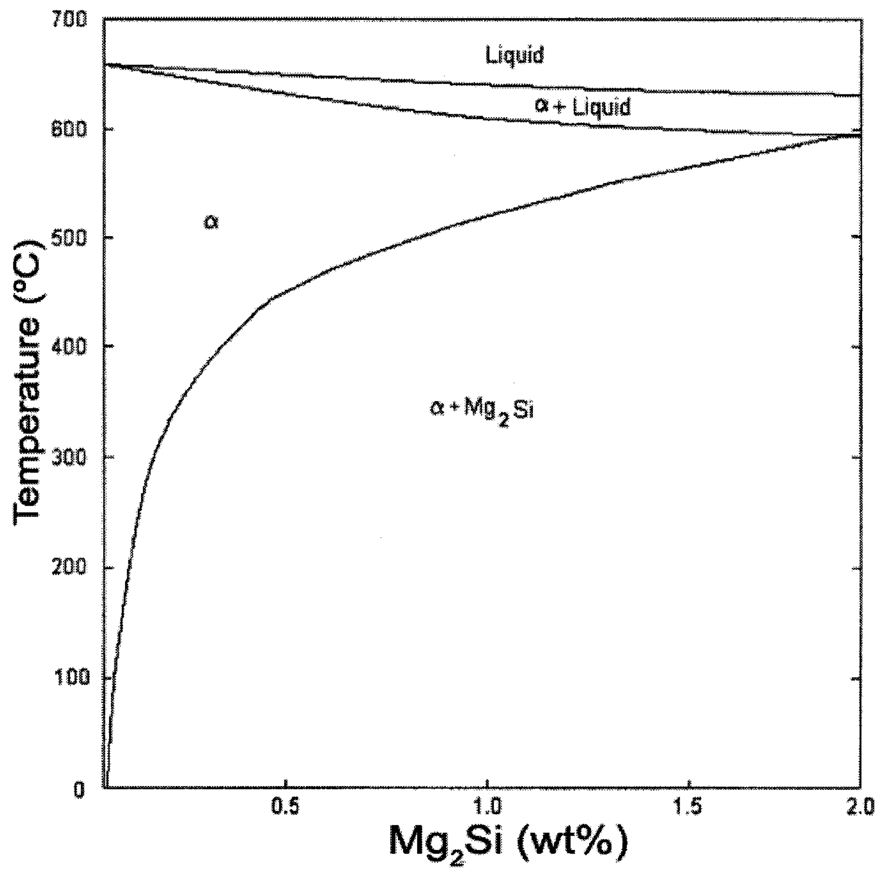

Figure 2.6 Pseudo-binary Al-Mg_2Si phase diagram.

Alloy 319, however, is a system based on the Al-Si-Cu system; therefore, the solution heat treatment aims to dissolve the copper present in the alloy, which is the element responsible for the age-hardening effect observed. The standard Mg content of this alloy is restricted to <0.1 wt%.

Li *et al.* [64] studied the factors which affect the dissolution of the $CuAl_2$ phase in alloy 319; they found that Sr-modification leads to segregation of the copper phase in regions away from the Al-Si eutectic, and that when iron is present in the alloy, the iron provides nucleation sites for the precipitation of the copper phase thus reducing the severity of $CuAl_2$ segregation caused by strontium. These factors are to be considered when solution heat-treating an aluminum casting containing copper, and which has been modified with strontium.

Figure 2.5 shows the aluminum-rich end of the binary phase diagram for the Al-Cu system since the copper content in alloy 319 is between 3% and 4%.

In order to reach the solid solution condition, the temperature should be maintained at a sufficiently high level, where the solution and diffusion conditions are optimum. The standard T6 treatment specifies that the solution heat treatment should be carried out at approximately 500°C and maintained for 4 – 12 hours depending on the casting method. Shorter periods of time are recommended for permanent mold castings and longer times for sand castings [4, 49, 58]. Figure 2.5 shows that this temperature is just above the solvus line and at a composition of 3 – 4% Cu the α-aluminum solid solution will be reached.

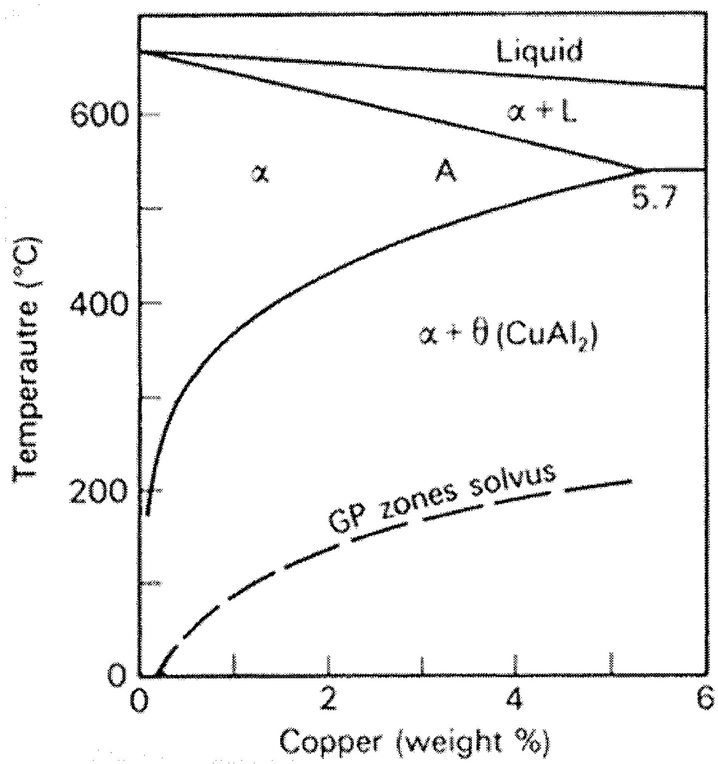

Figure 2.7 Al-rich section of the Al-Cu eutectic phase diagram [57].

Gauthier *et al.* [65, 66] studied the response of alloy 319 when subjected to solution heat treatments over a wide range of temperatures between 480°C and 540°C, close to the temperature at which the copper eutectic reaction takes place. They found that, with a copper content of 3.77%, this reaction occurs at 506°C under equilibrium solidification conditions; that is to say, at a cooling rate of ~0.4°C/sec. Their results show that optimum heat treatment is 8 h at 515°C, since such treatment yielded the best mechanical properties. They also obtained improved tensile values with an alternative solution treatment as follows: first, solution heat treating the product for 1.5 h at 540°C to allow for the spheroidization of the Si particles; followed by slow cooling to 515°C during which the undissolved molten Al_2Cu phase solidifies in the usual manner, and finally, maintaining this temperature for 1 h.

Alternative solution treatments in alloy 319 were studied by Sokolowski *et al.* [67]. They found that in some cases a two-step solution treatment is able to improve the mechanical properties of the casting; they also state that strontium modification raises the eutectic temperature of the Cu-rich phases and thus requires higher solution temperatures. This effect, however, might be ascribed to the copper segregation caused by strontium, as discussed earlier.

The selection of the solution heat treatment temperature for alloys of the Al-Si-Cu system should be carried out with care. The temperature should be restricted to a range below the solidification point so as to avoid the melting of Cu-containing phases. However, if full hardening is to be achieved by aging, the material must be heated to dissolve the copper it contains while at the same time taking into consideration the fact that if the solution temperature is too low, a reduction of mechanical properties will result.

Figure 2.6 shows that the lower the solution temperature for a 319 alloy, the lower the mechanical properties attained will be.

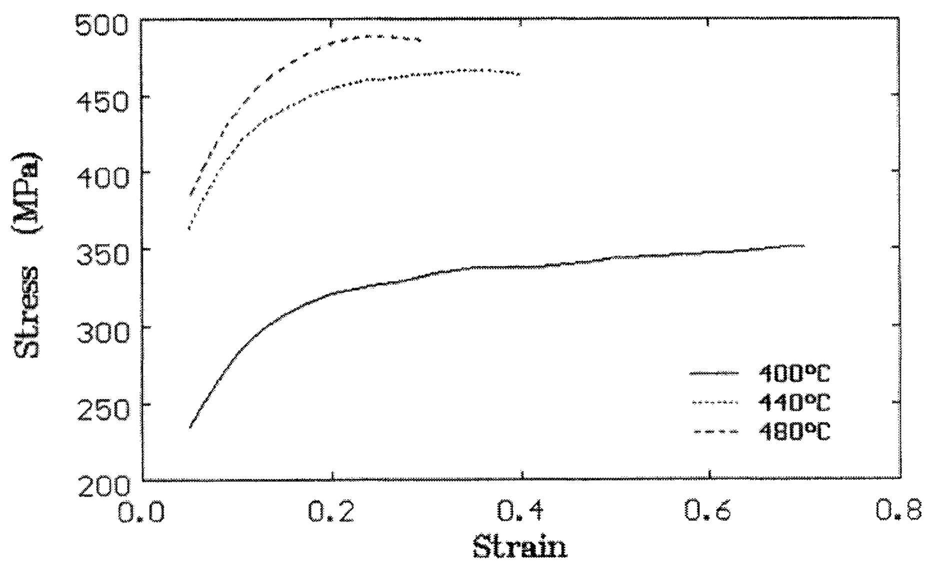

Figure 2.8 Stress-Strain curves obtained in compression of T4 samples from a 319 alloy solubilized at three different temperatures [4].

The melting of Cu-containing phases in a binary Al-Cu alloy was studied by Reiso *et al.* [68, 69]; their results show that melting starts to take place at the corresponding eutectic temperature, 547°C, and continues further with increasing temperatures as a result of the reduction in the Gibbs free energies. Certain researchers suggest that the solution heat treatment temperature should be limited to 500°C for copper contents of more than 2% [70, 71]. Parallel research [65, 66, 72, 73] indicates that, at higher temperatures, the melting of copper-containing phases occurs, thereby generating shrinkage porosity and a solidified structureless form of the copper phase which is detrimental to the mechanical properties of the alloys belonging to the Al-Si-Cu-Mg system. Incipient melting of the copper-containing phases may be avoided by minor additions of other elements; in a recent study carried out by Wang *et al.* [74], it was observed that the addition of beryllium (0.03 weight %) raises the Al – Al_2Cu eutectic temperature, thus reducing the risk of Al_2Cu melting.

There are a number of other effects associated with the solution-heat treatment stage. Among these may be included silicon spheroidization and coarsening which take place in an attempt to reduce the surface energy. The coarsening process, called Ostwald ripening, states that larger particles grow at the expense of smaller ones. Thus, the average size of the silicon particles increases, or coarsens, as the quantity decreases [75]. Intermetallic phases present in the casting, including those containing impurity elements, are normally thought to be unaffected by solution heat treatment. Limited changes, however, do occur [5]. For example, the β-Al_5FeSi phase present in alloy 319 is difficult to dissolve, but Gauthier and Samuel [66] observed that it is possible to dissolve this phase almost completely with long solution treatments of up to 24 h at high temperatures of between 515°C and 540°C. Similar observations on this phase were made by Crowell and Shivkumar [76] in a study carried out with Al-Si-Cu alloys.

Figure 2.7 shows the difference between the microstructures of an as-cast Al-Si-Cu-Mg alloy and a solution heat-treated one. Note the difference in the morphology of the eutectic silicon. Fragmentation of the silicon particles occurs in the solution heat-treated sample; also, some of the intermetallics observed in the as-cast sample are no longer visible.

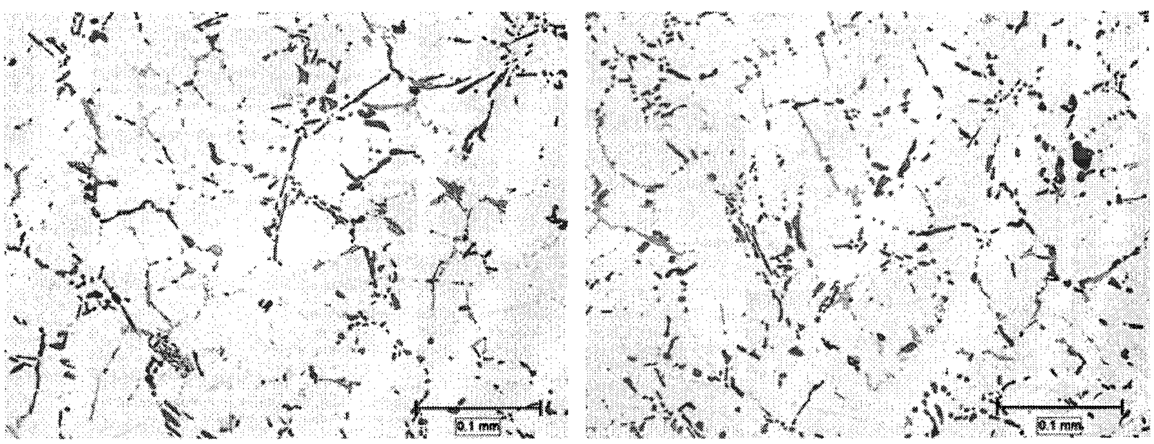

(a) As-Cast (b) Solution Heat Treated

Figure 2.9 Optical micrographs of the microstructures of (a) As-Cast and (b) Solution Heat Treated samples of an Al-Si-Cu-Mg Alloy.

The solution heat-treatment occurs at high temperatures, as stated earlier, which explains the occurrence of the effects discussed above. A quenching step is required in order to maintain the desirable conditions for obtaining precipitation-hardening.

2.3.2 Quenching

The objective of quenching is to maintain the highest possible degree of solution and amount of quenched-in vacancies, both of which are the optimum conditions for precipitation-hardening. The lowest level of induced residual stresses and the least distortion possible at room temperature are suitable conditions for avoiding a decrease in the mechanical properties of the final heat-treated product. After quenching, the metastable T4 supersaturated solid solution condition is achieved [4, 5, 9].

Rapid cooling from solution to room temperature involves critical aspects. A balance must be maintained between fast quenching and the minimization of residual stresses and distortion which occur with fast quenching. It should be noted that fast quenching is to be sought since excessive delays in quenching result in a temperature drop and rapid formation of coarse precipitates in a temperature range at which the effects of precipitation are ineffective for hardening purposes [19, 77]. The region where detrimental precipitation takes place is alloy-dependent. In quench-sensitive alloys, such as wrought alloy 7075, this region lies between 400 to 290 °C while in casting alloy 356 it is 400 to 260 °C; some sources quote this range, or a slightly different one, as the most critical for quenching any aluminum alloy [58]. For casting alloys, the delay in quenching should not exceed 45 s and a maximum quenching delay of 10 s is usually acceptable, as specified by ASTM standards [78].

The importance of the quenching medium lies in the fact that the quenching rate and heat extraction depend on it. Wrought alloys are commonly quenched by immersion in cold water, but quenching for castings and parts with complex shapes and thick sections is commonly performed in a medium with slower cooling rates, such as in hot water between 65°C and 80°C or solutions of polyalkaline glycol; or else in a different medium such as forced air or mist [79, 80].

Byczynski *et al.* [81] studied the effect of the quench rate on the mechanical properties of 319-type alloys and determined that quenching in water at 65°C, which is the highest cooling rate of all those used in the study, may be beneficial to the mechanical properties analyzed: Brinell hardness, ultimate tensile strength and dimensional growth.

After the quenching stage of the T6 treatment, the next stage is the aging or precipitation-hardening of the alloy.

2.3.3 Aging

The process of the decomposition of a super-saturated solid solution obtained after the application of a solution heat-treatment is called aging; it occurs as a result of a supersaturation in the matrix of a certain element or elements. There exists a driving force for the precipitation of equilibrium phases. Over time, some alloys age at relatively low temperatures, even at room temperature. This phenomenon is called natural aging and the rate at which it happens depends to a high degree on the alloy system. For example, casting alloys A356.0 and C355.0 age within 48 h with insignificant changes thereafter; alloy A520.0 age-hardens over a period of years and is therefore normally used in the T4 condition; several alloys which belong to the Al-Zn-Mg system are employed without heat treatment and exhibit changes in their properties over three to four weeks or with short heat treatments at relatively low temperatures [82].

Microstructural changes cannot be detected because these effects occur through zones forming within the solid solution [4, 5, 19, 57, 58]. Natural aging has been extensively studied in a variety of casting alloys, mainly those which belong to the Al-Si-Mg and Al-Mg-Cu systems; in general, it can be stated that the longer the natural aging stage, the more adversely affected the mechanical properties will be [83-85]. In order to avoid or inhibit the natural aging of alloys prone to this phenomenon, the castings may be kept at lower temperatures, usually subzero, until the artificial aging stage is completed; studies carried out by Murali *et al.* [86] determined that trace additions of elements such as In, Cd, Sn and Cu inhibit natural aging in Al-Si cast alloys.

The aging rate can be accelerated when treating the product at a higher temperature, so as to enhance the diffusion of solute atoms and precipitation of secondary phases. This process is called precipitation-hardening or artificial aging. The degree of strengthening will depend on the system involved, the volume fraction and size of the second phase particles, as well as on their interactions with the dislocations [57, 87-89].

The mechanisms which operate during the aging stage will be outlined in greater detail in the following section.

2.3.3.1 Precipitation Hardening Mechanisms

Complex temperature- and time-dependent changes occur in most precipitation-hardenable systems. The principal change to be observed in initial periods of artificial aging at low temperatures is a redistribution of solute atoms within the lattice to form ordered clusters or GP (Guinier-Preston) zones [90] which are enriched in solute [19, 57, 89].

In view of the fact that the mechanisms discussed here are similar in the majority of age-hardenable aluminum alloy systems and the conclusions are of general applicability [89], only the Al-Cu system will be used as an example. Figure 2.8 shows a schematic representation of a GP zone in an Al-Cu alloy system.

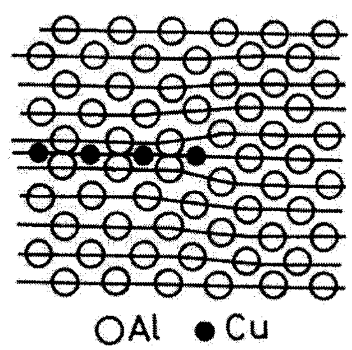

Figure 2.10 Section through a GP zone parallel to the (200) plane [91].

GP zones may precipitate in different shapes: rods, needles, spherical clusters, or monoatomic discs parallel to a crystallographic plane of the metal matrix; their form depends to a high degree on the specific alloy system. Silver, copper, magnesium and zinc are among the alloying elements which exhibit GP zones in aluminum alloys [89] and their formation requires the movement of solute atoms over relatively short distances so that they are finely dispersed in the matrix. The rate of nucleation and actual structure are influenced by an excess of vacant lattice sites, or vacancies, which are captured from the solution stage by quenching. These vacancies facilitate the transport of the solute atoms [19, 57, 91-93].

The appearance of GP zones produces a lattice distortion within the area they occupy and on several planes in the matrix, since they retain its structure and produce appreciable elastic strains due to the coherency they exhibit. Figure 2.9 shows a schematic representation of coherent, semi-coherent and non-coherent precipitates.

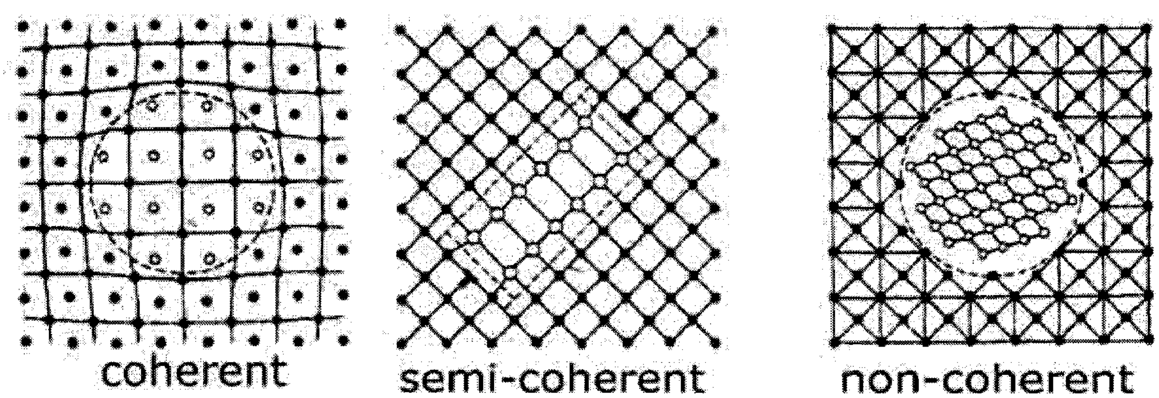

Figure 2.11 Schematic representation of precipitate coherency [89].

The strengthening effect observed in age-hardenable alloys may be explained by two basic concepts and their application in the dislocation theory [87]:

1. The interference to slip by particles precipitating on crystallographic planes, and

2. The number and size of the precipitating particles.

An increased number, or high volume fraction, of GP zones in the matrix increases the distortion and thus also the stress required to move dislocations and produce deformation, since a single GP zone on its own has only a minimal effect on impeding dislocation gliding [57, 89].

As dislocations traverse the GP zones they shear them, increasing the solute-solvent bonds across the slip planes as well as the energy needed by subsequent dislocations to cross the zones. This process eventually causes dislocation pile-ups at grain boundaries [9, 19, 89]. A representation of this phenomenon is shown in Figure 2.10.

Eventually, GP zones start forming metastable transition phases which are particles with a different crystal structure from that of the solid solution or the structure of the equilibrium phase. In most alloys, the metastable phases have crystallographic orientation relationships with the solid solution and the two phases remain semi-coherent; they are coherent only on some planes by adaptation of the matrix through elastic strain. The strengthening effect increases as the size of the precipitates increases, as long as the dislocations continue to cut through the precipitates. This stage is regarded as the *peak aging condition*, i.e. where the highest strength is achieved.

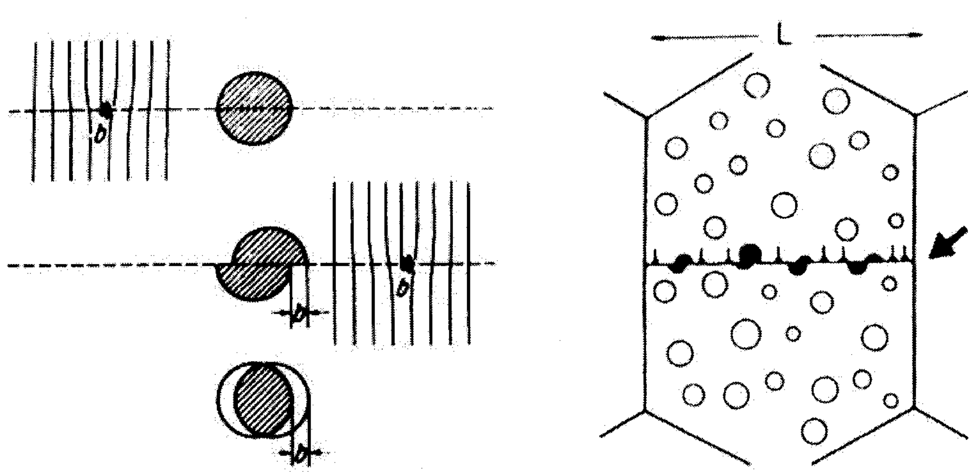

(a) (b)

Figure 2.12 (a) Shearing of a GP zone by a moving dislocation; (b) dislocation pile-ups at grain boundaries [57].

As aging progresses, these particles grow, thereby increasing coherency strains, until the interfacial bond is exceeded and coherency disappears. The precipitate then changes from transition to equilibrium form, in this case, strengthening is caused by the stress required to cause the dislocations to loop around and form dislocation tangles instead of going through the precipitates.

As precipitates grow and become more widely spaced, they can be readily bypassed by dislocations forming loops around them, a phenomenon known as the Orowan mechanism, shown in Figure 2.11, and causing the strengthening to decrease. This stage is called *overaging* [5, 9, 19, 57, 89].

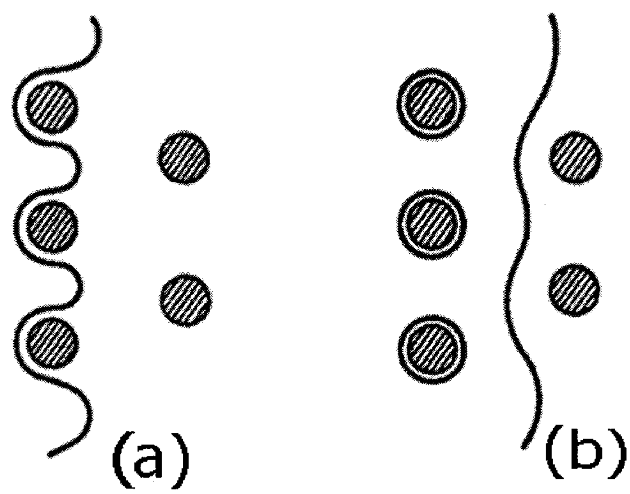

Figure 2.13 The Orowan process of dislocations: (a) bowing between precipitates, then (b) by-passing the particles by leaving a dislocation loop surrounding each one [89].

2.3.3.2 Precipitation in Common Aluminum Alloy Systems

In the Al-Cu system, GP zones initially form as two-dimensional discs with a diameter of between 3 to 5 ηm. As aging progresses, these zones increase in number and are ultimately replaced by the θ'' phase at aging temperatures above 100°C. This phase is tridimensional and remains semi-coherent with the α-Al matrix. Subsequently, the transition phase θ' forms and coexists with θ'' until the semi-coherency cannot be maintained and finally, there is the transformation of θ' to the non-coherent equilibrium phase θ (Al_2Cu) [4, 19, 89, 91, 94-96]. The structures and morphologies of the θ phases are presented in Figure 2.12.

The precipitation sequence is as follows:

$$SS \rightarrow GP\ (1) \rightarrow \theta'' \rightarrow \theta' \rightarrow \theta_{eq}$$

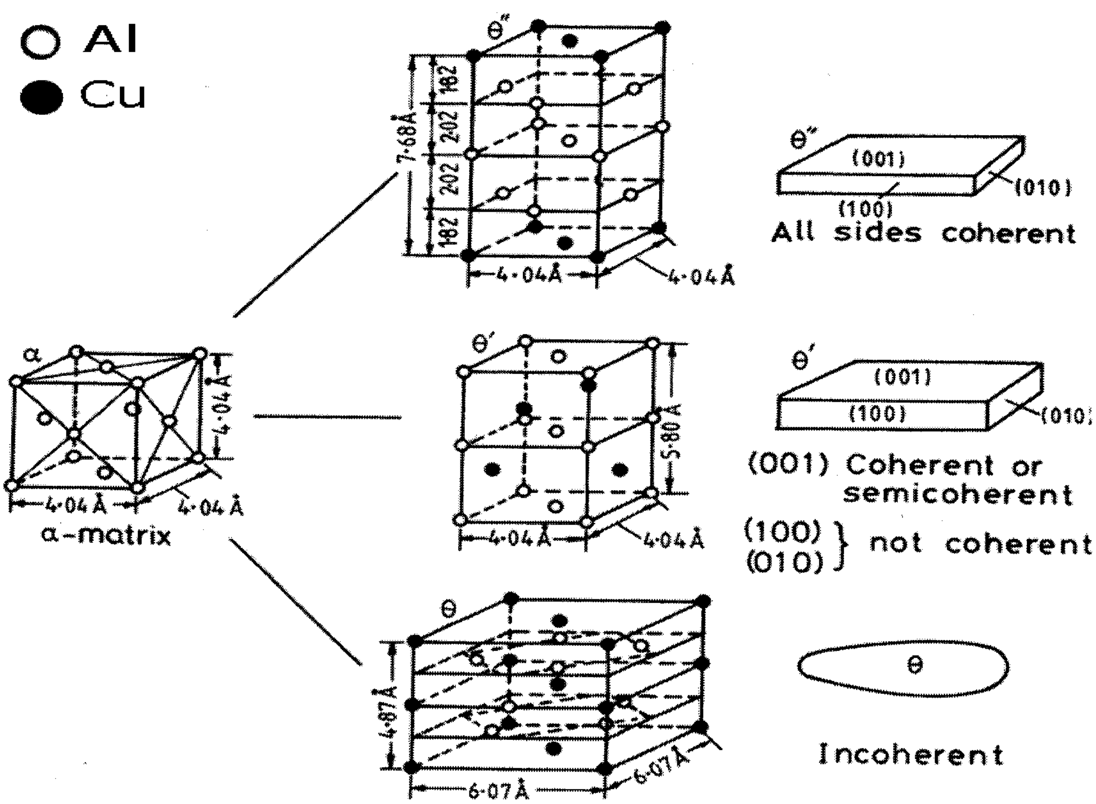

Figure 2.14 Structure and morphology of θ'', θ' and θ in Al-Cu [91].

Figure 2.13 shows a transmission electron micrograph of the θ'' phase, as fine particles, and the θ' phase as needles, which appear in an aged Al-Cu alloy at 150°C. The needles of the θ' phase are oriented in the <001> directions of the α-Aluminum matrix.

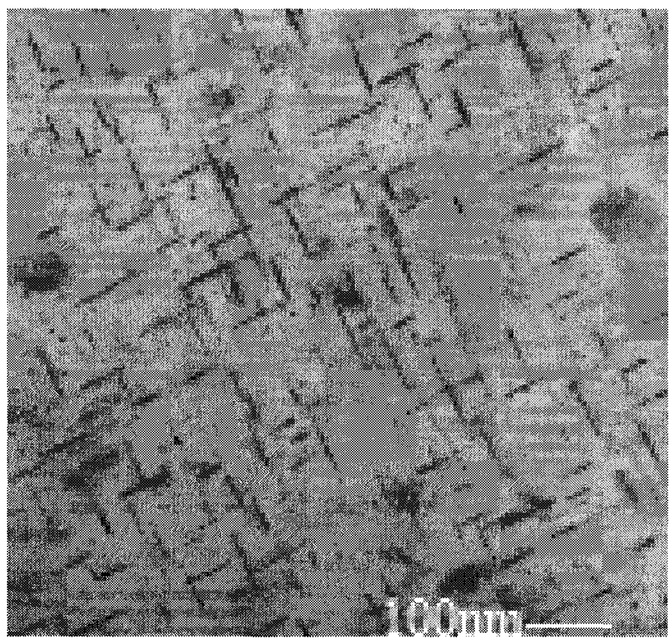

Figure 2.15 θ' phase as needles and θ'' phase as fine particles. Sample of an Al-4Cu alloy aged during 100 h at 150°C [95].

As regards an Al-Cu-Mg system, additions of magnesium to Al-Cu alloys accelerate and intensify natural precipitation-hardening. The precipitation mechanisms in this type of alloy is not as well documented as it is in Al-Cu alloys, but it is believed that the precipitates consist of groups of magnesium and copper atoms which collect on certain planes. Some of these alloys, at elevated temperatures, produce the transition phase S' (Al_2CuMg) which is coherent on {021} matrix planes. Overaging then forms the equilibrium S phase and loses coherency. It has also been found that, when additions of Si are made to this alloy, modified Si-containing lath-shaped GPB zones appear, in addition to GP zones. These zones are faceted in the $\{001\}_\alpha$ planes and elongated in the $<001>_\alpha$ directions [97-101]. Other more complex intermetallic phases may appear depending in the ratio of the different elements present in the alloy, these phases may include [19, 99, 102]: λ-$Al_5Cu_2Mg_8Si_5$, $Al_4CuMg_5Si_4$ among others. The identification of these phases, however, is difficult since most of them have the morphology of needles or very fine plates and for some precipitates it is extremely difficult to obtain a positive identification with the techniques used in this study, sometimes atomic resolution equipment is needed [103].

The precipitation sequence is thus:

$$SS \rightarrow GP/GPB \rightarrow S' (Al_2CuMg) \rightarrow S (Al_2CuMg)$$

Figure 2.14 shows a transmission electron micrograph of the S phases precipitating in an Al-Cu-Mg alloy at different aging times.

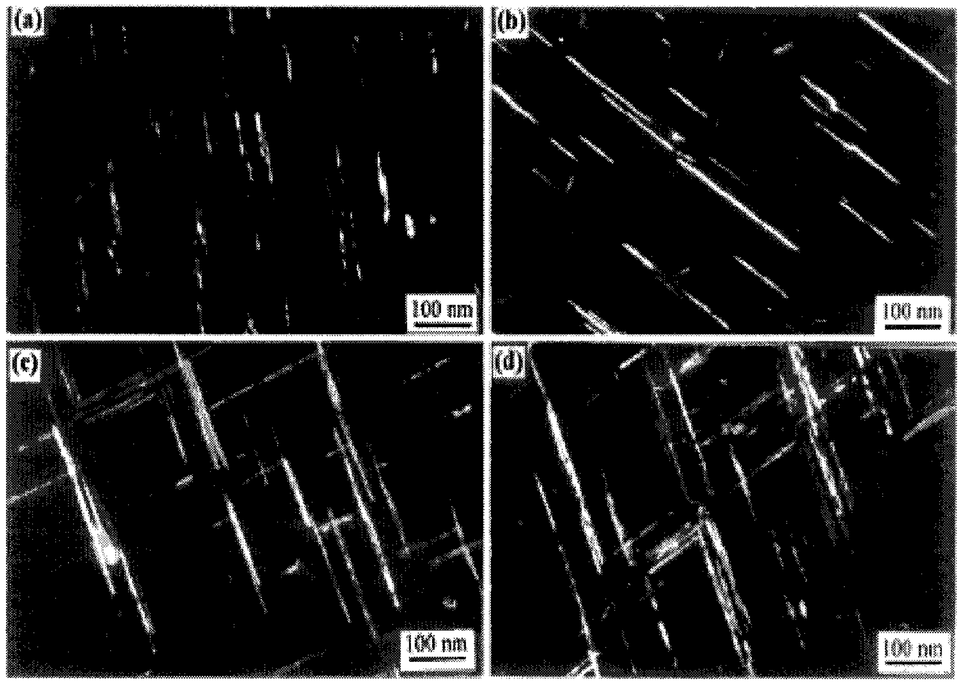

Figure 2.16 TEM micrograph showing plate/disc-shaped precipitates during the aging process in an Al-Cu-Mg alloy aged at 240°C, (a) after 0.75 h, (b) after 1.5 h, (c) after 4 h, (d) after 48 h [104].

In the Al-Mg-Si, system strengthening occurs over an extended period of time at room temperature. The formation of zones in these alloys has not been detected but in short aging times and temperatures of up to 200°C there is x-ray and electron diffraction evidence indicating the presence of very fine, needle-shaped zones. Researchers in the field [105-109] report that the zones are initially spherical and convert to needle-like forms with aging, while further aging causes growth of the zones to rod-shaped transition particles β'-Mg_2Si with a highly ordered structure; at higher temperatures the transition particles are transformed into the equilibrium phase β-Mg_2Si. No evidence of coherency strain was found in these phases.

The precipitation sequence is thus:

SS → GP → β' (Mg_2Si) → β (Mg_2Si)

Depending on the Si:Mg ratio, a different precipitation sequence might be observed. Other studies [110, 111] for example, suggest there are several stages in between the formation of transition and equilibrium phases as follows:

SS → Clusters of Si atoms and clusters of Mg atoms → Dissolution of Mg clusters → Formation of co-clusters Mg/Si → Small precipitates of unknown structure → β'' → B' and β'' → β (Mg_2Si) precipitates

Figure 2.15 shows the typical microstructure observed when analyzing a transmission electron microscope sample of an Al-Si-Mg sample, note the small spherical particles of the β'' phase and the β phase in the form of plates.

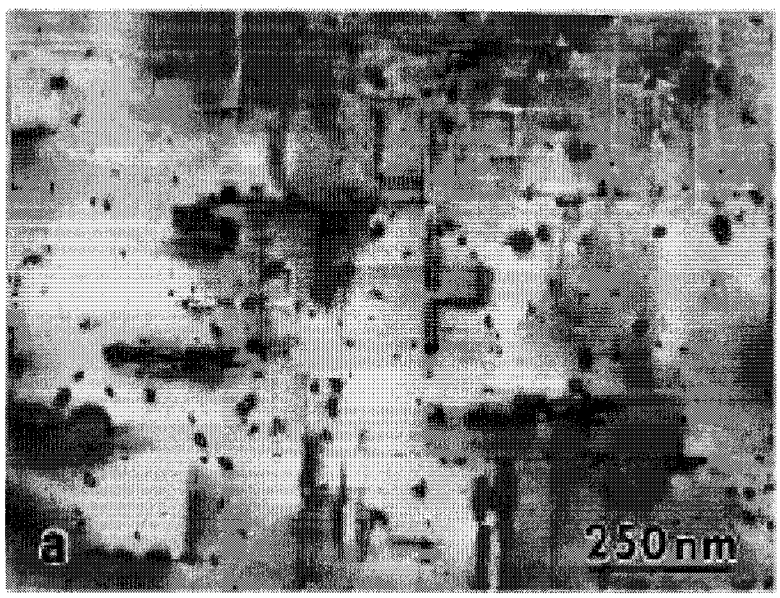

Figure 2.17 Transmission electron micrograph of an Al-Si-Mg alloy aged at 320°C for 1 hour [106].

Much research has been carried out in the Al-Mg-Si-Cu system concerning precipitates because of its relative complexity and convoluted precipitation process [102, 108, 112-117]. Hardening occurs with the precipitation of several phases depending on the Mg:Si ratio, copper concentration, and aging temperature. With an excess of Si, complex phases precipitate including Mg_2Si, Al_2Cu, Q (AlMgSiCu) and primary Si. The coherent and semi-coherent modifications of the two phases act as hardening agents up to aging temperatures of 200°C; above 200°C, the β'' phase is replaced by semi-coherent β' phases. The precipitation sequence is believed to be as follows:

SS→ GP → β'' → θ → Si → various modifications of β' (with copper) including Q'

→ Q (AlMgSiCu), Al_2Cu, Si

Figure 2.16 shows the microstructure of an Al-Cu-Mg-Si alloy showing the Q' and β'' phases in an alloy aged at 180°C for 1 h and for 7 h, respectively.

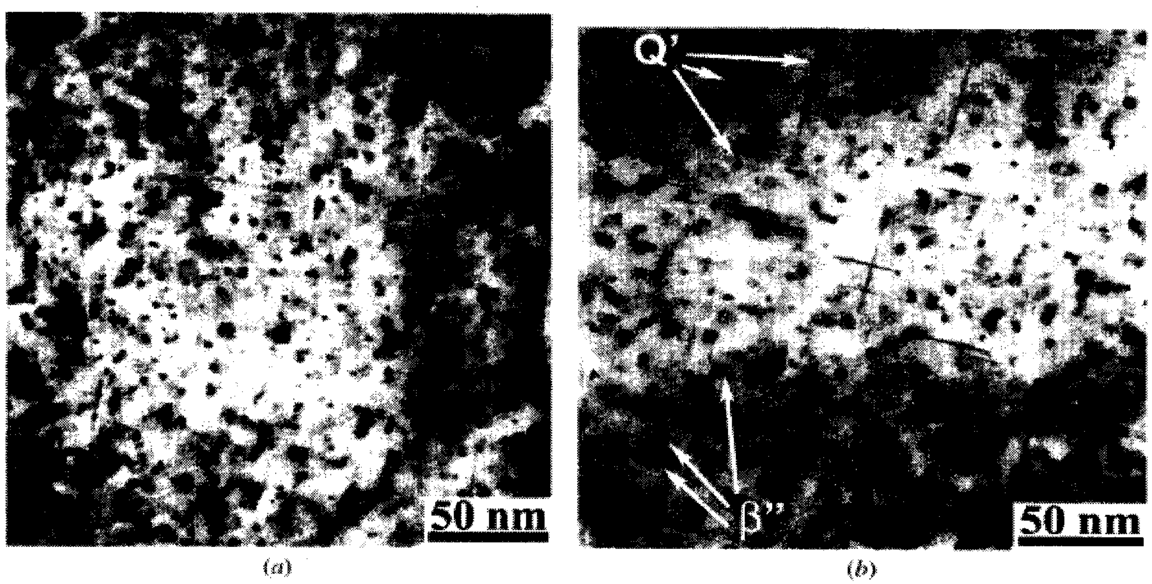

Figure 2.18 Transmission electron micrographs of samples aged at 180°C during (a) 1 h and (b) 7 h respectively [112].

Alloy 319 belongs to the Al-Si-Cu family of alloys, thus Mg additions are commonly made to improve its response to heat treatment, since this element in combination with Cu and Al produces several intermetallic phases which improve the mechanical properties of the alloy. As may be seen from the previous section, the complexity of the interactions between Al, Cu and Mg leads us to hypothesize the possibility of the presence of several intermetallic phases which are responsible for the precipitation hardening mechanisms. The following section will detail the available information for the mechanical properties of alloy 319 under different heat treatment conditions.

2.4 Mechanical Properties of 319-Type Alloys and their Improvement through Heat Treatment

The reported tensile and hardness properties of alloy 319 according to the literature[19] are presented in Table 1; F means the product was tested in its as-cast state, T5 and T6 indicate the heat treatment which was applied to the product before testing; solution heat treatment and artificial aging, are indicated accordingly. These values are regarded as standard and should not be used for design purposes since the mechanical properties are influenced by a wide variety of factors.

Other alloy characteristics, such as density (2796 kg/cm^3), thermal conductivity at 25 °C (0.25 SI units) and coefficient of thermal expansion, are not affected by the casting process or the heat treatment applied to the product [19].

Table 2.1: Properties of Alloy 319

	Tensile Strength (MPa)	Yield Strength (MPa)	% El in 50 mm	BHN
SAND CASTING				
F	186	124	2	70
T5	207	179	1.5	80
T6	250	164	2	80
PERMANENT MOLD				
F	234	131	2.5	85
T6	276	186	3	95

It is evident from Table 2.1 that permanent mold castings yield better properties than sand castings, and that the best properties may be achieved when the casting is heat treated using the T6 treatment.

Figure 2.17 shows the variation in tensile properties, namely strength and elongation, of alloy 319 over time at room temperature, which is the condition regarded as natural aging. The variation in the following conditions is shown: T4, solution heat treated and quenched; T6, solution heat-treated, quenched and artificially aged; and T7, solution heat-treated, quenched and overaged. Also, the results for samples prepared in permanent mold and sand mold are compared.

The strength values in these graphs are given in ksi; in order to convert to SI units (MPa) a simple multiplication must be made with the following equivalence: 1 ksi = 6.895 MPa. The graphs were taken from the literature [5] and the information to plot the graphs was produced at the Alcoa Laboratories, Cleveland Casting Research Division.

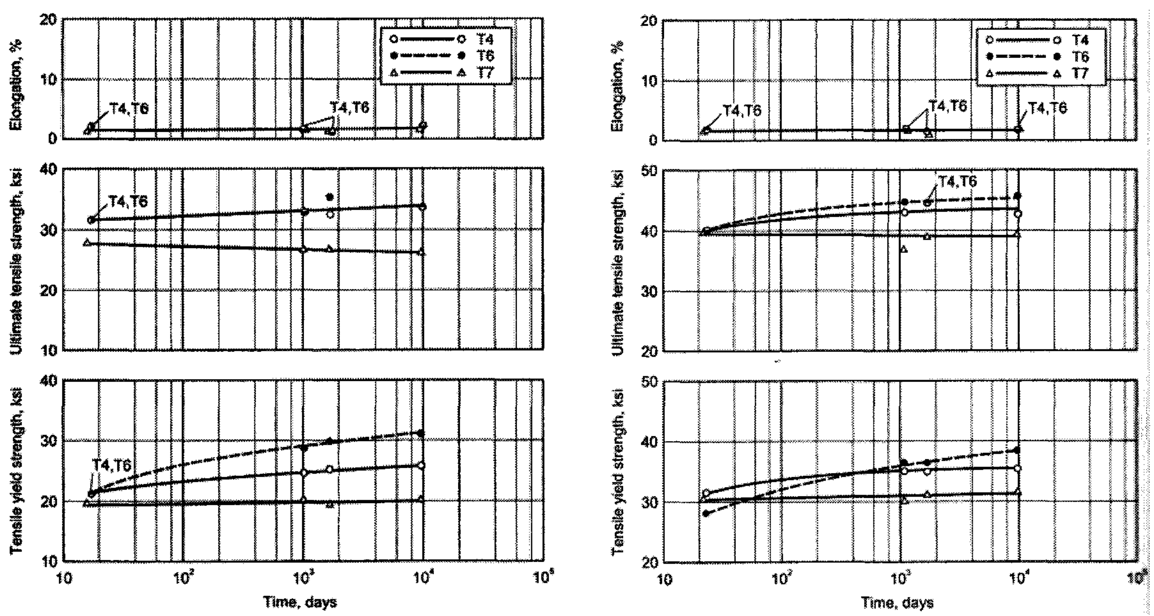

(a) Permanent Mold (b) Sand Cast

Figure 2.19 Natural aging of alloy 319 in the T4, T6 and T7 conditions. (a) Permanent mold and (b) Sand cast [5].

It will be observed that elongation does not exhibit much change for any of the treatment conditions that appear in the graphs, either for permanent mold or sand mold samples. The overaged condition, T7 treatment, shows that there is no variation of strength over time because all the hardening phases have already precipitated in the heat treatment applied; therefore no change will be observed thereafter.

As regards the conditions T4 and T6, ultimate tensile strength shows a slight increase over long periods of time; however, yield strength values are affected by natural aging, as evidenced in the corresponding graphs, indicating that this parameter is more sensitive to the aging process. It will be noted that the curve corresponding to the T6 condition shows the most dramatic increase of the three. This effect may be explained by an incomplete precipitation of the hardening phases, indicating that either the temperature was not high enough or the time was not sufficient to complete the precipitation. Unfortunately, such details as temperature at the time of heat treatment were not supplied.

Another set of data was provided in the same reference [5] labelled "319.0-F Sand Castings: typical tensile properties" where tensile samples were maintained at certain temperatures for the times indicated after casting. Figure 2.18 shows the curves plotted using this information.

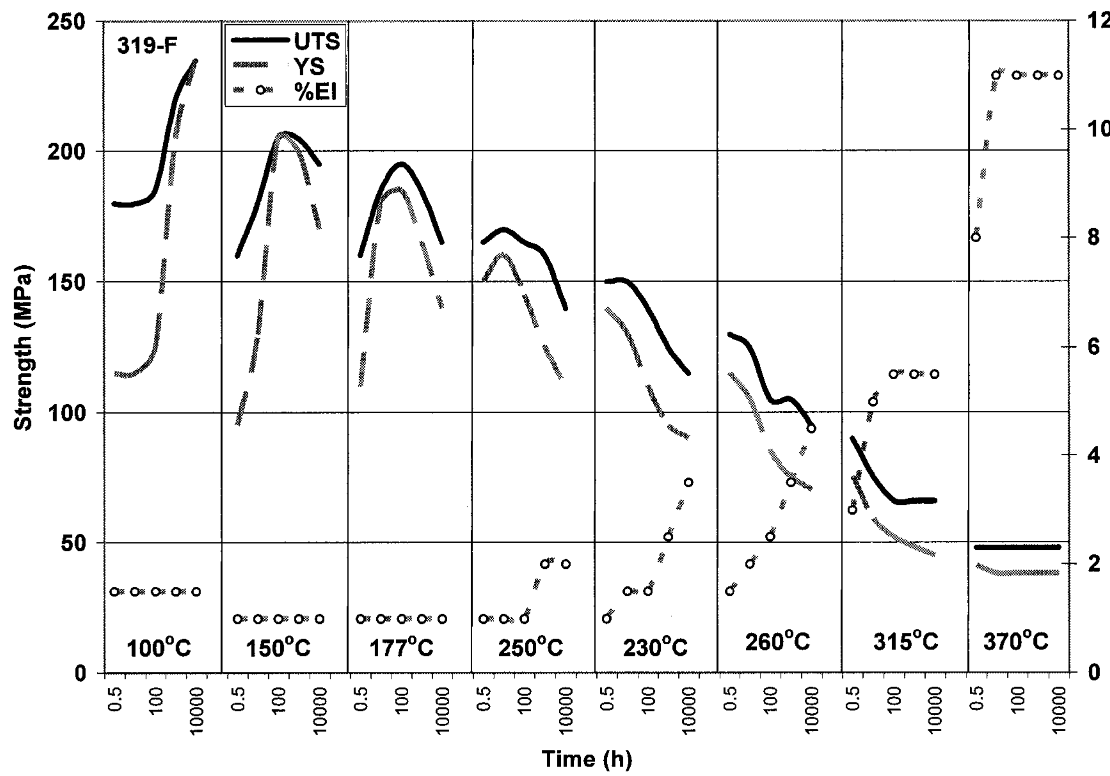

Figure 2.20 Tensile properties of alloy 319.0-F plotted from data from [5].

The behavior observed is the typical aging curve for aluminum alloys: strength tends to increase over time until the peak strength is reached, following which the strength lessens due to the growth of precipitates in the matrix, and overaging occurs, characterized by the loss in strength. When treating at higher temperatures, the peak strength occurs more rapidly and the elongation starts to increase. However, the tensile properties of castings are dependent on many factors such as the casting conditions, the solidification rate, the grain size, the chemical composition, the soundness of the casting and, the level of modification, to name but a few. Unfortunately, all of these details are not provided with the data; it should be noted that the samples were aged after casting, and as mentioned earlier, the best attainable properties are observed when applying the T6 treatment.

In a study by Purtee [118], the aging characteristics of a 319 alloy were studied. Cast bars were produced for tensile tests and Brinell hardness measurements, however, only 3 aging temperatures, 230°C, 257°C and 284°C, were used. The maximum aging time used was 6 hours and only the ultimate tensile strength, elongation and hardness values were presented. The highest hardness and strength values were obtained after aging for 6 hours at 230°C, which is expected since this is the lowest aging temperature in the study. The temperatures used resemble those used for treating aluminum castings in the T7 condition, or overaging. When treating with this condition, some advantages exist at the expense of reduced strength levels. These advantages include the improved dimensional stability of the products that has been evidenced by other studies [119, 120].

The aging behavior of Alloy 319 was studied by Gauthier *et al.* [121]. Tensile bars were cast and heat treated with the T6 treatment at different aging temperatures ranging from 155°C to 220°C for up to 24 hours. They found that the peak aging condition was reached after aging for 24 h at 155°C or 5 h at 180°C, the corresponding values were 403 MPa for tensile strength, 253 MPa for yield strength and an elongation of 1.2%.

They also found that such casting defects as inclusions and oxides have a marginal effect on the yield strength but detract from the tensile strength and the elongation values. The elongation values in heat-treated samples with casting defects were inferior to those obtained by samples in the as-cast condition. This effect is to be expected as the same deductions concerning inclusions, oxides and their relation to tensile properties were drawn from another study [122].

An extensive study was carried out by Li *et al.* [123, 124] where the mechanical properties of alloys of the 319-type were examined. Their findings show that factors such as decreasing the cooling rate and the addition of Sr are beneficial to the tensile properties; they also found that the presence of Fe-containing phases such as β-Al_5FeSi, and the segregation of the $CuAl_2$ phase, as well as its incomplete dissolution, are detrimental to the tensile properties. As regards impact properties, Sr-modification is beneficial while the β-Al_5FeSi phase may act as a crack initiation site, thereby reducing the impact toughness of the material. The elongation in tensile tests may be related to the impact toughness of the material: the more ductile the material, the higher the impact toughness values will be. The study also included a comparison of two heat treatment conditions, T5 and T6; the main difference being the presence of the solution heat treating stage and water quenching in the T6 condition. The results show that all of the properties analyzed are significantly improved when treating with the three stages of a typical T6 heat treatment regime.

The effect of Fe, among other elements, in cast alloys was studied by Caceres *et al.* [125]. According to the results of their study, they state that additions of Fe to Al-Si-Cu-Mg alloys will lower the ductility of these alloys considerably, and that the addition of a combination of Cu and Mg improves the strength of the alloy by the formation of the hardening-phases Al_2Cu, Mg_2Si and $Al_5Cu_2Mg_8Si_6$.

The effect of additions of Mg, specifically on the aging behavior of alloys of the 319-type, was studied by Ouellet and Samuel [126]. They determined that additions of 0.45% Mg enhance the response of the alloy to heat treatment, particularly in the T6 condition where improvements of more than 40% in strength were obtained in samples that contained Mg, in comparison with samples treated at the same temperature and time (8 h at 180°C) containing very low levels of Mg, about 0.06%.

Sepehrband *et al.* [127] studied the effects of adding Zr to a typical A319 alloy on its aging behavior; they found that this element improves the hardness of the alloy provided that solution treatment times are long enough to dissolve the Zr in the matrix. They also observed that there is a constant behavior in the aging curve after the peak aging condition is reached, which may be explained by the slow precipitation of the Al_3Zr phase. Additions of different elements have been studied in relation to the aging behavior of Al-Si-Cu-Mg alloys; for example, Wang *et al.* [128] studied the effect of additions of Be. They found that this element accelerates the age-hardening rate and increases the age-hardening response at an aging temperature of 160°C.

Other practices have also been stablished to obtain even better mechanical properties, i.e. higher hardness values and higher strengths with acceptable elongation levels. Among these are non-conventional aging treatments, which will be further detailed in the following section.

2.5 Non-Conventional Aging Treatments of Aluminum Alloys

Recent studies [1, 2, 95, 129-132] have been carried out to analyze the effects of experimental aging cycles on aluminum alloys. These studies claim that certain mechanical properties such as tensile strength, hardness and impact toughness may display improvements of up to 30% as compared to conventional aging cycles. The non-conventional cycles consist in preaging the alloy (that is to say, aging before the peak aging condition is reached); then maintaining it at a low temperature, anywhere between room temperature and 65°C, for extended periods of time, from a few hours to a few weeks, and finally resuming the aging to either the peak or overaging condition. These experimental aging cycles have a beneficial effect on some of the alloys studied. More detail, however, is not provided for specific alloy systems; most of the work was done for wrought alloys but for only a few cast alloys.

Considering that alloy 319 is commercially important and given its complexity, resulting from the presence of silicon, copper, magnesium and strontium, the study of its precipitation behavior, as well as of the mechanisms which operate during aging, will provide a more in-depth and detailed understanding of the response of the alloy in the context of mechanical properties.

Chapter 3
Experimental Procedures

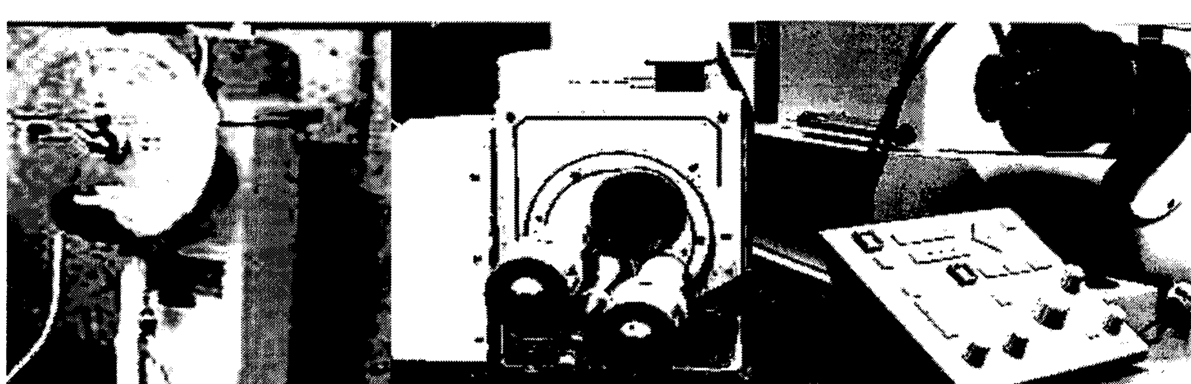

3.1 General

The experimental procedure designed for this specific work aims at investigating the effect of artificial aging conditions, including time and temperature as well as Mg additions and Sr-modification, on the mechanical properties and precipitation characteristics of a 319 Al-Si-Cu aluminum alloy when it is subjected to conventional and non-conventional artificial aging treatments.

The work may be described in the following stages: (i) materials, melting and casting procedures, (ii) heat treatment of the samples, (iii) mechanical properties testing, and (iv) microstructural analysis including optical, scanning and transmission electron microscopy.

3.2 Materials, Melting and Casting Procedures

Cast tensile and impact samples were produced in order to determine the effect of heat treatment on the mechanical properties. The chemical composition of the alloy used is shown in Table 3.1.

Table 3.1: Mean Chemical Composition of 319 Alloy

Element (wt%)							
Si	Cu	Fe	Mn	Mg	Zn	Ti	Sr
6.15	3.53	0.09	0.001	0.05	0.008	0.15	0.0001

The alloy was originally supplied in the form of ingots which were cut, dried and melted in a preheated (350 ± 5°C) silicon carbide crucible of 6-kg capacity using an electrical resistance furnace and maintaining the melting temperature at 750 ± 5°C. At this temperature, amounts of Sr in the form of an Al-10 %Sr master alloy and controlled amounts of Mg in the form of a pure metal were added, with the aid of a perforated graphite bell, in order to obtain four alloy conditions:

- base alloy 319, labelled 3
- alloy 319 + 200 ppm Sr, labelled 3S
- alloy 319 + 0.4% Mg, labelled 3M
- 319 + 0.4 %Mg + 200 ppm Sr alloy, labelled 3MS

The molten metal was degassed for 40 minutes using high purity dry argon injected into the melt with the hydrogen level maintained at less than 0.1 mL/100 g Al measured by an AlScan™ apparatus.

3.2.1 Preparation of Tensile Test Specimens

For each alloy condition, a permanent mold of the type ASTM B-108, shown in Figure 3.1, was used to cast 250 tensile test bars, the dimensions of which are presented schematically in Figure 3.2. The average DAS, Dendrite Arm Spacing, of the sample in the testing gauge was 25 μm.

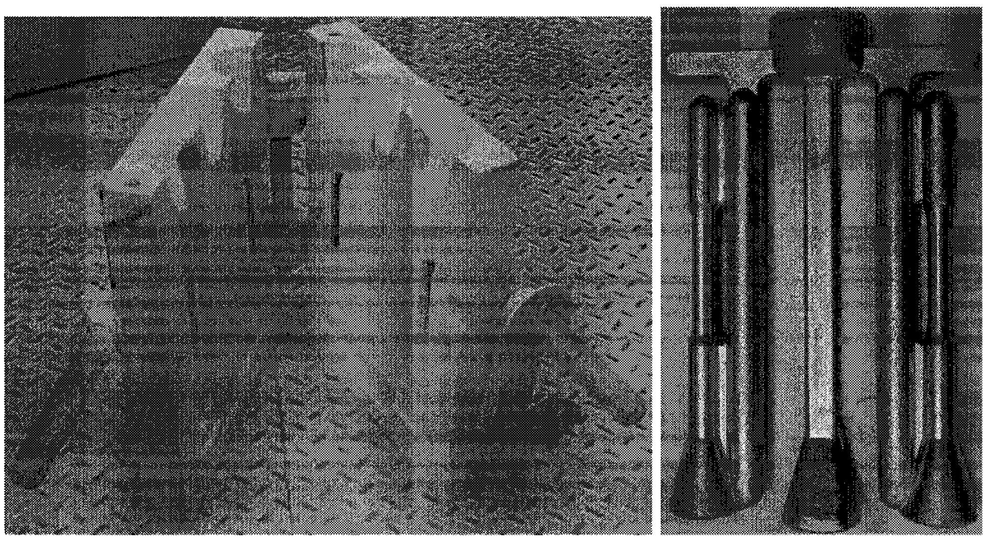

(a) (b)

Figure 3.1 (a) Permanent mold used to cast tensile samples, b) Casting showing the tensile bars with the risering and gating system.

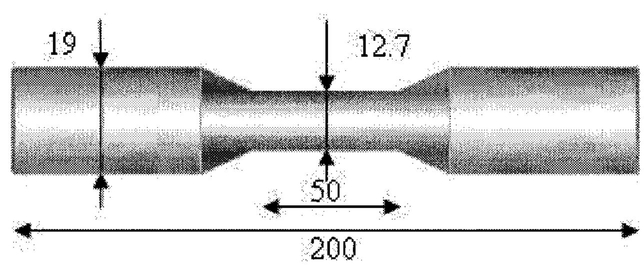

Figure 3.2 Dimensions of the tensile bars produced from the permanent mold (in mm) according to the ASTM-B108 Standard.

3.2.2. Preparation of Impact Tests Specimens

Unnotched impact samples were also cast, according to the ASTM E23 standard in a permanent mold as shown in Figure 3.3. After casting, the surface of the sample was ground with sandpaper to eliminate any surface irregularities which might affect the test. The dimensions of the samples were 10x10x55 mm.

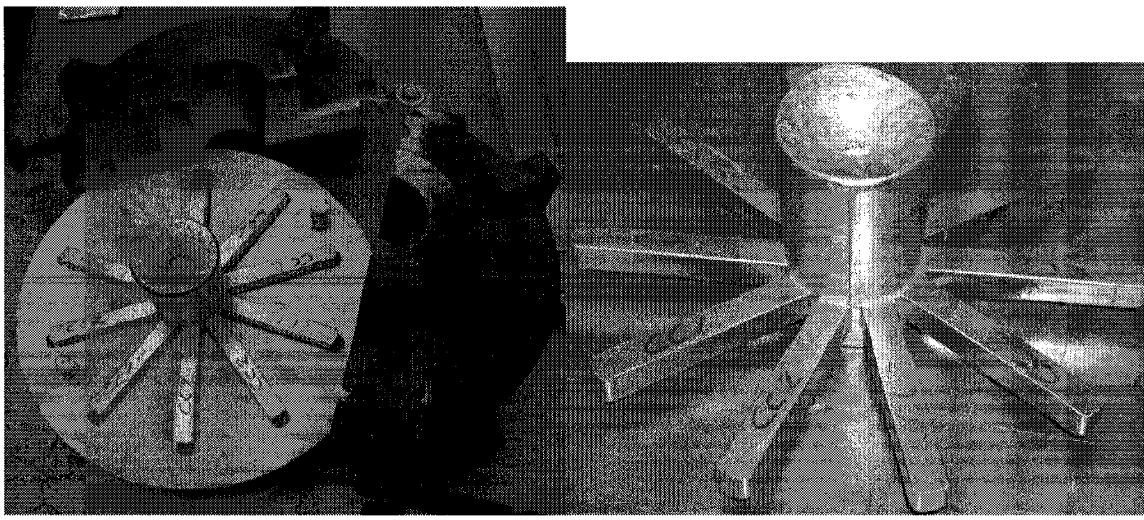

(a) (b)

Figure 3.3 (a) Permanent mould used to cast impact samples, (b) Casting showing the samples with the risering system.

3.3 Heat Treatment of the Samples

The samples were solution heat-treated at 495°C for 8h in a Lindberg/Blue M electric resistance air-forced furnace where the temperature could be controlled to within ±1°C, as shown in Figure 3.4, and then were immediately quenched in warm water at 60°C; after that, the artificial aging treatment was carried out using either continuous, multi-temperature or interrupted cycles, in the same furnace. After cooling the samples from the solution heat treatment stage, they were stored in a freezer at approximately -20°C until the time came for the artificial aging cycle to be carried out in order to avoid natural aging effects.

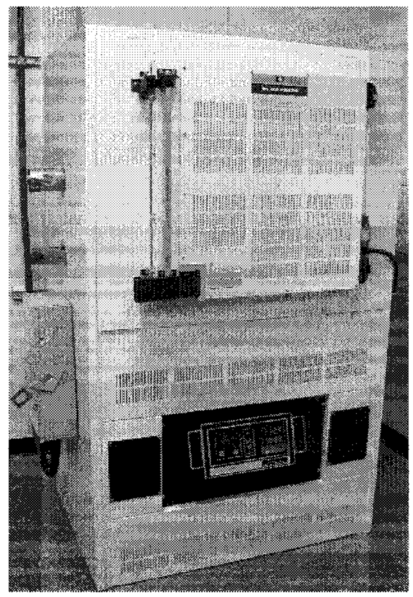

Figure 3.4 Electric resistance air-forced furnace where the heat treatments were carried out.

The continuous cycles are the artificial aging treatments performed conventionally, and the results obtained serve as a baseline for comparison with the new proposed cycles. These cycles were applied at five different temperatures (150°C, 170°C, 190°C, 220°C and 240°C) for 2, 4, 6 and 8 h.

The details for the multi-temperature aging cycles performed are summarized in Table 3.2.

Table 3.2: Multi-Temperature Aging Cycles

A – 2 h at 150°C and 1 h at 180°C	J – 2 h at 150°C and 3 h at 240°C
B – 2 h at 150°C and 3 h at 180°C	K – 2 h at 150°C and 5 h at 240°C
C – 2 h at 150°C and 5 h at 180°C	L – 2 h at 150 °C and 10 h at 240°C
D – 2 h at 150°C and 10 h at 180°C	M – 24 h at 100°C and 2 h at 240°C
E – 2 h at 190°C and 1 h at 180°C	N – 24 h at 130°C and 2 h at 240°C
F – 2 h at 190°C and 3 h at 180°C	O – 1 h at 170°C, 1 h at 190°C and 2 h at 240°C
G – 2 h at 190°C and 5 h at 180°C	P – 1 h at 150°C, 1 h at 170°C and 2 h at 240°C
H – 2 h at 190°C and 10 h at 180°C	Q – 2 h at 170°C and 2 h at 240°C
I – 2 h at 150°C and 2 h at 240°C	R – 2 h at 190°C and 2 h at 240°C

Multi-temperature aging cycles were designed using temperatures typically used in several foundries, also certain commonly used cycles such as 1 h at 170°C, 1 h at 190°C and 2 h at 240°C. A number of these multi-temperature cycles end at a relatively high temperature, 240°C. Several researchers found evidence [119, 120] suggesting that the products do not reveal a profound volumetric change after heat treatment at these temperatures.

Interrupted aging, similar to that described in the work of Lumley *et al.* [1, 2, 95, 129-132] for several wrought alloys, was also carried out. These aging cycles consist of an underaging step applied just after the warm water quench, followed by a low temperature stage at room temperature for periods of either 24 or 100 h, and lastly, aging is then resumed at a higher temperature. For these interrupted aging cycles, the combination of temperatures and times selected were taken from the multi-temperature cycles which produced the best mechanical properties, such as tensile strength and microhardness. The cycles are shown in Table 3.3.

Table 3.3: Interrupted Aging Cycles

1h at 170°C, 1h at 190°C, 24 h at 25°C, and 2h at 240°C
1h at 170°C, 1h at 190°C, 100 h at 25°C, and 2h at 240°C
2h at 190°C, 24 h at 25°C, and 3h at 180°C
2h at 190°C, 100 h at 25°C, and 3h at 180°C

3.4 Mechanical Properties Testing

In this part of the work, tensile and impact testing was performed and microhardness measurements obtained so as to monitor the effect of heat treatment on those properties.

3.4.1 Tensile Testing

Five tensile test bars were used for each tensile experiment. These bars were pulled to the point of fracturing at room temperature by means of an MTS™

Servohydraulic mechanical testing machine at a strain rate of 4 x 10^{-4}/s; a picture of this machine is shown in Figure 3.5. A strain gauge extensometer was attached to the test bars to measure alloy ductility. The yield strength (measured at 0.2% offset strain), the ultimate tensile strength and the total percent of elongation before fracture, as reported in this thesis, were obtained by means of a data acquisition system attached to the machine. This system provided the load-elongation curve; an example of which is shown in Figure 3.6.

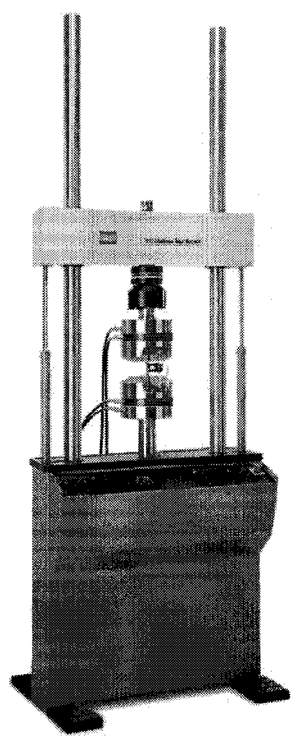

Figure 3.5 MTS servohydraulic mechanical testing machine.

This curve has the same shape as the engineering stress-strain curve because it may be obtained by dividing the load and elongation by constant factors. The elastic region is the first portion of the curve, where the load and elongation are linearly proportional until the elastic limit is reached (labelled E.L. in the figure) and gross plastic deformation starts taking place; then at 0.2% elongation, a line is drawn parallel to the elastic line and its intersection with the curve provides the yield strength, labelled Y.S. Plastic deformation proceeds, producing strain hardening and increasing the load to produce continuous plastic deformation; finally, fracture occurs due to the formation and propagation of cracks at one or more points of stress concentration. Where fracture takes place, the ultimate tensile strength is obtained, and is labelled U.T.S. on the curve.

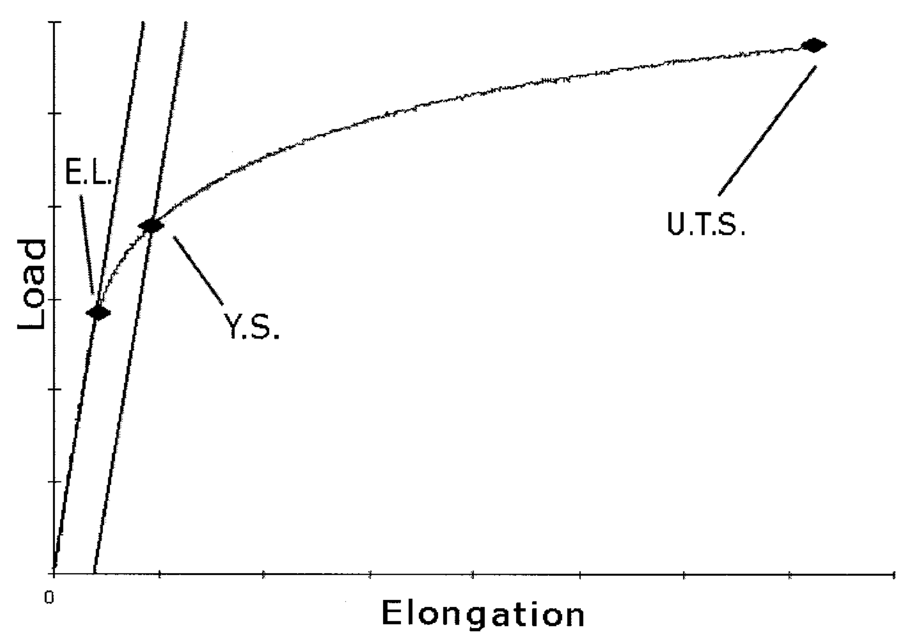

Figure 3.6 Example of a Load-Elongation Curve.

Those bars that were to be tested in the as-cast and solution heat treatment condition were kept in a freezer at ~-20°C before the actual testing took place. Such testing was not performed until the test bar was at room temperature, in order to avoid any natural aging effects.

3.4.2 Impact Testing

Impact toughness was measured on unnotched samples using the Charpy test. The specimen dimensions were 10x10x55 mm and the specimen surface was polished with sandpaper to remove any surface irregularities. A data acquisition system was connected to a SATEC™ pendulum impact machine to monitor the behavior of the test specimen, so as to measure the load and energy values as a function of time and the total absorbed energy (E_t). The setup is shown in Figure 3.7. The error bars shown in all the figures, in the results and discussion section, represent the standard deviations observed for each experiment which consisted of testing 5 samples.

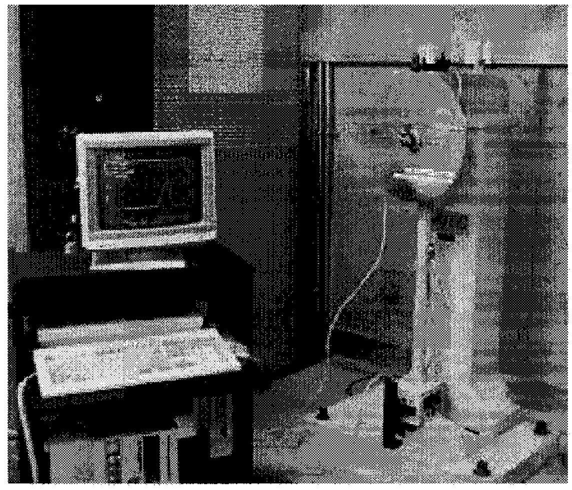

Figure 3.7 Impact machine and data acquisition system setup.

Figure 3.8 shows a typical result obtained from the instrumented impact test. The X-axis represents the time while the load and the energy are recorded on the Y-axes. The total absorbed energy, E_t (absorbed by a fractured specimen when tested under rapid loading conditions) represents the sum of the energies required for crack initiation, E_i, and crack propagation, E_p, and serves to describe the impact toughness of the alloy. The initial load increase, where it varies linearly with time, corresponds to the elastic region up to the yield load P_y. The first load fluctuation is no more than an artifact of the test caused by the inertial loading which results from the acceleration of the specimen from the resting position. As the load increases prior to attaining the maximum load point, P_{max}, the specimen displays plastic deformation; beyond this point, the load decay indicates controlled crack propagation.

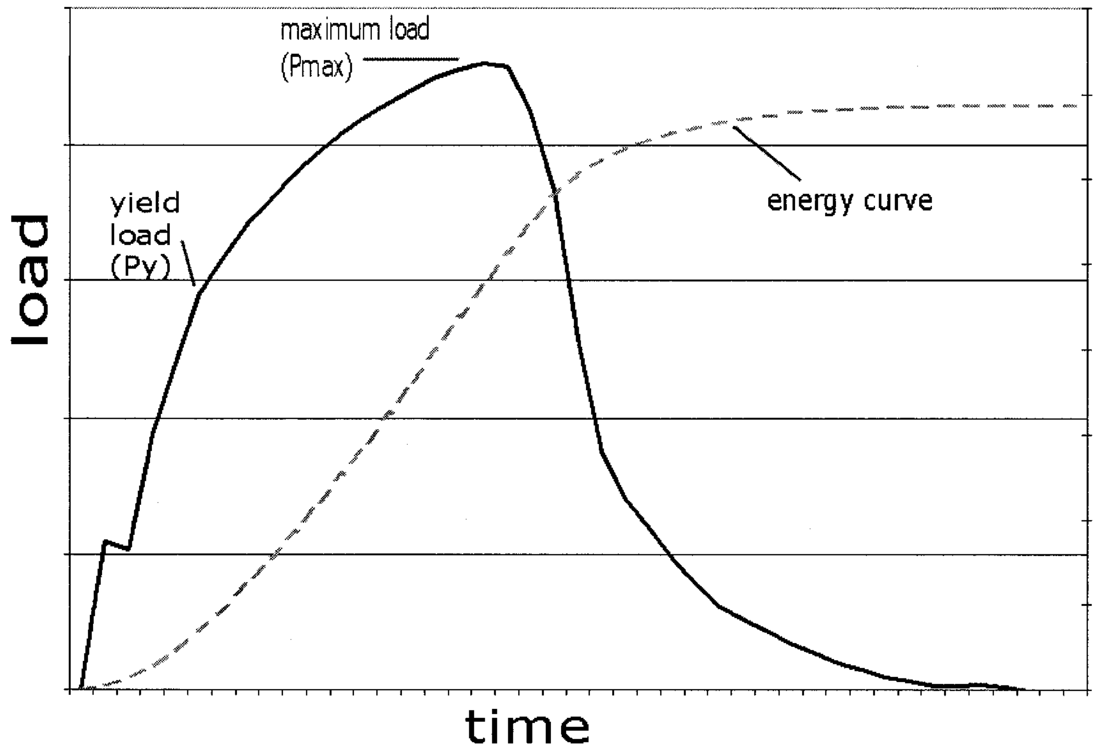

Figure 3.8 Typical impact toughness curve obtained by means of the data acquisition system.

3.4.3 Microhardness Measurements

Microhardness measurements were obtained from fractured tensile bars. Two coupons, 1 cm in length, were obtained from a cross-sectional area about 1 cm from the fracture surface of each bar. These coupons were mounted in cold mounting resin, then ground and polished as is customary for metallographic samples: (i) grinding with SiC paper #120, #320, #400, #600, #1200; (ii) polishing with 5 μm and 3 μm alumina powder and finally; (iii) polishing with 0.05 μm colloidal silica in order to obtain a flat mirror-like surface. In order to ensure a symmetrical indentation, the mounted coupons were placed in a universal clamp and levelling device when tested.

Five microhardness readings were taken for each coupon using a Vickers hardness tester brand Future Tech, model F11-7 equipped with a diamond indenter of a square-shaped base and an angle of 136° between faces. The range of loads for this tester goes from 25 gf to 10 Kgf, and the load selected here was 100 gf. The size of the indentation was measured at a magnification of 400X with a micrometer integrated to a microscope attached to the device. The measurement was then converted to a Vickers hardness value (VHN) by a microprocessor with a digital read-out display. The tester was checked for calibration by taking ten hardness readings on a standard test block before proceeding to measure the treated samples: all the values fell within the range indicated in the standard. Figure 3.9 shows a picture of the tester. For each aging condition, the average of the values obtained from four coupons is presented together with its respective standard deviation value.

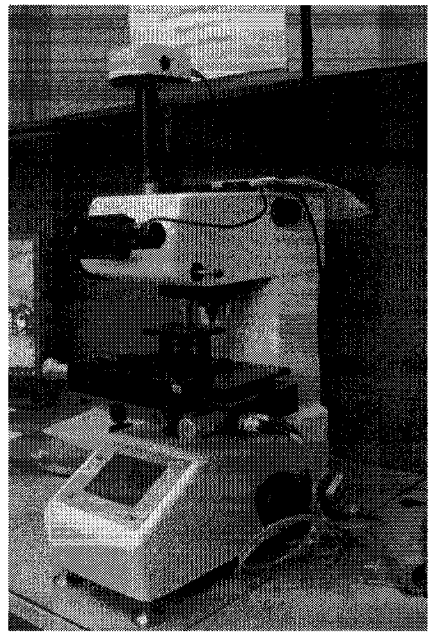

Figure 3.9 Microhardness tester used to assess the effect of aging.

3.5 Microstructural Analysis.

The surfaces of selected tensile and impact test samples were examined in order to determine the types and morphologies of the phases obtained in the as-cast condition and after the various heat treatments. The examination was carried out using optical-, scanning- and transmission electron-microscopy. Optical microscopy was used to analyze the microstructure obtained in the alloy at high magnifications ranging from 100 to 300X. Scanning electron microscopy was used to analyze the fracture surface of certain samples, while transmission electron microscopy was used to reveal and identify the very tiny precipitates that appeared in the microstructure as a result of the precipitation hardening due to aging.

3.5.1 Optical Microscopy

The samples used for analysis in an optical microscope were prepared in the same traditional way as metallographic samples are usually prepared. They were cut and mounted in cold mounting resin, then ground and polished in the same sequence as that described previously for microhardness samples, and were finally etched with Keller's reagent (95 ml H_2O, 2.5 ml HNO_3, 1.5 ml HCl and 1 ml HF) to reveal such features of interest in the microstructure as α-Al dendrites, Al-Si eutectic, Cu and Mg-containing phases, and so forth.

3.5.2 Scanning Electron Microscopy

Scanning Electron Microscopy micrographs were taken for several samples so as to characterize the fracture surface. A JEOL JSM-6360LV Scanning Electron Microscope equipped with an EDAX™ chemical analysis system was used for this purpose. The accelerating voltage for imaging was 15 keV, the emission current 60 µA, and the beam diameter of less than 0.5 µm. Figure 3.10 shows a picture of this type of microscope.

The samples used for chemical analyses were the same ones as those which provided the coupons for the microhardness assessment. The samples were cleaned with high-purity ethanol in an ultrasonic agitator to prevent dirt or any other particles to interfere with the image acquisition process. The surface of fractured tensile specimens is not suitable for chemical analyses in an SEM due to the irregularities that are present; therefore, certain microhardness samples were used. These samples were coated with gold to render the surface conductive and appropriate for use in an SEM.

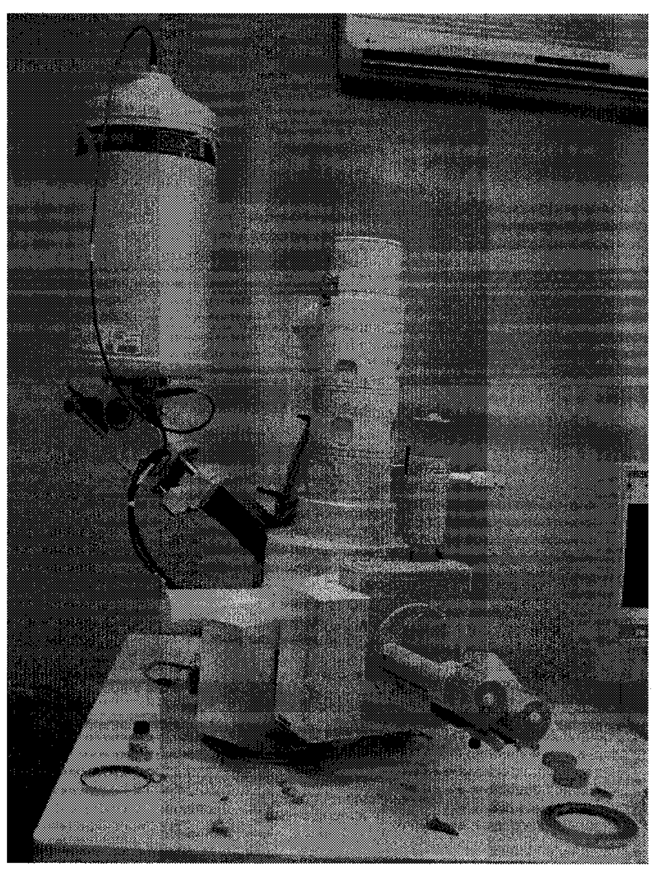

Figure 3.10 JEOL JSM-6360LV scanning electron microscope used for this work.

3.5.3 Transmission Electron Microscopy

Transmission Electron Microscopy was used to identify the precipitates on a very small scale, using a JEOL™ JEM-2100F Field Emission Electron Microscope equipped with an advanced control system which permits the integration of an EDAX™ chemical analysis system, STEM, and EELS. The microscope was operated at an acceleration voltage of 200 keV. Figure 3.11 shows a picture of this type of microscope.

The specimens for Transmission Electron Microscopy were prepared by cutting very thin sections (about 1 mm thick) from the bulk samples using a high precision diamond disk cutter at low speeds to avoid deformation from the cutting process. These thin sections were then ground to a thickness of approximately 100 μm, while small disks (3 mm diameter) were obtained with a puncher. The small disks were then transferred to a Struers™ Tenupol 3 jet polishing cell for further thinning. The etchant used was a solution of 30% Nitric Acid, and 70% Methanol and the temperature was maintained at -25°C. The optimum operating conditions used to obtain a specimen suitable for observation were a voltage of 3.5 V and a current of 0.5 A. Figure 3.12 shows a picture of the jet polishing cell setup.

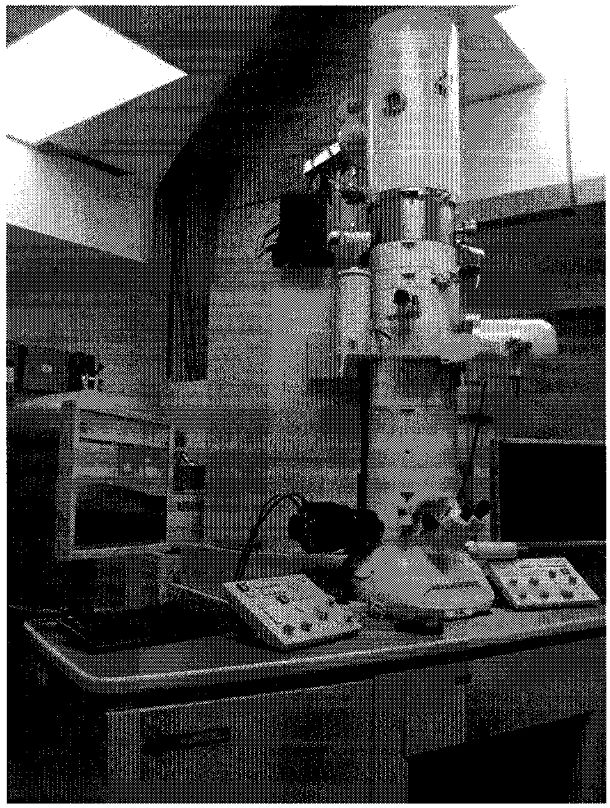

Figure 3.11 JEOL™ JEM-2100F Field Emission Electron Microscope.

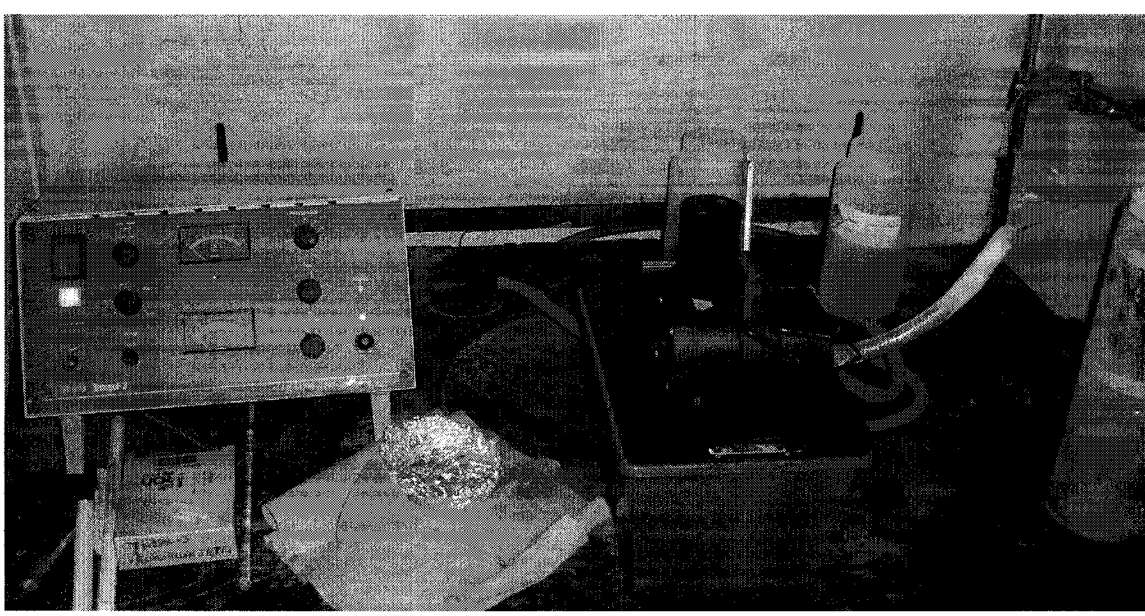

Figure 3.12 Struers™ Tenupol 3 jet polishing cell

Chapter 4

Results and Discussion

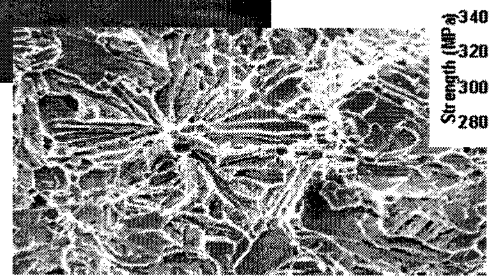

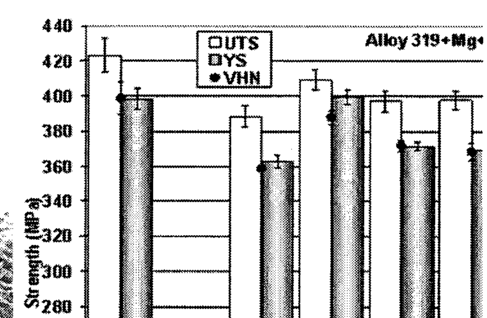

This chapter will present the results that were obtained by carrying out the tests described in the chapter on Experimental Procedures. As one of the main objectives of this thesis was to investigate the effects of several artificial aging treatments, the mechanical properties, as obtained, will be divided according to the aging treatment applied. This will be followed by a detailed analysis of the effects of these aging cycles on the precipitation process resulting from each treatment type, as monitored by scanning and transmission electron microscopy.

4.1 Mechanical Properties Obtained after Continuous Aging Treatment

The four 319 alloy types used, namely the 319 base alloy, 319+Sr, 319+Mg and 319+Mg+Sr alloys were subjected to conventional (or continuous) aging cycles. The data obtained from these experiments will serve as a baseline to compare the response of the alloys to the non-conventional treatments such as the multi-temperature and interrupted aging cycles used in this study.

The graphs presented in the following sections represent the average values of tensile properties and microhardness obtained from the different treatments for each alloy. The error bars shown in each graph represent the scatter in data obtained over five tensile/impact bars tested for each sample condition.

4.1.1 Alloy 319 (Base Alloy)

Figure 4.1 shows the ultimate tensile strength (UTS) and yield strength (YS), as well as the Vickers microhardness values obtained for the base alloy.

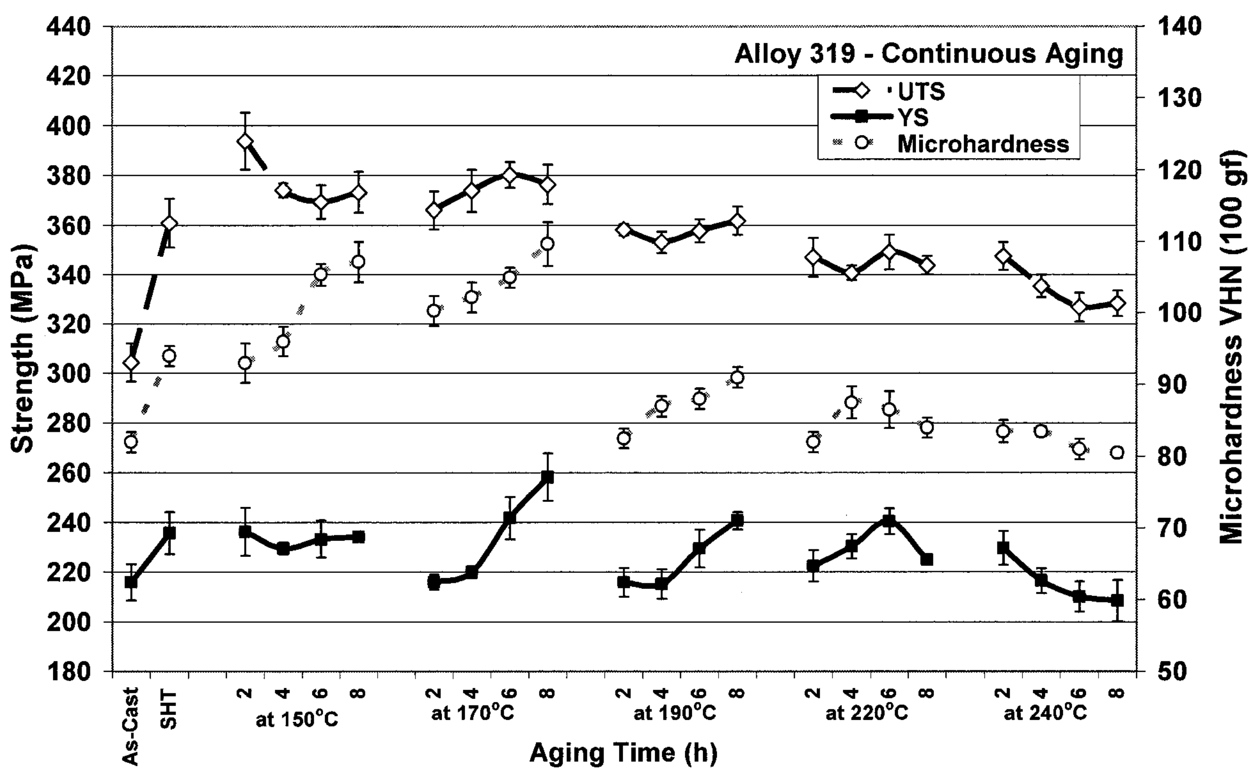

Figure 4.1 Average values of ultimate tensile strength (UTS), yield strength (YS), and microhardness (VHN) obtained for the 319 base alloy under different heat treatment conditions (using continuous aging cycles).

The X-axis represents the treatment or condition in which the samples were tested, covering the as-cast, solution heat-treated, and artificially aged conditions (at 150°C, 170°C, 190°C, 220°C and 240°C for 2, 4, 6 and 8 h), respectively. The primary Y-axis represents the strength values (UTS, YS), while the secondary Y-axis represents the Vickers microhardness values obtained for each condition.

From Figure 4.1, it will be observed that there is an initial improvement in all the properties after solution heat treatment and quenching, commonly known as the T4 condition, and labelled SHT in the graph. This improvement is to be expected since the solution heat treatment homogenizes the casting, fragments and partially spheroidizes the eutectic-silicon particles, and dissolves the intermetallic phases into the α-Al matrix, thereby strengthening it [4, 65, 66, 76, 133]. All of these features may be observed in Figure 4.2 which shows the difference in the microstructure of the (a) as-cast, and (b) solution heat-treated samples. It is interesting to observe the difference in the morphology of the silicon phase and the reduction in the amount of undissolved intermetallics in the latter case.

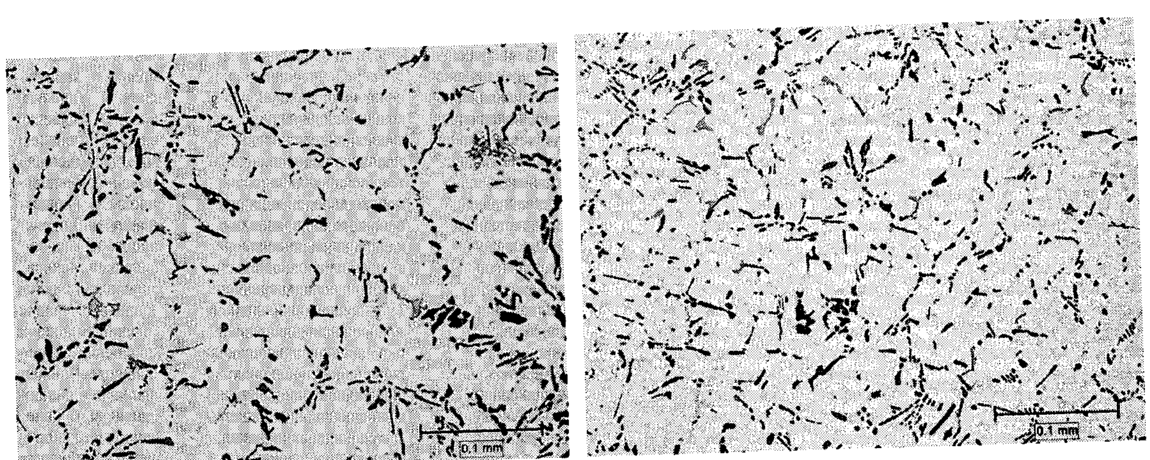

(a) (b)

Figure 4.2 Optical micrographs showing the microstructures of the (a) as-cast, and (b) solution heat-treated base alloy 319.

After solution heat treatment, artificial aging is carried out at 150°C. The ultimate tensile strength shows a maximum of strength after 2 h of aging at this temperature; as aging time is increased, however, the values are close to those obtained after solution heat treatment. Ultimate tensile strength values obtained at higher aging temperatures, i.e. 170°C and 190°C, are similar to those of the solution heat-treated condition, where aging at 170°C for long times, i.e. 6 and 8h, shows a slight peak in tensile strength. At the highest aging temperatures, 220°C and 240°C, a decrease in ultimate tensile strength is observed with increased aging time.

Yield strength values tend to be more responsive to artificial aging since this property is less influenced by the soundness of the casting than ultimate tensile strength and more influenced by the microstructural condition of the alloy [5, 19, 83]. Artificial aging at 150°C does not show an appreciable improvement in yield strength; however, when the aging temperature is increased to 170°C a clear increase in YS is observed over time. The same behavior is observed at 190°C although the attained values are not as high as those obtained by aging at 170°C. At 220°C a decrease in yield strength, characteristic of overaging behavior may be noted after aging for 6 h, while at 240°C overaging occurs with increasing aging time.

The tensile strength values reflect the condition of the bulk casting (tensile test bars in this case), since casting defects such as inclusions and pores may affect the values obtained during testing [66, 122, 125]. Microhardness, in turn, reflects the condition of the α-Al matrix, since the test is carried out only in the matrix, on a very small area of the bulk specimen. In Figure 4.1, an increase in the properties is observed with increasing time when aging is carried out at 150°C and 170°C, peak hardness being observed after aging at 170°C for 8 h. When the aging is carried out at 190°C, a drop in the microhardness followed by a slow recovery is observed with increasing aging time, indicating that the strengthening effect due to the artificial aging had already been reached at lower aging temperatures. The hardness values show a decrease over time, as expected, when the artificial aging temperature is increased to 220°C and 240°C.

The standard T6 heat treatment specifies that artificial aging for the 319 alloy should be carried out at 155°C for 2 to 5 hours [9, 19, 58]. From the results shown in Figure 4.1, however, it will be observed that the best combination of properties, i.e. high tensile strength and microhardness, is achieved when aging is carried out at 170°C for 8 h. This condition will thus be considered to represent the best T6 treatment for the base alloy. The corresponding tensile properties are 376 MPa for UTS, 258 MPa for YS, and 110 VHN for the microhardness.

The T7 treatment, representing the overaged condition, is sometimes preferred when heat treating aluminum castings. This treatment usually involves artificial aging at a high temperature, i.e. 240°C, to achieve an overaged condition where the castings are dimensionally stable, however, at the expense of strength and ductility [119, 120]. From Figure 4.1 it will be observed that aging for 2 h at 240°C yields the best combination of properties for the T7 treatment. The corresponding strength and microhardness values are 348 MPa UTS, 230 MPa YS, and 83.5 VHN, respectively.

Figure 4.3 shows the variation in elongation and total absorbed impact energy values for 319 base alloy, obtained after continuous aging over the same range of aging temperatures, 150°C to 240°C, and times. The primary Y-axis represents percentage elongation and the secondary Y-axis represents the total absorbed impact energy in Joules.

As can be seen, the elongation and impact toughness values also improve on going from the as-cast state to the solution heat-treated (T4) condition. Peak values for both properties are attained when artificial aging is carried out at 150°C for 4 h, after which the values tend to decrease over time. The improvement in the impact toughness values and in the elongation values may be explained by the even distribution of microconstituents and their dissolution in the aluminum matrix achieved through the solution heat treatment/quenching step [123, 124, 134]. Also, the fragmentation, dissolution and spheroidization processes taking place during solution heat treatment reduce the amount of acicular particles such as eutectic Si and Fe-containing phases initially existing in the as-cast sample, as well as the amount of undissolved Cu-containing phases. These phases are hard particles that play a key role in the fracture propagation process and may act as crack initiation sites [44, 64, 65, 76, 124].

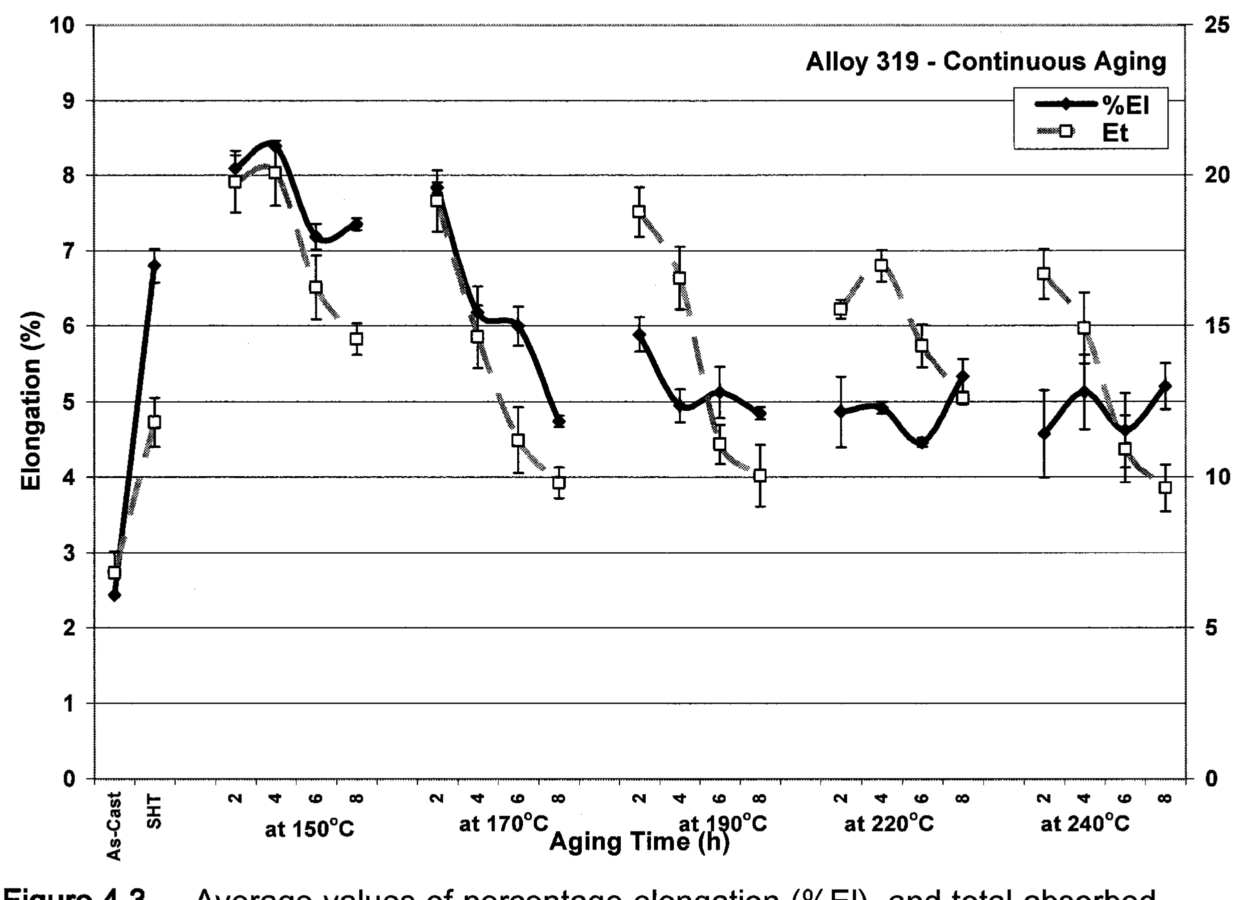

Figure 4.3 Average values of percentage elongation (%El), and total absorbed impact energy (E_t) obtained for the 319 base alloy under different heat treatment conditions (using continuous aging cycles).

Figure 4.3 also shows that when artificial aging is carried out at 170°C, both properties decrease with increasing aging time. The same behavior may be observed for the aging cycles at 190°C, but the decrease is more marked for the impact toughness. Such a decrease is expected since it is in these aging cycles that the highest strength and microhardness values are obtained. At higher artificial aging temperatures, i.e. 220°C and 240°C, impact toughness values again decrease with time. Elongation, however, shows a slight recovery at long aging times, i.e. 8 h at 220°C. There is a good correlation between the elongation and impact toughness values, since both properties show similar tendencies when subjected to artificial aging; however, tensile and impact tests are essentially different because of the strain rate at which the material is tested. This difference explains why both properties are not affected by artificial aging in the exact same way. The corresponding values of elongation and total absorbed impact energy for the best T6 treatment, 8 h at 170°C, are 4.74% and 9.82 J, respectively. The corresponding values for the best T7 treatment, 2 h at 240°C, are an elongation of 4.57% and 16.72 J of total absorbed impact energy.

4.1.2 Alloy 319 + Sr (Sr-Modified Alloy)

Figure 4.4 shows the ultimate tensile strength and yield strength, as well as the Vickers microhardness values obtained for the Sr-modified 319 alloy. The same behavior as in the 319 base alloy is observed after solution heat treatment: there is an increase in all the properties in comparison with the as-cast condition. The maximum tensile strength is observed after artificial aging at 150°C for 2 h; thereafter the UTS values obtained decrease over time. The values of UTS at higher temperatures, i.e. 170°C and 190°C, are close to those obtained after solution heat treatment, indicating that artificial aging has little effect on this property of the Sr-modified 319 alloy.

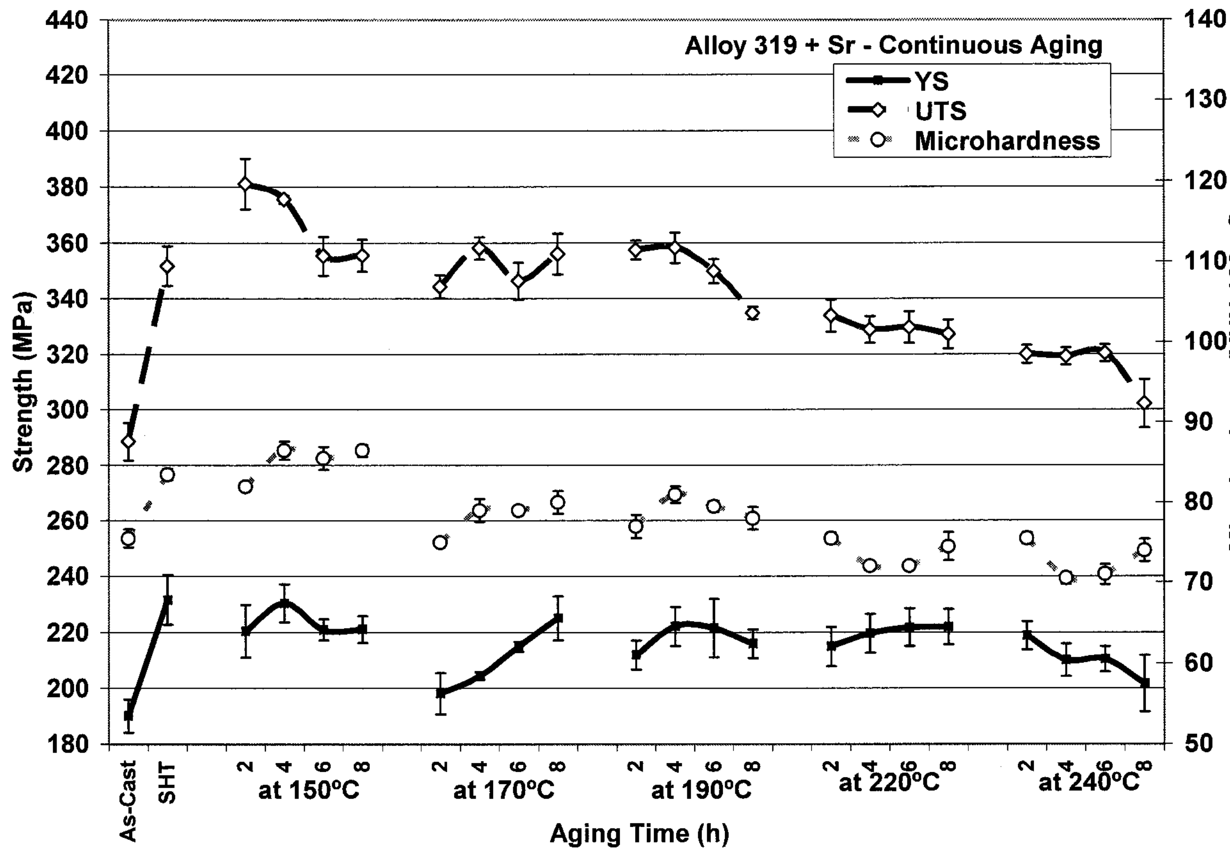

Figure 4.4 Average values of ultimate tensile strength (UTS), yield strength (YS), and microhardness (VHN) obtained for the 319+Sr alloy under different heat treatment conditions (using continuous aging cycles).

The yield strength values reach a peak after solution heat-treatment or after aging at 150°C for 4 h. Aging at 170°C shows a slow improvement over aging time, whereas aging at higher aging temperatures, such as 190°C and 220°C, shows almost no change over the aging times studied. The overaging occurs when aging is carried out at 240°C.

The microhardness behavior is very similar to that of yield strength, where the highest value is achieved after aging at 150°C for 4 h, and increasing the aging temperature further only decreases the values which may be obtained. The best combination of properties for the T6 treatment are found after aging at 150°C for 4 h, the corresponding values being 376 MPa UTS, 230 MPa YS, and 86.5 VHN for microhardness. With respect to the T7 treatment, the best combination of properties is found after aging at 240°C for 2 h, and the corresponding strength and microhardness values are 320 MPa UTS, 219 MPa YS, and 75.5 VHN, respectively.

Figure 4.5 shows the variation in elongation and total absorbed impact energy values for the Sr-modified 319 alloy when subjected to continuous aging cycles over the same range of aging temperatures and times. It will be observed that the values are higher in this case compared to those exhibited by the base alloy. This is to be expected, since these properties depend to a high degree on the morphology and distribution of the brittle Si, Fe and Cu phases mentioned previously, which are responsible for the fracture in this type of alloy [46, 135]. Thus, modifying the eutectic silicon phase is expected to improve the ductility and impact toughness of the alloy as evidenced by Figure 4.5.

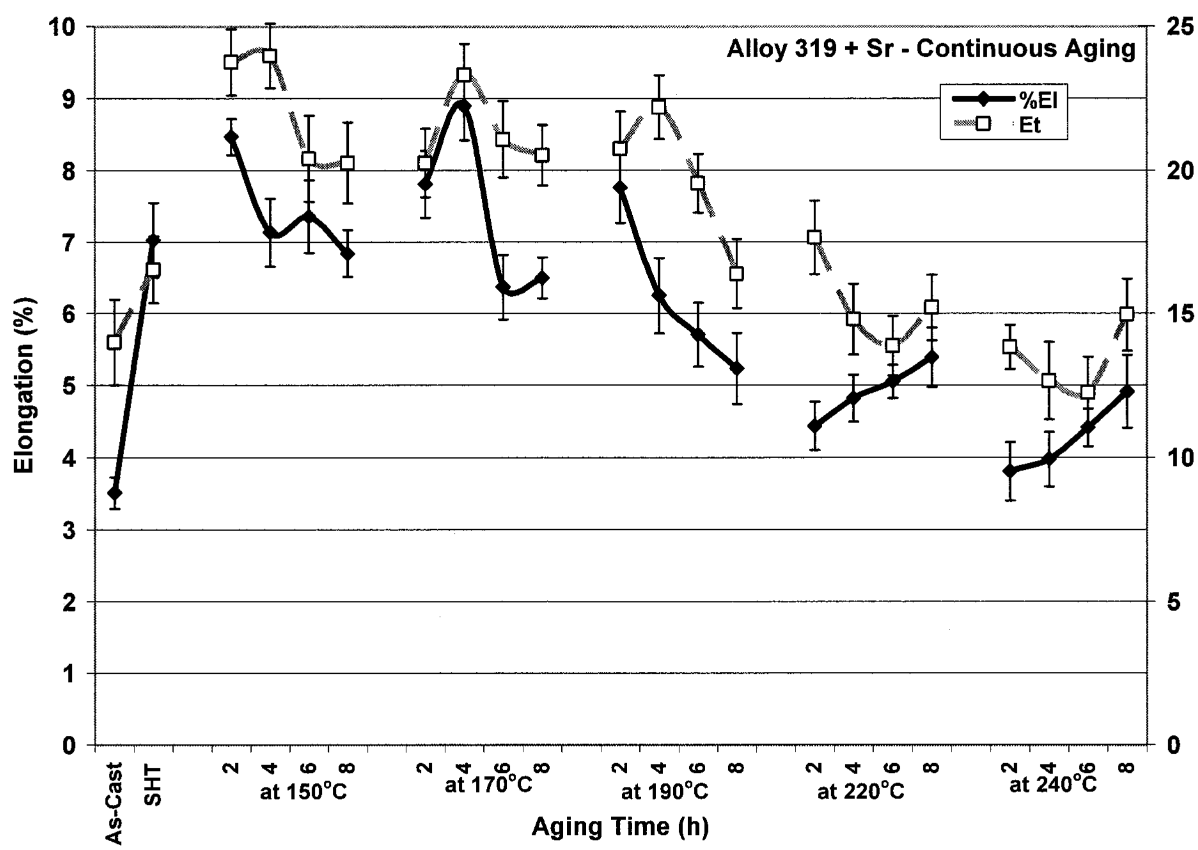

Figure 4.5 Average values of percentage elongation (%El), and total absorbed impact energy (E_t) obtained for the 319+Sr alloy under different heat treatment conditions (using continuous aging cycles).

From the initial improvement in elongation and absorbed energy values after solution heat treatment, a peak may be seen after aging at 150°C for 2 h. It is for this aging cycle that the highest impact toughness is observed. Increasing the aging time at the same temperature is seen to decrease the value obtained. Aging at 170°C shows an improvement in toughness for the first 4 h, where the peak is observed, thereafter the values decrease over time. The same behavior, i.e. decrease in elongation and impact energy over time, is observed when aging is carried out at 190°C. At higher aging temperatures, i.e. 220°C and 240°C, a slow recovery in elongation and toughness is observed when aging is carried out for long periods, such as 6 h and 8 h.

The corresponding values of elongation and total absorbed impact energy for the best T6 treatment, 4 h at 150°C, are 7.13% and 24 J, respectively. Those for the best T7 treatment, 2 h at 240°C, are 3.81% and 13.83 J, respectively.

4.1.3 Alloy 319 + Mg (Magnesium-Containing Base Alloy)

Figure 4.6 shows the variation in ultimate tensile strength, yield strength, and Vickers microhardness values obtained for the 319+Mg alloy. The addition of Mg greatly enhances the artificial aging response of the alloy, as evidenced by the properties presented in Figure 4.6. It is interesting to note the improvement in strength and microhardness that can be achieved in this alloy compared to the 319 base and Sr-modified alloys. Significant increases in the three properties presented in the graph may be observed, and there is excellent correspondence between the yield strength and the microhardness results.

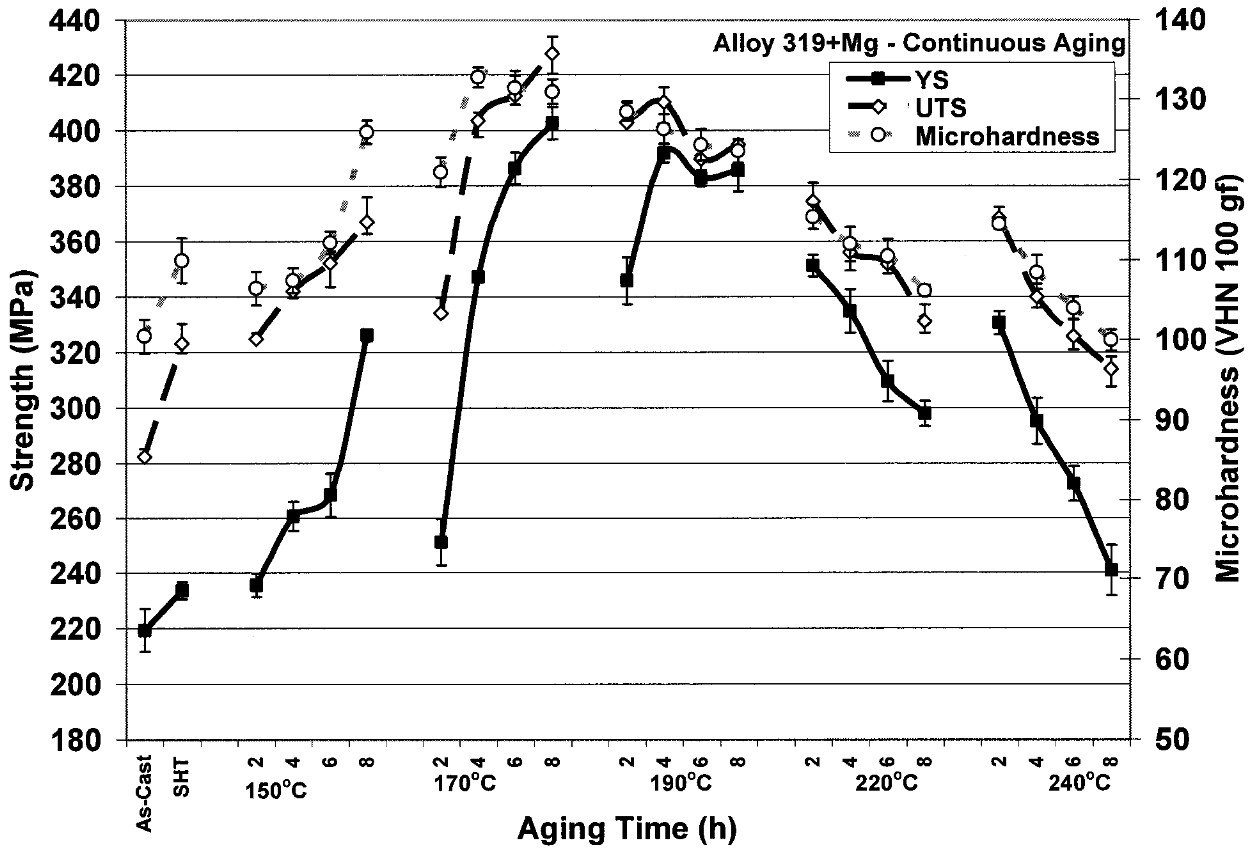

Figure 4.6 Average values of ultimate tensile strength (UTS), yield strength (YS), and microhardness (VHN) obtained for the 319+Mg alloy under different heat treatment conditions (using continuous aging cycles).

Following the initial increase in properties from the as-cast to the solution heat-treated (T5) condition, aging at 150°C and 170°C further increases these values over the range of times studied. Strength and hardness peaks are achieved after aging at 170°C for 8 h. At 190°C aging temperature, an improvement in UTS and YS is observed up to 4 h, after which no further improvement is observed at increased aging times; in fact, a slight decrease in the strength may be observed. Regarding microhardness, the values decrease slightly. At the higher aging temperatures, i.e. 220°C and 240°C, overaging is observed, as characterized by the loss of strength and hardness over time.

The best combination of properties is achieved after aging at 170°C for 8 h and the corresponding properties observed are 428 MPa UTS, 403 MPa YS, and 131 VHN for the microhardness. This condition may therefore be considered as the appropriate T6 treatment for the 319+Mg alloy. The best properties in the T7 (overaged) condition is achieved after aging at 240°C for 2 h where the corresponding properties are 368 MPa UTS, 331 MPa YS, and 114 VHN.

Figure 4.7 shows the variation in percentage elongation and total absorbed impact energy values obtained for the 319+Mg alloy after continuous aging over the range of temperatures studied. From a comparison of Figure 4.7 with Figures 4.3 and 4.5, it is evident that these values tend to be lower than those exhibited by the base 319 and Sr-modified alloys [14, 62]. While addition of Mg increases the strength and hardness of the alloy, it does so at the expense of ductility [19, 57, 126, 136].

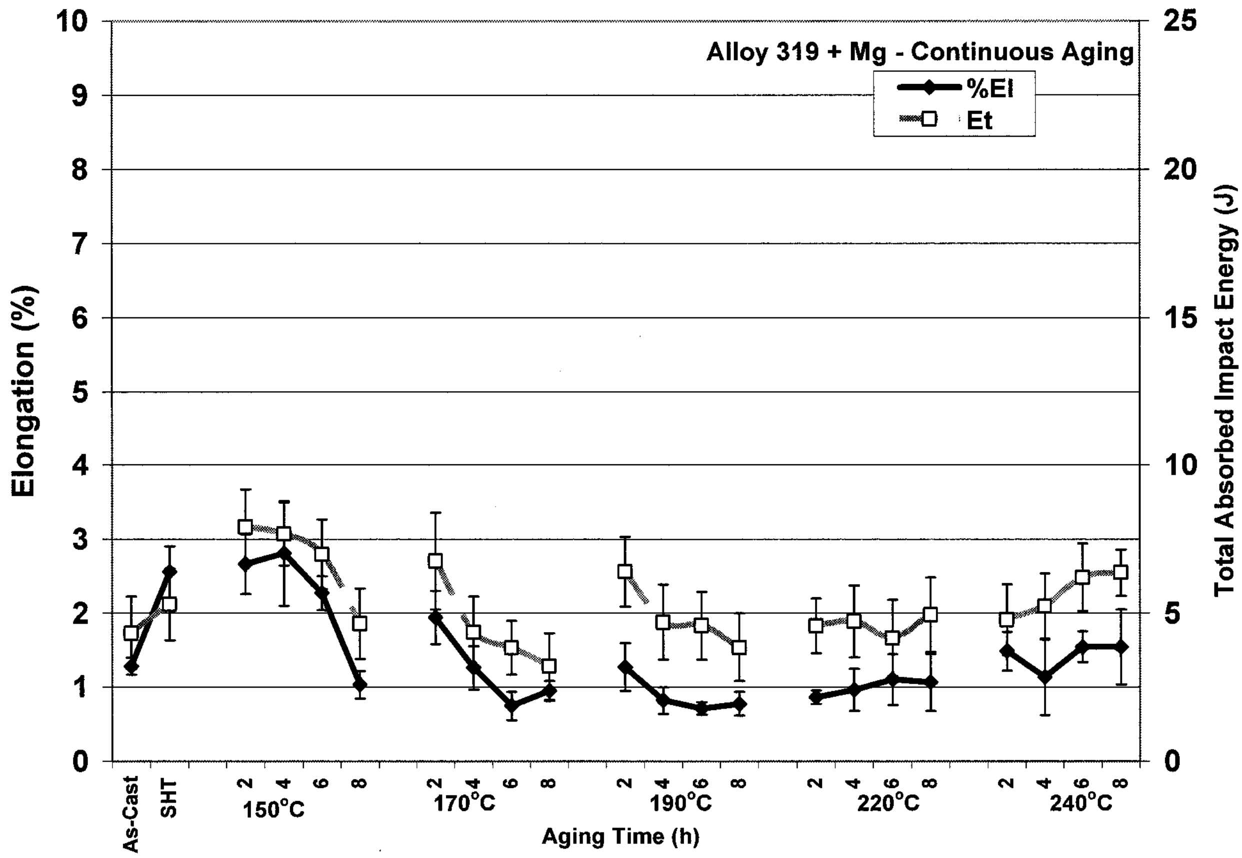

Figure 4.7 Average values of percentage elongation (%El), and total absorbed impact energy (E_t) obtained for the 319+Mg alloy under different heat treatment conditions (using continuous aging cycles).

Starting from the as-cast condition, an improvement in properties is obtained with the T5 treatment (solution heat treatment). Additional aging at 150°C improves the values still further up to an aging time of 4 h; beyond this point the values begin to decrease. The same tendency is observed when aging at 170°C over the same range of times. At 190°C aging temperature and after 2 h of aging, the elongation achieved is the same as that observed in the as-cast condition. Increasing the aging time to 4 h slightly reduces the elongation which thereafter remains more or less stable for longer aging times. A similar behavior may also be observed at 220°C, since the values remain unchanged over the aging time. Finally, at 240°C, a slight recovery can be observed for both the percent elongation and the absorbed impact energy. The corresponding values of elongation and total absorbed impact energy for the best T6 treatment, i.e. 8 h at 170°C, are 0.95% and 3.21 J, respectively. The corresponding values for the best T7 treatment, i.e. 2 h at 240°C, are 1.49% and 4.79 J.

4.1.4 Alloy 319 + Mg + Sr (Mg-Containing Sr-Modified Alloy)

Figure 4.8 shows the variation in ultimate tensile strength, yield strength, and Vickers microhardness values obtained for the Sr-modified 319+Mg alloy. In comparison with the 319+Mg alloy, the properties obtained are slightly lower, although, the behavior and the tendencies are similar. An initial increase in the values is achieved after solution heat treatment, mainly for the microhardness and ultimate tensile strength.

Aging at 150°C does not show any substantial improvements in the strength values while microhardness starts increasing after aging for 6 h or 8 h. The best aging response is obtained after aging at 170°C, where the values increase over the range of aging times studied, with peak aging being observed after 8 h. Accordingly, this may be considered as the best combination of properties for the

T6 treatment for the 319+Mg+Sr alloy, and the corresponding values are 423 MPa UTS, 398 MPa YS, and 134 VHN for microhardness. Overaging begins to occur at 190°C, and a decrease in properties is observed. The same tendency is observed at the higher temperatures of 220°C and 240°C. The best combination of properties for the T7 (overaged) condition at 240°C is found after aging for 2 h, the corresponding properties being 355 MPa UTS, 306 MPa YS, and 95 VHN.

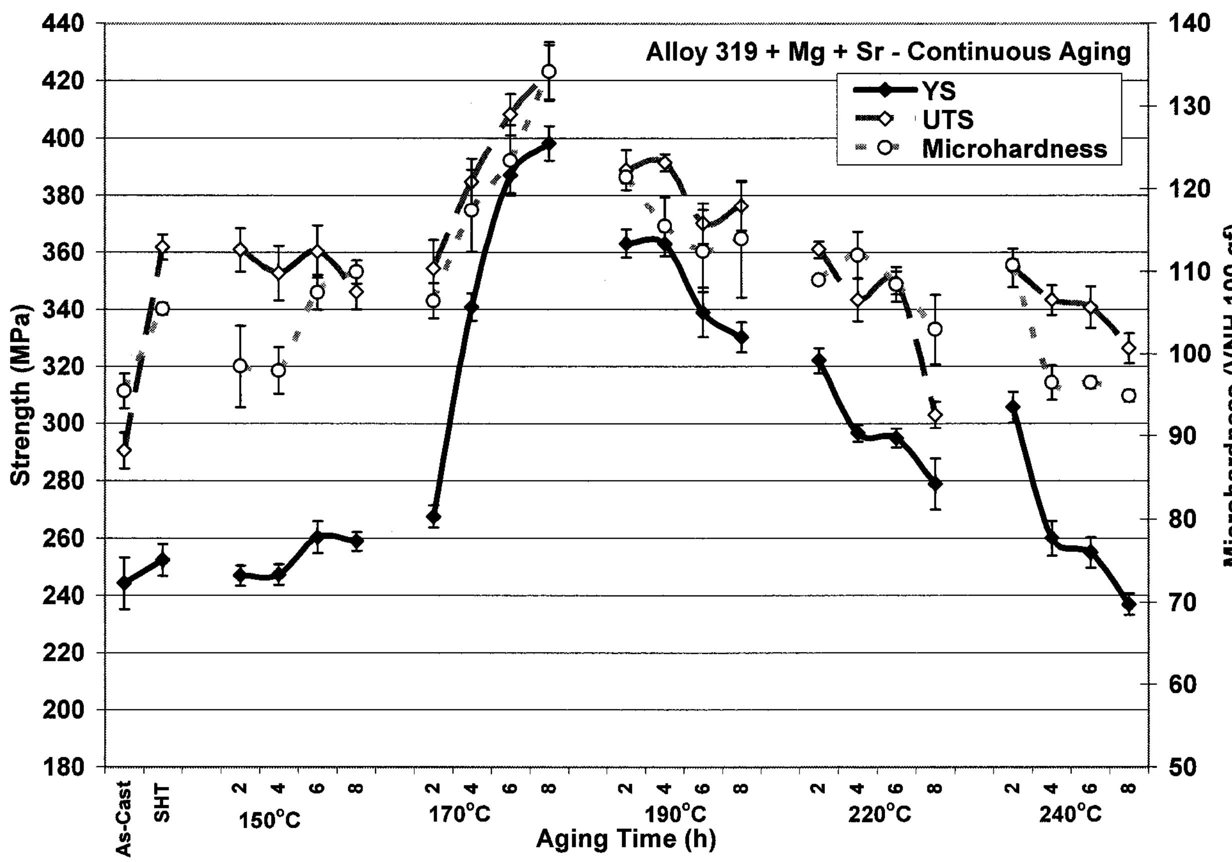

Figure 4.8 Average values of ultimate tensile strength (UTS), yield strength (YS), and microhardness (VHN) obtained for the 319+Mg+Sr alloy under different heat treatment conditions (using continuous aging cycles).

Figure 4.9 shows the variation in elongation and total absorbed impact energy values for the Sr-modified 319+Mg alloy obtained after continuous aging over the range of temperatures and times studied. In comparison with the unmodified 319+Mg alloy, the modified alloy (319+Mg+Sr) shows higher ductility and absorbed impact energy values, as expected [14, 15, 62].

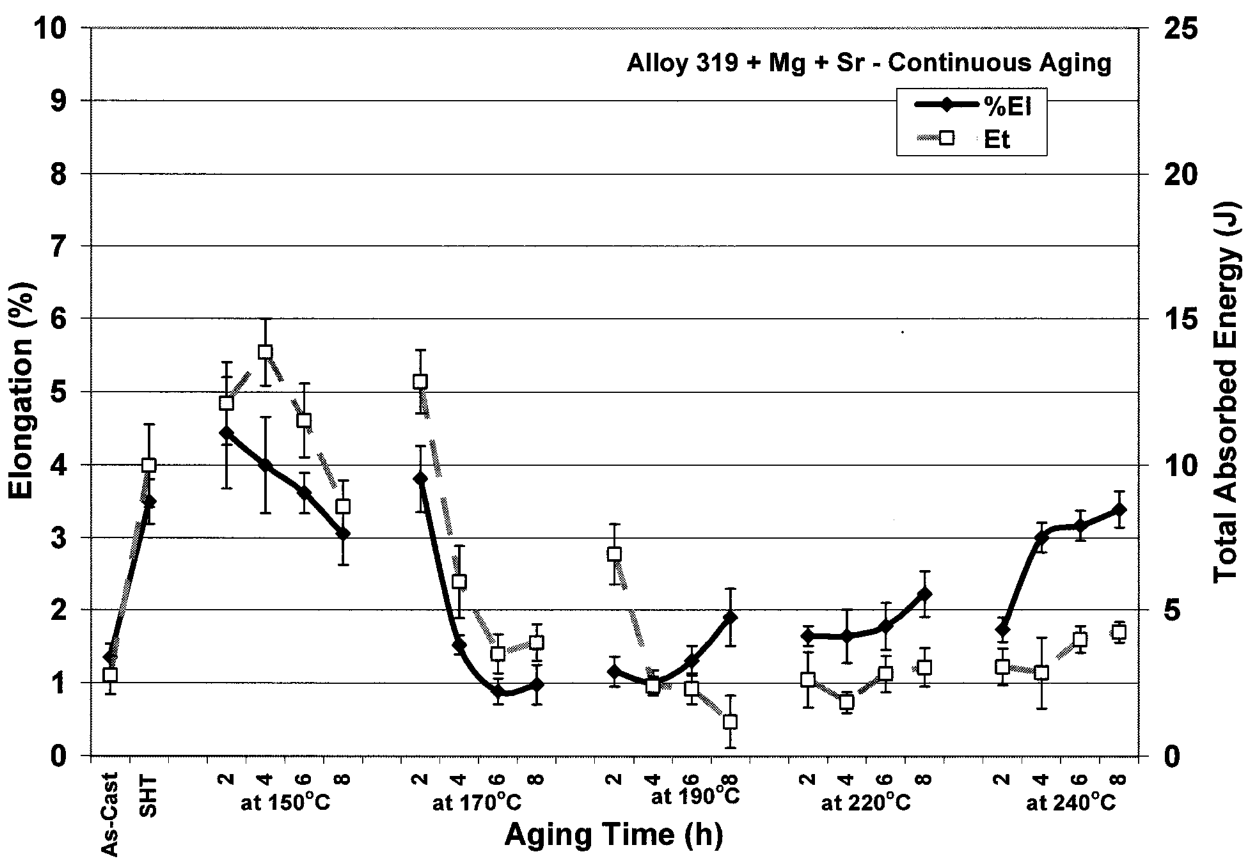

Figure 4.9 Average values of percentage elongation (%El), and total absorbed impact energy (E_t) obtained for the 319+Mg+Sr alloy under different heat treatment conditions (using continuous aging cycles).

Due to the presence of Mg, both alloys exhibit the same response to aging: an increase in properties is initially observed on going from the as-cast to the solution heat-treated condition. Aging at 150°C and 170°C, however, shows a loss in properties over the aging times studied. The highest strength and microhardness values are observed after aging at 170°C for 8 h, which represents the best T6 treatment in this case. The elongation and impact absorbed energy values are 0.98% and 3.21 J, respectively.

Aging at 190°C produces an increase in elongation values when aging is carried out for longer times, i.e. 6 h and 8 h, whereas the absorbed impact energy values continue to decrease over time to reach a minimum after 8 h of aging at this same temperature. At higher aging temperatures, i.e. 220°C and 240°C, the properties improve with increasing aging time. The T7 condition for this alloy, i.e. 2 h at 240°C, yields an elongation of 1.73% and 3.06 J for the total absorbed impact energy.

The results for the tensile strength and microhardness values obtained for the four 319-type alloys under the different heat treatment/continuous aging conditions are summarized together in Figure 4.10 to facilitate comparison. The various codes entered along the X-axis in the figure represent the alloy type and heat treatment condition in each case, as listed in Table 4.1.

With respect to the following table, it should be mentioned that for the T7 treatment, the aging temperature and time were the same for all the alloys, i.e. 240°C for 2h, whereas in the case of the T6 treatment the conditions differed, depending upon the alloy, namely 170°C/8 h for all alloys except for the 319+Sr alloy (3S), where the best T6 condition corresponded to 150°C/4 h.

Table 4.1 Alloy and heat treatment codes used in Figure 4.10.

Alloy	Alloy Code	Heat Treatment/Condition	Code
Base 319	3	As-cast	F
319+Sr	3S	SHT + quenched	T4
319+Mg	3M	SHT + quenched + aging*	T6
319+Mg+Sr	3MS	SHT + quenched + aging (240°C)	T7

*artificially aged to the highest achievable strength

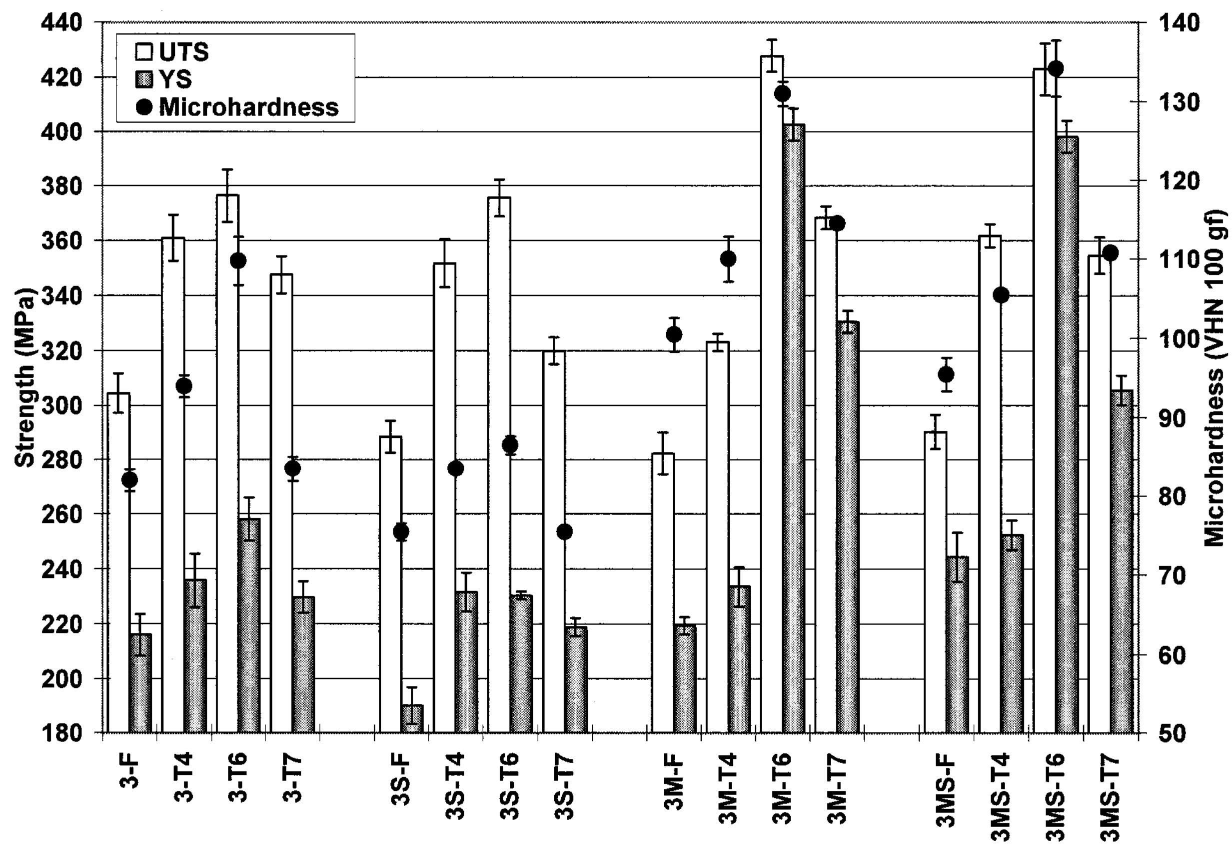

Figure 4.10 Summary of the average values of ultimate tensile strength (UTS), yield strength (YS), percentage elongation (%El), total absorbed impact energy (E_t), and microhardness (VHN) obtained for the four alloys under different heat treatment conditions (using continuous aging cycles).

4.2 Mechanical Properties Obtained after Multi-Temperature Aging Treatments

The T6 treatment is usually preferred when heat treating 319 alloy castings. This treatment has the advantage of producing the highest strength achievable with, however, a corresponding reduction in ductility [5, 19, 58, 137]. In some cases the T7 treatment is considered a better alternative. This treatment consists in artificially overaging the alloy at high temperatures in the range of 200°C –

240°C. Among the advantages of overaging is the reduction of residual stresses, increased performance, as well as stabilization of the alloy, particularly in applications which involve exposure of the casting to elevated temperatures and thermal fatigue [119, 120]. In this study, the multi-temperature aging cycles investigated may be divided in two categories similar to the T6 and T7 treatments, i.e. aging at lower temperatures (150°C – 190°C) and aging at higher temperatures (220 – 240°C), respectively. The results are presented in the following sections, accordingly.

4.2.1 T6-Type Multi-Temperature Aging Treatments

Table 4.2 shows the details of the T6-type multi-temperature aging cycles that were used and their respective codes. These same codes have been used in all the figures presented in this section. The temperatures for these cycles was selected based on those continuous aging treatments which provided optimum properties, the objective being to seek further possible improvement in these properties through the use of multi-temperature aging treatments.

Table 4.2: T6-Type Multi-Temperature Aging Cycles.

A – 2 h at 150°C and 1 h at 180°C	E – 2 h at 190°C and 1 h at 180°C
B – 2 h at 150°C and 3 h at 180°C	F – 2 h at 190°C and 3 h at 180°C
C – 2 h at 150°C and 5 h at 180°C	G – 2 h at 190°C and 5 h at 180°C
D – 2 h at 150°C and 10 h at 180°C	H – 2 h at 190°C and 10 h at 180°C

4.2.1.1 Alloy 319 (Base Alloy)

Figure 4.11 compares the tensile strength and microhardness values obtained with the T6 continuous aging treatment (8 h @ 170°C) with those obtained from the T6-type multi-temperature treatments (A through H). As mentioned previously, the error bars shown in this and subsequent figures represent the scatter in data obtained over five samples tested for each condition (treatment).

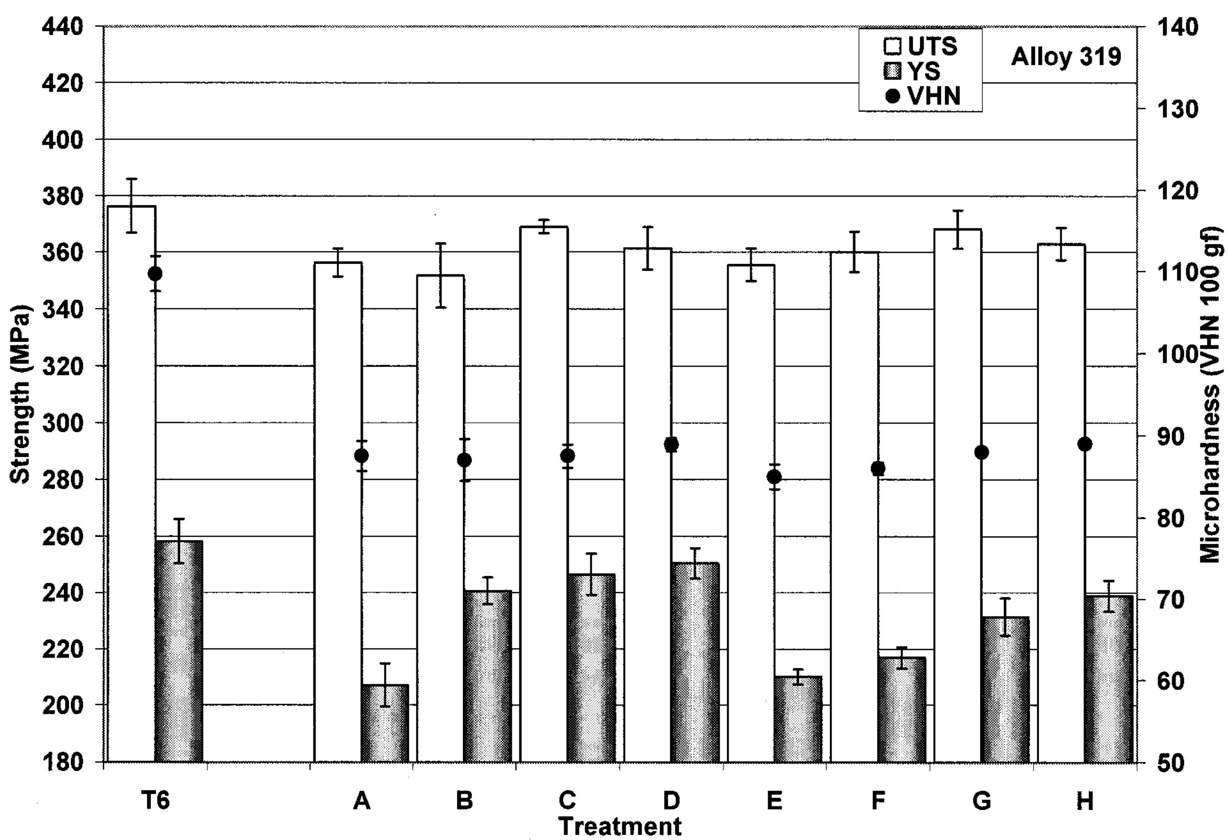

Figure 4.11 Average values of ultimate tensile strength (UTS), yield strength (YS), and microhardness (VHN) obtained for the 319 base alloy after T6 continuous aging and T6-type multi-temperature aging treatments.

From Figure 4.11 it will be observed that none of the multi-temperature treatments are beneficial, since the T6 continuous aging treatment yields higher strength and microhardness values. It is noticeable however, that the yield strength tends to increase slightly when aging time is increased as evidenced by treatments A, B, C and D; the same behavior may be noticed in the remainder of the multi-temperature aging treatments although this is not beneficial on the whole, when compared to the values obtained from the T6 treatment. The microhardness does not seem to be affected by the multi-temperature treatments, and the values obtained are all lower than that obtained from the T6 treatment. Therefore, the T6 continuous aging treatment is best suited for obtaining maximum strength and microhardness.

Figure 4.12 shows a comparison of elongation and impact toughness values obtained from the T6 continuous aging, and the multi-temperature aging treatments. In this case, the properties are slightly improved after the multi-temperature treatments. This is to be expected since the corresponding strength values are lower compared to that shown by the T6-treated sample(s). Although the impact toughness or elongation values are higher in the multi-temperature cycles than those observed for the T6 treatment, the reduction in tensile strength or microhardness is more significant, thus indicating that T6 treatment is the better choice.

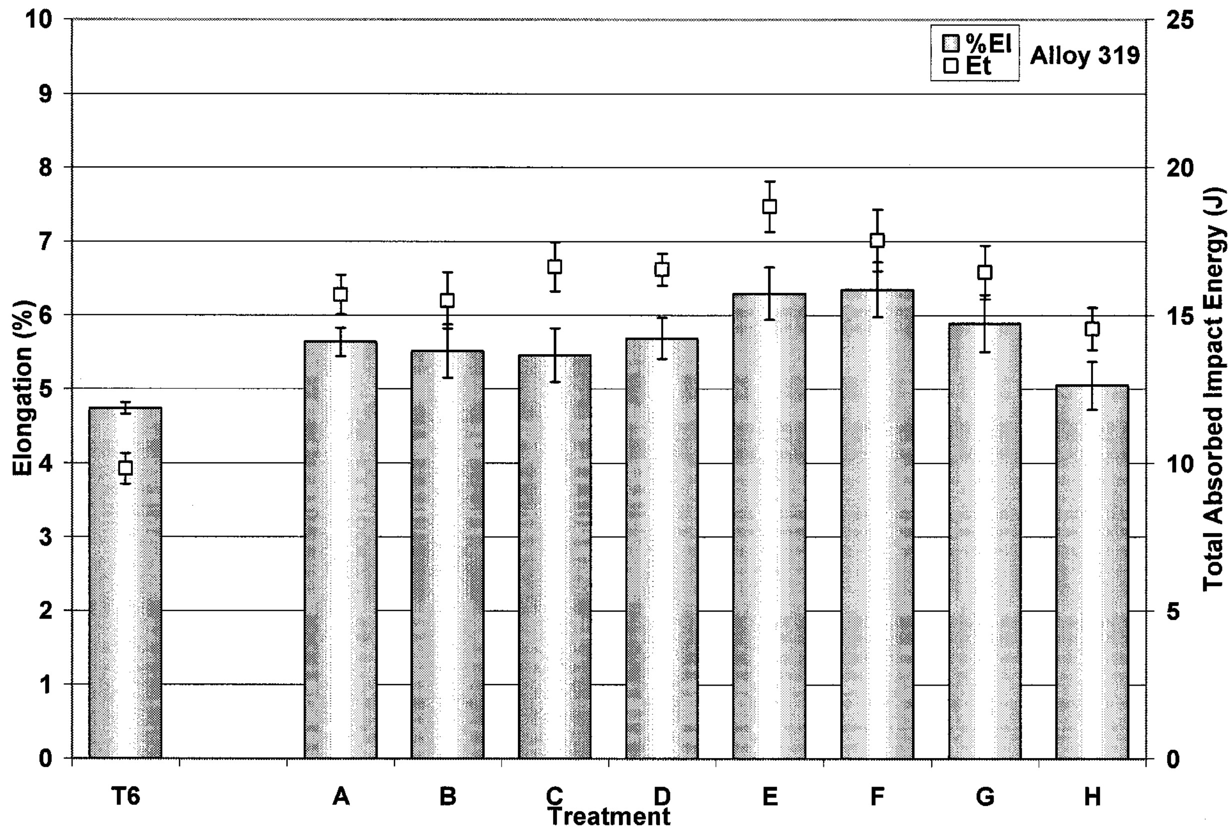

Figure 4.12 Average values of percentage elongation (%El), and total absorbed impact energy (E_t) obtained for the 319 base alloy after T6 continuous aging and T6-type multi-temperature aging treatments.

4.2.1.2 Alloy 319+Sr (Sr-Modified Alloy)

Figure 4.13 compares the tensile strength and microhardness values obtained with the T6 continuous aging treatment (4 h @ 150°C) with those obtained from the T6-type multi-temperature treatments (A through H). It may be noted that the continuous T6 treatment temperature and time in this case are different from those observed for the base alloy (170°C for 8 h).

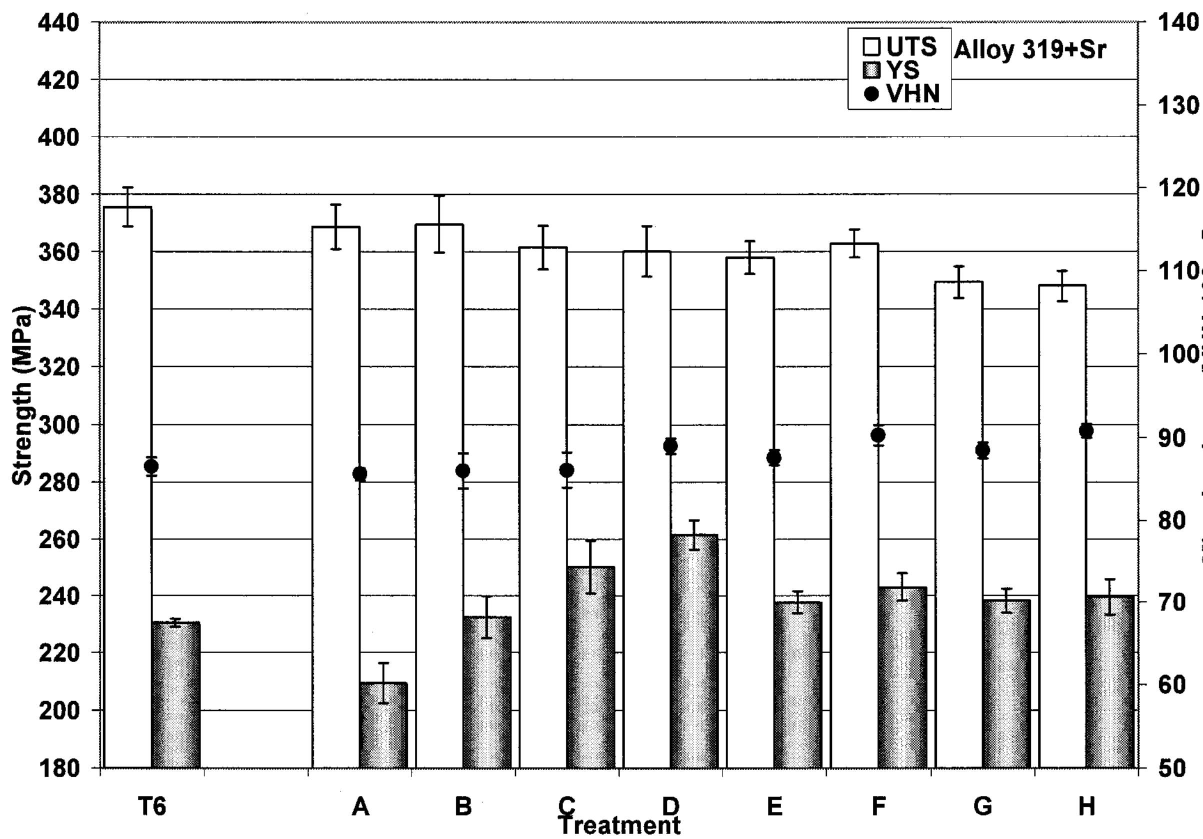

Figure 4.13 Average values of ultimate tensile strength (UTS), yield strength (YS), and microhardness (VHN) obtained for the 319+Sr alloy after T6 continuous aging and T6-type multi-temperature aging treatments.

From Figure 4.13 it will be observed that the values obtained with the use of the T6 continuous aging treatment and the multi-temperature treatments are closely similar; treatments C and D show higher yield strength values than the T6 treatment, but the ultimate tensile strength and microhardness values are similar. Treatments E through F show closely similar values for all properties, the UTS values being lower, and the YS and microhardness being slightly higher than the corresponding T6 treatment values. Thus these multi-temperature treatments may be considered to be somewhat beneficial for the 319+Sr alloy, since the latter properties appear to be more sensitive than the ultimate tensile strength to the heat treatment conditions.

Figure 4.14 shows a comparison of the values obtained for elongation and impact toughness when the 319+Sr alloy is subjected to T6 continuous aging treatment and multi-temperature aging treatments. As expected, the elongation and impact toughness values are lower than those obtained using the T6 treatment, since the yield strength obtained from the multi-temperature treatments was higher. A tendency observed in the case of all treatments is that there is a decrease in the values of both these parameters upon extending the aging time. This behavior is normal since the strength and microhardness values that may be achieved increase with an increase in aging time.

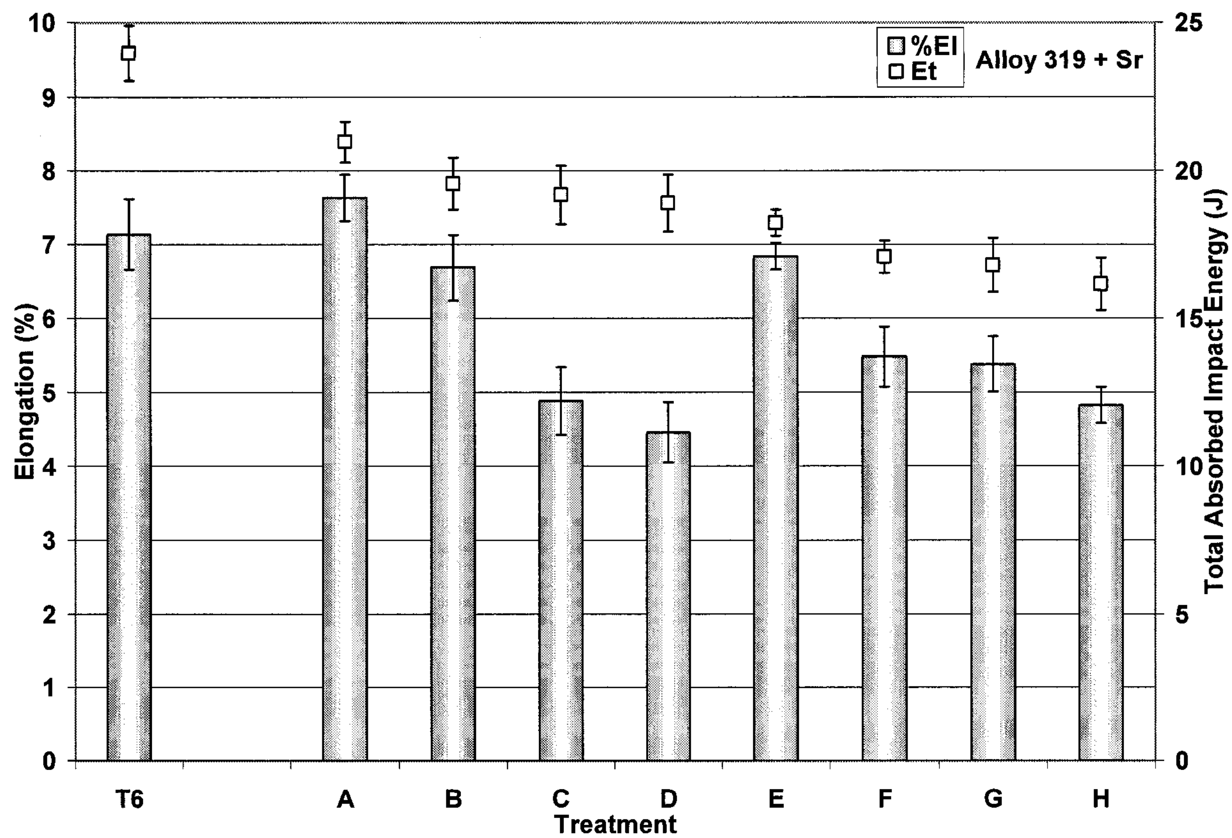

Figure 4.14 Average values of percentage elongation (%El), and total absorbed impact energy (E_t) obtained for the 319+Sr alloy after T6 continuous aging and T6-type multi-temperature aging treatments.

4.2.1.3 Alloy 319+Mg (Mg-Containing Base Alloy)

Figure 4.15 compares the tensile strength and microhardness values obtained with the T6 continuous aging treatment with those obtained from the T6-type multi-temperature treatments (A through H). The T6 treatment in this case was 8 h at 170°C.

It will be observed that the T6 treatment yields higher strength and microhardness values than almost all of the multi-temperature aging cycles, with the exception of treatment C which comprises in aging at 150°C for 2 h followed by aging at 180°C for 5 h. With the use of this cycle, the strength values attained are almost identical to those obtained after T6 treatment, and the microhardness is also slightly higher (cf. 137 VHN with 131 VHN for the T6 case).

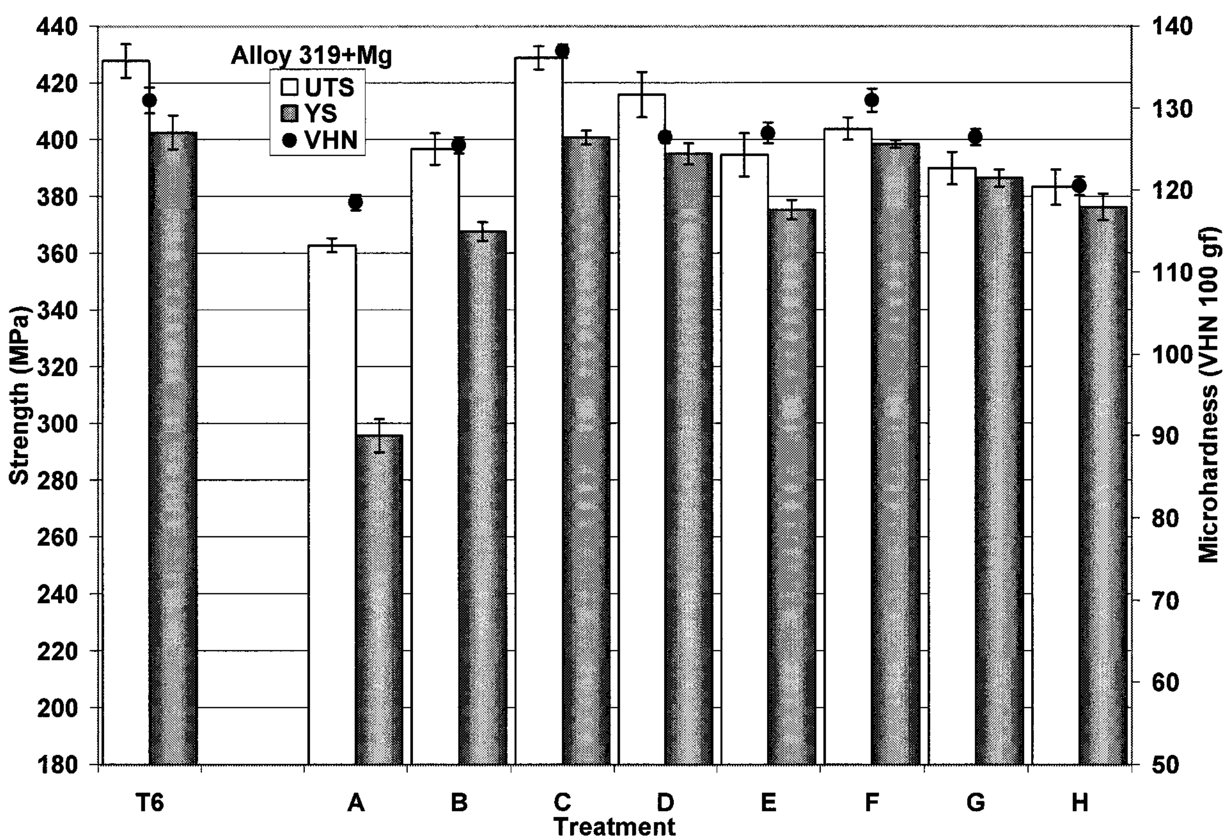

Figure 4.15 Average values of ultimate tensile strength (UTS), yield strength (YS), and microhardness (VHN) obtained for the 319+Mg alloy after T6 continuous aging and T6-type multi-temperature aging treatments.

It is interesting to note that, even at prolonged aging times such as in treatment D (3 h at 150°C + 10 h at 180°C), the strength and microhardness values obtained for are still high, showing that resistance to softening persists even after long aging times. The same tendency may be observed at higher temperatures, such as in treatment H, which consists of aging at 190°C for 2 h followed by 10 h at 180°C, where the properties are seen to be comparable to those obtained after continuous aging at 190°C.

Figure 4.16 shows the elongation and impact toughness values obtained for the 319+Mg alloy when subjected to the T6 and multi-temperature aging treatments. It can be seen that, although the percentage elongations obtained from the multi-temperature treatments are closely similar to the T6 treatment value, treatments A to D show slightly better ductility, while treatments E to H produce lower elongations. The total absorbed impact energy is also improved somewhat with the multi-temperature aging treatments. Overall, taking into consideration both microhardness and the tensile and impact properties, the multi-temperature aging treatments may be considered to be more advantageous for the 319+Mg alloy.

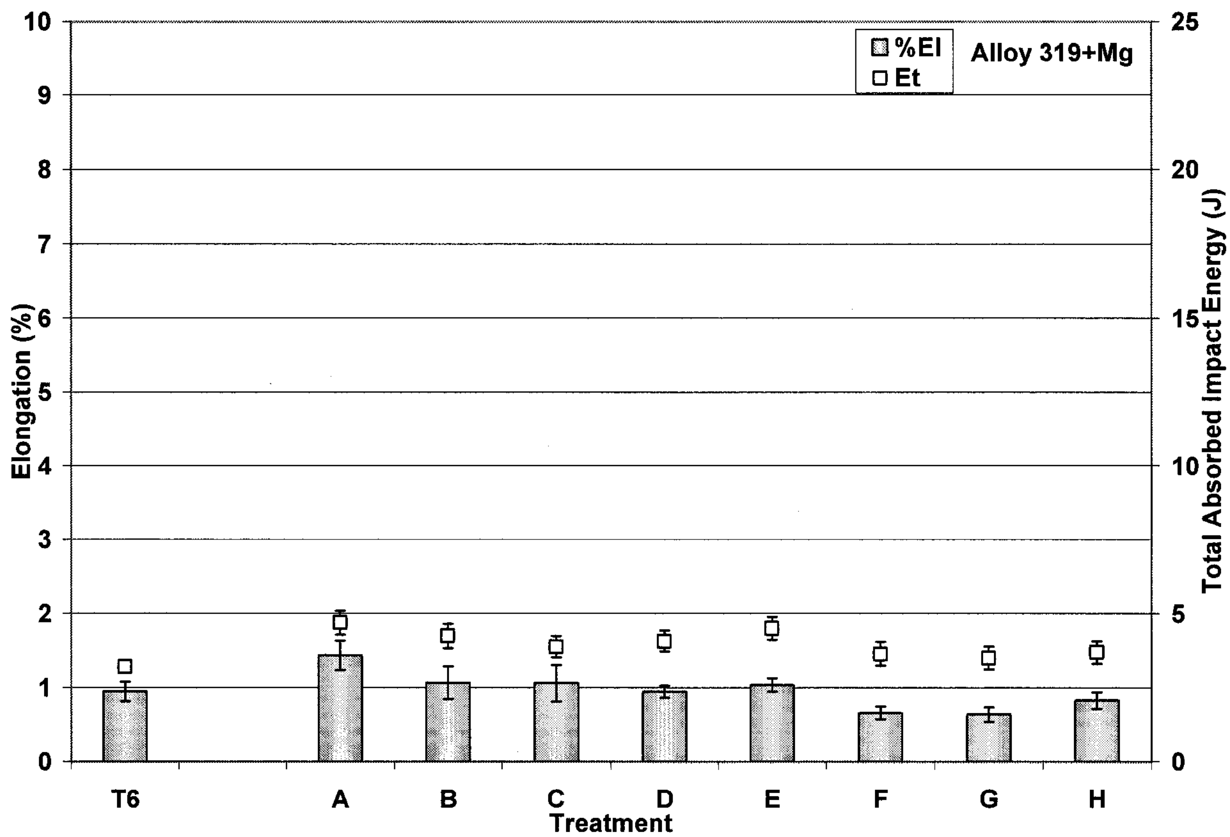

Figure 4.16 Average values of percentage elongation (%El), and total absorbed impact energy (E_t) obtained for the 319+Mg alloy after T6 continuous aging and T6-type multi-temperature aging treatments.

4.2.1.4 Alloy 319+Mg+Sr (Sr-Modified Mg-Containing Alloy)

Figure 4.17 compares the tensile strength and microhardness values obtained with the T6 continuous aging treatment (8 h @ 170°C) with those obtained from the T6-type multi-temperature treatments (A through H).

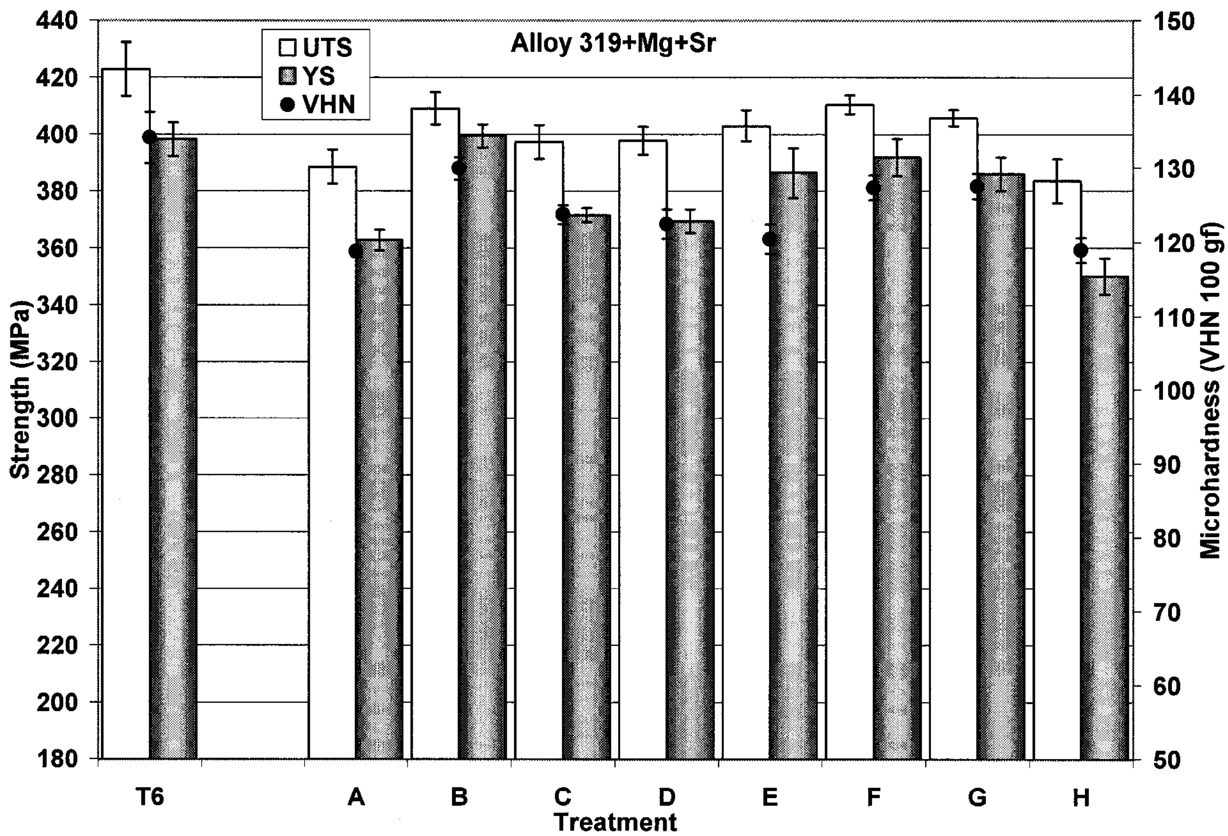

Figure 4.17 Average values of ultimate tensile strength (UTS), yield strength (YS), and microhardness (VHN) obtained for the 319+Mg+Sr alloy after T6 continuous aging and T6-type multi-temperature aging treatments.

As may be seen, the T6 continuous aging yields higher properties than the multi-temperature treatments, indicating that no further improvements could be obtained using such treatments. However, Treatment B exhibited properties closely similar to those obtained from the T6 condition.

Figure 4.18 shows the elongation and impact toughness values obtained for the 319+Mg+Sr alloy when subjected to the T6 and multi-temperature aging treatments. Some treatments, such as Treatment D, which comprises aging at 150°C for 2 h followed by aging at 180°C for 10 h, showed a higher elongation value of 1.39% as opposed to 0.98% obtained using the T6 continuous aging treatment. In general, it may be said that the elongation values are slightly improved after the multi-temperature treatments; the same tendency may be observed in the case of impact toughness, where the improvement is noticeable to a larger extent.

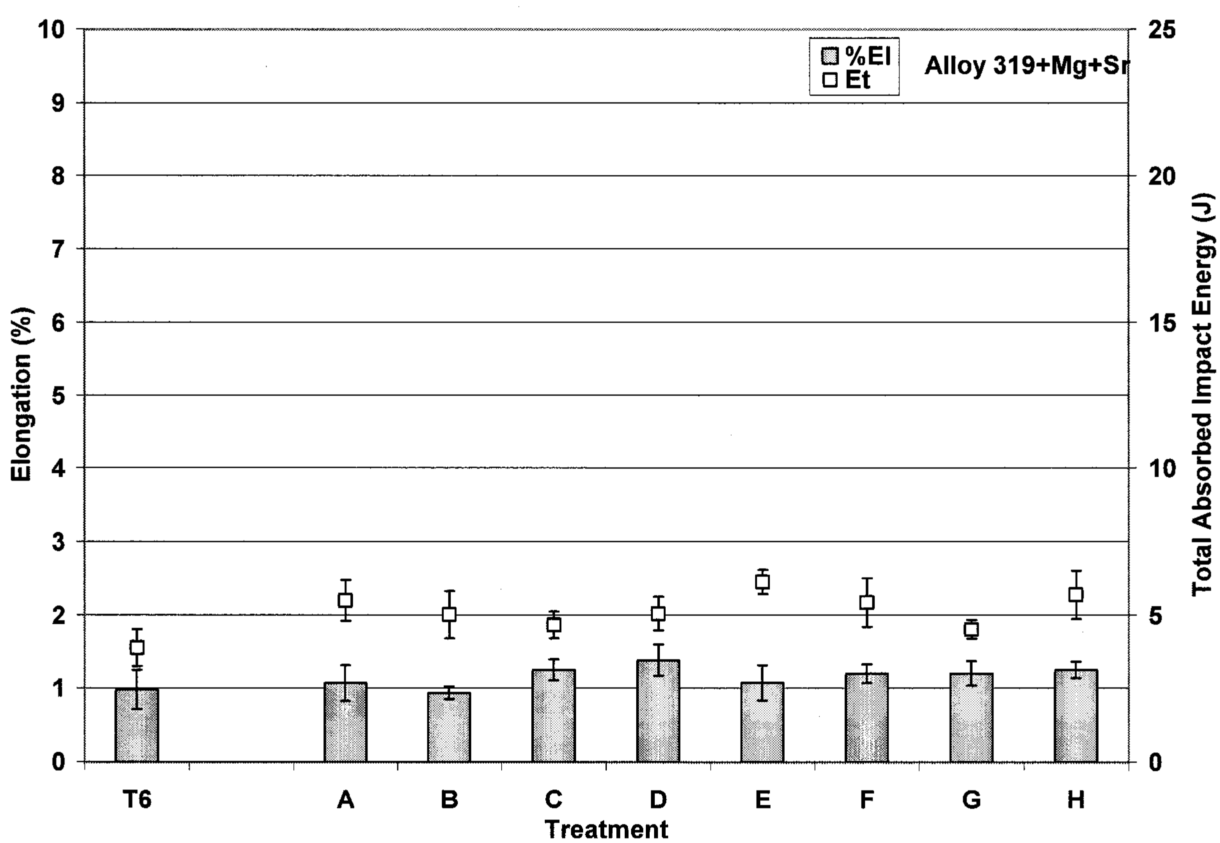

Figure 4.18 Average values of percentage elongation (%El), and total absorbed impact energy (E_t) obtained for the 319+Mg+Sr alloy after T6 continuous aging and T6-type multi-temperature aging treatments.

There is no noticeable improvement observed upon comparing the tensile strength and microhardness values obtained from the multi-temperature aging cycles with those obtained after T6 treatment, since the latter yields higher properties. However, when considering the ductility and impact toughness, a clear benefit is observed: a more ductile material with higher impact toughness and similar strength values can be obtained with the multi-temperature aging cycles. The same behavior may be observed in the 319+Mg alloy, suggesting that the presence of Mg in 319 alloy benefits from multi-temperature treatments.

4.2.2 T7-Type Multi-Temperature Treatments

Table 4.3 shows the details of the T7-type multi-temperature aging cycles that were used and their respective codes. As in the previous section, these codes (I through R) have been used in all the figures presented in this section. The temperatures for these cycles was selected based on those continuous aging treatments which provided optimum properties, as well as a number of others commonly used in certain foundries which prefer using the T7 temper. In the discussion that follows, the treatments will be regarded as having two stages: (i) the underaging stage carried out at low temperatures (100°C, 130°C, 150°C, 170°C or 190°C), and (ii) the overaging stage carried out at 240°C. Table 4.3 lists the details of the treatments used. Similar to the case of the T6-type multi-temperature treatments, here also these cycles were investigated to determine if such treatment could further improve the properties.

Table 4.3: T7-Type Multi-Temperature Aging Cycles

Codes and Multi-Temperature Treatment Regimes					
I	2 h @ 150°C	+	2 h @ 240°C		
J	2 h @ 150°C	+	3 h @ 240°C		
K	2 h @ 150°C	+	5 h @ 240°C		
L	2 h @ 150°C	+	10 h @ 240°C		
M	24 h @ 100°C	+	2 h @ 240°C		
N	24 h @ 130°C	+	5 h @ 240°C		
O	1 h @ 170°C	+	1 h @ 190°C	+	2 h @ 240°C
P	1 h @ 150°C	+	1 h at 170°C	+	2 h @ 240°C
Q	2 h @ 170°C	+	2 h @ 240°C		
R	2 h @ 190°C	+	2 h @ 240°C		

4.2.2.1 Alloy 319 (Base Alloy)

Figure 4.19 compares the tensile strength and microhardness values obtained with the T7 continuous aging treatment (2 h @ 240°C) with those obtained from the T7-type multi-temperature treatments (I through R). It ought to be mentioned that the same T7 continuous aging conditions were used for all the four alloys studied.

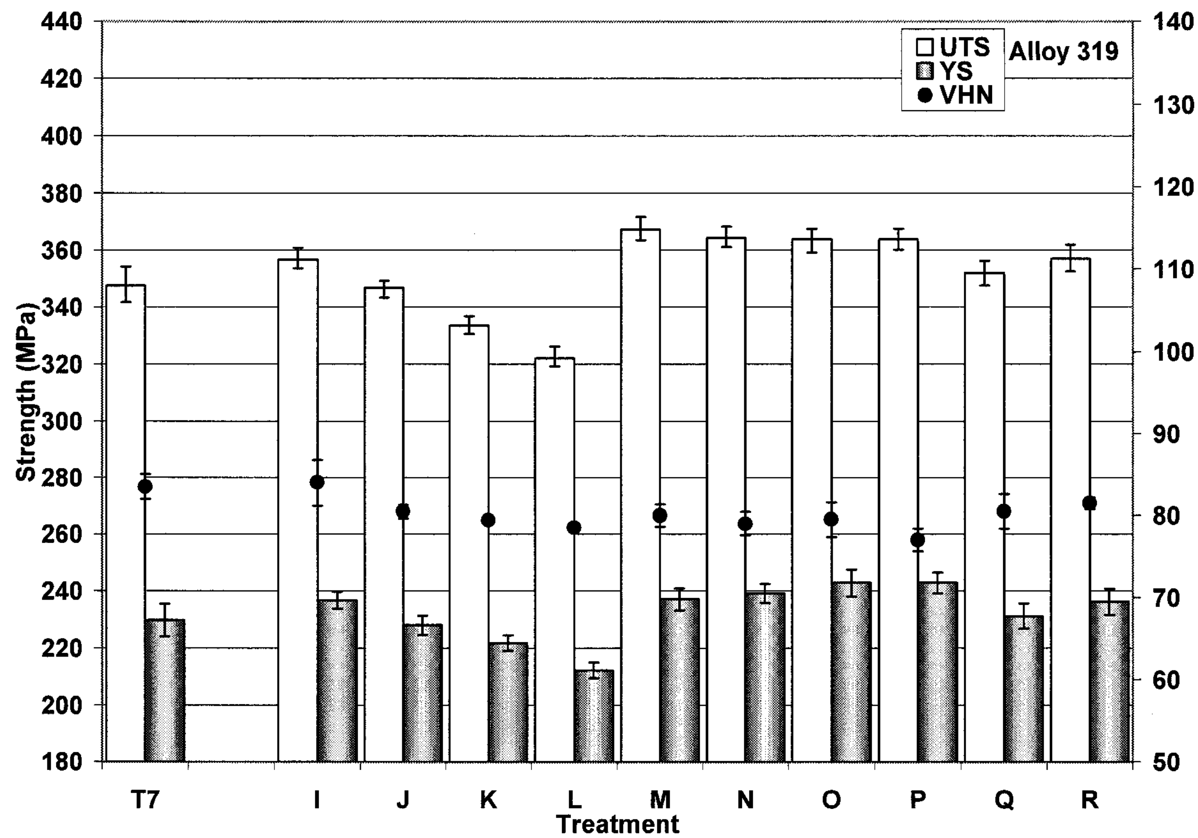

Figure 4.19 Average values of ultimate tensile strength (UTS), yield strength (YS), and microhardness (VHN) obtained for the 319 base alloy after T7 continuous aging and T7-type multi-temperature aging treatments.

It will be observed from Figure 4.19 that in some cases, such as treatments M and N, the multi-temperature aging cycles provide slightly higher tensile strengths than the T7 continuous aging treatment. These treatments, however, involve an extended underaging stage, i.e. 24 h at either 100°C or 130°C, followed by overaging for 2 h at 240°C. Treatments I through K demonstrate the progression of overaging as a function of time, where a loss in all three properties is observed upon increasing the aging time from 2 h to 10 h. Although the use of treatments

O and P provide the highest strength achievable, the microhardness values are lower than those obtained after T7 treatment. Finally, treatments Q and R display similar properties to those obtained from T7 continuous aging.

Figure 4.20 shows a comparison of elongation and impact toughness values obtained from the T7 continuous aging, and the T7-type multi-temperature aging treatments. An increase in properties may be observed on going from treatment I to treatment L, where the elongation increases by about 30% and the impact toughness by about 20%. This is to be expected, since overaging results in a loss in strength with a recovery in ductility and impact toughness. Accordingly, treatment L displays high elongation (~6%) and impact energy (~18.5 J) values among all the multi-temperature cycles studied, it also displays the lowest strength and microhardness values.

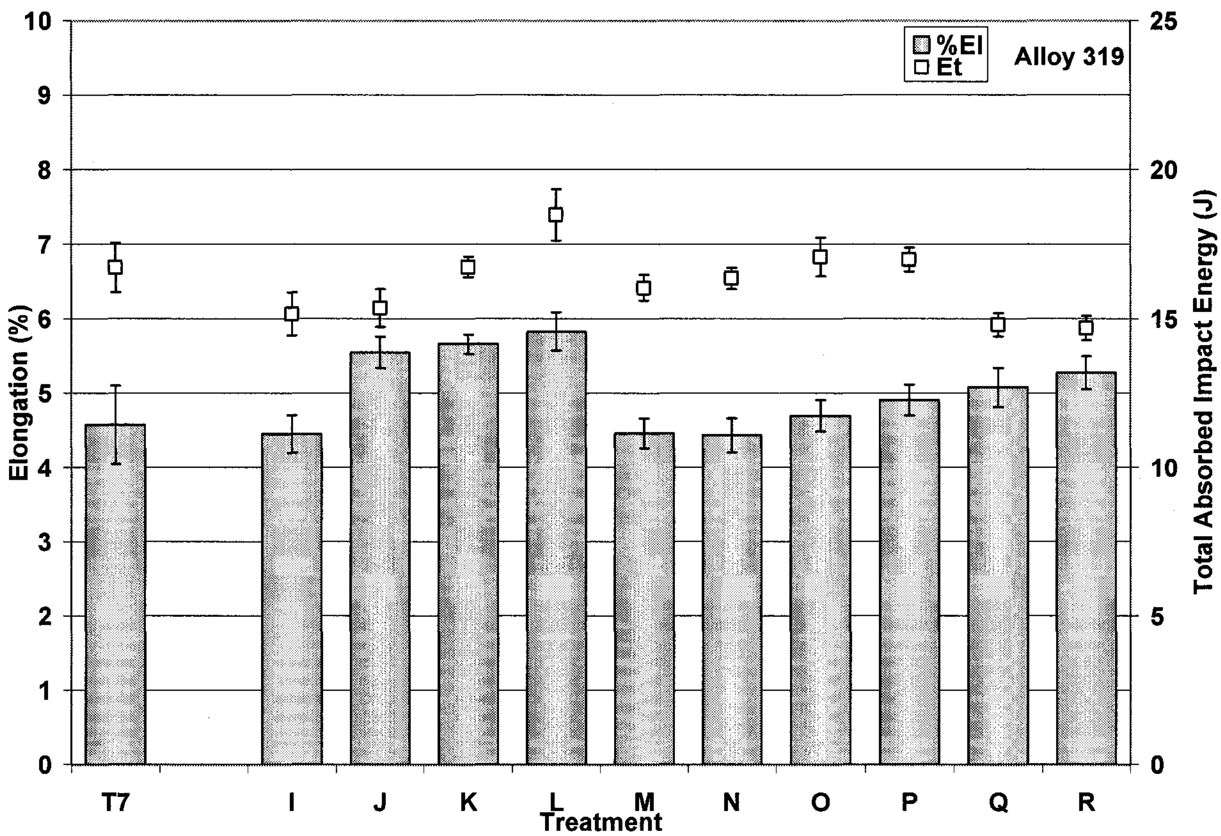

Figure 4.20 Average values of percentage elongation (%El), and total absorbed impact energy (E_t) obtained for the 319 base alloy after T7 continuous aging and T7-type multi-temperature aging treatments.

Treatments M through P show values for elongation and impact toughness similar to those obtained using T7 continuous aging. In consideration of the fact that these treatments produce higher strength values, it would thus be more productive to use these cycles for the 319 alloy rather than the T7 continuous regime. Finally, treatments Q and R display slightly higher elongation values and somewhat lower impact toughness values compared to the T7 treatment.

Effectively, therefore, these treatments would not provide any improvements over the T7 regime.

4.2.2.2 Alloy 319+Sr (Sr-Modified Alloy)

Figure 4.21 shows a comparison of tensile strength and microhardness values obtained with the T7 continuous treatment and the T7-type multi-temperature aging cycles in the Sr-modified 319 alloy. As may be seen, the multi-temperature cycles provide higher properties in some cases.

Treatments I through L show that this alloy produces slightly higher strength values than the continuous T7 regime for ultimate tensile strength and yield strength even after prolonged aging times, such as treatment L which consists of aging at 150°C for 2 h followed by aging at 240°C for 10 h. In these treatments, the microhardness values remain almost constant. The longest treatments, M and N, display higher strength values compared to the former (treatments I through L and T7). Of these, treatment N (24 h at 130°C + 2 h at 240°C) displays the highest strength and microhardness values obtained from the multi-temperature treatments. The improvement in strength is particularly noticeable when it is compared to the T7 continuous regime: there is an increase of about 10% in both YS and UTS. The remaining multi-temperature treatments; O through R; display similar microhardness values, comparable to that obtained from the T7 continuous treatment; the UTS and YS values are slightly higher, however, the improvement is not observantly significant, i.e. about 5% for treatment O.

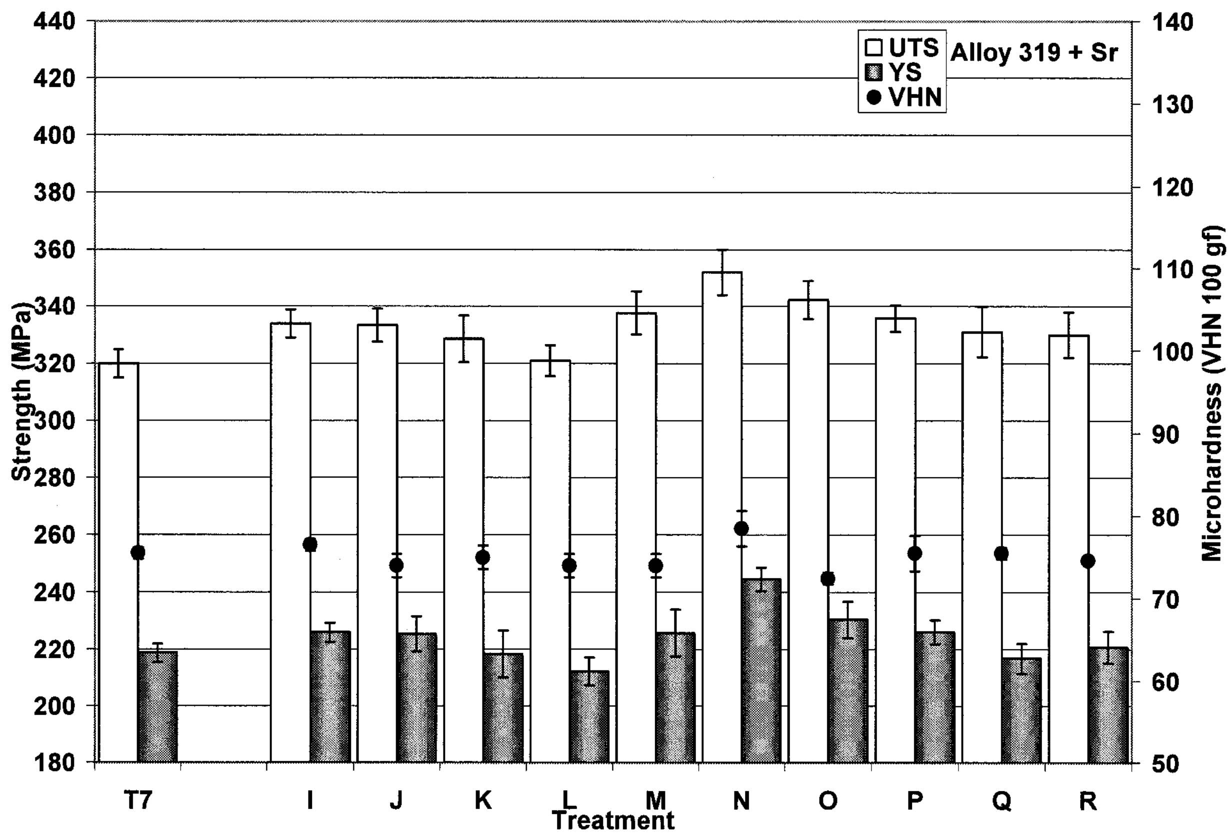

Figure 4.21 Average values of ultimate tensile strength (UTS), yield strength (YS), and microhardness (VHN) obtained for the 319+Sr alloy after T7 continuous aging and T7-type multi-temperature aging treatments.

Figure 4.22 shows a comparison in elongation and impact toughness values obtained from the T7-type multi-temperature treatments for the 319+Sr alloy. It will be observed that treatments I through L increase the impact toughness and ductility with increasing aging time, the highest values being obtained for treatment L which consists of aging at 150°C for 2 h followed by aging at 240°C for 10 h.

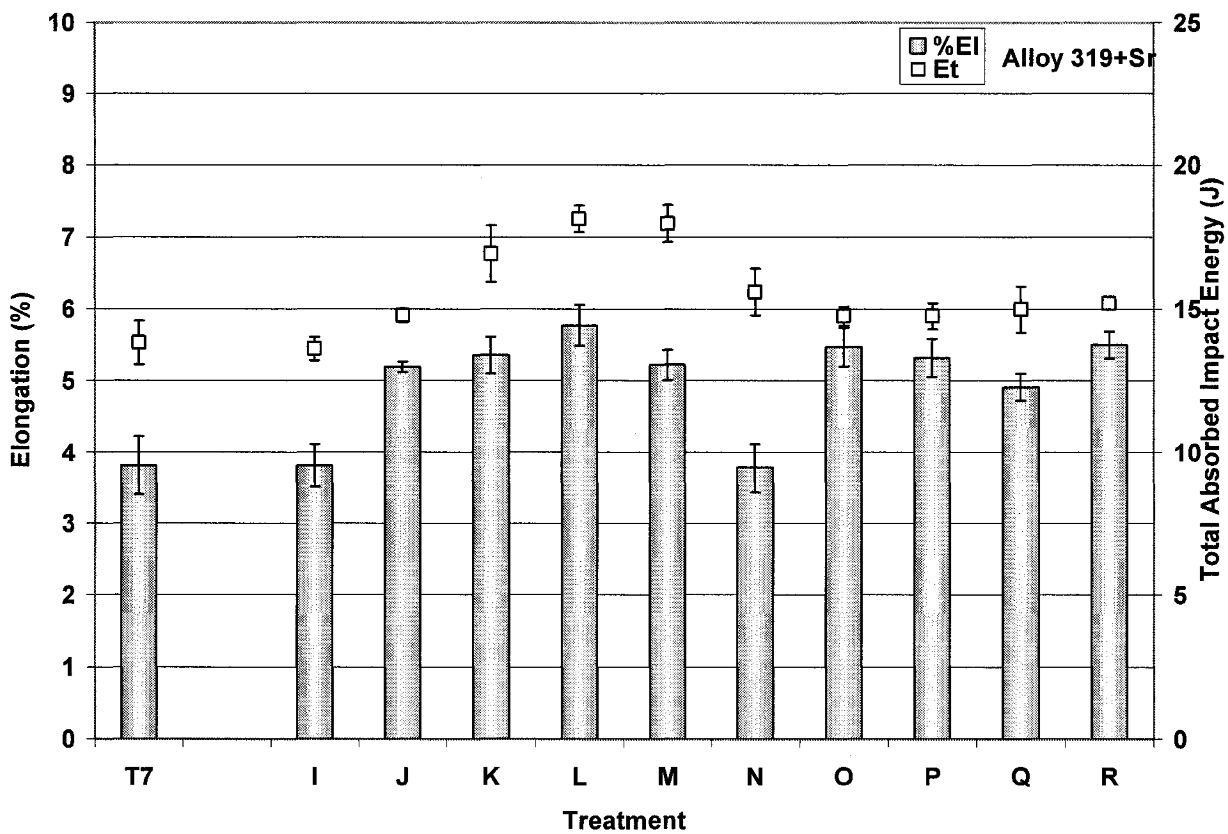

Figure 4.22 Average values of percentage elongation (%El), and total absorbed impact energy (E_t) obtained for the 319+Sr alloy after T7 continuous aging and T7-type multi-temperature aging treatments.

With treatment L, the corresponding improvement in properties over those provided by the T7 treatment is an increase in elongation of about 50% and an increase in the total absorbed impact energy of about 22%, with comparable strength values. Similarly, treatment M also provides comparatively higher elongation and impact toughness values. Treatment N, where the highest strength and elongation values were obtained, showed a minimal decrease in elongation (~1%) although the impact toughness improved somewhat (~12%). The Sr-modified 319 alloy benefits from these treatments (L, M and N) since they either improve the strength of the alloy and provide comparable elongation and impact toughness values, or they improve the elongation and impact toughness and provide comparable strength levels. Finally, treatments O through R improve only the elongation, while the impact toughness remains almost constant.

In general it may be said that the T7-type multi-temperature aging treatments are beneficial to the 319+Sr alloy because the ductility and impact toughness can be improved by as much as 50% and 20%, respectively, and maintaining practically the same strength levels as that obtained from T7 continuous aging. In this regard, treatment L (2 h @ 150°C + 10 h @ 240°C) shows the best combination of strength and ductility values.

4.2.2.3 Alloy 319+Mg (Mg-Containing Base Alloy)

Figure 4.23 shows the comparison of tensile strength and microhardness values obtained using the T7 continuous aging and the T7-type multi-temperature aging cycles for the 319+Mg alloy. It will be noted that the T7 treatment provides higher properties, except for treatment I, where the properties obtained are virtually the same for all intents and purposes.

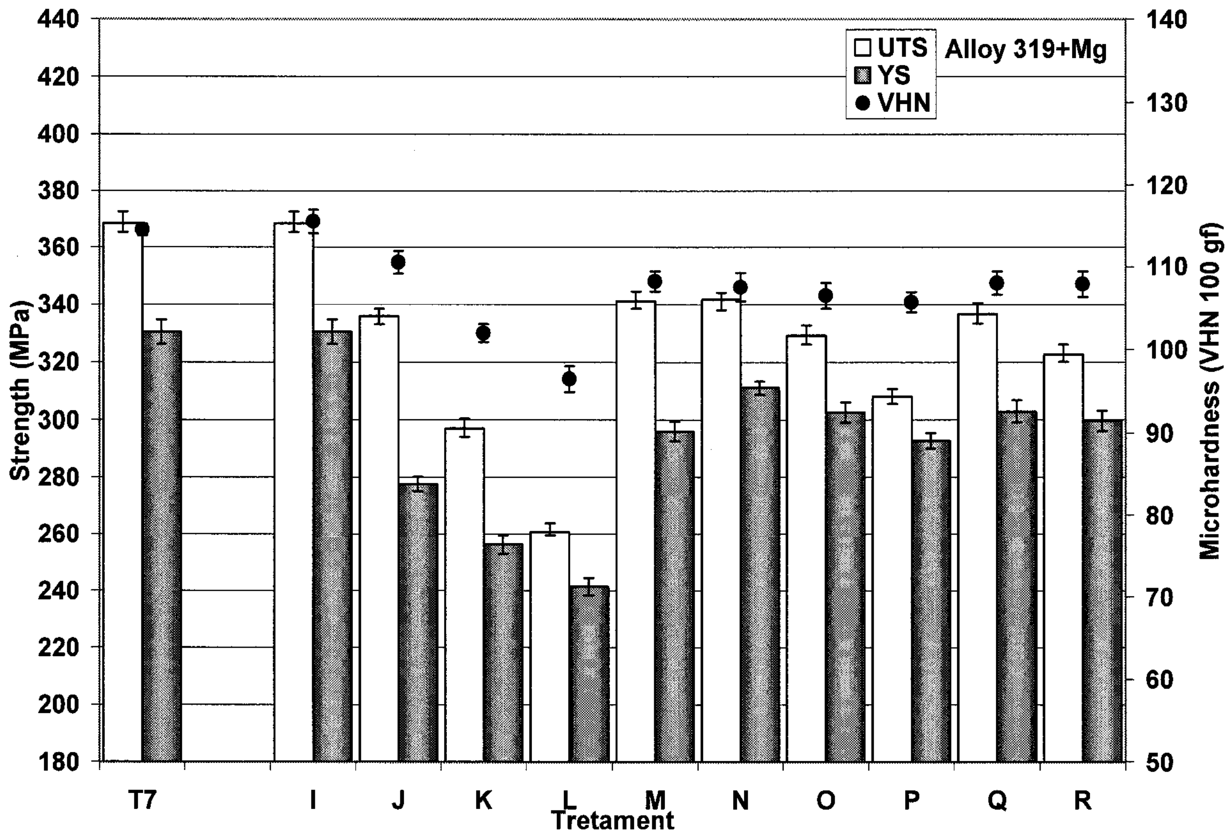

Figure 4.23 Average values of ultimate tensile strength (UTS), yield strength (YS), and microhardness (VHN) obtained for the 319+Mg alloy after T7 continuous aging and T7-type multi-temperature aging treatments.

Treatments J, K and L show a decrease in the strength and microhardness as the overaging period is increased from 3 through 5 to 10 hours, respectively (see Table 4.3 for details). The longer treatments, M and N, which involve a 24 h underaging stage (compared to 2 h for treatments J, K and L), show similar properties, but lower than those obtained from the T7 continuous treatment, suggesting that the strength of this alloy cannot be further improved by multi-temperature aging. The remaining multi-temperature treatments, O through R, show almost the same values for strength and microhardness but in all cases these values are still lower than those obtained using the T7 continuous aging treatment.

Figure 4.24 compares the elongation and impact toughness values obtained using T7-type multi-temperature treatments with those obtained from the T7 treatment. It will be observed that the elongation values are not improved with the use of any of the multi-temperature treatments, while the impact toughness is only slightly increased in some cases.

From Figure 4.24 it may be observed that treatments I through L display closely similar values to those obtained using the T7 treatment, thus indicating the latter is the better choice for this alloy because, in general, it provides higher strength values than these treatments (except for treatment I). Treatments M through R display lower elongation values but slightly improved total absorbed impact energies compared to treatments I – L, the best case being treatment O (1 h @ 170°C + 1 h @ 190°C + 2 h @ 240°C) showing about 10% improvement in elongation compared to the T7 continuous treatment. However, strength-wise, the latter is preferable since it yields higher values.

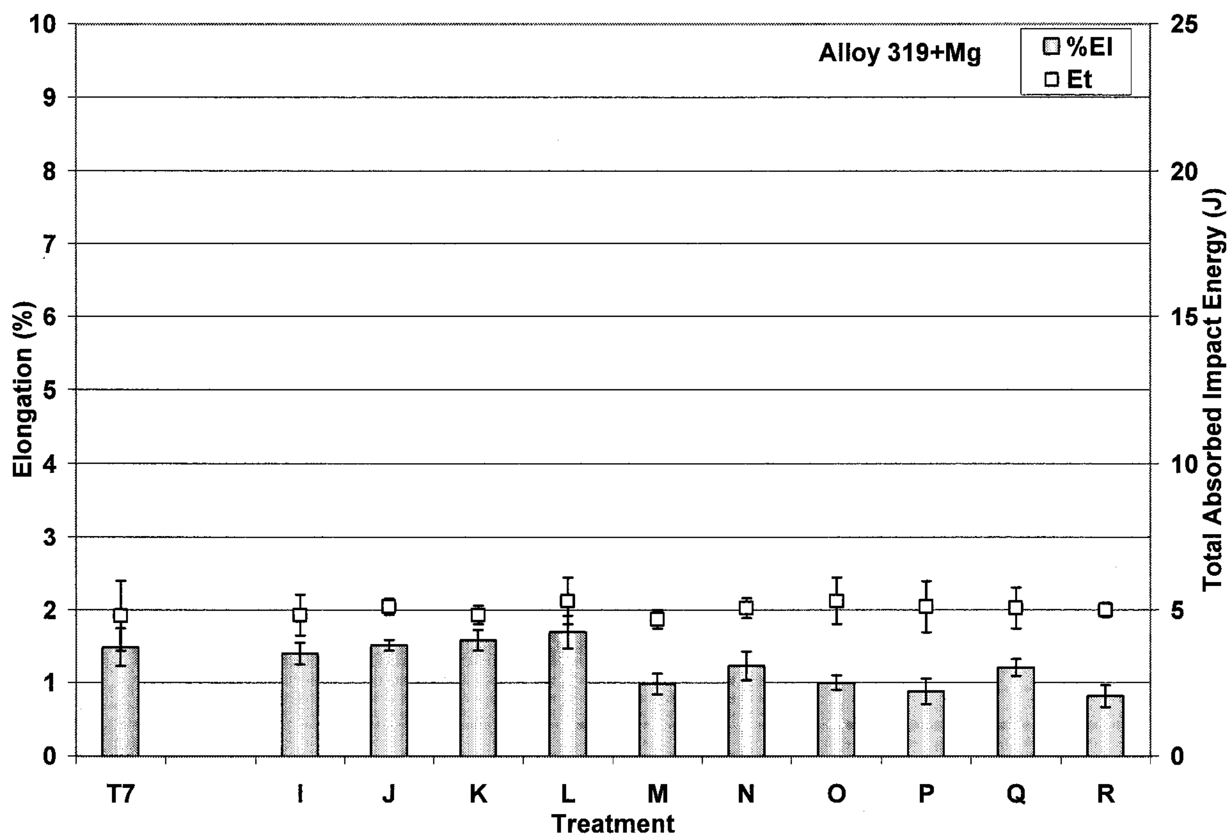

Figure 4.24 Average values of percentage elongation (%El), and total absorbed impact energy (E_t) obtained for the 319+Mg alloy after T7 continuous aging and T7-type multi-temperature aging treatments.

4.2.2.4 Alloy 319+Mg+Sr (Sr-Modified Mg-Containing Alloy)

Figure 4.25 shows a comparison of the values obtained for the UTS, YS and microhardness for the 319+Mg+Sr alloy subjected to the T7 continuous aging, and T7-type multi-temperature aging treatments. It will be observed from the graph, that only one multi-temperature treatment yields higher properties. This treatment, Treatment O, consisted in underaging for 1 h at 170°C, 1 h at 190°C and finally overaging for 2 h at 240°C. The improvement, however, is not great since at most, only a 5% increase is observed. Treatments I through L do not improve the properties above that obtained with continuous aging, the best results being obtained for Treatment J which exhibits comparable values. The same behavior was observed here as in the other alloys: there is a further decrease in properties with an increase in treatment time. However, the loss is not as marked as that noted in the 319+Mg alloy, indicating that modification helps in the stabilization of mechanical properties after heat treatment.

The remaining treatments M, N, and P through R show values comparable to those of treatments I through L, although they are still not as high as those obtained with the T7 continuous treatment. These results indicate that multi-temperature treatments have little effect on this alloy as regards tensile strength and microhardness.

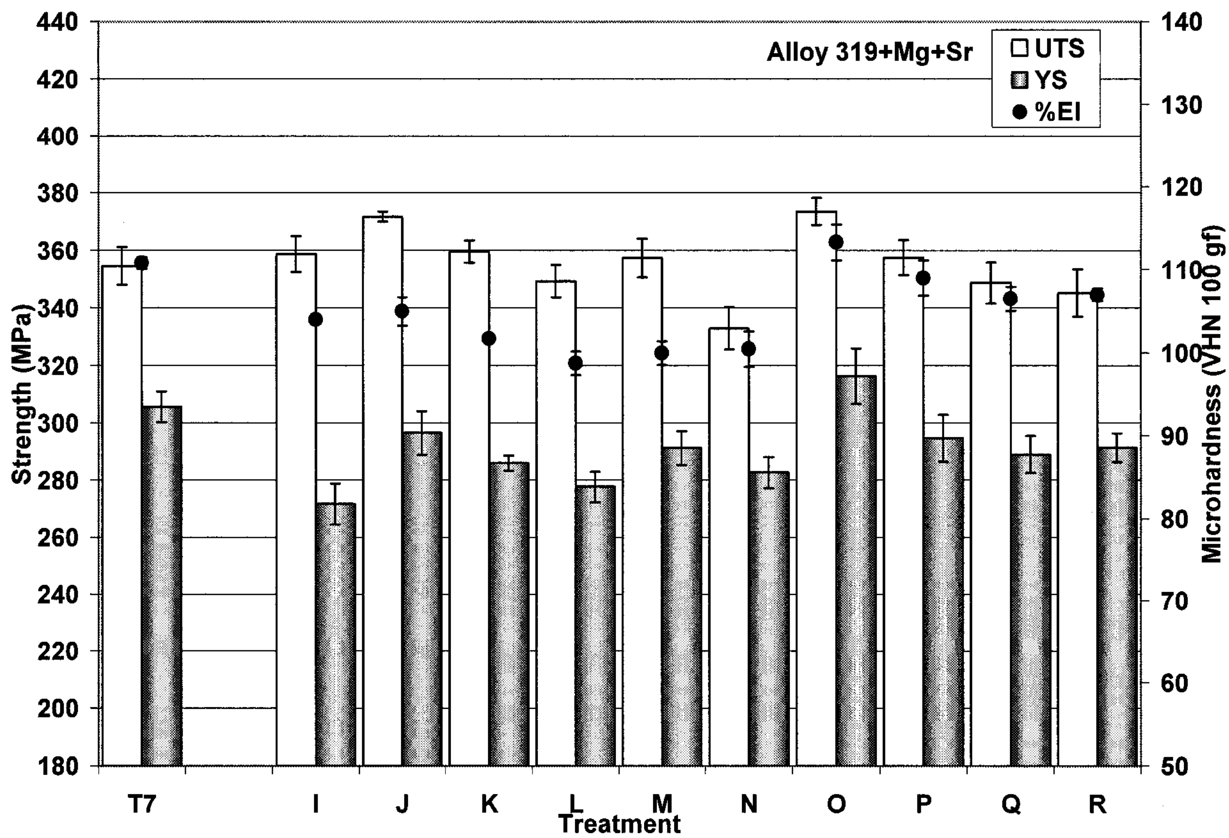

Figure 4.25 Average values of ultimate tensile strength (UTS), yield strength (YS), and microhardness (VHN) obtained for the 319+Mg+Sr alloy after T7 continuous aging and T7-type multi-temperature aging treatments.

Figure 4.26 shows the elongation and impact toughness values obtained for the 319+Mg+Sr alloy when subjected to the T7 and T7-type multi-temperature aging treatments. It will be observed, from the graph, that all the multi-temperature treatments improve these values as compared to T7 continuous aging treatment.

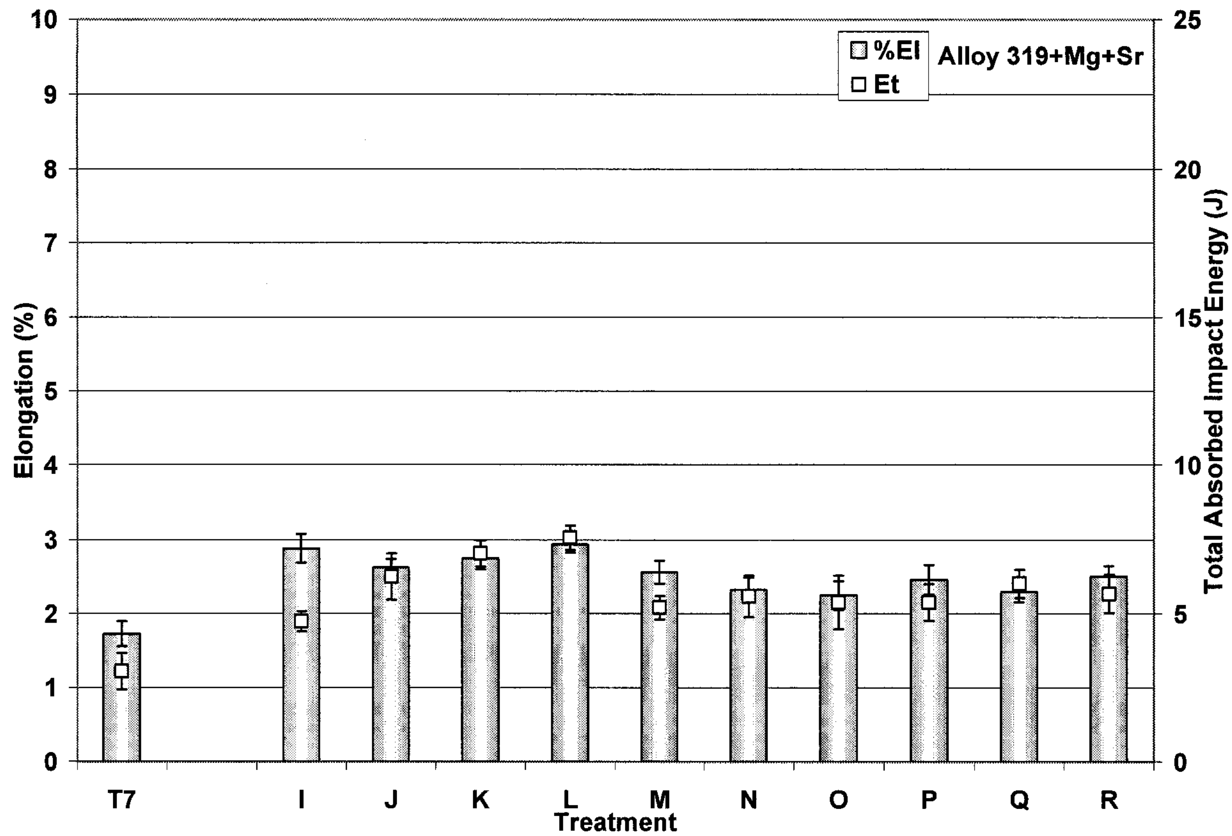

Figure 4.26 Average values of percentage elongation (%El), and total absorbed impact energy (E_t) obtained for the 319+Mg+Sr alloy after T7 continuous aging and T7-type multi-temperature aging treatments.

Treatments I through L show an increase in the elongation and impact toughness values with an increase in overaging time, as was to be expected [119, 120]. The rest of the multi-temperature treatments show fairly similar values for both properties. It is clear, then, that treatment O (1 h @ 170°C + 1 h @ 190°C + 2 h @ 240°C) is beneficial to this alloy since it produces improved elongation and impact toughness values and a slightly higher level of strength. An increase in elongation of about 30% (from 1.73% to 2.25%) and an increase in impact toughness of nearly 70% (from 3.06 J to 5.39 J) may be observed in treatment O when comparing it with the values obtained after treating using T7 continuous aging treatment.

4.3 Mechanical Properties Obtained using Interrupted Aging Cycles

As reported in the literature [1, 2, 95, 129-132], interrupted aging cycles have been used in a number of wrought and cast aluminum alloys, but there are no published works to date indicating that this specific type of aging treatment has been used for 319 alloys. Thus, studying the response of this alloy to interrupted aging will prove to be of significant importance. For this, two multi-temperature treatments were selected to put interrupted aging to the test; both of these treatments were ones which produced the best combination of properties: the first one is similar to the T6 continuous treatment, while the second is similar to the T7 continuous regime.

The corresponding treatments selected for interrupted aging were Treatment F consisting of underaging at 190°C for 2 h, followed by aging at 180°C for 3 h (T6-type); and Treatment O consisting of underaging at 170°C for 1 h, then aging at 190°C for 1 h, followed by overaging at 240°C for 2 h (T7-type). In each case, an interruption time was inserted before the final aging step for periods of 24 h and

100 h at room temperature. The results obtained for these cycles are presented in the following sections.

4.3.1 Tensile Properties

Figure 4.27 compares the ultimate tensile strength values obtained for the four 319-type alloys following the T6-type interrupted aging treatment, and using various interruption times (0, 24 and 100 h). It will be observed, from the figure, that there is no noticeable improvement or loss in UTS with the change in interruption time for any of the alloys.

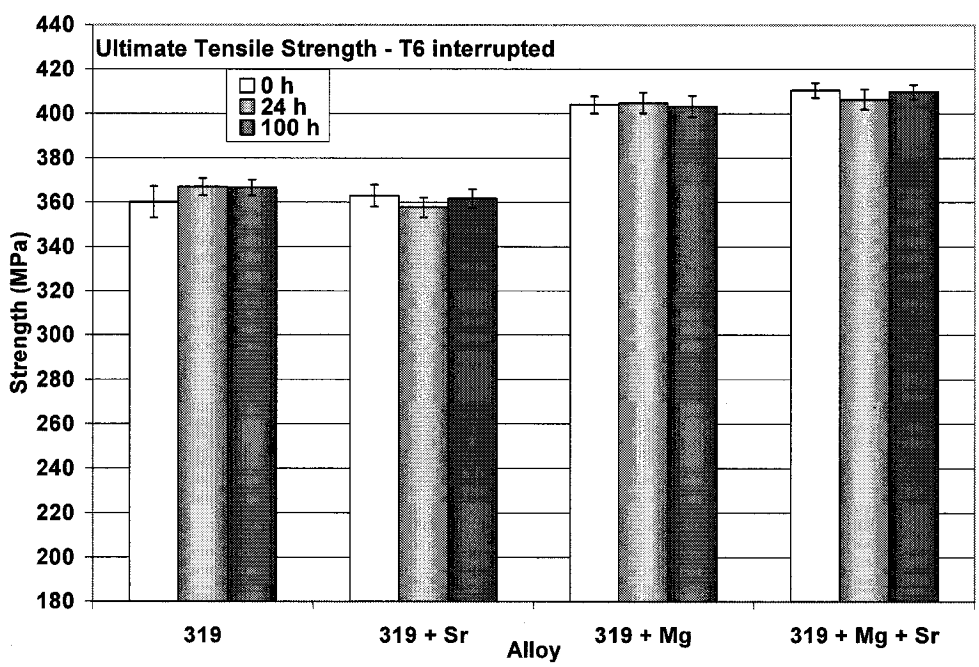

Figure 4.27 Comparison of UTS values obtained for the four 319-type alloys following the T6-type interrupted aging treatment using interruption times of 0, 24 and 100 h.

Figure 4.28 compares the UTS values for the same alloys subjected to T7-type interrupted aging treatment using interruption times of 0, 24 and 100 h.

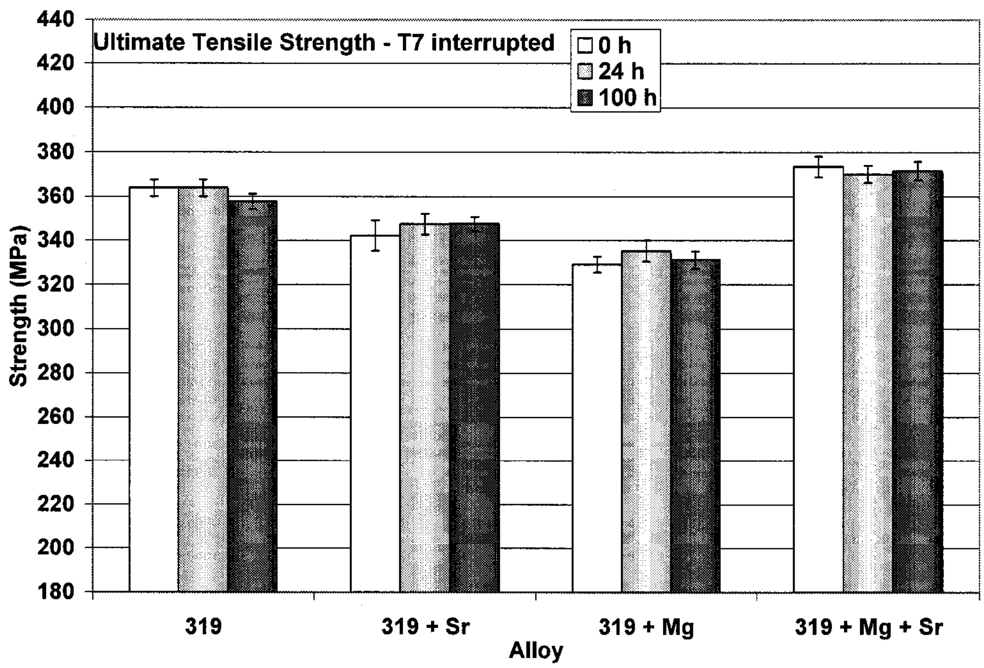

Figure 4.28 Comparison of UTS values obtained for the four 319-type alloys following the T7-type interrupted aging treatment using interruption times of 0, 24 and 100 h.

From Figure 4.28, it is evident that the interrupted aging cycles have no effect on the ultimate tensile strength of any of the alloys, since there is no appreciable tendency for this property to increase or decrease when the interruption stage is included in the multi-temperature aging cycle concerned. The values obtained with interrupted aging are almost identical to those obtained using the T7-type multi-temperature treatment (Treatment O).

Comparisons of the YS values obtained for the four alloys after interrupted aging treatments corresponding to the T6- and T7-type multi-temperature treatments are displayed in Figures 4.29 and 4.30, respectively. Again, it will be observed from both figures that there is no clear tendency that the values obtained increase or decrease with a change in interruption time. As the yield strength is usually more affected than the UTS by the heat treatment applied [83], and in view of the fact that no clear tendency is observed in the present figures, it may be reasonable to conclude that using interrupted aging is not useful in the case of these 319-type alloys for purposes of increasing the strength.

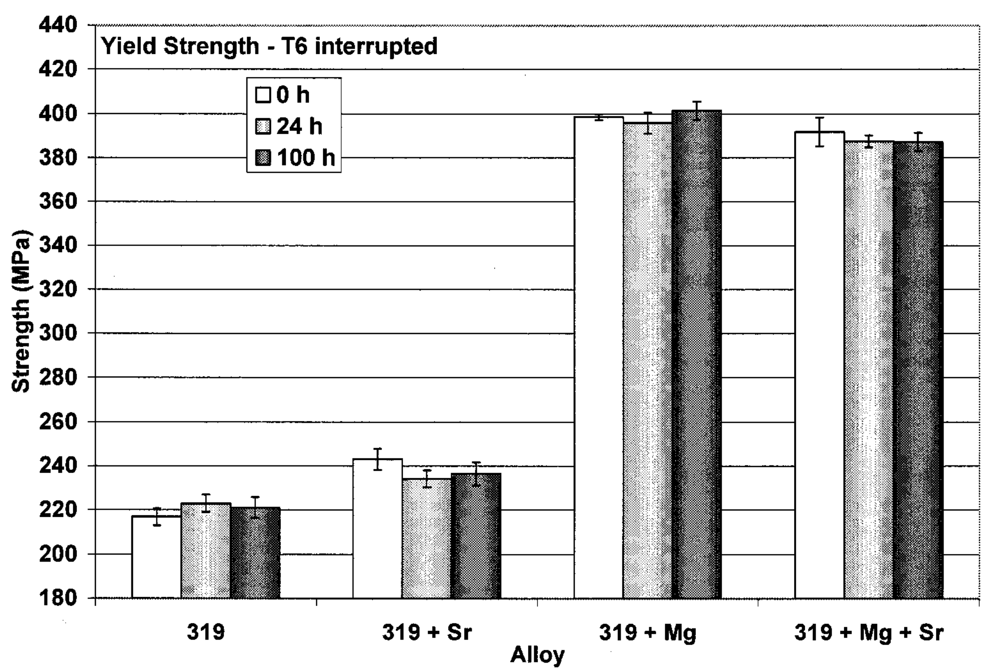

Figure 4.29 Comparison of YS values obtained for the four 319-type alloys following the T6-type interrupted aging treatment using interruption times of 0, 24 and 100 h.

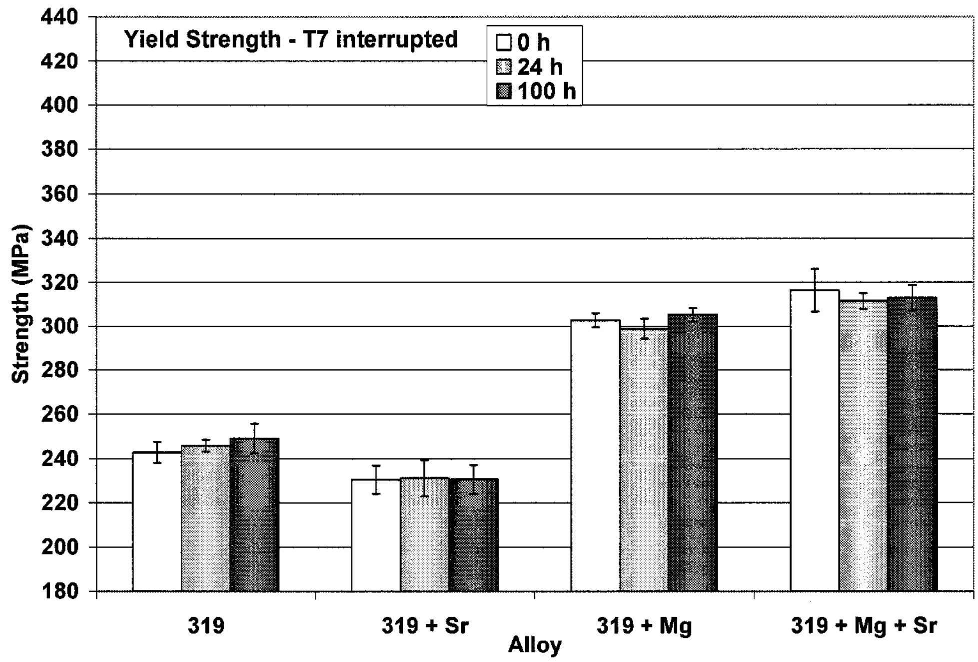

Figure 4.30 Comparison of YS values obtained for the four 319-type alloys following the T7-type interrupted aging treatment using interruption times of 0, 24 and 100 h.

Comparisons of the elongation values obtained for the four alloys after interrupted aging treatments corresponding to the T6- and T7-type multi-temperature treatments are displayed in Figures 4.31 and 4.32, respectively. As Figure 4.31 shows, with the use of interrupted aging and increase in interruption time, a decrease in elongation of about 5% is observed in the case of the 319 base alloy. The interruption time appears to have no effect on the 319+Sr alloy, whereas both 319+Mg and 319+Mg+Sr alloys show a slight increase in elongation values with increase in the interruption time. This increase, however, may be neglected since it falls within the range of standard deviation.

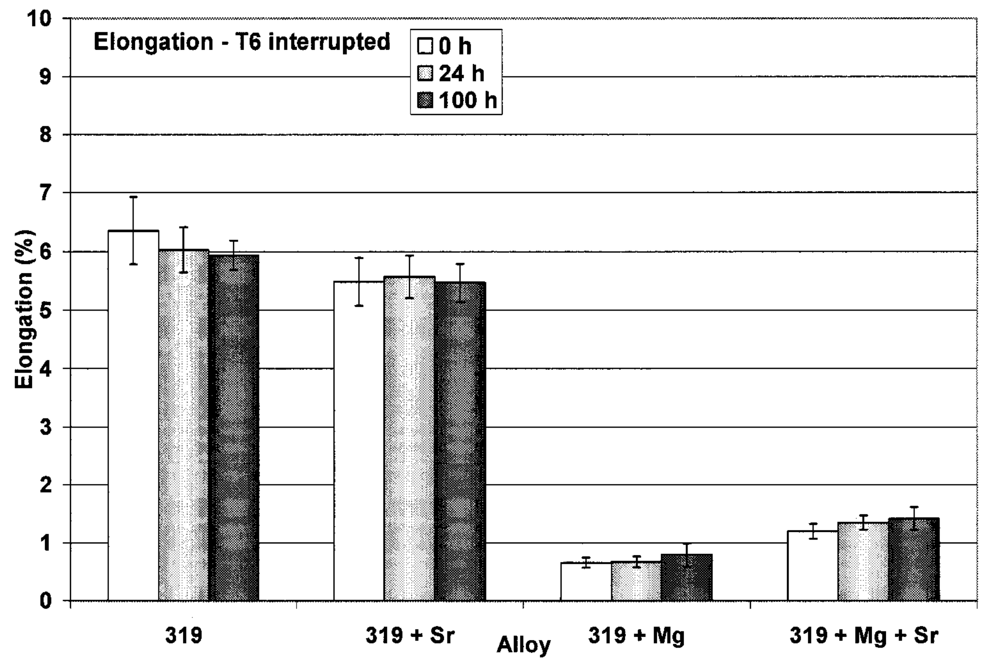

Figure 4.31 Comparison of percentage elongation values obtained for the four 319-type alloys following the T6-type interrupted aging treatment using interruption times of 0, 24 and 100 h.

As Figure 4.32 shows, for the base 319 and the Sr-modified 319 alloys, no clear tendency for either an increase or decrease in elongation is observed with change in interruption time. The addition of Mg to the base alloy shows a slight but definite decrease in elongation as the interruption time is increased. The elongation values are improved to almost twice their values with the addition of Sr. In this case, increase in the interruption time shows a tendency to improve the elongation. The variations in elongation with the use of interrupted aging cycles may be neglected, however, since most of the changes fall within the standard deviation range.

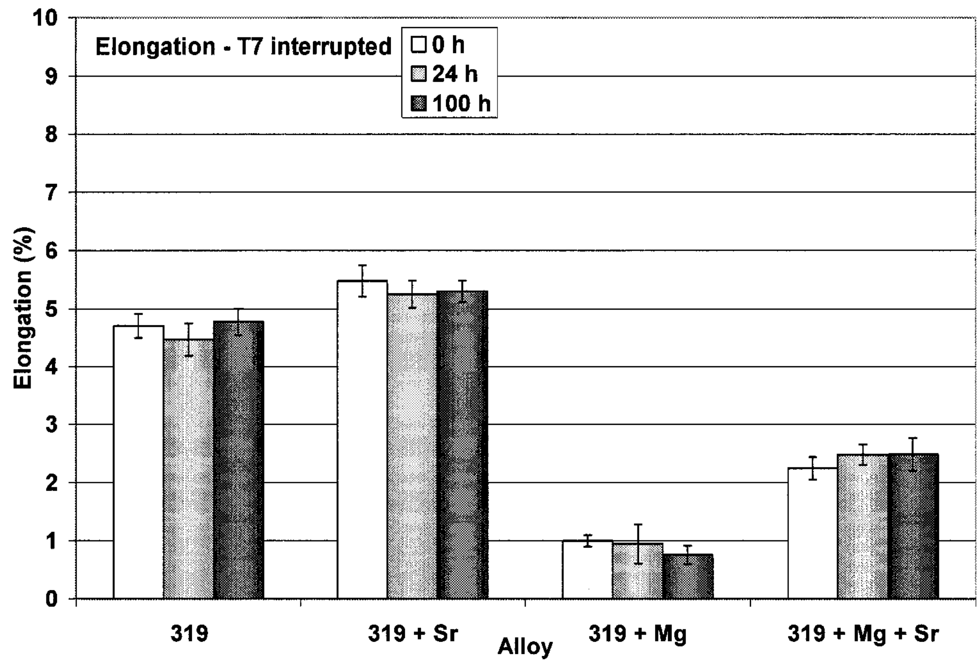

Figure 4.32 Comparison of percentage elongation values obtained for the four 319-type alloys following the T7-type interrupted aging treatment using interruption times of 0, 24 and 100 h.

4.3.2 Microhardness and Impact Toughness

Figures 4.33 and 4.34 compare the microhardness values obtained for the four alloys when subjected to T6- and T7-type interrupted aging cycles, respectively. The graph in Figure 4.33 is similar to that observed in Figure 4.29 depicting the yield strength values under the same heat treatment conditions (i.e. T6-type interrupted aging cycles). This is to be expected since the yield strength is the tensile property most affected by heat treatment [9, 19, 83]. The microhardness tends to correspond very well to the tendencies observed for the yield strength, although it is usually a more sensitive property as seen previously in Figures 4.29

and 4.30 for both the T6 and T7 continuous aging and the T6- and T7-type multi-temperature aging cycles.

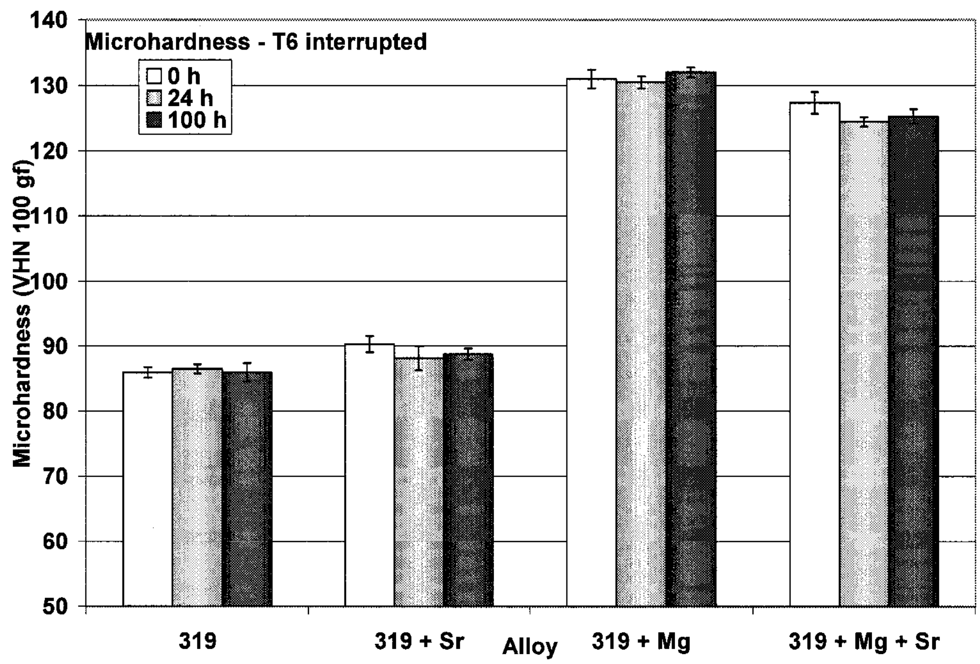

Figure 4.33 Comparison of the microhardness values obtained for the four 319-type alloys following the T6-type interrupted aging treatment using interruption times of 0, 24 and 100 h.

Figure 4.34 does not show an identical match with the yield strength values shown in Figure 4.29 obtained after T7-type interrupted aging treatments but otherwise the same observations may be made: the variations observed for microhardness are not significant, indicating the interruption of the aging treatment does not have a marked effect on this particular property either. The most noticeable variation in microhardness values was observed in the 319+Mg alloy, where the microhardness decreased from 106.5 VHN to 104.3 VHN after interrupting the aging for 24 h, namely, a decrease of approximately 2%.

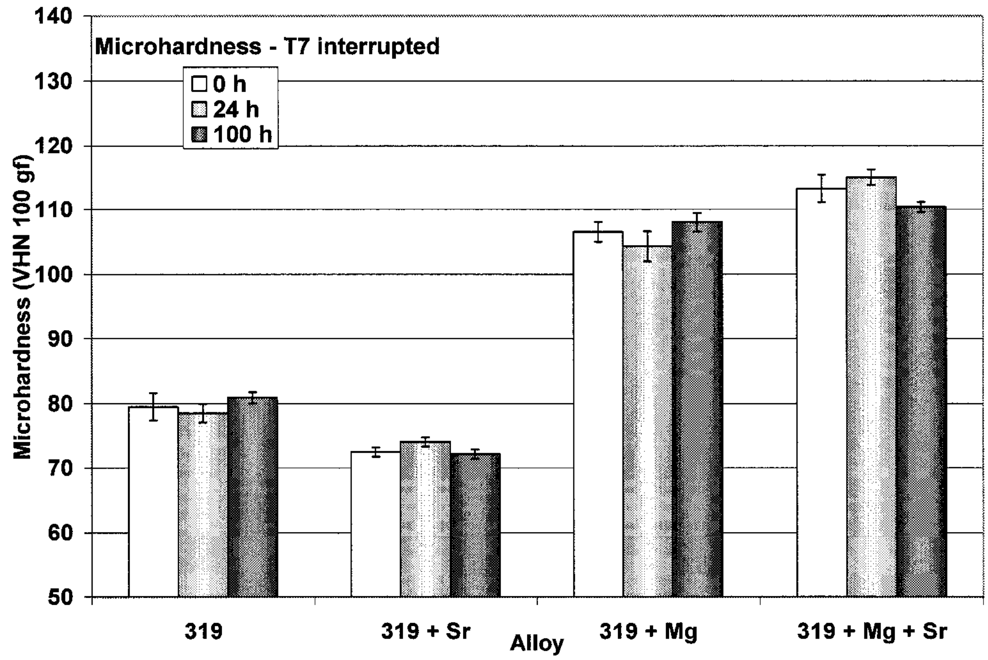

Figure 4.34 Comparison of the microhardness values obtained for the four 319-type alloys following the T7-type interrupted aging treatment using interruption times of 0, 24 and 100 h.

Figures 4.35 and 4.36 show the variation in impact toughness values observed for the four alloys when subjected to the T6- and T7-type interrupted aging cycles, respectively. It will be observed from both figures, that there is no marked tendency to an increase or decrease in the values obtained as opposed to those observed in the graphs corresponding to percentage elongation, namely Figures 4.32 and 4.31.

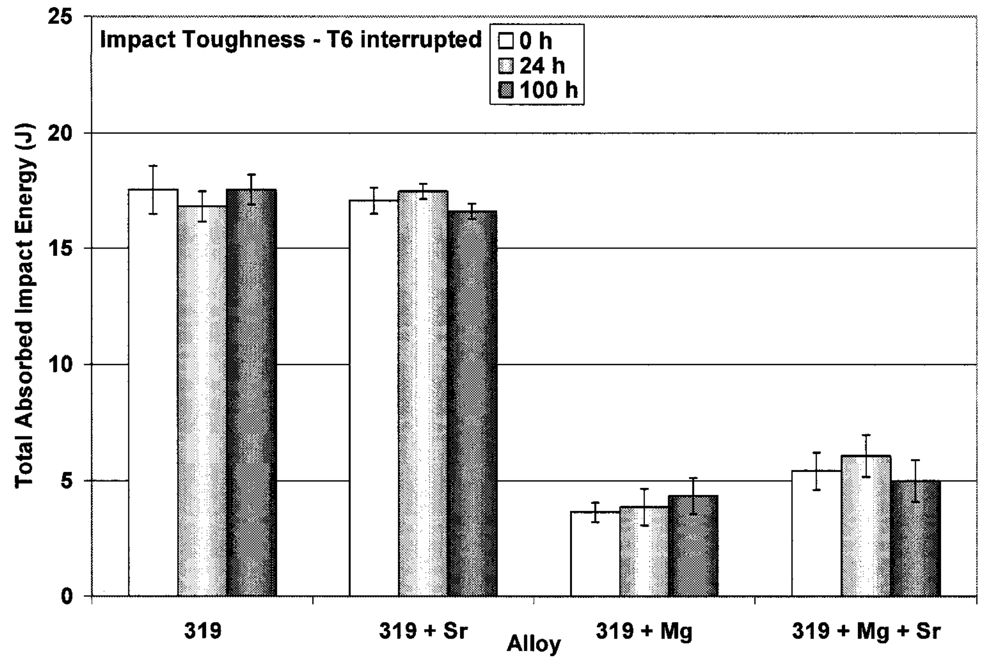

Figure 4.35 Comparison of the impact toughness values obtained for the four 319-type alloys following the T6-type interrupted aging treatment using interruption times of 0, 24 and 100 h.

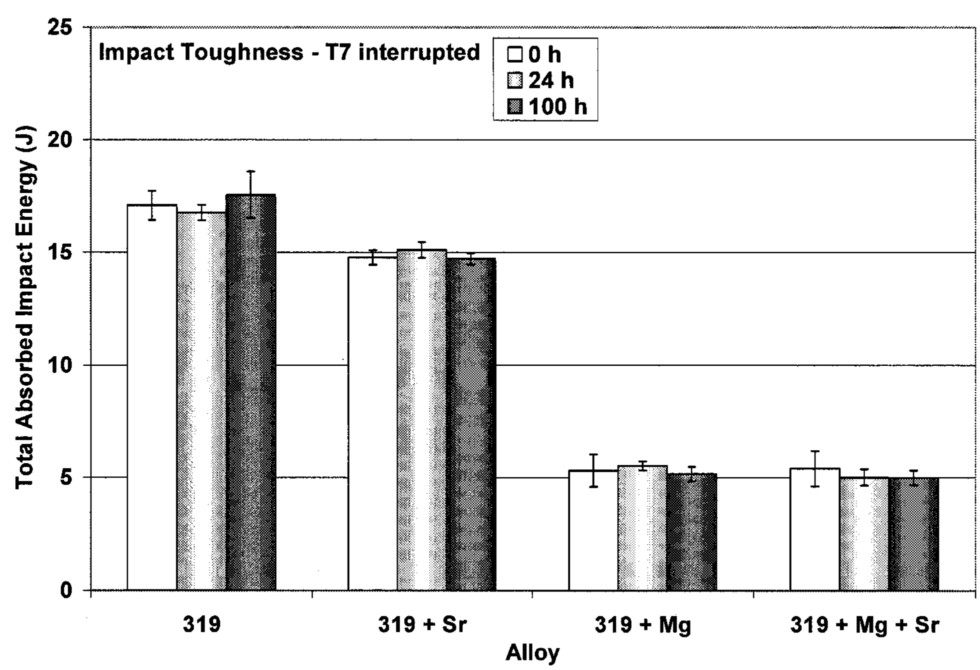

Figure 4.35 Comparison of the impact toughness values obtained for the four 319-type alloys following the T7-type interrupted aging treatment using interruption times of 0, 24 and 100 h.

After detailed analysis of the tensile properties (UTS, YS and %El), microhardness, and the impact toughness values obtained for the four alloys using interrupted aging cycles, it may be stated that this type of aging does not have any marked effect on the 319-type alloys investigated in this study, with respect to an improvement in properties. It may also be stated that the mechanisms which take place during precipitation hardening of this alloy system are not affected by the inclusion of an interruption stage at room temperature before the last stage of any of the multi-temperature aging treatments studied.

To summarize, the 319-type alloys included in this study do not benefit from the standard T6 treatment, since aging at 170°C for 8 h produces better properties. The best properties were observed in the 319+Mg+Sr alloy and they cannot be further improved by T6-type multi-temperature aging treatments. In the case when an overaged (T7) condition is desired, the optimum treatment consists of underaging at 170°C for 1 h, at 190°C for 1 h, and finally overaging at 240°C for 2 h. It was also observed that interrupted aging does not affect the achievable properties obtained.

4.4 Microstructural Results

This section presents the results of the microstructural analysis carried out by means of electron microscopy. A scanning electron microscope was used to analyze the fracture surface of tensile test specimens because of its greater depth of field [138]. The identification of tiny precipitates present in the aluminum dendrites was performed using a transmission electron microscope because of its high resolution, in conjunction with excellent chemical and crystallographic analysis capabilities [139].

4.4.1 Scanning Electron Microscopy

The first set of micrographs presented in this section refers to the modified alloy with additions of Mg, since this alloy displays a greater degree of noticeable differences on the fracture surface. Figure 4.37 shows the surface of a fractured tensile test specimen in the as-cast state. The surface exhibits ductile fracture features in general, with crack initiation mostly observed in the eutectic silicon particles, since the latter are more brittle than the matrix itself and act as preferred crack initiation sites [66, 123, 124, 135].

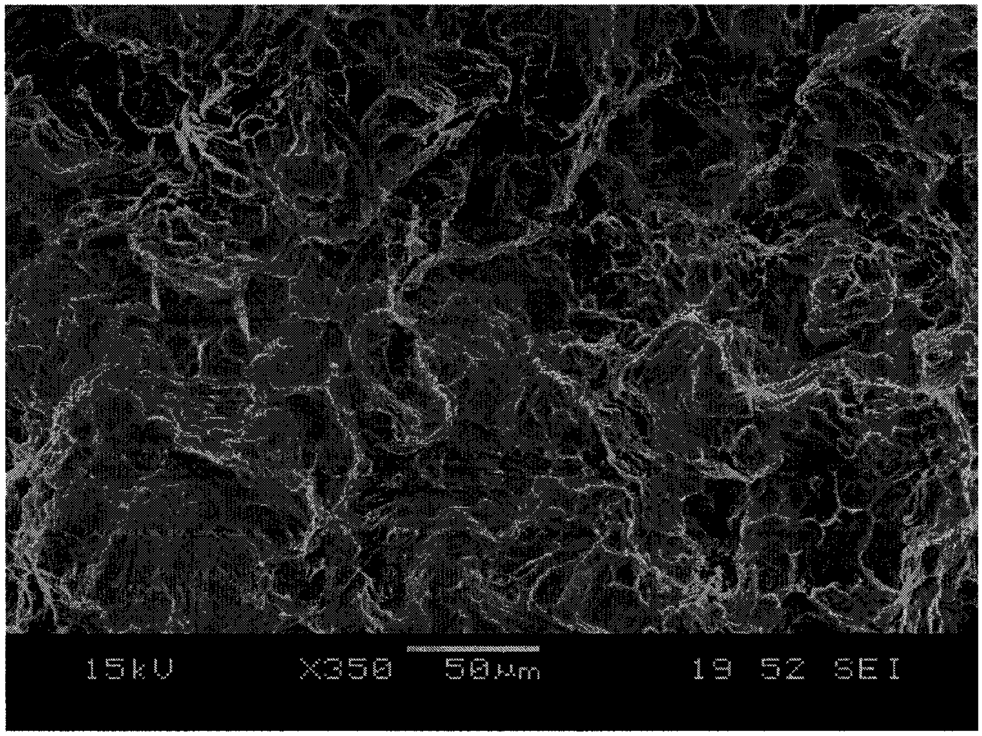

Figure 4.37 Fracture surface of a tensile specimen of the 319+Mg+Sr alloy in the as-cast state.

Figure 4.38 presents the fracture surface of a solution heat-treated specimen at the same magnification. The difference in the fracture mode between the as-cast sample and that shown in Figure 4.38 may clearly be noted as being of higher ductility, evidenced by the greater amount of smaller dimples observed. These dimples are produced as a result of the spheroidization and fragmentation of the eutectic Si phase and the dissolution of the intermetallic precipitates containing Cu and Mg in the matrix, thereby increasing the area of the ductile α-aluminum matrix which, being ductile, fails by void coalescence leaving many small dimples on the fracture surface. These observations are in good agreement with published work dealing with the fractography of this specific alloy system [46, 66, 126, 135].

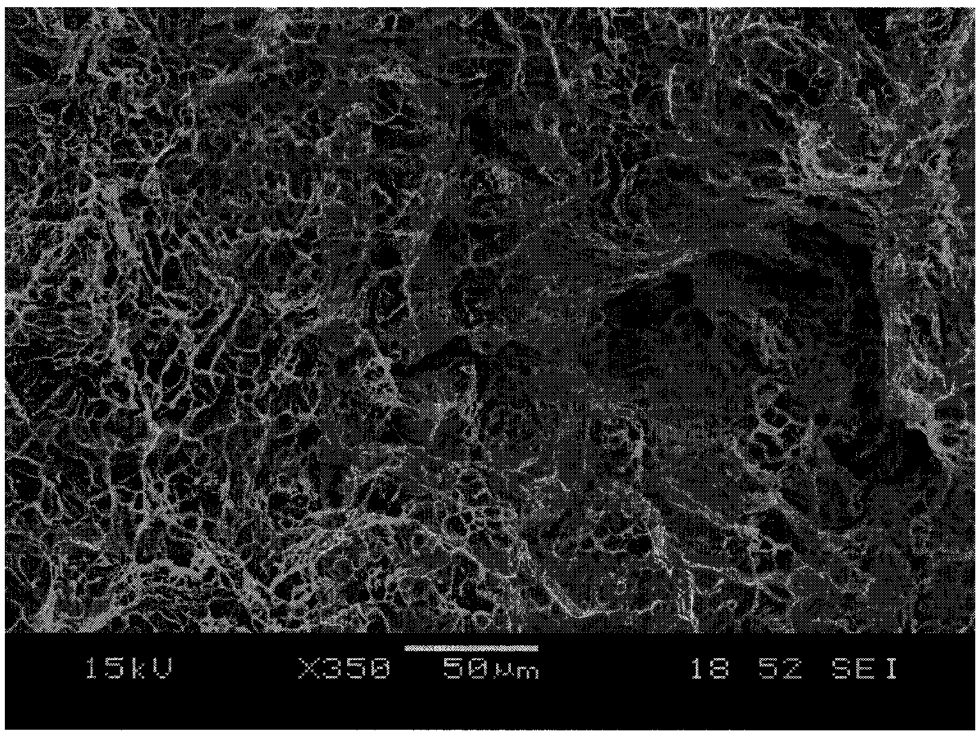

Figure 4.38 Fracture surface of a tensile specimen of the 319+Mg+Sr alloy in the solution heat-treated condition.

Figure 4.39 shows the fracture surface of a sample in the peak-aged condition (T6), aged at 170 °C for 8 h, at which the highest tensile strength was obtained. The nature of the fracture surface appears to be relatively more brittle than the fracture observed in the solution heat-treated sample.

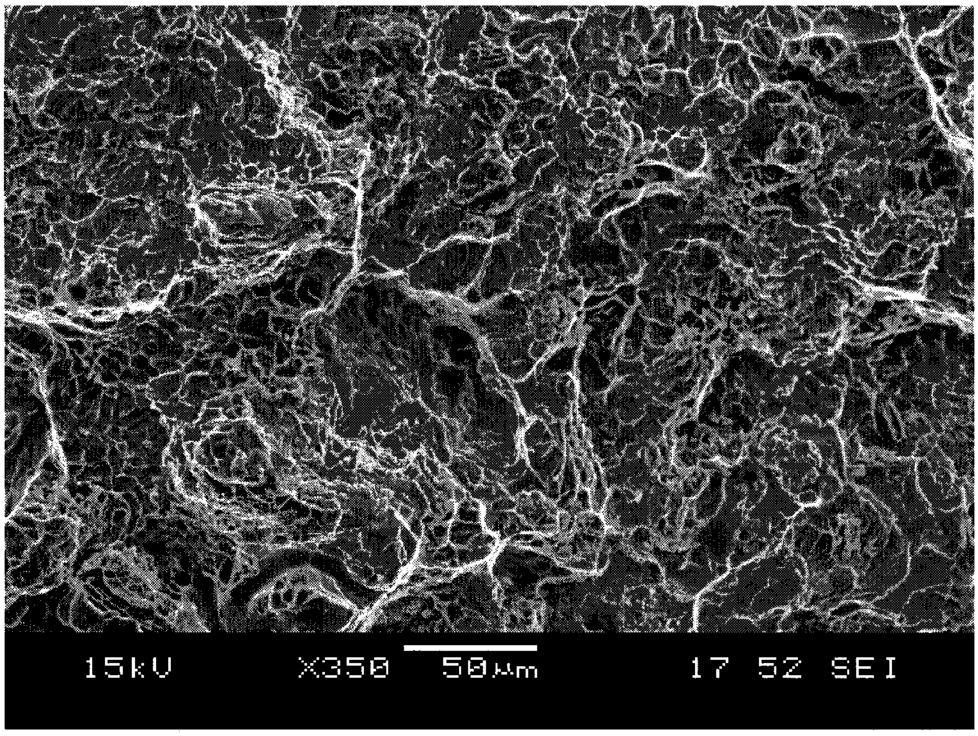

Figure 4.39 Fracture surface of a tensile specimen of the 319+Mg+Sr aged at 170°C for 8 h.

Figure 4.40, taken at a higher magnification, shows the presence of many secondary cracks in the interdendritic regions indicating that the fracture starts mostly with cracks in the Si, Al_2Cu and Fe and Mg brittle intermetallic phases, rather than at their interfaces with the matrix [46, 66, 123]. In the figure these cracks are indicated by white arrows.

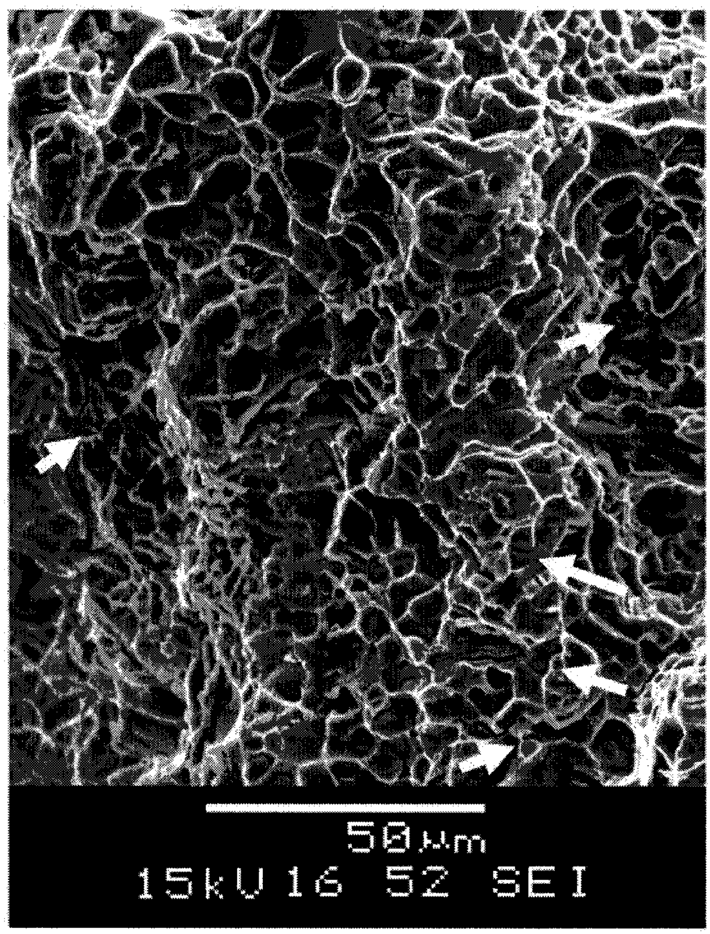

Figure 4.40 Detail of the fracture surface of a tensile specimen of the 319+Mg+Sr alloy aged at 170°C for 8.

Figure 4.41 shows a micrograph of the fracture surface of a sample in the overaged condition, aged at 240 °C for 4 h. The fracture mode is a combination of ductile and brittle fracture, the ductile part being the α-Al matrix and the brittle part pertaining to the more brittle phases such as the eutectic Si and the Cu and Mg intermetallics.

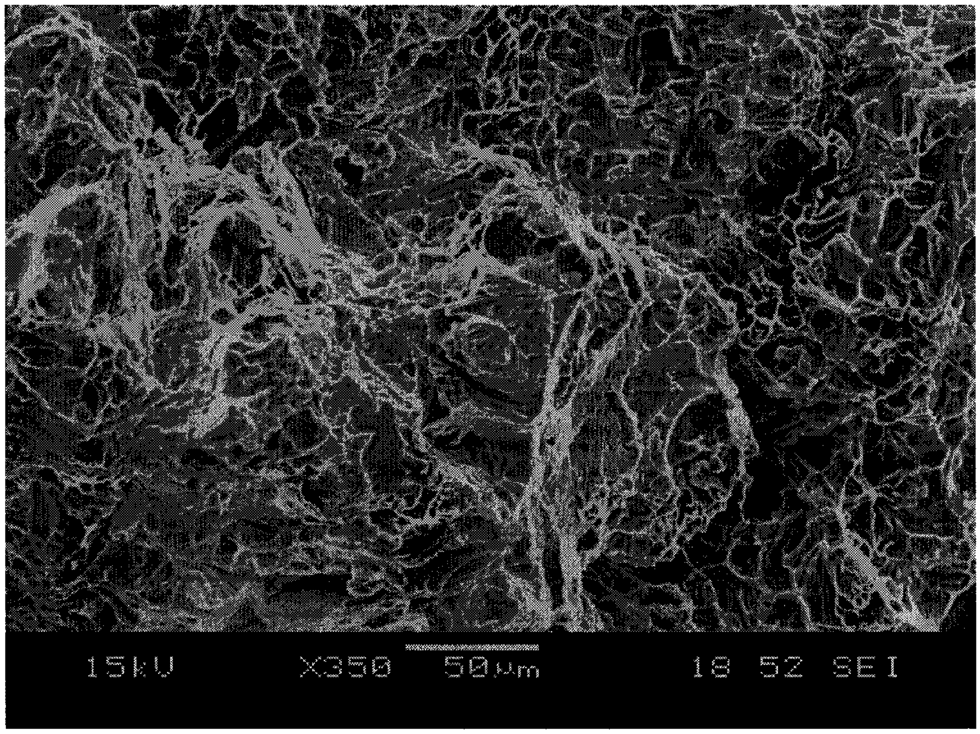

Figure 4.41 Fracture surface of a tensile specimen of the modified alloy with additions of Mg aged for 4 h at 240°C.

In the overaged condition, the precipitates coarsen beyond the critical strengthening size. This coarsening has a detrimental effect on tensile strength [9, 57, 87, 89, 92], thereby explaining why there is a decrease in the strength obtained when testing samples in this condition.

Figure 4.42 shows a brittle area of the fracture in greater detail, surrounded by the type of small dimples characteristic of ductile fracture.

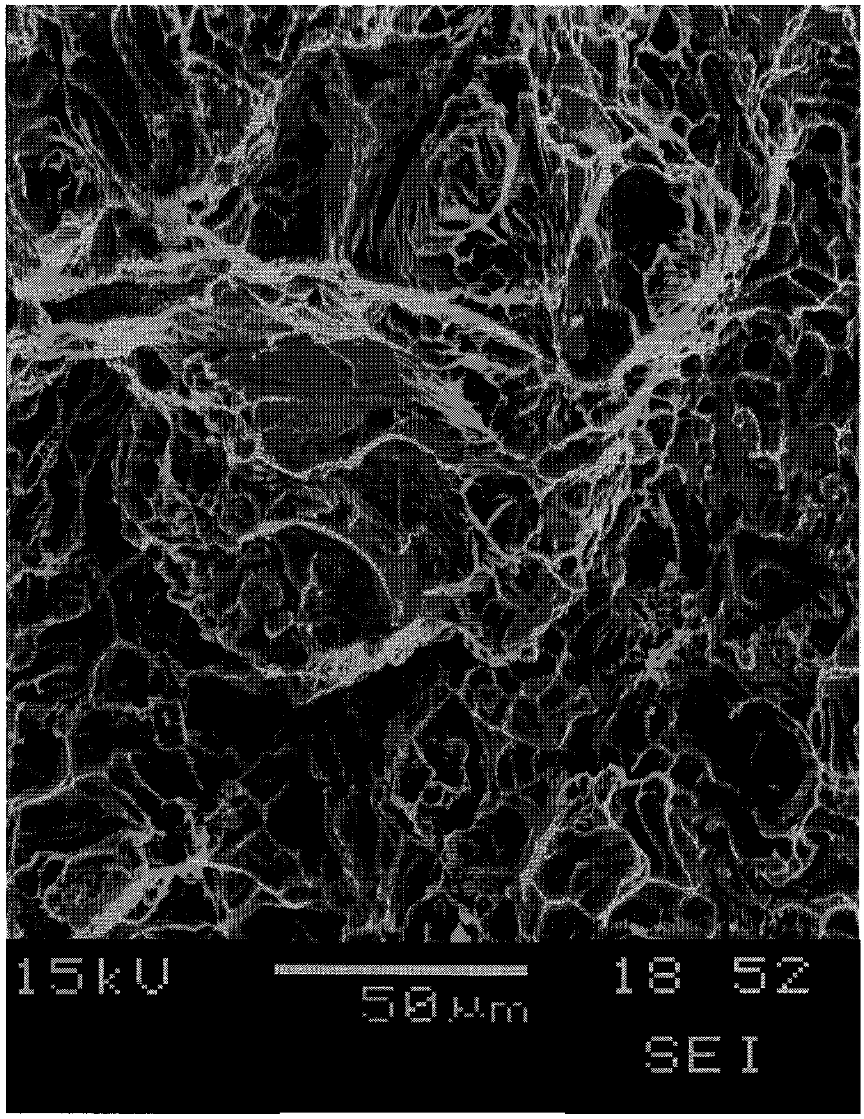

Figure 4.42 Detail of the fracture surface of a tensile specimen of the 319+Mg+Sr alloy aged at 240°C for 4 h.

Besides the change in the fracture mode observed when varying the artificial aging conditions, other noticeable features emerged during the SEM analysis. A number of these features will be presented here, including the fracture characteristics of the eutectic silicon phase.

Figure 4.43 depicts the characteristic star-shaped fracture of the brittle unmodified eutectic silicon phase. This micrograph was taken from the 319 base alloy where no Si phase modifiers such as Sr were added. Also, some secondary cracks on the brittle Si phase particles indicated by the arrows may be observed in the surrounding area.

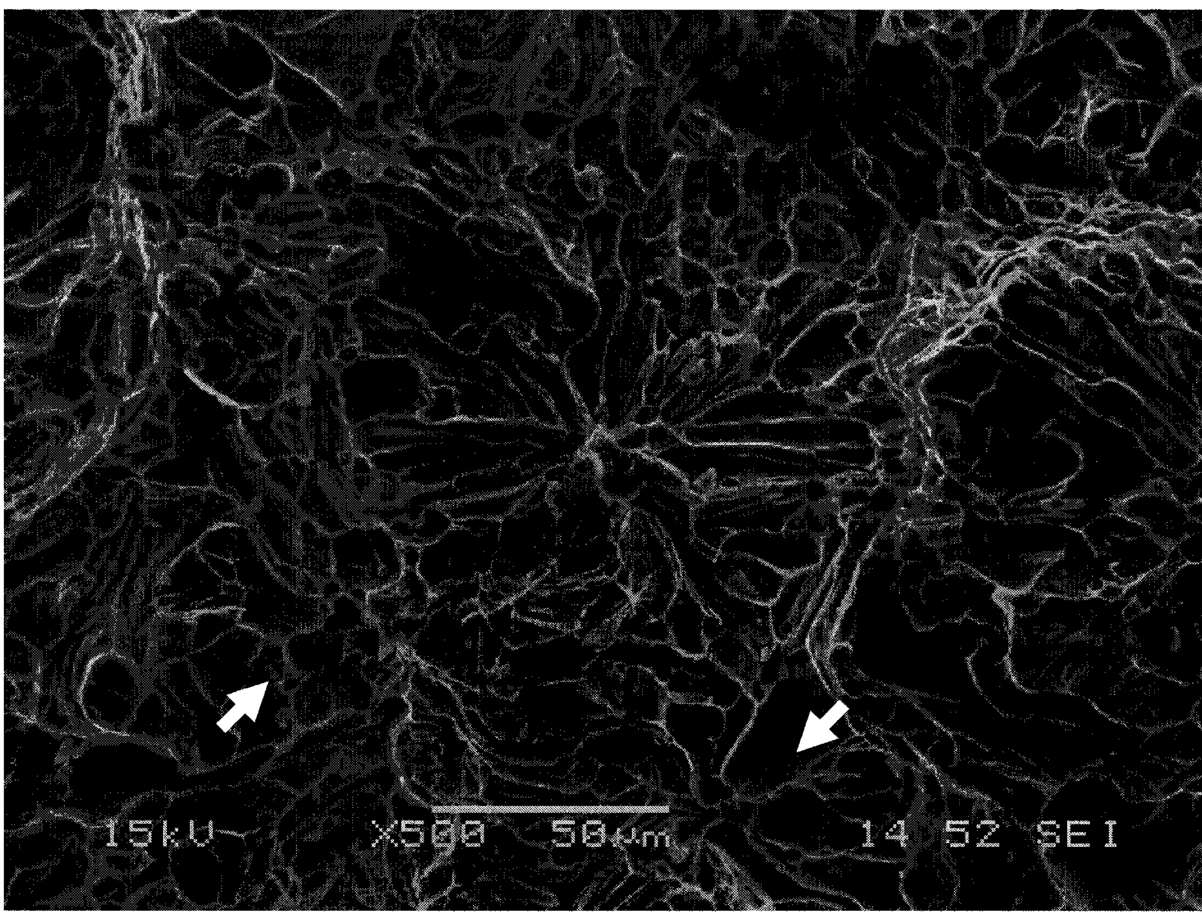

Figure 4.43 Micrograph showing the fracture surface of a tensile sample of the 319 base alloy in the absence of Sr showing the star-shaped fracture of the unmodified Si eutectic phase.

The following images are backscattered electron (BSE) images obtained from the various conditions of the alloys studied, namely, 319, 319+Sr, 319+Mg, and 319+Mg+Sr. These images provide elemental information since the contrast depends on the atomic number of the elements within the specimen. Backscattered electrons have higher energy than secondary electrons and are thus less influenced by any electronic charge build-up, in non-conductive areas of the specimen such as oxides or surface contaminants. The amount and direction of backscattered electrons vary with: (i) chemical composition of the sample (higher atomic number elements appear brighter than lower atomic number elements), (ii) surface topography, (iii) crystallinity and (iv) magnetism of the specimen [138, 140, 141].

The bright areas in the following images consist of precipitates containing heavier elements such as Cu. A polished sample was used to take the BSE image, in view of the fact that it is difficult to analyze the chemical composition of constituents appearing on the surface of fractured specimens due to the topography. Figure 4.44 shows this image with the typical precipitates which appear in this type of alloy, while Figure 4.45 shows the three EDS spectra corresponding to the positions shown in Figure 4.44. In the spectra, the presence of Au is due to the fact that this element was used to coat the sample in order to render it conductive since it was mounted in bakelite.

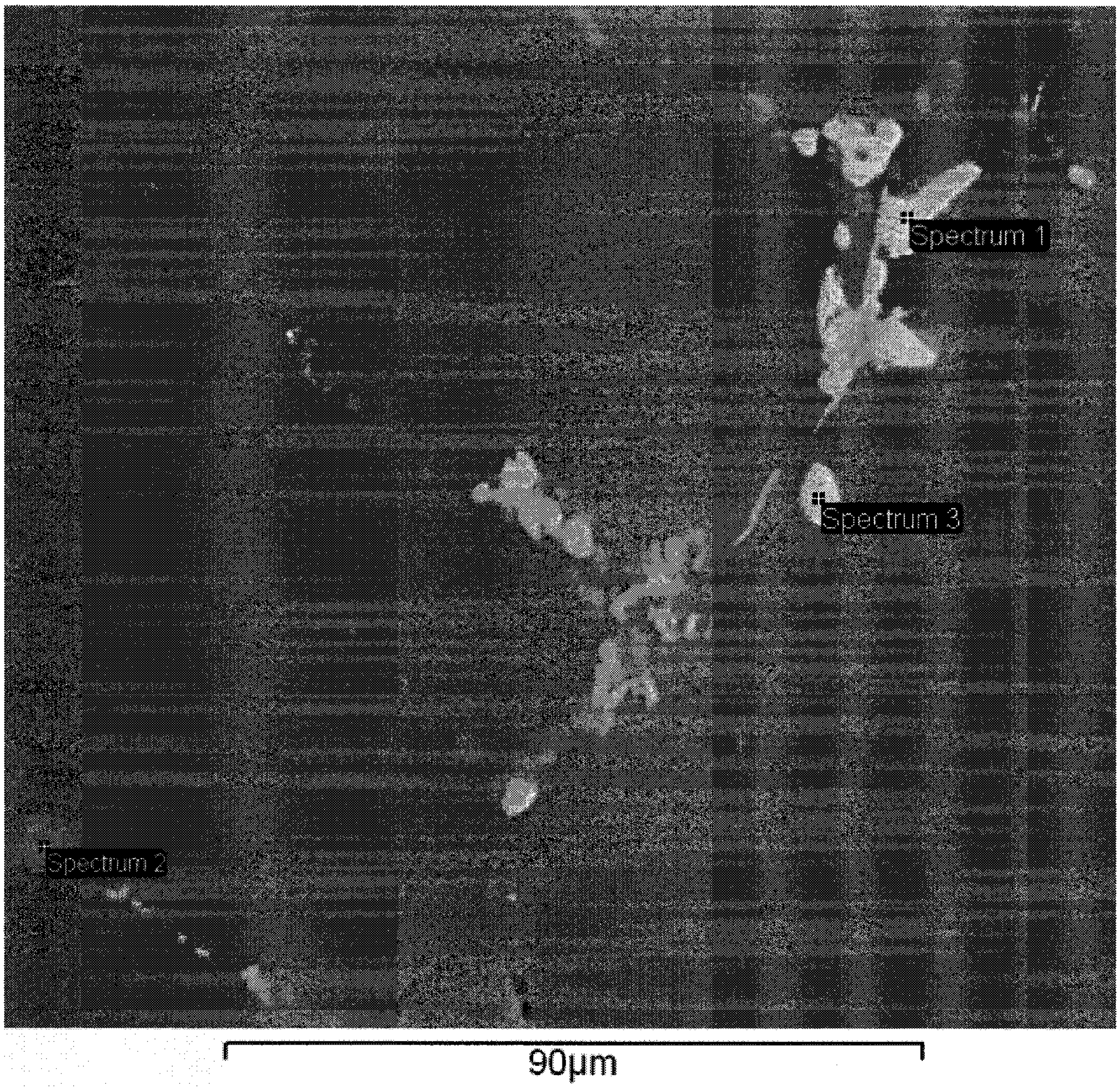

Figure 4.44 BSE image obtained from a polished sample of the 319+Mg+Sr alloy.

Spectra 1 and 3 show the presence of Cu, while spectrum 2 shows the presence of both Cu and Mg. The brighter, white precipitates contain Cu and the grey ones contain Mg. These particles appear together in the same area, and as will be seen in Figure 4.44, smaller Mg-containing phases appear around or very close to those containing Cu. The presence of these precipitates is typical of the alloy and they do not change when experimentally varying the aging conditions –an indication that the mechanisms which operate in artificial aging cannot be detected with the SEM analysis.

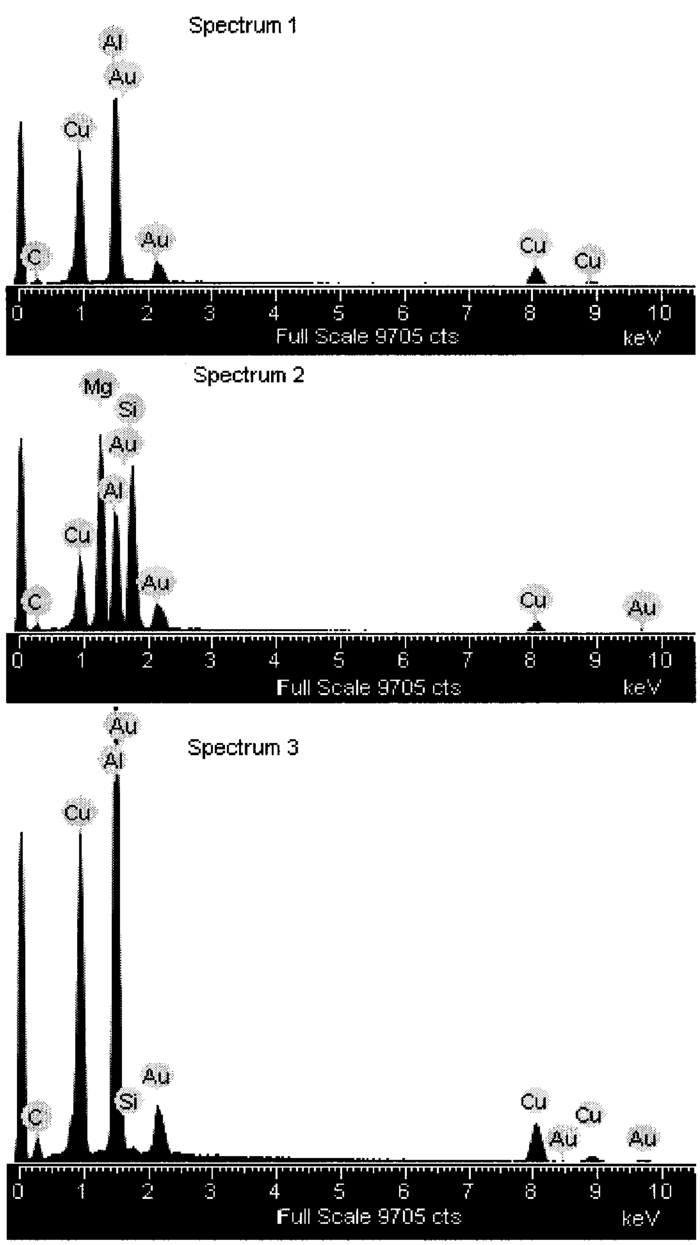

Figure 4.45 Spectra corresponding to the positions shown in Figure 4.44.

The segregation of the Cu-containing phases occurs when the alloy is modified with Sr [64, 73], this effect becomes apparent when the scanning electron microscope is applied for fracture surface analysis. Figures 4.46 through 4.49 show backscattered electron micrographs of the four alloys used in this study. Figure 4.46 corresponds to the 319 base alloy; Figure 4.47 corresponds to the 319+Mg alloy; Figure 4.48 shows the 319+Sr alloy; and, lastly, Figure 4.48 shows the 319+Mg+Sr alloy.

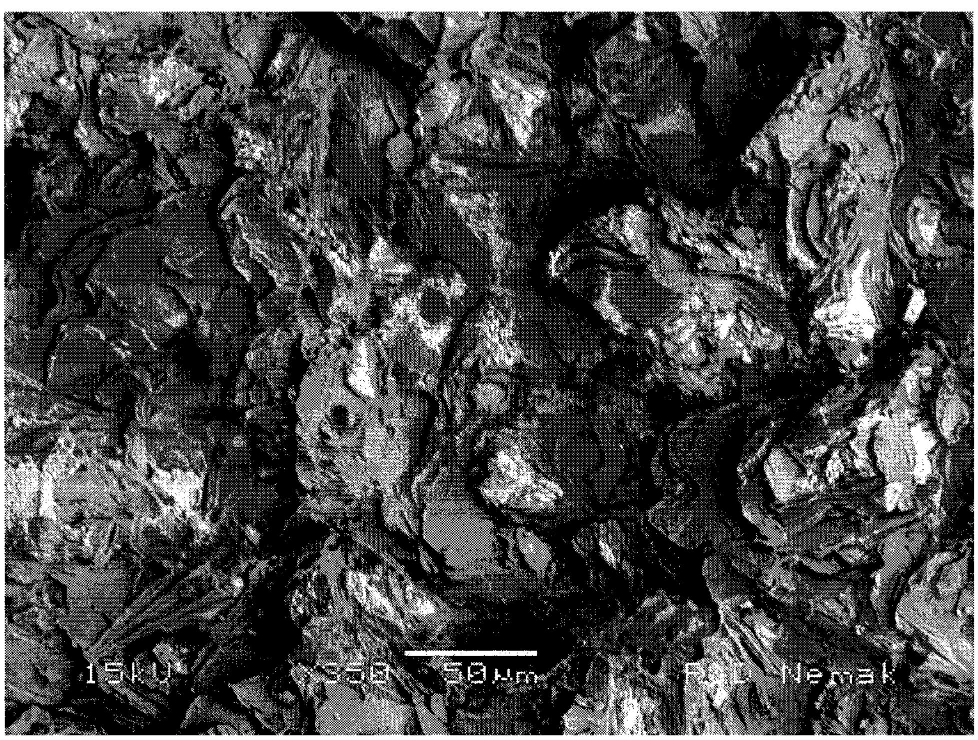

Figure 4.46 BSE image of the fracture surface obtained from alloy 319 (as-cast condition).

All of these micrographs were obtained from the fracture surfaces of the corresponding as-cast samples. No noticeable difference is observed when comparing the images in Figures 4.46 and 4.47, considering that they correspond to alloys which have not been modified with Sr. It should be noted that a few bright areas observed in these images correspond to the Al_2Cu phase.

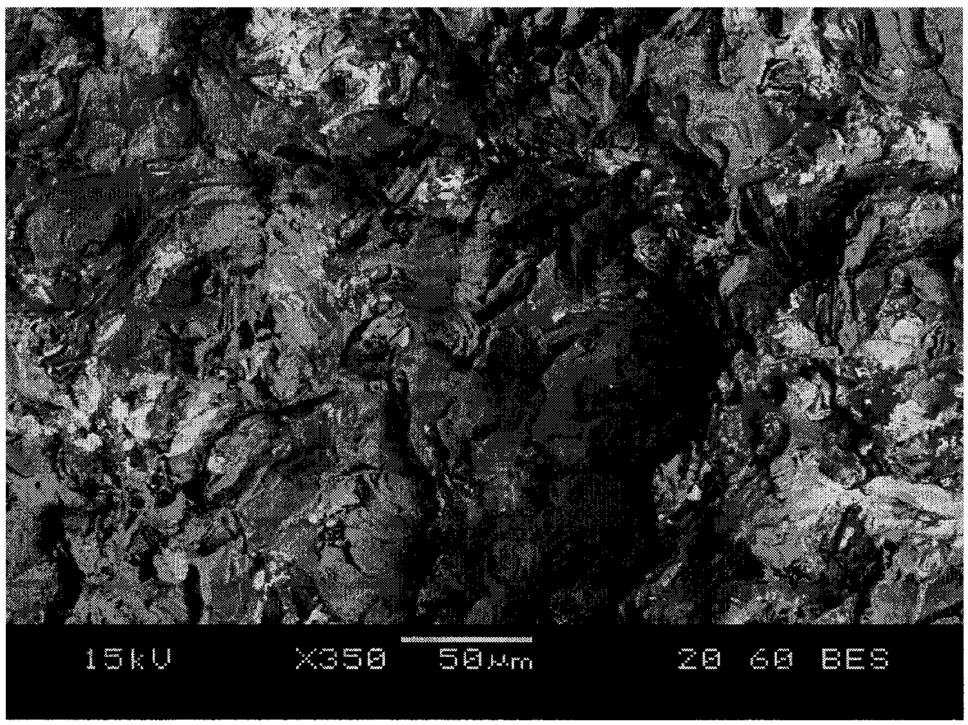

Figure 4.47 BSE image of the fracture surface obtained from the 319+Mg alloy (as-cast condition).

Figures 4.48 and 4.49 correspond to the Sr-modified alloys. The larger extents of bright areas on the fracture surfaces of these samples indicate that more Cu-phases are present on the surface.

The process of modification leads to an increase in the amount of Si particles in the aluminum matrix. These Si particles serve as nucleation sites for the Al_2Cu

phase. Although the precipitation of the Al_2Cu phase is not prevented by the modification process the segregation effect tends to predominate [64, 73]. This effect is demonstrated by the micrographs presented in Figures 4.46 to 4.49, also artificial aging practices do not have a significant effect on avoiding or promoting this phenomenon.

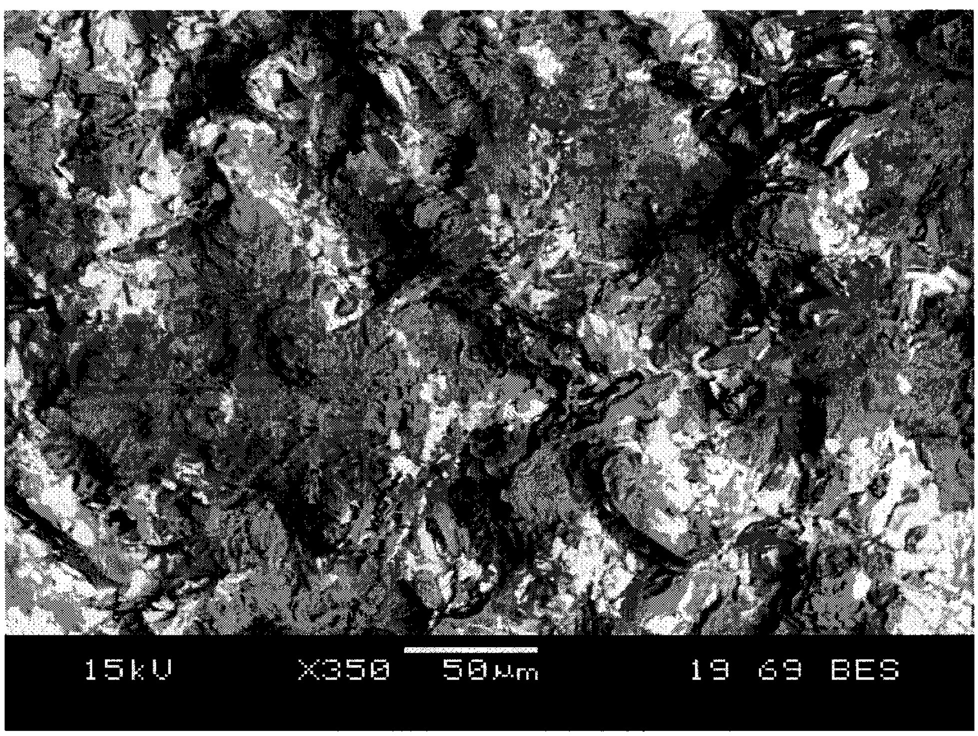

Figure 4.48 BSE image of the fracture surface obtained from the 319+Sr alloy (as-cast condition).

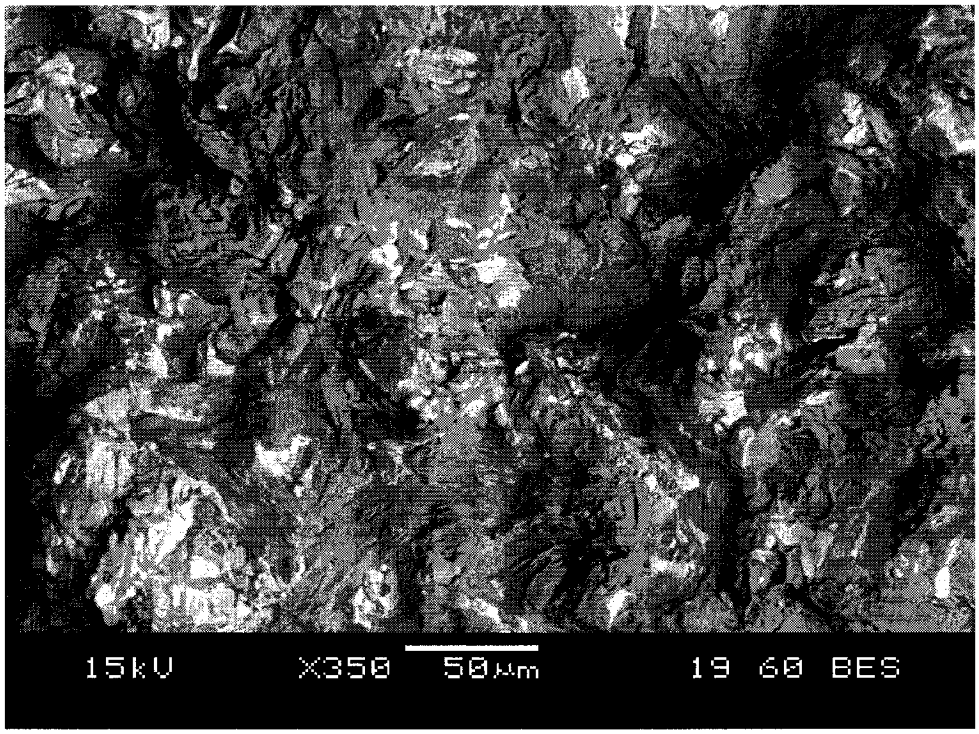

Figure 4.49 BSE image of the fracture surface obtained from the 319+Mg+Sr alloy (as-cast condition).

A further feature observed when using the scanning electron microscope is decohesion of the Si particles which occurs at the overaged stage, when the aging is performed at the higher temperatures used for this study namely, 220°C and 240°C. A loss of strength and hardness is generally observed when aging is carried out at these temperatures, while a slow recovery of percent elongation and total absorbed impact energy usually occurs at this time [9, 19, 58, 78, 137]. The BSE micrograph images shown in Figures 4.50 and 4.51 were obtained from the 319+Sr alloy aged at 240°C, revealing this effect.

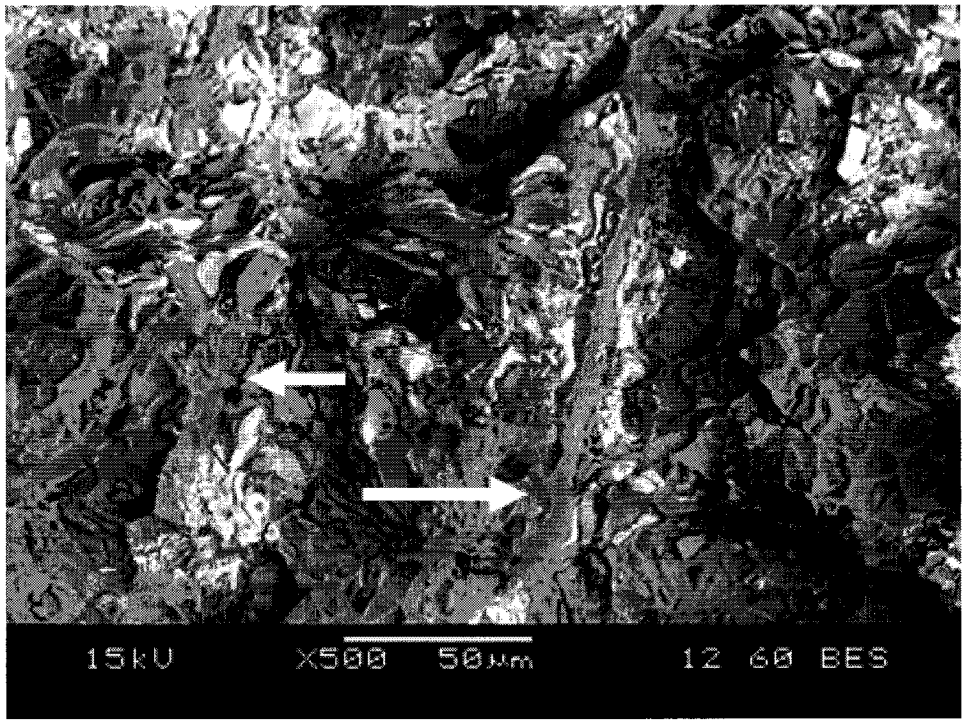

Figure 4.50 BSE image of the fracture surface obtained from the 319+Sr alloy (aged at 240°C for 2 h).

The regions marked with white arrows in Figures 4.50 and 4.51 show the site where the fracture and decohesion of Si particles takes place. As aging time is increased, this effect becomes more marked. Figure 4.51 shows the fracture surface of a sample of the same alloy aged at the same temperature for a greater length of time, namely, 8 hours. The magnification shown in Figure 4.51 is lower than in the previous figures, to demonstrate that the same type of fracture and decohesion of Si particles occurs over the entire surface as if in a network.

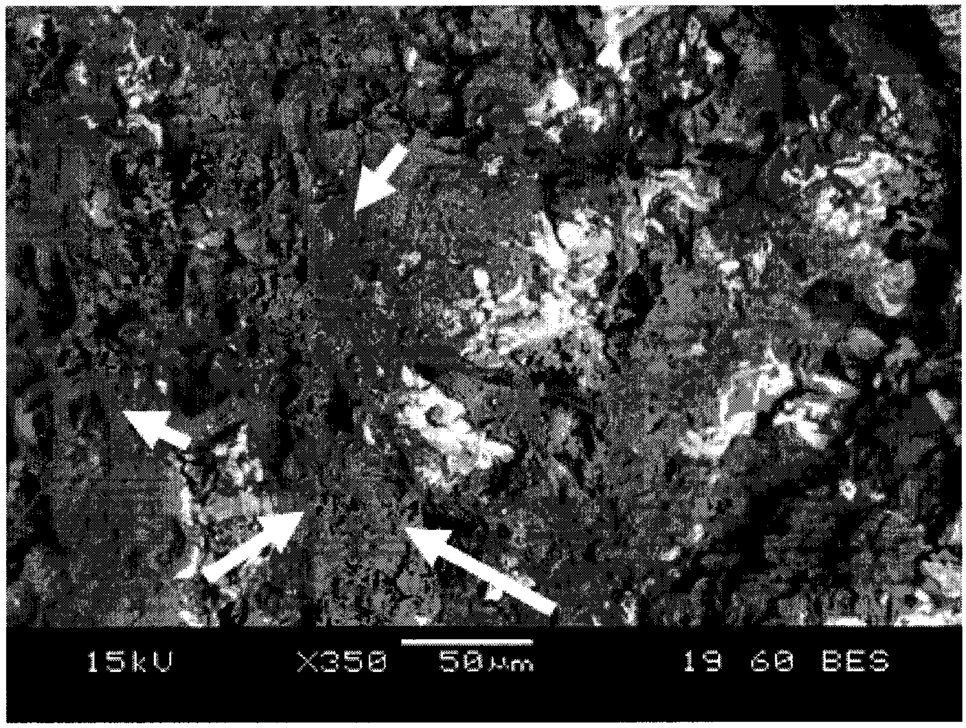

Figure 4.51 BSE image of the fracture surface obtained from the 319+Sr alloy (aged at 240°C for 8 h).

The soundness of the casting is of major importance when taking the mechanical properties of the cast alloy into consideration, since casting defects such as increased porosity and the presence of inclusions often affect the performance of the product [122-124]. Very few samples in this study displayed the above-named defects: about 4 or 5 samples per 250-sample batch, representing approximately 2% of the total of samples produced. The values which were affected were the UTS, the percent elongation and the total absorbed impact energy. In such cases, when the results of the test were affected, they were excluded from the analysis.

Figure 4.52 presents a micrograph showing several oxide inclusions in a sample obtained from the 319+Mg alloy in the as-cast condition. Since the oxides are non-conductive, they become electronically charged and appear as bright particles in secondary electron images of the fracture surface [138]. It is expected that these oxide inclusions would appear on the fracture surface since they tend to act as stress raisers and cause the material to fail.

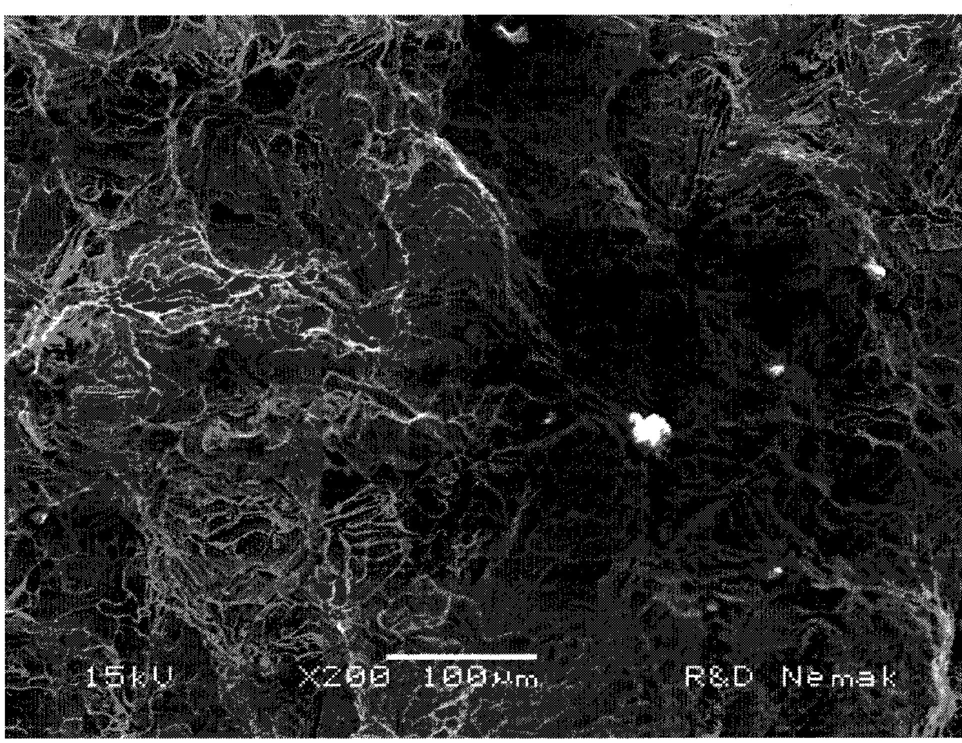

Figure 4.52 Micrograph showing oxide inclusions present in a sample obtained from the 319+Mg alloy (as-cast condition).

Figure 4.53 shows a BSE image obtained from the fracture surface of a tensile test sample of the 319+Mg alloy where a certain amount of porosity may also be observed. The presence of pores is clear from the smooth surface of the dendrites appearing on the left side of the image. This sample was aged at 240°C for 8 h and small precipitates may be observed, in the form of tiny bright spots, on the smooth surface of the dendrites indicated by arrows.

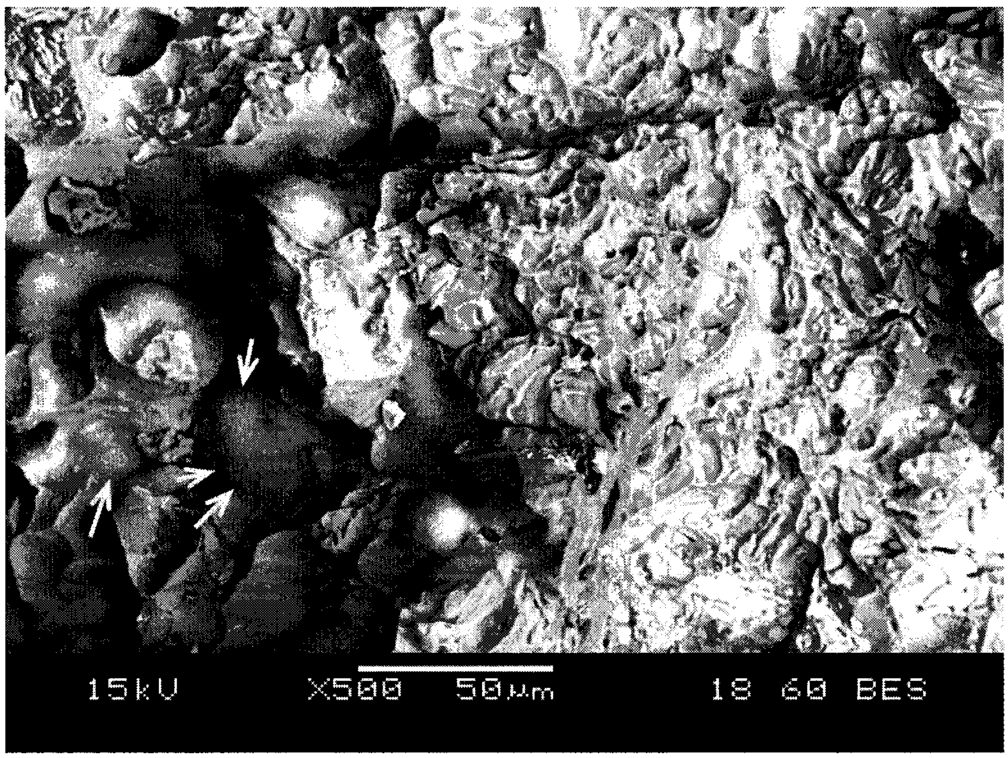

Figure 4.53 BSE image of a fracture surface obtained from a tensile test specimen of the 319+Mg alloy aged at 240°C for 8 h.

4.4.2 Transmission Electron Microscopy

Transmission electron microscopy was used in order to study the effects of aging in greater depth, by using an instrument with hightened resolution capacity so as to facilitate identifying the precipitates present in the aluminum dendrites. The following sections will present images obtained from samples aged under continuous aging regimes versus multi-temperature aging cycles for comparison purposes.

4.4.2.1 Images Obtained from Samples after Continuous Aging Treatments

Figure 4.54 shows a micrograph of the microstructure observed in the as-cast 319+Mg+Sr alloy; unless otherwise indicated, all the images presented in this section were obtained from samples of this alloy. No heat treatment was applied to this material; thus the presence of large particles (~0.75 μm) of Si and $TiAl_3$ is to be observed in the microstructure.

Figure 4.55 shows the EDS spectrum obtained from the matrix and Figure 4.56 shows a selected area diffraction (SAD) pattern obtained exclusively from the α-Al matrix. An analysis of the pattern obtained reveals the interplanar distances of the diffracting planes (111) and (220), 2.32 Å and 1.41 Å, respectively. The zone axis is $[\bar{1}12]$.

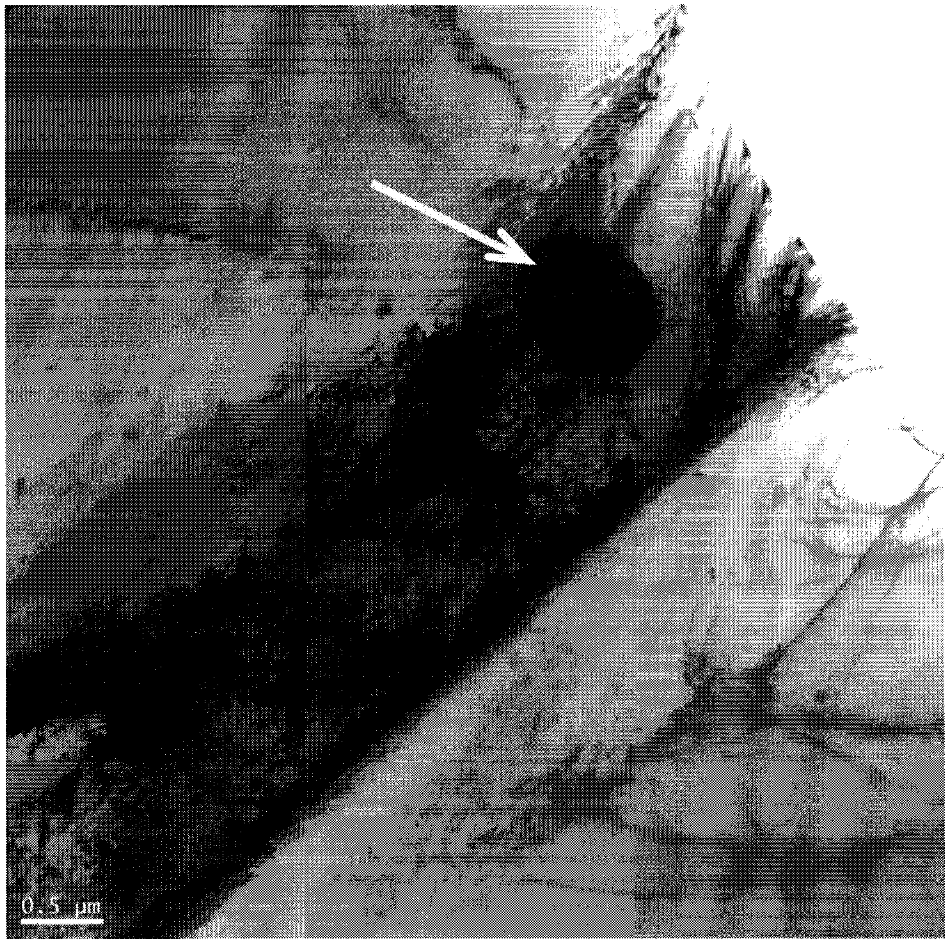

Figure 4.54 Bright Field TEM image of the microstructure observed in the as-cast 319+Mg+Sr alloy.

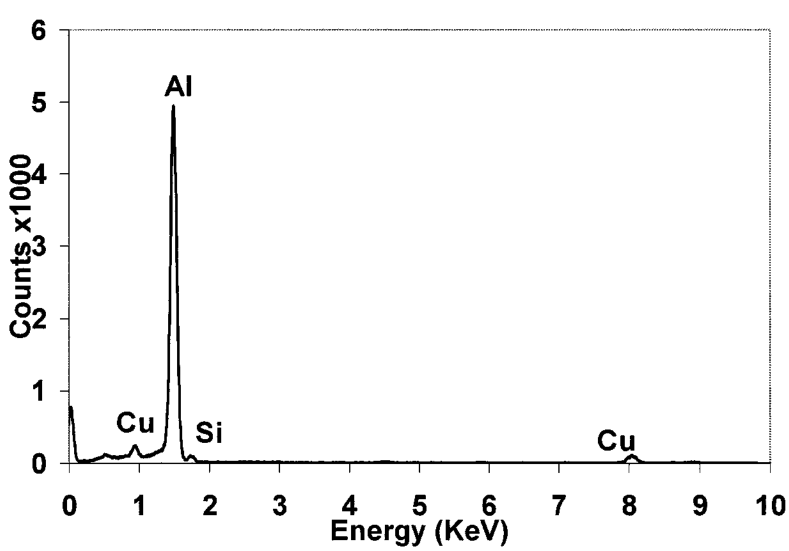

Figure 4.55 EDS spectrum obtained from the matrix in Figure 4.54.

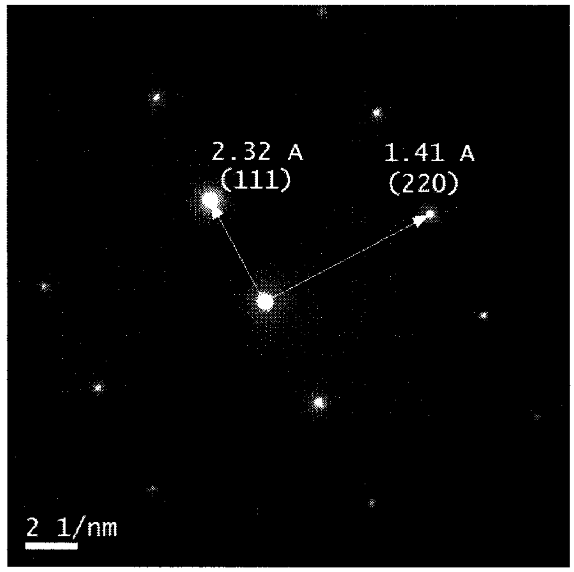

Figure 4.56 SAD pattern of the aluminum matrix shown in Figure 4.54.

Figure 4.57 shows the EDS spectrum taken from the particle, showing a large Si peak; when comparing both spectra in Figures 4.55 and 4.57, a clear difference may be observed between the Si peaks. In order to obtain further information on the large Si particle observed in Figure 4.54 indicated with the arrow, the sample was tilted following the Kikuchi lines to obtain different diffraction patterns at several zone axes. These patterns, as obtained from several zone axes, are presented in Figures 4.58 to 4.60. It should be noted that, included in the image are the interplanar distances of the diffracting planes as well as the angles to which the sample was tilted.

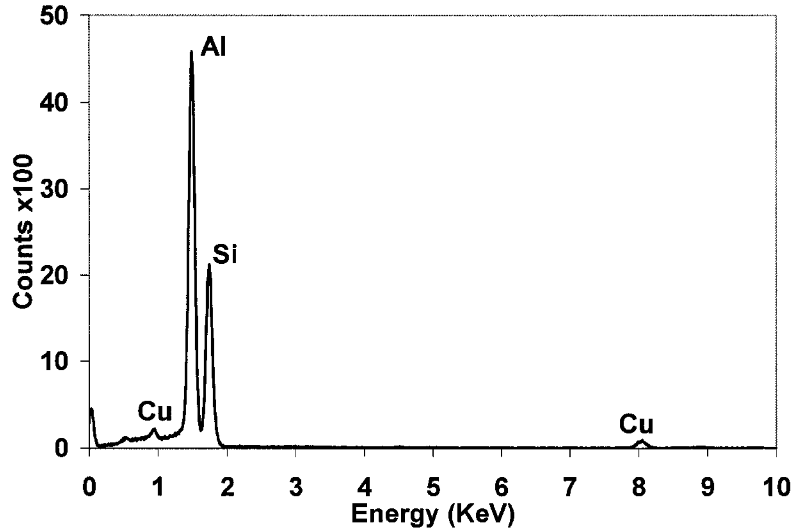

Figure 4.57 EDS spectrum obtained from the large dark particle observed in Figure 4.54.

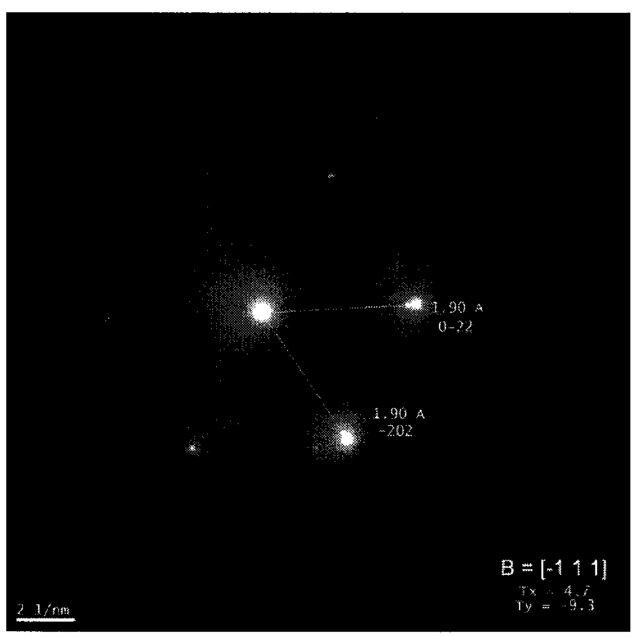

Figure 4.58 SAD pattern of the Si particle in Figure 4.54, zone axis [$\bar{1}$ 1 1].

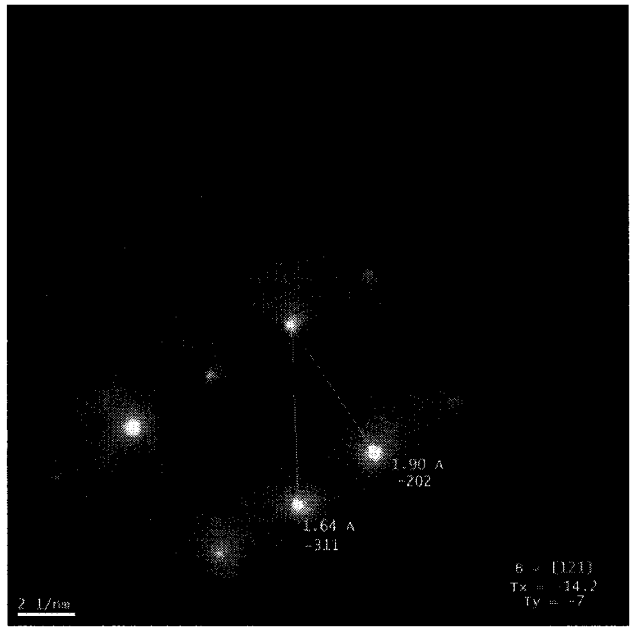

Figure 4.59 SAD pattern of the Si particle in Figure 4.54, zone axis [1 2 1].

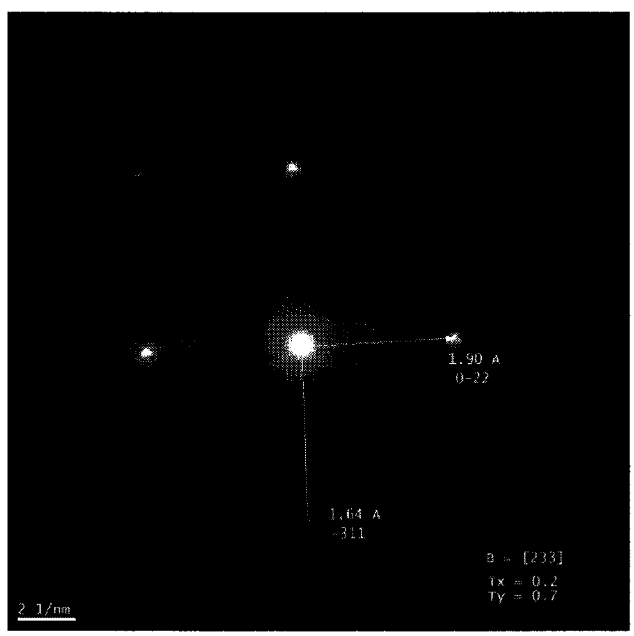

Figure 4.60 SAD pattern of the Si particle in Figure 4.54, zone axis [2 3 3].

In this as-cast condition of the alloy, some $TiAl_3$, $Al_{15}(Fe,Mn)_3Si_2$ and undissolved Cu-rich phases were identified as well. Figure 4.61 shows an image of the same sample taken in scanning transmission electron microscope (STEM) mode where these particles are present.

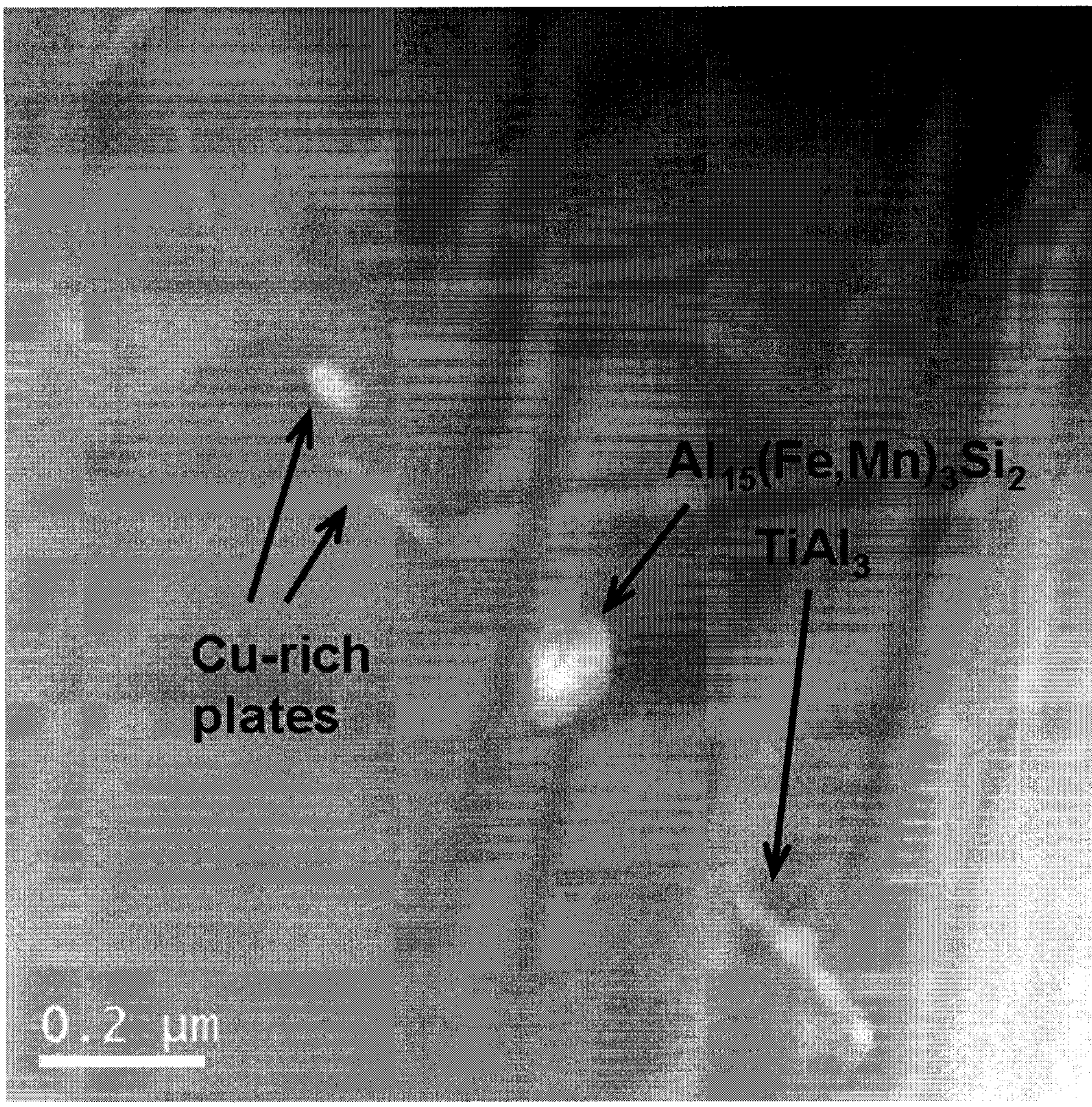

Figure 4.61 STEM image of the as-cast sample (319+Mg+Sr alloy) showing elongated Cu-rich precipitates, $TiAl_3$ and $Al_{15}(Fe,Mn)_3Si_2$ particles.

Figure 4.62 shows the corresponding EDS spectrum of the Ti_3Al and $Al_{15}(Fe,Mn)_3Si_2$ particles seen in Figure 4.61. It is of interest to observe the presence of the peaks produced by Fe, Mn and Ti.

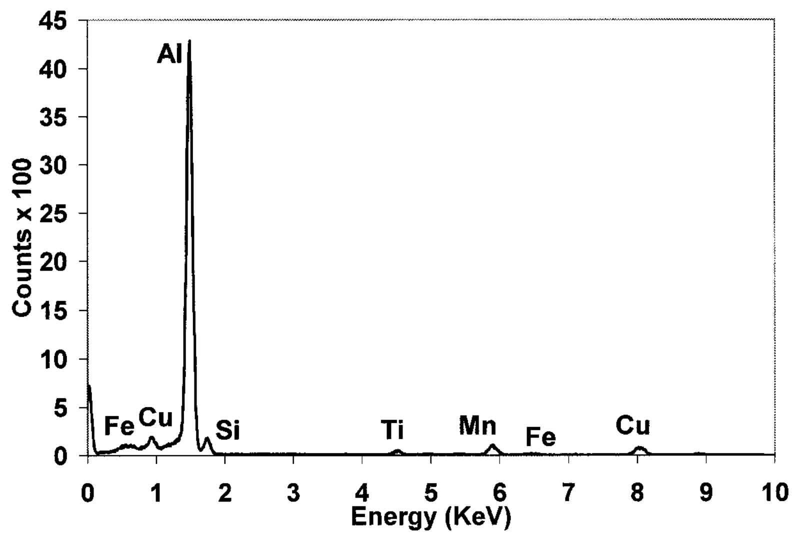

Figure 4.62 EDS spectrum of the Ti_3Al and $Al_{15}(Fe,Mn)_3Si_2$ particles shown in Figure 4.61.

When a solution heat treatment is applied to the material, some undissolved $TiAl_3$ and Si plates may still be observed, although they are much smaller in size than the ones present in the as-cast condition. Figure 4.63 shows a bright field TEM image of a 319+Mg+Sr sample in the solution heat-treated condition where Si plates may be observed, as indicated by the white arrows. Elongated particles of Ti_3Al may also be observed, and are marked with black arrows. Dislocations may be observed in Figure 4.63; they can be seen more easily, however, in the bright field image presented in Figure 4.64.

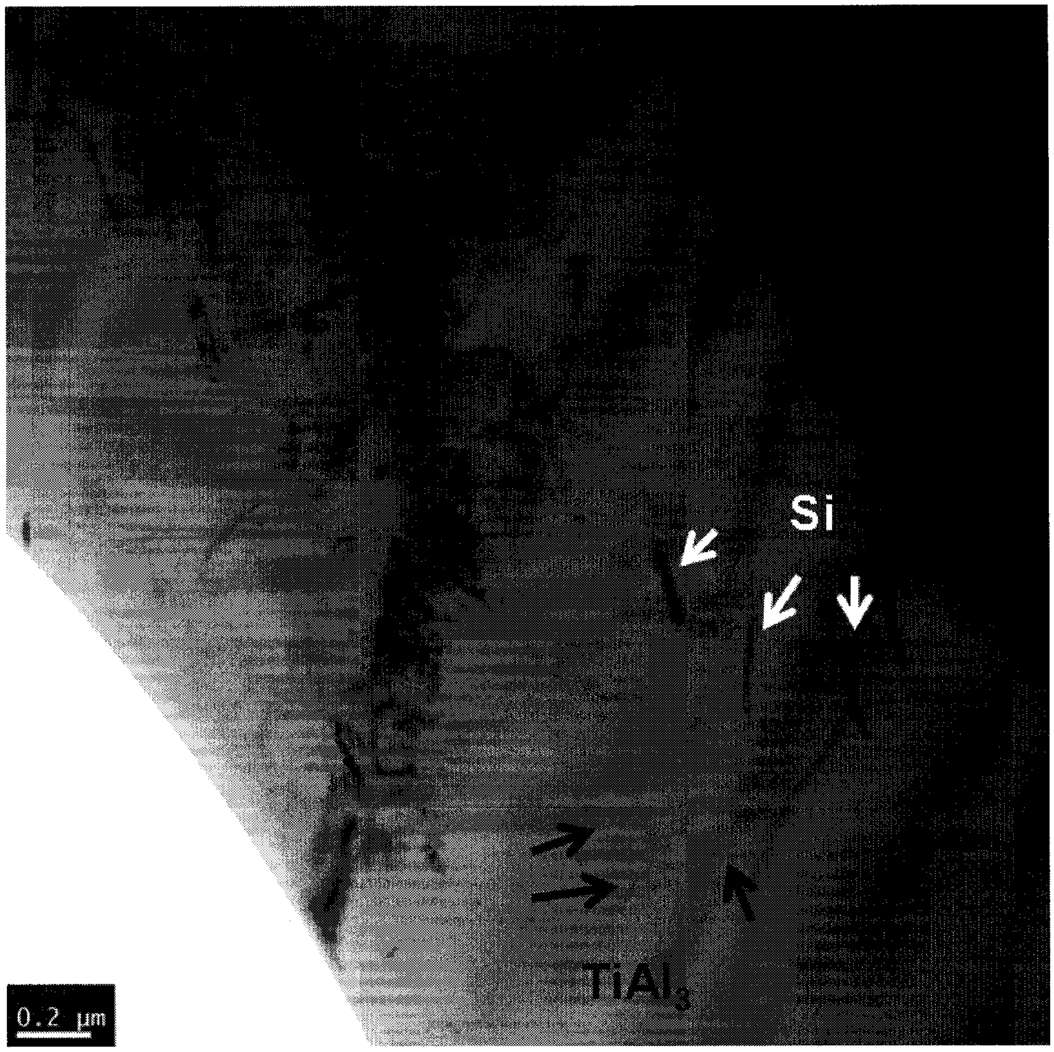

Figure 4.63 Bright field TEM image of a sample of the 319+Mg+Sr alloy in the solution heat-treated condition.

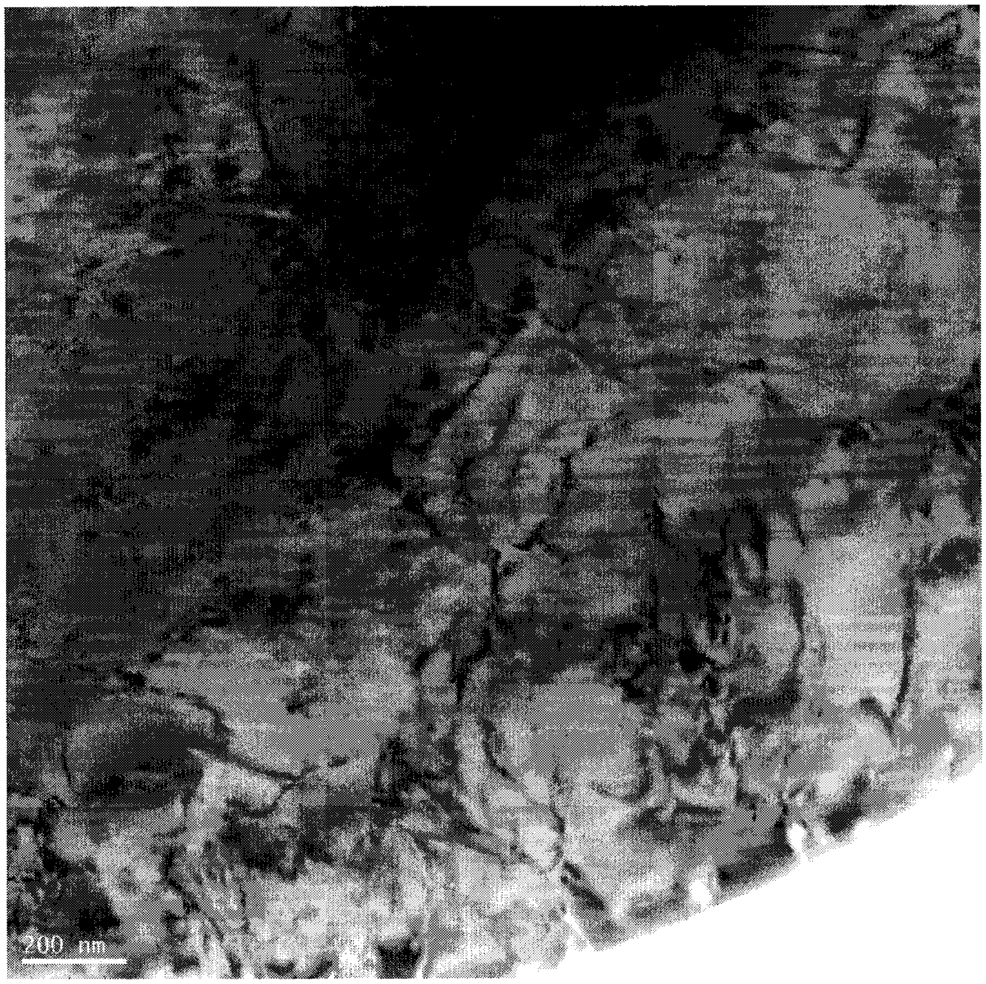

Figure 4.64 Bright field TEM image of the sample in the solution heat-treated condition showing the dislocation tangles (alloy 319+Mg+Sr).

The difference in coefficients of thermal expansion between the matrix and the intermetallic phases present will cause dislocations to appear. These dislocations release thermal stress generated during the quenching from the high solution treatment temperature and tend to form tangles together with the equiaxed Si particles present in the α-Al matrix [87, 89, 102].

The dark field image corresponding to Figure 4.64 is shown in Figure 4.65 where precipitates in the form of rods may be observed. EDS analysis reveals that they contain both Cu and Mg, leading to the conclusion that they constitute the ternary phase S-$CuMgAl_2$ which does not dissolve with solution heat treatment [101].

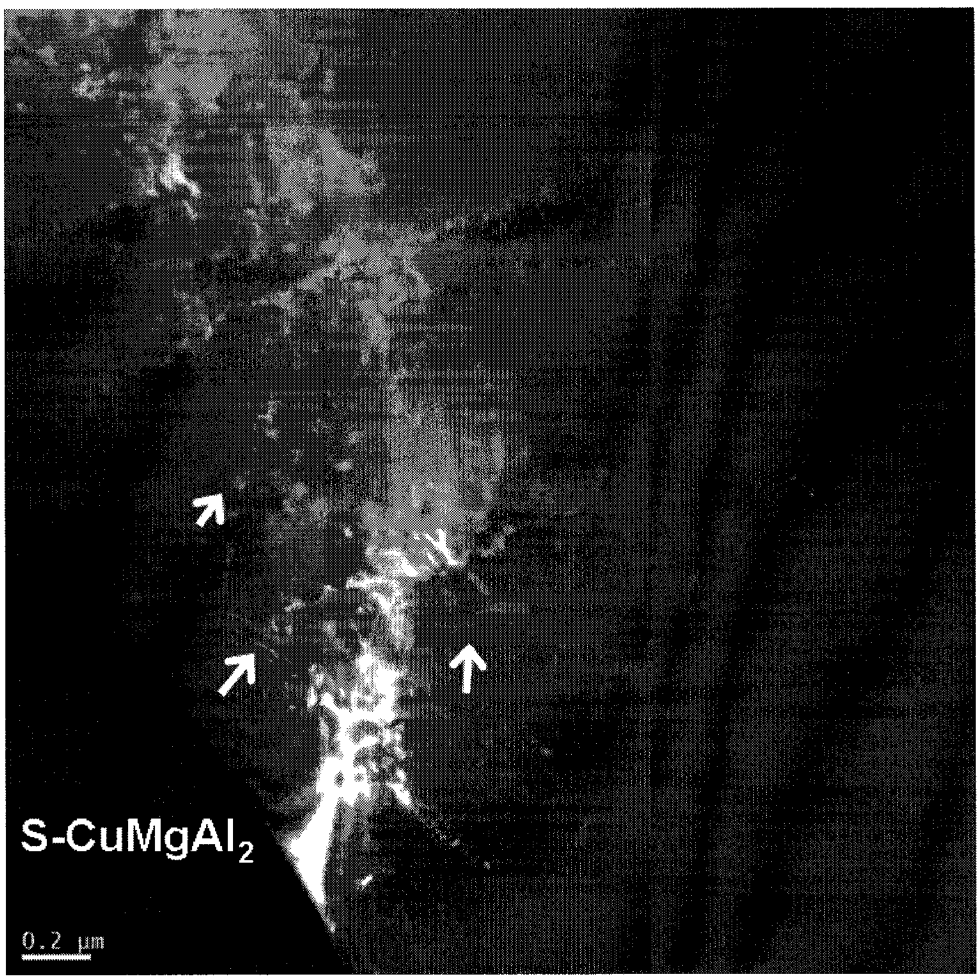

Figure 4.65 Dark field TEM image of the sample in the solution heat-treated condition showing $CuMgAl_2$ precipitates (alloy 319+Mg+Sr).

A further interesting feature which may be observed in this specimen is the particular appearance of the dislocation movement in a zigzag fashion within the matrix, presented in detail at a higher magnification in Figure 4.66.

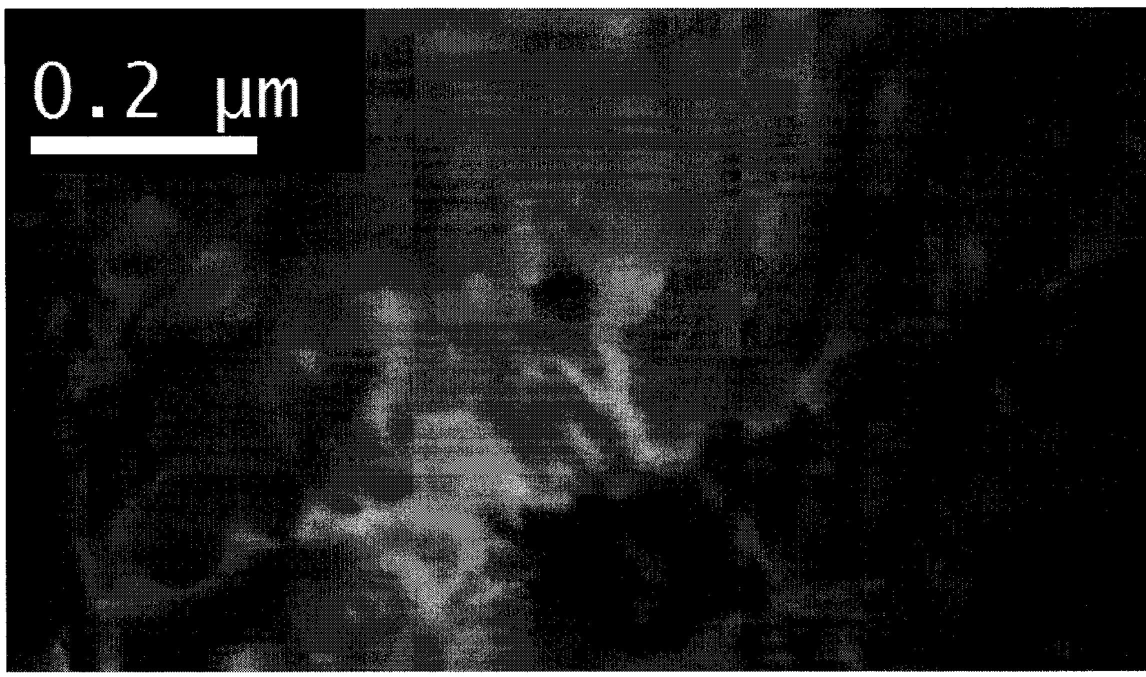

Figure 4.66 High magnification detail of the dislocations present in the solution heat-treated sample shown in Figure 4.64 (alloy 319+Mg+Sr).

Figure 4.67 shows a bright field image of the same sample. The image was obtained in a double beam condition near the [001] zone axis. The morphology of the equiaxed Silicon particles is more evident, these particles are marked with the white arrows. Small β-Mg_2Si plate precipitates, slightly bigger than the Si equiaxed particles, can be observed as well. These particles measure approximately 50x10 nm which is in good agreement with the literature [85, 103, 105, 106, 109, 111, 114]. These precipitates are marked with black arrows in Figure 4.67.

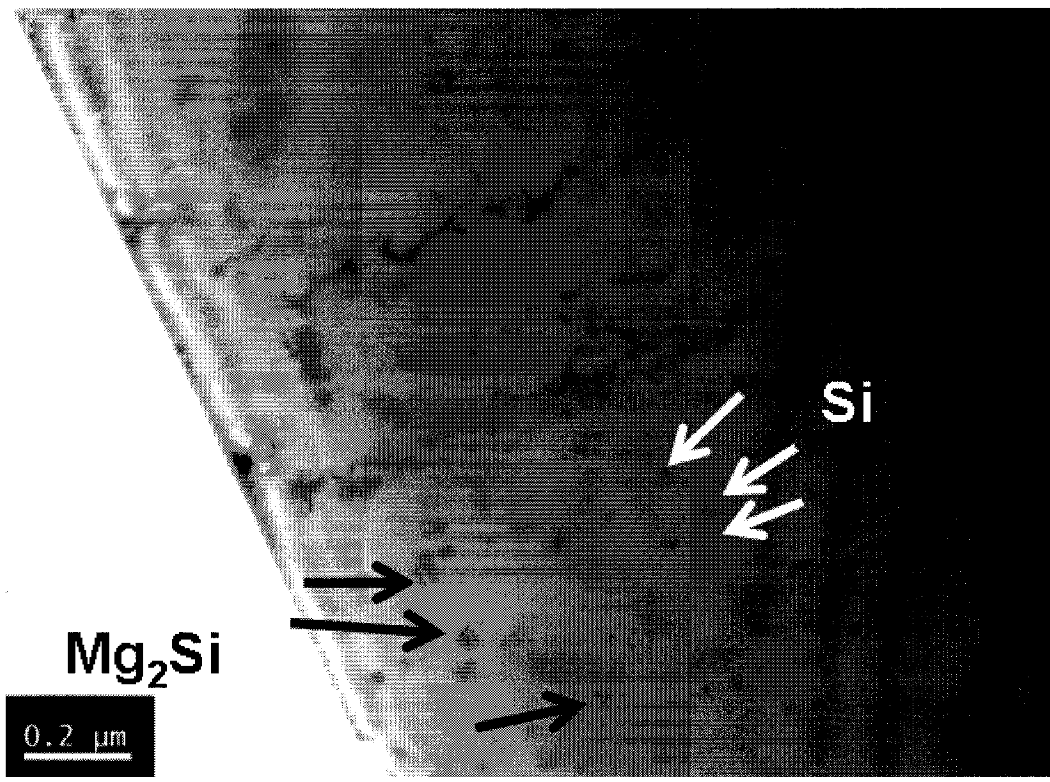

Figure 4.67 Bright Field TEM image of the sample in the solution heat-treated condition showing Mg_2Si and Si precipitates.

It is possible that the β phase particles present in the matrix did not dissolve since the solution temperature required to dissolve the Mg present in the alloy is usually higher than the temperature used for this research work [5, 58, 78, 137]. For example, the solution temperature generally used for ternary Al-Si-Mg alloys, such as alloy 356, is ~540°C; alloys of the 319-type, however, contain Cu and therefore, the solution temperature should be kept at a lower level (maximum

500°C) to avoid the incipient melting of the Cu-rich phases during the solution treatment [64, 70, 72, 73], a situation which would be detrimental in terms of the mechanical properties.

Figure 4.68 shows a bright field TEM image of a sample aged at 170°C for 4 h; at this point in the aging process the hardening effect is instigated. The microstructure consists of large sized elongated precipitates undissolved by the solution heat treatment, and tiny needlelike Al_2Cu precipitates.

Figure 4.68 Bright field TEM image of a sample aged at 170°C for 4 h (alloy 319+Mg+Sr.

The early mechanisms of the aging process have already been discussed extensively by different researchers [98-100]. It is generally accepted that the mechanism which causes the first increase in strength and hardness is the formation of Guinier-Preston zones (GP_{zones}) in the α-Al matrix. This process of zone formation may occur easily and rapidly at relatively high temperatures (180°C – 200°C). These zones may be difficult to detect by means of traditional microscopy or X-ray analysis techniques.

Figure 4.69 shows a high-magnification bright field image obtained from the same sample with the electron beam parallel to the [001] zone axis; the insert in the image is the selected area diffraction pattern obtained from this image. In this figure, the needlelike θ'-Al_2Cu precipitates are oriented in the <001> orthogonal directions of the α-Al matrix and are clearly to be seen. The streaking along the <100> directions is a typical indication of the presence of GP zones within the matrix.

Figure 4.70 shows a STEM image of the same sample, in which $TiAl_3$ and Si particles may be observed. The morphology of the Cu-containing precipitates is more evident in STEM images than in either bright field or dark field TEM images. The Al_2Cu particles appear as bright needles with a specific orientation in STEM images.

Figure 4.69 Higher magnification bright field TEM image obtained from a sample aged at 170°C for 4 h (alloy 319+Mg+Sr) with the electron beam parallel to the [001] zone axis; the insert is the corresponding selected area diffraction pattern.

The square indicates the area from which the X-ray mapping was obtained. It is noticeable that the mapping for the $Mg_{K\alpha}$ energy indicates that this element is distributed all over the area indicated by the square and that no Mg-containing precipitates may be distinguished. Elements such as Ti, Si and Cu seem to appear in the same region of the elongated precipitate. Figure 4.71 shows another STEM image, at increased magnifications, of a region where the $TiAl_3$, Si and Cu precipitates appear.

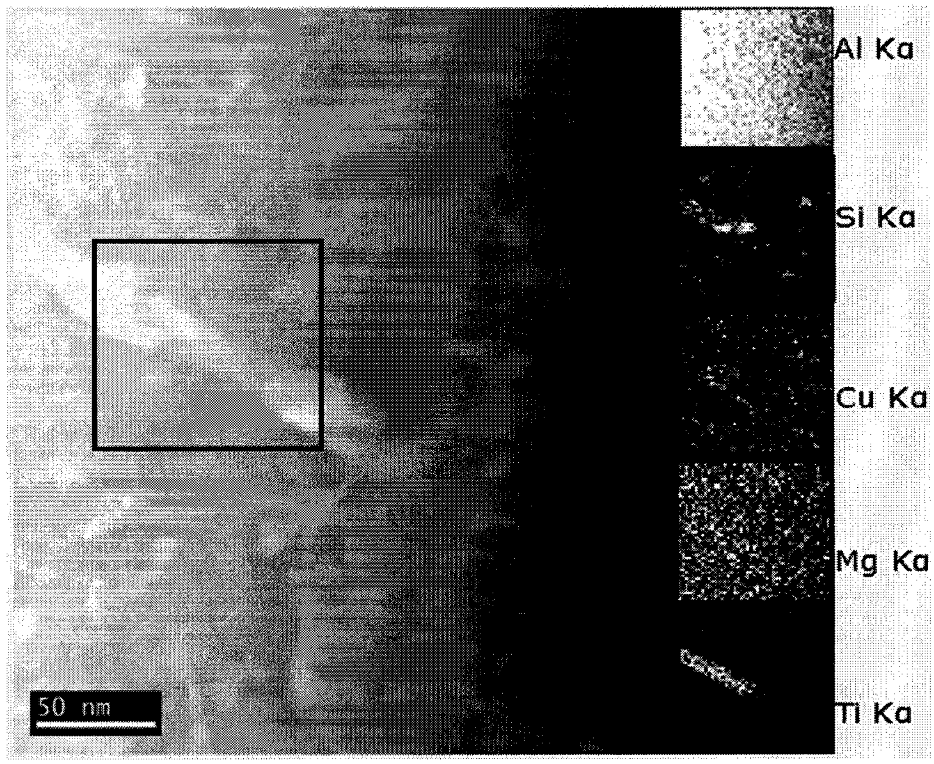

Figure 4.70 STEM image of the sample aged at 170°C for 4 h (alloy 319+Mg+Sr), and the corresponding X-ray mapping of the region indicated in the black square.

It will be observed, from the x-ray mappings, that particles containing Si and Cu seem to be located underneath the Ti-containing particle which has a rhomboid shape. The brighter area in the square corresponds to the Cu particle. The Ti present in the alloy comes from the grain refiner used during the casting process: TiB_2.

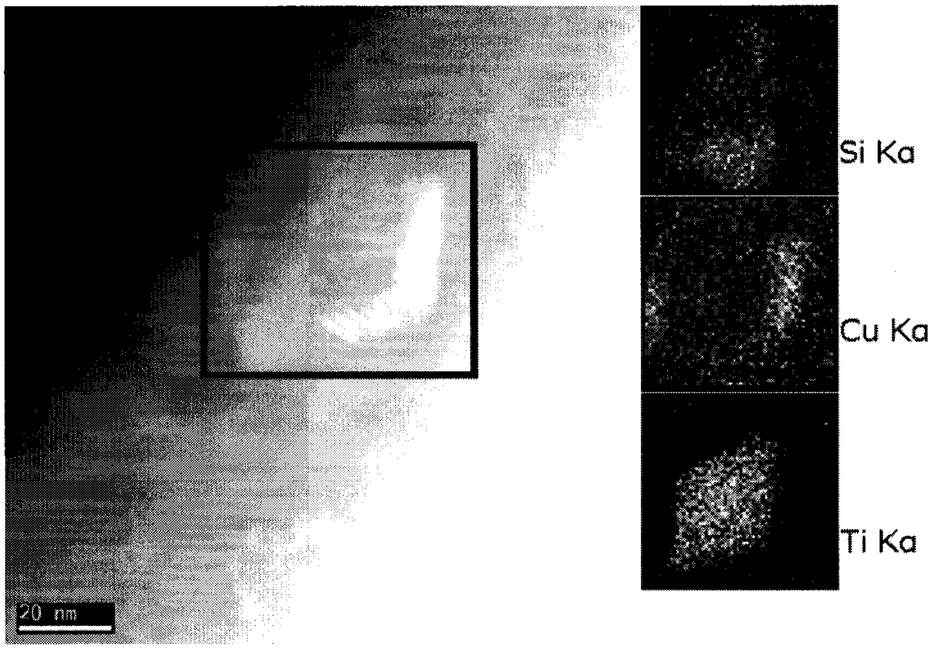

Figure 4.71 STEM image of the sample aged at 170°C for 4 h (alloy 319+Mg+Sr) at a higher magnification, and the corresponding X-ray mapping of the region indicated in the black square.

Figure 4.72 shows a bright field TEM image, obtained in the two-beam condition near the zone axis [001], showing the microstructure observed in a sample which has been aged at 170°C for 8 h. This aging condition is the one which yielded the strength and hardness peak.

A denser precipitation of θ'-Al_2Cu will be observed in Figure 4.72 as compared to the images presented earlier. This behavior is to be expected since Al_2Cu precipitates are the ones responsible for the strengthening mechanism and this sample was aged to the maximum strength or T6 condition [57, 87-89, 92].

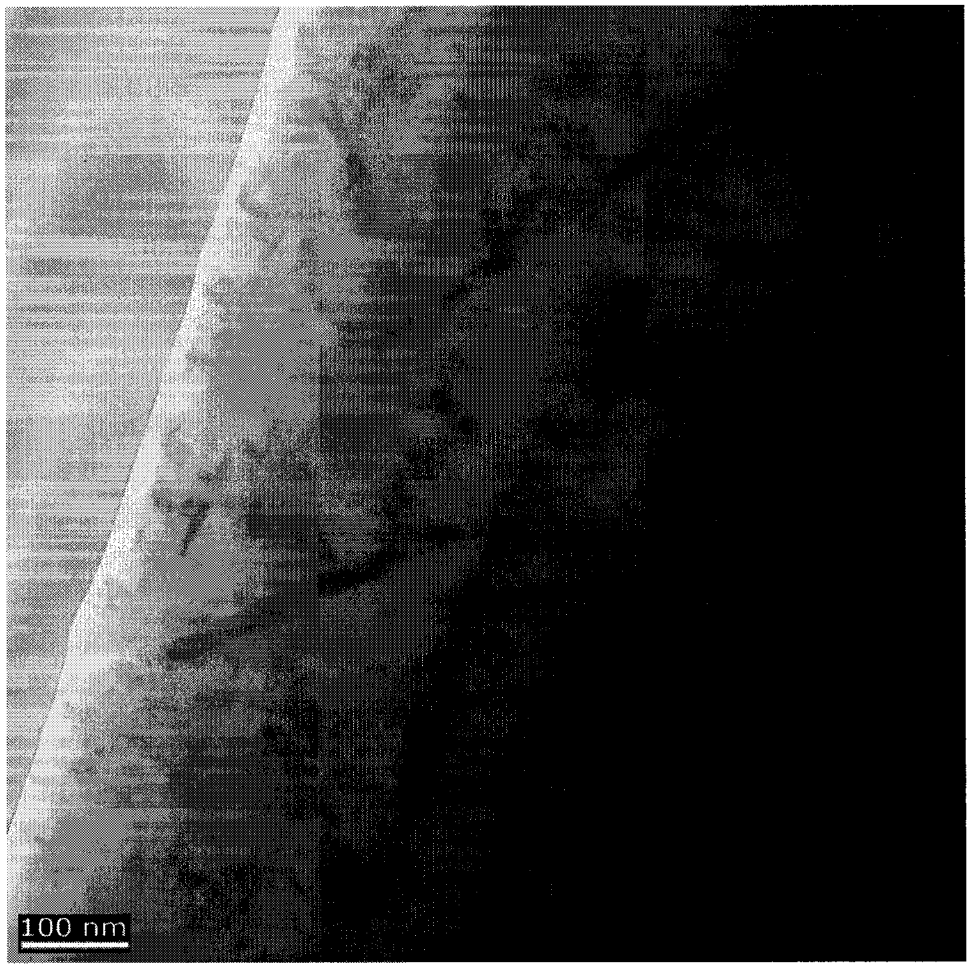

Figure 4.72 Bright field TEM image of a sample aged at 170°C for 8 h (alloy 319+Mg+Sr).

Figure 4.73 shows the dark field image of the same sample in the same position. It may happen occasionally that the deformation fringes in the samples make observation of the precipitates difficult, and this is why it is relatively easier to detect them in images obtained in STEM mode since the contrast displayed is dependent on the atomic number of the elements present in the sample, or also called compositional contrast [138, 140].

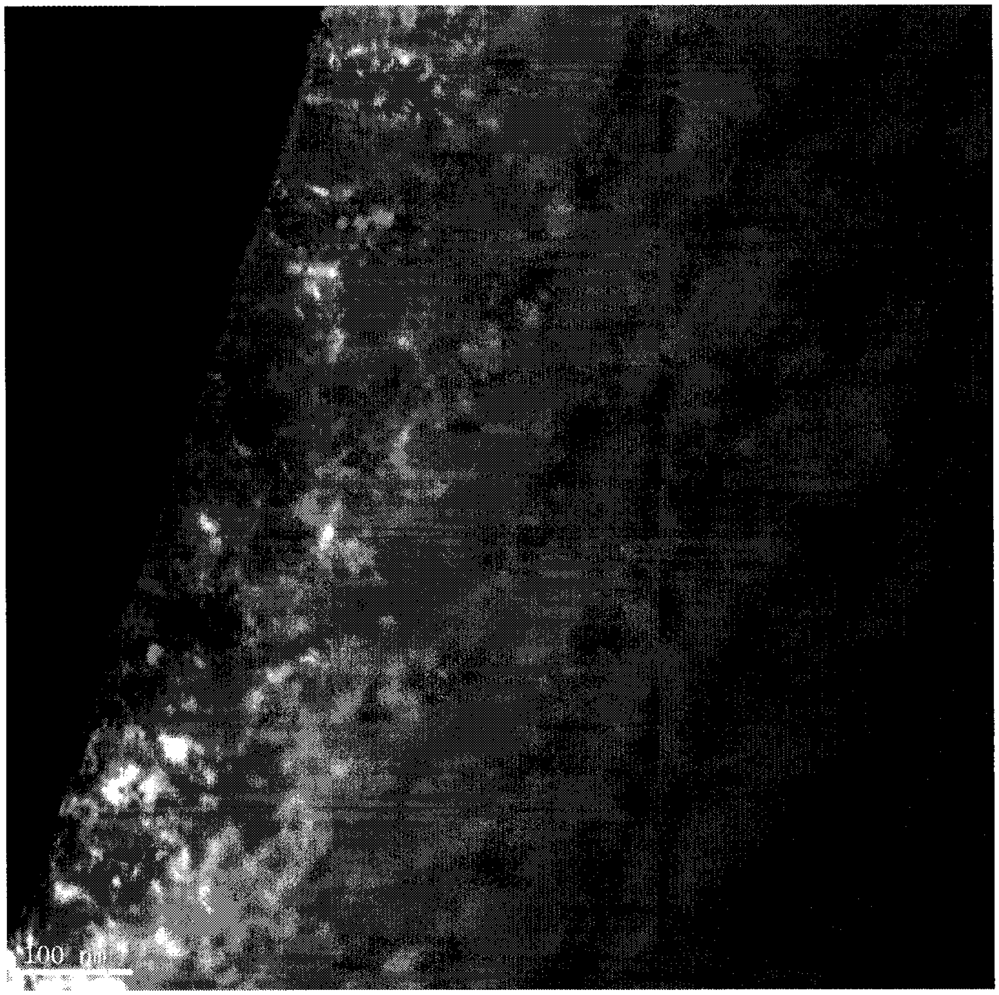

Figure 4.73 Dark field TEM image of a sample aged at 170°C for 8 h (alloy 319+Mg + Sr).

Figure 4.74 presents high magnification images of the Al_2Cu precipitates in the form of needles present in this sample. Figure 4.74(a) shows the bright field image, while Figure 4.74(b) shows the dark field image and Figure 4.74(c) shows a STEM image.

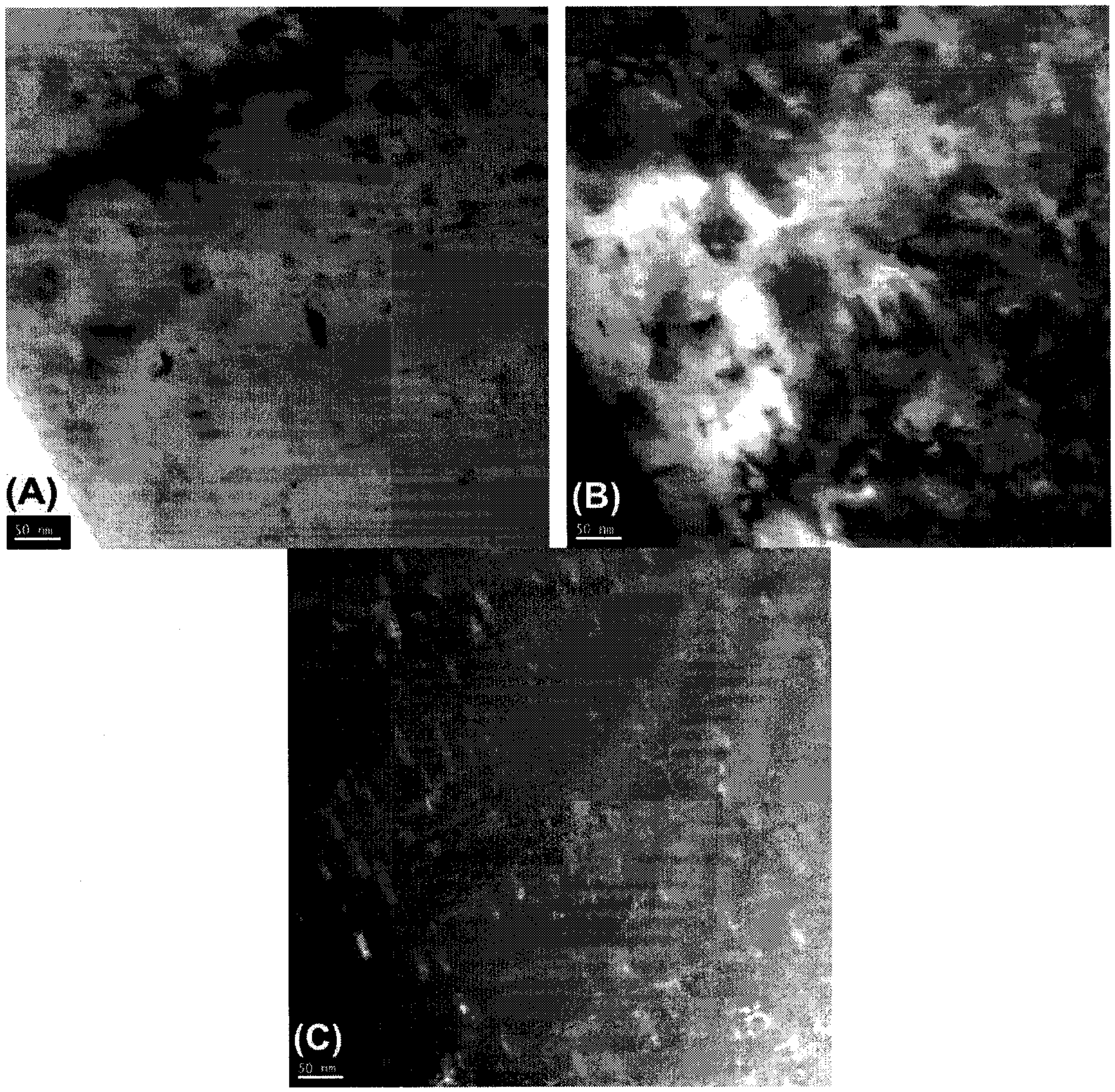

Figure 4.74 High magnification images of the Al_2Cu precipitates present in the sample aged at 170°C for 8 h: (a) bright field, (b) dark field and (c) STEM.

The Al_2Cu needles to be observed in Figure 4.74 have an average size of 35x5 ηm. They precipitate in the <100> directions of the matrix [57, 91], and although it may appear that there is a second kind of particle precipitating at about 90° to the needles, it is the same phase but seen from a perpendicular direction; these particles appear to have a platelike morphology because of the two-dimensional projection due to the fact that these images were not taken near the [001] zone axis but near a [011] axis.

Figure 4.75 shows the microstructure to be observed in a sample which has been treated by means of the overaging condition: aged at 240°C for 8 h. The microstructure consists of θ-Al_2Cu particles in the α-Al matrix which have grown to acquire platelike morphology instead of acicular. The image was obtained by means of the two beam condition and the corresponding selected area diffraction pattern is presented in Figure 4.76, the zone axis being [011]; it should be noted that there are discrete diffraction maxima appearing as additional spots in the diffraction pattern. The additional spots belong to the diffracting planes of the θ-Al_2Cu phase.

Figure 4.77 shows a higher magnification of an area first seen in Figure 4.75 where the θ-Al_2Cu needles may easily be examined. They precipitate in the orthogonal <100> directions of the matrix; also precipitates in the form of plates may be observed.

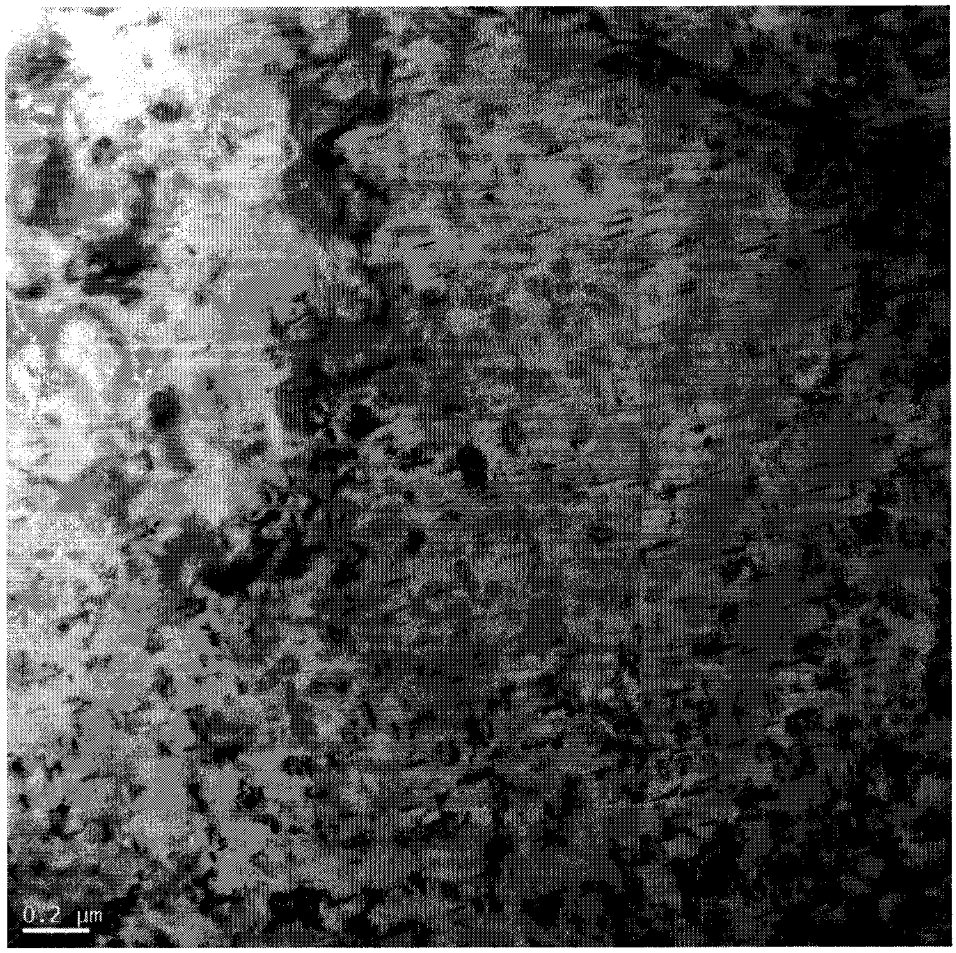

Figure 4.75 Bright field TEM image of the microstructure observed in the sample aged at 240°C for 8 h (alloy 319+Mg+Sr).

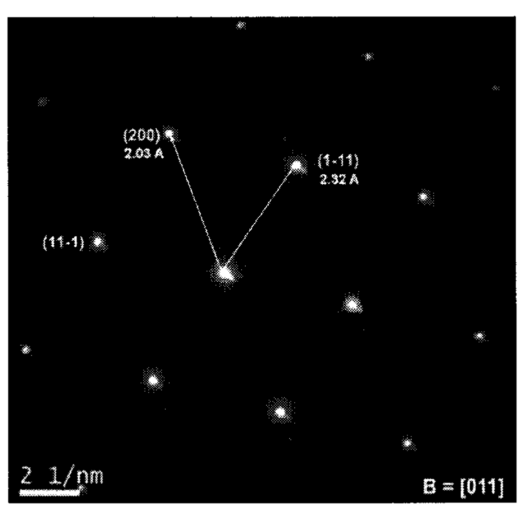

Figure 4.76 Selected area diffraction pattern of Figure 4.74 showing additional spots belonging to the θ-Al_2Cu phase.

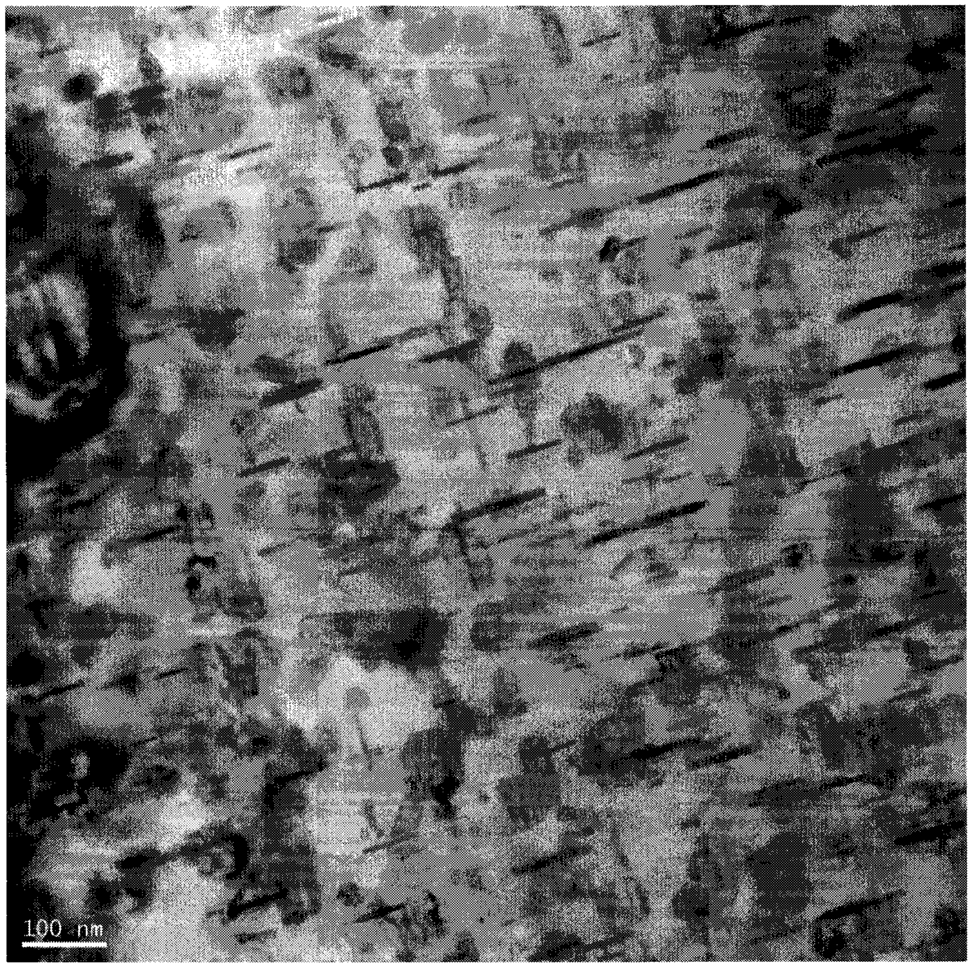

Figure 4.77 Bright field TEM image at a increased magnification of an area in Figure 4.74 (319+Mg+Sr alloy).

EDS spectra and X-ray maps were obtained in order to obtain compositional information from the precipitates observed in the previous image. Figure 4.78 presents the microstructure observed in samples having undergone an overaging treatment when imaged by the STEM technique. The inserts show X-ray maps for the different elements present in the alloy. The X-ray maps for the different elements present correspond to the area indicated by the white square in the image. As expected, the aluminum map indicates that this element is present throughout the area; silicon particles in the form of equiaxed precipitates may also be seen, indicated by black arrows in the image. The white arrows indicate where the Cu needles and plates may be observed. The Mg map indicates that the tiny plates, measuring ~20x5 ηm, observed close to the Cu-containing needles, contain Mg. The map for Ti indicates that it is not present in the area; thus large $TiAl_3$ rods were not observed in the instance of this particular aging condition.

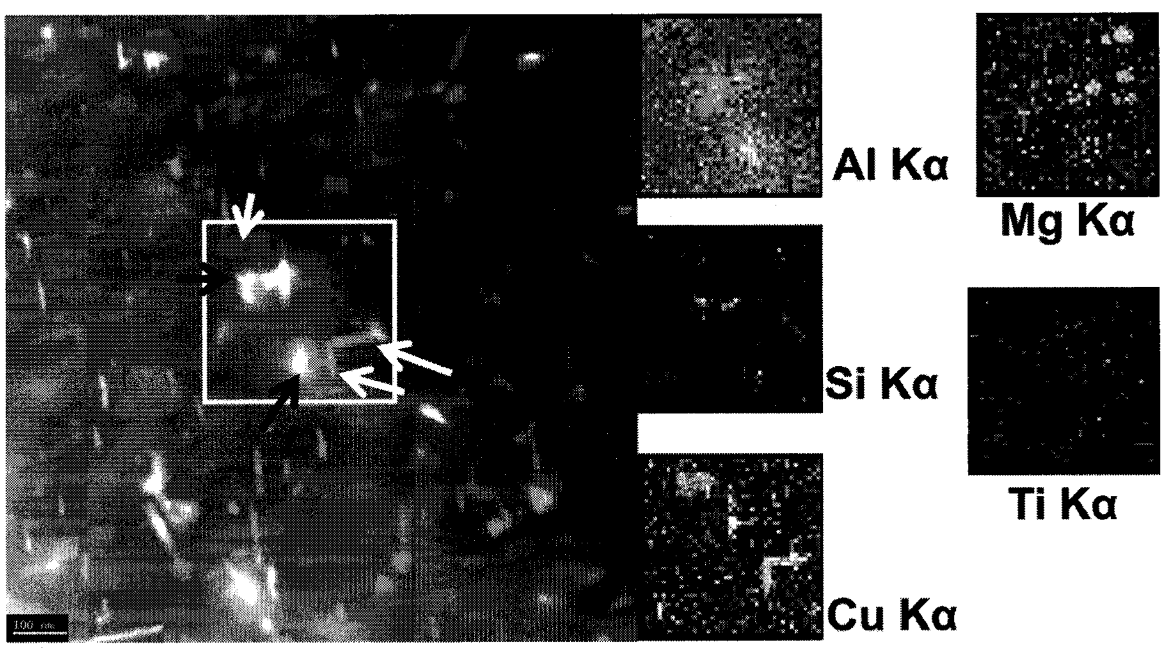

Figure 4.78 STEM image of the microstructure observed in the overaged sample and X-ray maps of several elements.

Figure 4.79 shows another STEM image at increased magnifications where an X-ray mapping and an X-ray line scan were obtained. The area indicated within the white square is the one from which the x-ray mapping was obtained, while the maps shown in the Figure pertain to those of Si, Cu and Mg only, since there were no other noticeable changes in the Al and Ti maps. The line scan is marked with the black line from point A to point B. It will be noted from the X-ray maps present in Figure 4.79 that the Mg is distributed evenly in the area and that there is no evidence of the presence of any Mg-containing precipitates; two Al_2Cu needles are present close to a Si equiaxed particle, which may indicate that Cu-containing phases are prone to nucleate on Si particles.

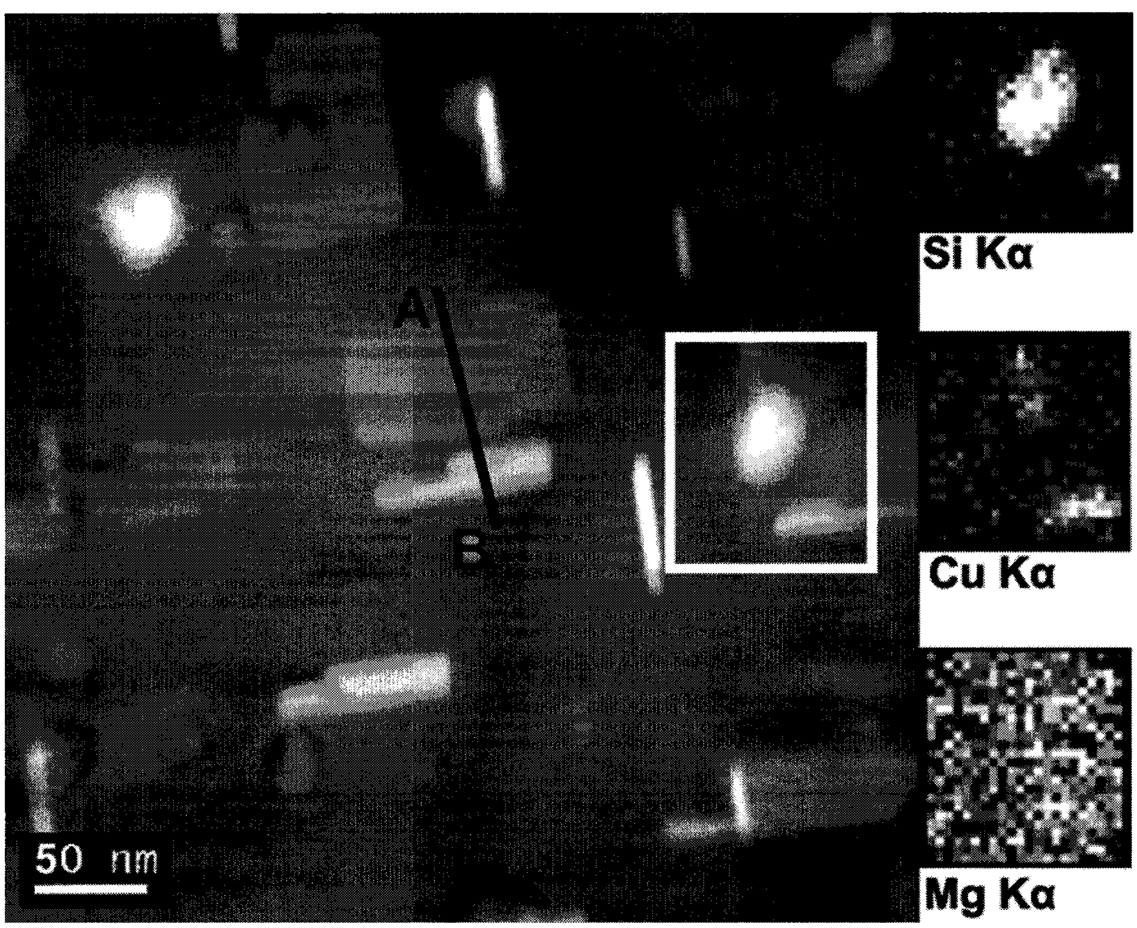

Figure 4.79 STEM image obtained at a higher magnification from the overaged sample, showing the area from which X-ray maps and a line scan were obtained.

Figure 4.80 shows a graph depicting the intensity of the characteristic X-ray emitted by Al, Si, Cu and Mg within the black line shown in Figure 4.79. It will be observed that the plate contains Al and Cu; the next particle might possibly be a small needle of the quaternary phase Q ($Al_5Cu_2Mg_7Si_7$) since the intensity of all the elements present in the graph increases; this type of particle, however, would be present only as a minor species [103, 108]. A needle of Al_2Cu can observed next to the particle that contains the four elements presented in the graph, since only these two elements are present based on the intensity obtained.

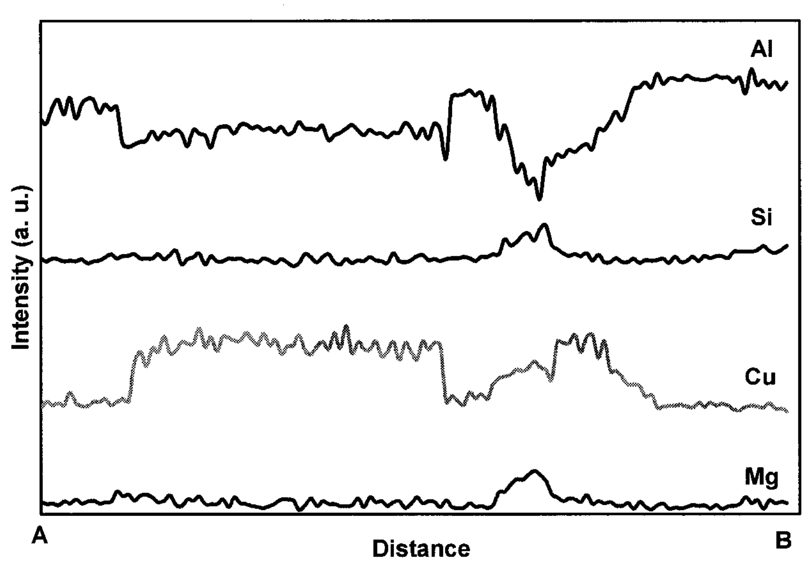

Figure 4.80 Graph of the X-ray intensities obtained in the line scan indicated in Figure 4.78

Figure 4.81 presents a high resolution bright field TEM image of a particle with acicular morphology close to an almost equiaxed Si particle. The image was taken with the beam parallel to a [011] axis which goes to explain the amount of diffraction contrast which may be observed.

Figure 4.81 High resolution bright field TEM image of a needlelike particle close to an equiaxed Si particle present in the overaged sample.

Figure 4.82 shows a high resolution image taken at increased magnifications where the atomic planes of the α-Al matrix, the needlelike particle and the Si particle may clearly be observed.

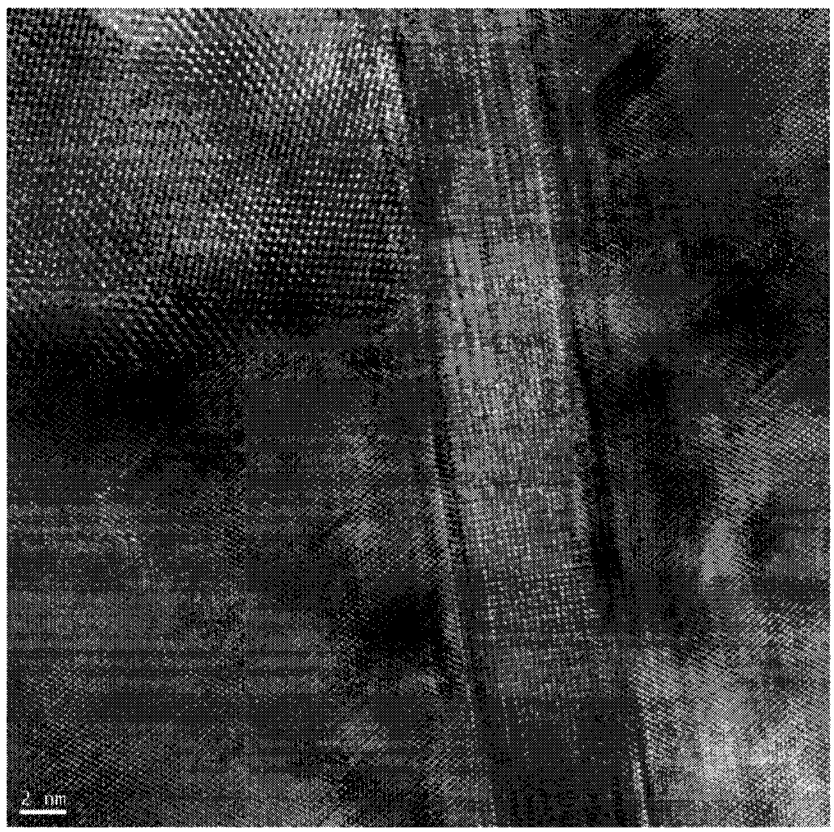

Figure 4.82 High resolution bright field TEM image of a needlelike particle close to an equiaxed Si particle present in the overaged sample.

It has been reported, for other cast alloys [103] such as alloy 339, that particles of the quaternary phase Q tend to nucleate on Si particles. There is a distinct possibility that this might be the case in the previous two images; these small needles which measure approximately 50x5 ηm are present in the microstructure only as a minor species.

4.4.2.2 Comparison of Images: Samples from Continuous, Multi-Temperature vs. Interrupted Aging Treatments

Figure 4.83 presents the comparison between the microstructures of two samples: the image from sample (a) aged continuously to the peak-aged condition T6, this is to say at 170°C for 8 h, while the image from sample (b) aged by applying a T6-type multi-temperature aging cycle, 2 h at 190°C followed by 5 h at 180°C, labeled as Treatment G. The values obtained for UTS, YS and microhardness were slightly lower for the sample aged using the multi-temperature treatment.

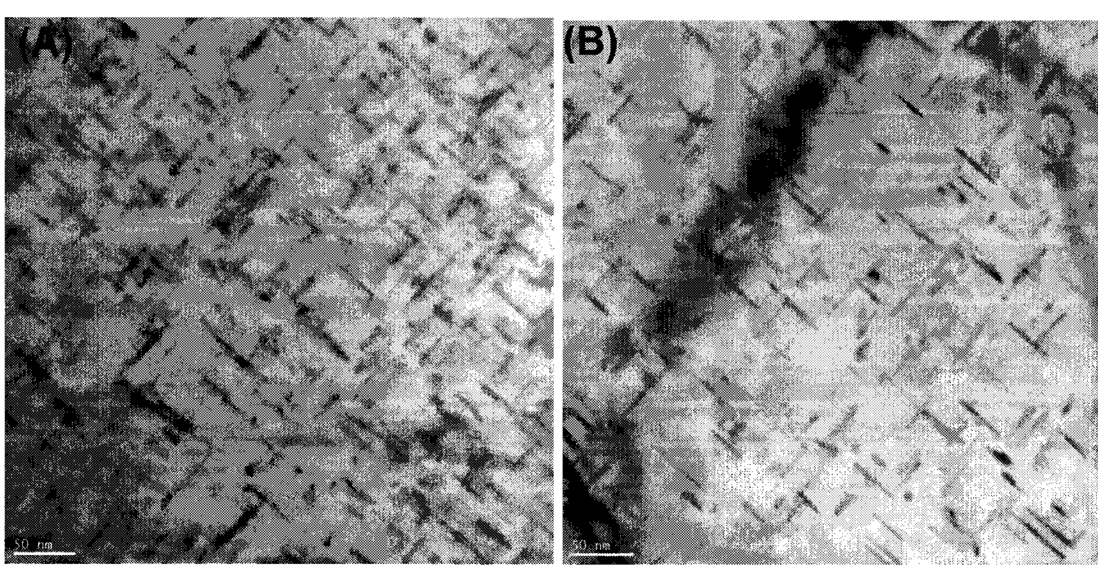

Figure 4.83 Bright field TEM images of: (a) peak aged sample; and (b) sample aged for 2 h at 190°C and 5 h at 180°C.

It is worthy of note, from the comparison in Figure 4.83, that the needlelike particles are more widely spaced in the sample which was aged by applying the multi-temperature treatment than in the preceding sample, aged using continuous aging, this wider spacing may explain the lower strength and microhardness values displayed as compared to the values produced by the sample which was aged using a continuous T6 treatment: 8 h at 170°C. A dense precipitation of intermetallic species will impede the movement of dislocations through the matrix more effectively, rendering the material stronger; when the precipitates are widely dispersed the dislocations can cross between them [87, 89, 91].

Figure 4.84 shows a comparison between a sample which was aged applying treatment G, 2 h at 190°C and 5 h at 180°C, and a sample which was aged using the same treatment but with the addition of an intermediate interruption stage at room temperature, that is to say, aging for 2 h at 190°C, 100 h at 25°C and 5 h at 180°C.

It will be observed from Figure 4.84 that the type of precipitate is the same in both samples, indicating that interrupted aging does not have an effect on the precipitation of this alloy; this was to be expected since the mechanical properties studied were very similar as well, not showing a clear improvement or loss when applying an interrupted aging cycle.

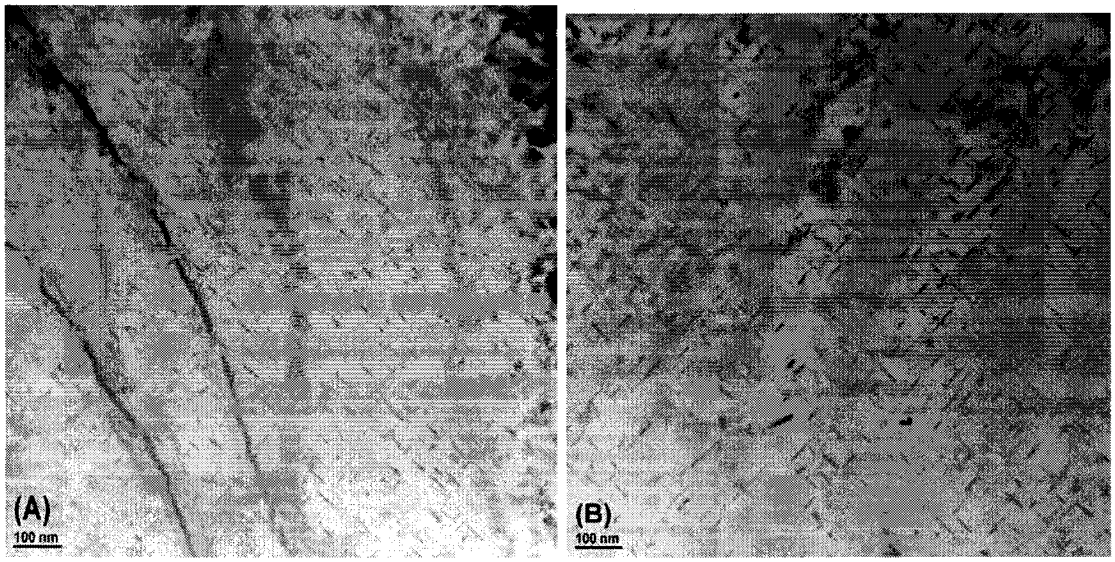

Figure 4.84 Bright field TEM images of: (a) sample aged for 2 h at 190°C and 5 h at 180°C; (b) sample aged for 2 h at 190°C, 100 h at 25°C and 5 h at 180°C.

Figure 4.85 presents a comparison between a sample aged by the application of a T7 condition, 2 h at 240°C, and a sample which had undergone aging by means of a T7-type multi-temperature treatment, in other words, 1 h at 170°C, 1 h at 190°C and 2 h at 240°C. It will be observed in Figure 4.85(a) that when overaging is instigated, a characteristic coarsening of the Al_2Cu needles occurs. This coarsening of needles will lead to the microstructure present in Figure 4.77 which shows a higher density of coarse Cu-containing precipitates; Figure 4.77 pertains to the completely overaged material which was aged at 240°C for 8 h. Figure 4.85(b) shows the microstructure of the material aged through a T7-type multi-temperature treatment, 1 h at 170°C, 1 h at 190°C and 2 h at 240°C, which yielded the best mechanical properties studied. Both images presented in Figure

4.85 were obtained with the double beam condition and the transmitted beam parallel to the [001] zone axis. The equiaxed precipitates which are present in both images are the ternary phase S-$CuMgAl_2$. More of these precipitates may be observed in Figure 4.85(b). These particles display rodlike morphology where the rods measure about 100ηm in length and 10 ηm in thickness. The orientation of this phase is parallel to the zone axis of the images, therefore, they will appear as dots or equiaxed particles [101, 103, 142, 143].

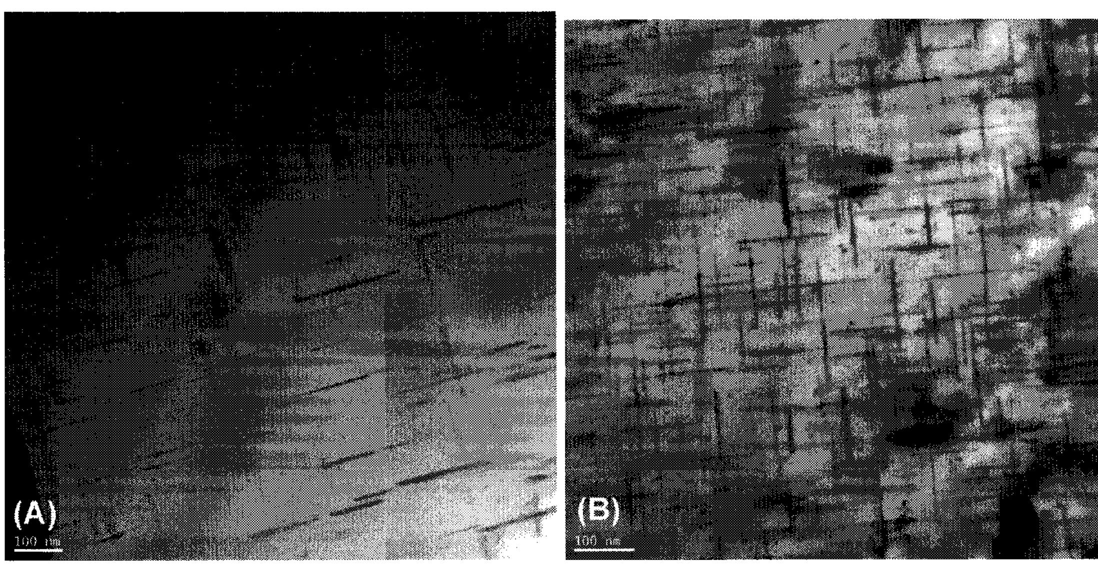

Figure 4.85 Bright field TEM images of: (a) sample aged at 240°C for 2 h; and (b) sample aged for 1 h at 170°C, 1 h at 190°C and 2 h at 240°C.

There is a distinct difference to be observed between the two microstructures presented in Figure 4.85, in view of the fact that the coarsening of the Al_2Cu needles is not present and there is still a high concentration of needlelike precipitates; this behavior indicates that the inclusion of certain underaging stages before the actual overaging stage would be beneficial to the material since it holds back the overaging process. This delay may be explained by the fact that underaging, carried out at lower temperatures ranging from 150°C to 190°C, will cause nucleation of early metastable phases and later on when the temperature has risen to the overaging temperature, or 240°C, these metastable phases will disappear; there will, however, be a local enrichment of the atoms contained in the metastable phases which in turn will produce a smaller and better distributed stable phase during overaging, thereby improving the mechanical properties of the material.

The application of an underaging stage before overaging does not always improve the mechanical properties, as was observed in earlier sections of this chapter (see Figure 4.25). Figure 4.86 shows a bright field TEM image obtained from a sample aged by means of the treatment labeled N, 24 h at 130°C and 2 h at 240°C, this multi-temperature treatment was the one which yielded the lowest values for strength and microhardness. The image was obtained by means of the double beam condition, with the transmitted beam parallel to the [001] zone axis. The microstructure observed in the sample shows Al_2Cu needles still remaining distributed homogeneously in the matrix. Some Al_2Cu plates may also be observed, in the form of thick plates, indicating that the transformation of the Al_2Cu needles to the stable θ_{eq} has occurred. The Al_2Cu plates are indicated in

Figure 4.86 by the white arrows. The darker particles present in the microstructure consist of Si plates; these are indicated by continuous black arrows. S-$CuMgAl_2$ rods are also present and they are marked with the dotted black arrows.

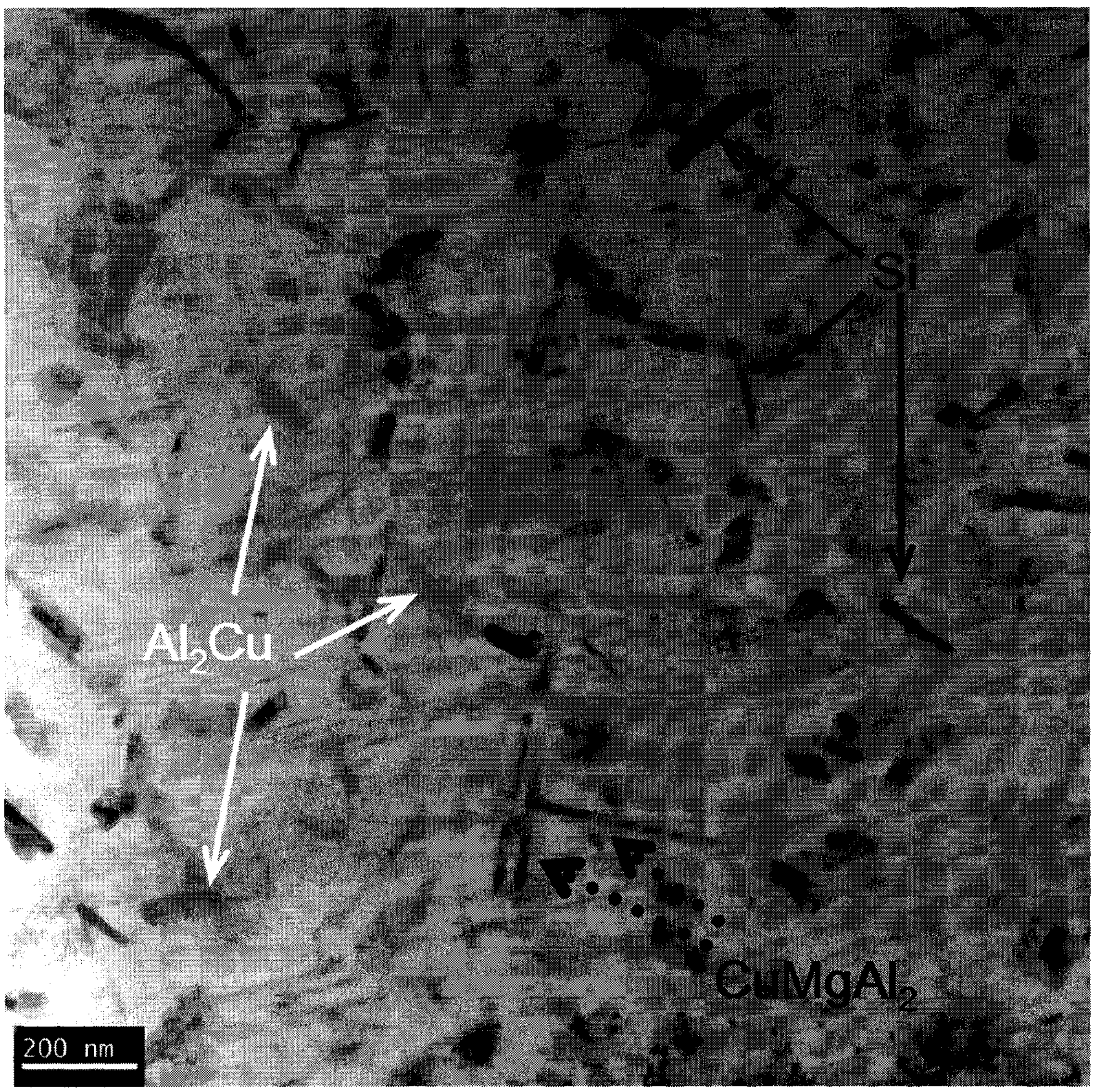

Figure 4.86 Bright field TEM image obtained from a sample aged for 24 h at 130°C and 2 h at 240°C (alloy 319+Mg+Sr).

The coarsening of strengthening precipitates such as Al_2Cu, Mg_2Si, $CuMgAl_2$, and so forth may have a detrimental effect in the mechanical properties of the alloy. The T7-type multi-temperature aging cycle, 24 h at 130°C and 2 h at 240°C, yields lower properties than the continuous T7 overaging cycle. This behavior is expected, since the underaging stage of the multi-temperature treatment is relatively long, 24 h, there is sufficient time for the previously mentioned phases to coarsen and form the thick plates and particles which may be observed in Figure 4.86.

It will be noted upon observing the figures presented in these sections, that the optimum combination of temperatures and times to obtain a material of high strength (in peak aged condition) would be continuous aging at a relatively low temperature of ~170°C, since this type of treatment yields a microstructure consisting of a high density of small homogeneously distributed precipitates.

In the case where an overaged material is desired, the best combination would consist of a short underaging stage, ~2 h, at a similar temperature used for the peak aging condition, i.e. 170°C to 190°C, then subsequently applying the overaging stage for a short period of time (2 h at 240°C) as in the case of aging for 1 h at 170°C, 1 h at 190°C and 2 h at 240°C. Such a treatment yields the most desirable microstructure, namely one with a high density of precipitates which improves the mechanical properties of the alloy.

Chapter 5

Summary of Results

This chapter presents a general summary of the results obtained in this study. The first section focuses on conventional aging cycles; the second one concentrates on non-conventional aging; and the third one highlights the information obtained by the microstructural results. A summary of the best properties obtained by each alloy is presented at the end of the chapter in the section called industrial significance.

5.1 Conventional Aging Cycles

The standard T6 artificial aging treatment specified by the Aluminum Association of America for 319 alloys, that is, solution heat treatment for 8 h at 495°C and artificial aging for 2 – 5 h at 155°C, does not produce a noticeable improvement in mechanical properties such as ultimate tensile strength, yield strength and microhardness of the 319 base alloy used in this study. On the other hand, percent elongation and impact toughness seem to benefit from this treatment. Higher strength and microhardness values than those obtained from the standard T6 treatment may be obtained by artificially aging for longer times at 170°C, as the corresponding properties prove, however, at the expense of percent elongation and impact energy.

A satisfactory correspondence between the tensile strength values and the microhardness measurements obtained from the alloy may be observed. The variation in microhardness is a better indication of the effect of the aging treatment than the variation in tensile values. The former represent the changes in the aluminum matrix, *per se*, while the latter may be influenced by other factors such as casting defects because they are obtained from a bulk specimen. Conversely, there is a satisfactory correspondence between percent elongation and impact toughness values since they seem to be affected in the same way by the artificial aging practices used in this study.

The process of the modification of the eutectic silicon present in the alloy by means of the addition of strontium does not affect the aging behavior of the 319 base alloy. The values obtained for ultimate tensile strength and yield strength are similar, whether the alloy is Sr-modified or not. On the other hand, microhardness values seem to decrease with Sr-modification, as opposed to the values obtained for percent elongation and impact toughness which, as expected, increase after the Sr-modification.

The addition of magnesium to 319 base alloy noticeably enhances its response to artificial aging by increasing the achievable strength and microhardness, although this occurs at the expense of ductility. The standard T6 artificial aging treatment is not optimal for alloy 319+Mg since the highest strength and microhardness are observed after aging at 170°C for 8 h.

Sr-modification of the alloy containing Mg slightly improves its properties by increasing the percent elongation and impact toughness obtained after aging. This slight increase is beneficial since at the same time the strength and microhardness are maintained at a similar level. The best treatment for this alloy is the same as that used for the unmodified Mg-containing alloy, or artificial aging for 8 h at 170°C.

The combination of factors for obtaining optimum quality material is: a Sr-modified alloy with Mg in the T6 condition, or in other words: solution heat-treatment, water quenching and artificial aging at 170°C for 8 h. The corresponding properties are: 423 MPa UTS, 398 MPa YS, 134 VHN, 0.98% elongation and 3.21 J for total absorbed impact energy.

5.2 Non-Conventional Aging Cycles

The 319 base alloy does not seem to show any improvement in terms of tensile strength or microhardness with any of the multi-temperature cycles proposed when compared to the T6 continuous aging treatment. Higher percent elongation and impact toughness values may be obtained with T6-type multi-temperature treatments. These improvements, however, are not significant if the reductions in strength or microhardness are taken into account. The same may be said of the T7-type multi-temperature treatments: there is no clear improvement in the properties if a comparison is made between them and those obtained by multi-temperature and T7 continuous aging treatments.

The Sr-modified 319 alloy seems to benefit from certain multi-temperature treatments, such as treatments C (2 h at 150°C and 5 h at 180°C) and L (2 h at 150°C and 10 h at 240°C). With Treatment C the achievable yield strength obtained is higher by approximately 11% than that obtained with the T6 continuous aging treatment. This improvement, however, involves a reduction in the percent elongation and impact toughness values. Treatment L improves the ductility of this alloy by approximately 50% and the impact toughness by approximately 20% compared to the continuous T7 treatment. In this case, the strength and microhardness values remain almost the same, indicating that certain multi-temperature T7 treatments are beneficial to this alloy.

Multi-temperature aging cycles seem to yield lower strength and microhardness values for the 319+Mg alloy, except in the case of treatment C, 2 h at 150°C and

5 h at 180°C, where the values observed are almost identical to those obtained with the T6 continuous aging treatment. It is interesting to note, however, that this alloy displays a resistance to softening over time, as in the case of treatment H: 2 h at 190 °C and 10 h at 180 °C, where the aging takes place over 12 h. T7-type multi-temperature aging cycles are not beneficial to this alloy since no improvement in properties was observed, indicating that the T7 continuous treatment is the best option to select for overaging the alloy.

The Sr-modified 319+Mg alloy (319+Mg+Sr alloy) displays slightly higher strength and microhardness values when aged using the T6 continuous treatment than when aged with the T6-type multi-temperature aging process. A number of these aging treatments, however, improve the percent elongation and impact toughness of the alloy to a slight degree. The T7-type multi-temperature aging treatments do not improve the strength or microhardness of this alloy considerably when compared to the continuous T7 treatment; the most beneficial treatment is Treatment O: 1 h at 170°, 1 h at 190°C and 2 h at 240°C. This treatment improves the percent elongation displayed by the alloy by ~30% and the impact toughness by ~50%, which is a considerable improvement since the strength and microhardness values are also improved slightly with this treatment.

The results obtained using the interrupted aging cycles show neither a clear improvement nor a decline in the properties, indicating that the mechanisms which affect the precipitation hardening phenomenon are not affected by the inclusion of an interruption stage in the aging cycle.

5.3 Microstructure

The information obtained by means of the scanning electron microscope reveals that the initiation of cracks responsible for the failure of the material occurs in the brittle phases such as eutectic Si, Al_2Cu and Mg-containing phases rather than at their interfaces with the matrix which fails in a ductile manner. The failure of the matrix is a result of void coalescence and the corresponding fracture surface is characterized by the appearance of dimples. Two features of significant interest to be observed were the segregation of the Cu-containing phases and decohesion of Si particles which are both responsible for failure of the material in the overaged condition.

The results obtained using the transmission electron microscope showed that several of the phases which are present in the α-aluminum matrix are responsible for the strengthening response of this alloy when aging the material by means of different aging cycles. In the as-cast and solution heat-treated conditions big Si, TiAl3 and $Al_{15}(Fe,Mn)_3Si_2$ particles are present. Precipitates of $CuMgAl_2$ and Mg_2Si were also identified in the solution heat-treated condition; these phases, however, are present only as a minor species.

The dislocation tangles which were observed in the solution heat-treated samples had been introduced into the material so as to release the thermal stresses generated during the quenching from the solution treatment temperature. These tangles result from the difference in the thermal expansion coefficients between the matrix and the intermetallic particles present.

In the early stages of the aging process, namely after aging for 4h at 170°C, it is possible to observe a microstructure displaying homogeneous precipitation of θ-Al_2Cu needles oriented in the <001> orthogonal directions in the matrix; also, upon analysis of the corresponding diffraction pattern, the presence of GP zones was detected.

As expected, once aging proceeds and attains the peak-aged condition, the microstructure consists of a homogeneous dense precipitation of θ-Al_2Cu needles; it thus becomes clear that this phase is the major contributor to the hardening of the material.

5.4 Industrial Significance

Table 5.1 presents a summary of the highest properties obtained for the four 319 type alloys after artificial aging and the corresponding aging treatments by which these optimum properties were achieved. The highlighted cells in the table emphasize the maximum values attainable property-wise.

Table 5.1 Summary of the highest properties obtained after the specified artificial aging treatment.

<table>
<tr><th>Alloy</th><th colspan="2">319</th><th colspan="2">319 + Sr</th><th colspan="2">319 + Mg</th><th colspan="2">319 + Mg + Sr</th></tr>
<tr><td>UTS (MPa)</td><td>376</td><td rowspan="3">8h@170°C</td><td>376</td><td rowspan="3">4h@150°C</td><td>428</td><td rowspan="3">8h@170°C</td><td>423</td><td rowspan="3">8h@170°C</td></tr>
<tr><td>YS (MPa)</td><td>258</td><td>230</td><td>403</td><td>398</td></tr>
<tr><td>VHN</td><td>110</td><td>86.5</td><td>134</td><td>133</td></tr>
<tr><td>%El</td><td>8.4</td><td rowspan="2">4h@150°C</td><td>8.9</td><td>4h@170°C</td><td>2.8</td><td>4h@150°C</td><td>4.43</td><td>2h@150°C</td></tr>
<tr><td>E_t (J)</td><td>20</td><td>24</td><td>4h@150°C</td><td>7.9</td><td>2h@150°C</td><td>13.4</td><td>4h@150°C</td></tr>
</table>

It will be observed that the highest UTS, YS and microhardness values are obtained for the 319+Mg alloy after aging at 170°C for 8 h , i.e., with the T6 continuous aging treatment. Thus, the addition of Mg proves to be an excellent way of achieving a high level of tensile strength and microhardness, however, at the expense of elongation and impact toughness, since the highest values of these properties (2.8% and 7.9 J) for this alloy are much less than those exhibited by the other 319 alloys.

The Sr-modified alloy (alloy 319+Sr), on the other hand, yields the highest values for elongation and impact toughness, showing that the modification of the morphology of the Si eutectic phase from acicular to fibrous with the use of strontium enhances the ductility of the alloy. However, if the alloy contains little or no magnesium, its response to artificial aging will be limited. Therefore, a balance between strength/hardness and ductility/impact toughness should be sought.

Industrially, 319 alloys are used in the fabrication of automotive engine blocks and cylinder heads where the requirements for mechanical properties require that desirable values range from 250 to 300 MPa for yield and ultimate tensile strength, 1% for elongation, 10 J for impact toughness and 100 VHN for microhardness [4]. It may be noted from Table 5.1 that the 319+Mg+Sr alloy provides high tensile strength/microhardness values through heat treatment, comparable to those obtained with the 319+Mg alloy, while Sr-modification enhances its ductility and impact toughness to values far above those provided by the latter. Even if these values (4.4% El and 13.4 J) lie halfway between the maximum and minimum values observed in Table 5.1, they are sufficiently higher than the desired/required levels. For these reasons, the 319+Mg+Sr alloy would be considered to possess the best combination of mechanical properties for such applications.

Chapter 6 and 7

Conclusions and Statement of Originality

The following conclusions may be drawn after taking into consideration the results obtained by this study:

1. The 319-type aluminum alloy with the optimum combination of mechanical properties consists of a Sr-modified alloy with additions of Mg. The Sr-modification process does not affect the aging behavior of the alloy while the addition of Mg enhances its response to artificial aging.

2. The strengthening effect observed in the alloy is due mainly to the presence of θ-Al_2Cu particles which precipitate in the form of needles and plates.

3. The degree of strengthening that may be obtained depends directly on the amount and homogeneity of the θ-Al_2Cu phase.

4. Other phases such as Mg_2Si, $CuMgAl_2$, and Q-$Al_5Cu_2Mg_7Si_7$ are present in the alloy as well but only as minor constituents and do not contribute significantly towards strengthening.

5. The optimal properties in the T6, peak-aged, condition are not attained by applying the standard aging treatment but by continuously aging at 170°C for 8 h.

6. The properties obtained after the T6 continuous aging treatment mentioned earlier cannot be further improved by means of non-conventional aging cycles, either multi-temperature or interrupted, indicating that this is the optimum T6 aging treatment.

7. The properties obtained after applying the standard T7 treatment can be improved by means of a multi-temperature cycle such as 1 h at 170°C, 1 h at 190°C and 2 h at 240°C. This treatment is therefore considered as the optimum T7 aging treatment.

8. The optimum T7 cycle consists of a short, underaging stage at similar temperatures as those used for the peak aging condition, i.e. 170°C to 190°C, and then applying the overaging stage for a short period of time. This allows for the early nucleation of metastables phases and the later precipitation of the stable phase in a fine and well distributed fashion.

The following points, in that they are derived from the information obtained in this study, are deemed to be original contributions to knowledge in this field:

1. A comparison was carried out between the conventional continuous aging cycle used for this particular alloy and non-conventional, multi-temperature and interrupted, aging cycles in terms of mechanical properties such as ultimate tensile strength, yield strength, microhardness, percent elongation and impact toughness.

2. The optimum artificial aging treatments for the T6, peak-aged, and T7, overaged, conditions were proposed according to the results obtained. It has been concluded, therefore, that multi-temperature treatments do not improve the properties of the alloy in the T6 condition; while, on the other hand, a carefully selected multi-temperature treatment in the T7 condition may lead to superior properties. Interrupted aging does not have any appreciable effect on the properties analyzed by this study.

3. A theory as to why the mechanical properties are improved by some multi-temperature treatments has hereby been formulated. It proposes that the nucleation of early metastable phases and their later dissolution in the

matrix when the temperature is increased, cause a local enrichment which will ultimately produce smaller and better distributed stable phases.

4. An analysis of the phases which are present in this type of alloy was carried out using advanced characterization techniques. It was discovered that ternary and quaternary precipitates are present only as minor constituents and do not contribute significantly to the strengthening mechanism which operates in the artificial aging treatment. The phase responsible for the strengthening of the material is Al_2Cu although many phases are present in the material and the precipitation observed displays a form of complexity which is due to the presence of Al, Si, Cu and Mg.

Chapter 8

Suggestions for Future Work

Suggestions for Future Work

The research work presented in this thesis covers an extensive study of the artificial aging treatments for 319-type alloys, with the aim of optimizing their mechanical properties. A certain amount of transmission electron microscopy (TEM) was also used to examine the precipitation behavior during the aging process. However, the complexity of the precipitation observed suggests that TEM analysis could be used to advantage for future research. Suggestions for possible future work in this area could include:

- A study of the early mechanisms of aging using alloys of the 319-type prepared under highly controlled conditions (fabrication and treatment). In this context, other advanced characterization techniques [144, 145] such as differential scanning calorimetry, image simulation, atomic resolution microscopy and quantitative chemical analysis could also be used, in order to detect minute variations in the alloy and obtain positive identification of all the precipitates that are present in such alloys.

- A study of the potential formation of co-clusters in the heat ramp-up period during the first stages of heat treatment, by varying the heating rate and, consequently, the precipitation kinetics.

- Quantification of the volume fraction of precipitates and its correlation to the mechanical properties [146].

- The use of statistical tools for experimental design and analysis of the results obtained [147].

References

[1] R. N. Lumley, I. J. Polmear, A. J. Morton, "Development of Mechanical Properties during Secondary Aging in Aluminum Alloys", *Materials Science and Technology*, Vol. 21 (2005) 1025 - 1033.

[2] R. N. Lumley, I. J. Polmear, A. J. Morton, "Development of Properties During Secondary Ageing of Aluminum Alloys", *Materials Science Forum*, Vol. 426 - 432 (2003) 303 - 308.

[3] J. E. Gruzleski, B. Closset, *The Treatment of Liquid Aluminum Silicon Alloys*, American Foundrymen's Society, Des Plaines, IL, 1990.

[4] G. E. Totten, D. S. MacKenzie (Eds.), Handbook of Aluminum, Marcel Dekker, Inc., New York, NY. Basel, Switzerland., 2003, p. 1296.

[5] J. G. Kaufman, E. L. Rooy, *Aluminum Alloy Castings: Properties, Processes, and Applications*, ASM International, Materials Park, OH, 2004, p. 340.

[6] L. Bäckerud, G. Chai, J. Tamminen, *Solidification Characteristics of Aluminum Alloys Vol.2: Foundry Alloys*, American Foundrymen's Society/Skanaluminium, Des Plaines, IL, 1990.

[7] J. L. Jorstad, "Hypereutectic Al-Si Casting Alloys: 25 Years, What's Next?" *AFS Transactions*, Vol. 104 (1996) 669 - 671.

[8] E. S. Lee, "A Study of the Economics of Hypereutectic Aluminum-Silicon (Al-Si) Alloy Machining", *The International Journal of Advanced Manufacturing Technology*, Vol. 16 (2000) 700 - 708.

[9] D. L. Zalensas (Ed.) Aluminum Casting Technology, American Foundrymen's Society, Inc., Des Plaines, IL, 1993, p. 356.

[10] J. Chang, I. Moon, C. Choi, "Refinement of Cast Microstructures of Hypereutectic Al-Si Alloys Through the Addition of Rare Earth Metals", *Journal of Materials Science*, Vol. 33 (1998) 5015 - 5023.

[11] H. J. Kim, "Effect of Calcium on Primary Silicon Particle Size in Hypereutectic Al-Si Alloys", *Materials Science and Technology*, Vol. 19 (2003) 915 - 918.

[12] C. R. Ho, B. Cantor, "Modification of Hypoeutectic Al-Si alloys", *Journal of Materials Science*, Vol. 30 (1995) 1912 - 1920.

[13] J. E. Gruzleski, "The Art and Science of Modification: 25 Years of Progress", *AFS Transactions*, Vol. 100 (1992) 673 - 683.

[14] F. Paray, J. E. Gruzleski, "Effect of Modification on Aluminum Matrix of Al-Si-Mg Alloys", *Materials Science and Technology*, Vol. 10 (1994) 757 - 762.

[15] F. Paray, B. Kulunk, J. E. Gruzleski, "Impact Properties of Al-Si Foundry Alloys", *International Journal of Cast Metals Research*, Vol. 13 (2000) 17 - 39.

[16] K. Nogita, P. L. Schaffer, S. D. McDonald, L. Lu, A. K. Dahle, "Modification of Al-Si alloys", *Aluminium*, Vol. 81 (2005) 330 - 335.

[17] D. Apelian, G. K. Sigworth, K. R. Whaler, "Assessment of Grain Refinement and Modification of Al-Si Foundry Alloys by Thermal Analysis", *AFS Transactions*, Vol. 92 (1984) 297 - 307.

[18] H. Beumler, A. Hammerstad, B. Wieting, R. DasGupta, "Analysis of Modified 319 Aluminum Alloy", *AFS Transactions*, Vol. 96 (1988) 1 - 12.

[19] J. E. Hatch (Ed.) Aluminum: Properties and Physical Metallurgy, American Society for Metals, Materials Park, OH, 1984, p. 424.

[20] L. Wang, S. Shivkumar, "Influence of Sr Content on the Modification of Si Particles in Al-Si Alloys", *Zeitschrift für Metallkunde*, Vol. 86 (1995) 441 - 445.

[21] G. K. Sigworth, "Theoretical and Practical Aspects of the Modification of Al-Si Alloys", *AFS Transactions*, Vol. 91 (1983) 7 - 16.

[22] R. Elliot, *Eutectic Solidification Processing: Crystalline and Glassy Alloys*, Butterworths and Co. Ltd., London, 1983, p. 370.

[23] P. B. Crossley, L. F. Mondolfo, "The modification of Al-Si alloys", *Modern Casting*, Vol. 49 (1996) 89 - 100.

[24] C. C. Chama, "Mechanisms of silicon crystal growth", *Journal of Materials Science Letters*, Vol. 17 (1998) 1857 - 1859.

[25] M. Shamsuzzoha, L. M. Hogan, "Twinning in Fibrous Eutectic Silicon in Modified Al-Si Alloys", *Journal of Crystal Growth*, Vol. 72 (1985) 735 - 737.

[26] M. Shamsuzzoha, L. M. Hogan, "Crystal Morphology of Unmodified Aluminum-Silicon Eutectic Microstructures", *Journal of Crystal Growth*, Vol. 76 (1986) 429 - 439.

[27] M. M. Makhlouf, S. Shankar, Y. W. Riddle, "Mechanisms of Formation and Chemical Modificaton of the Morphology of the Eutectic Phases in Hypoeutectic Aluminum-Silicon Alloys", *AFS Transactions*, Vol. 113 (2005) 145 - 162.

[28] M. D. Hanna, S. Lu, A. Hellawell, "Modification in the Aluminum-Silicon System", *Metallurgical Transactions A*, Vol. 15A (1984) 459 - 469.

[29] S. Lu, A. Hellawell, "Modification of Al-Si Alloys: Microstructure, Thermal Analysis, and Mechanisms", *JOM*, Vol. 47 (1995) 38 - 40.

[30] S. Lu, A. Hellawell, "The Mechanism of Silicon Modification in Aluminum-Silicon Alloys: Impurity Induced Twinning", *Metallurgical Transactions A*, Vol. 18A (1987) 1721 - 1733.

[31] D. Argo, J. E. Gruzleski, "Porosity in Modified Aluminum Alloy Castings", *AFS Transactions*, Vol. 96 (1988) 65 - 74.

[32] S. D. McDonald, K. Nogita, A. K. Dahle, J. A. Taylor, D. H. St.John, "Eutectic Solidification and Porosity Formation in Al-Si Alloys: Role of Strontium", *AFS Transactions*, Vol. 108 (2000) 463 - 470.

[33] Z. Zhang, X. Bian, X. Liu, "Effect of strontium addition on hydrogen content and porosity shape of Al-Si alloys", *International Journal of Cast Metals Research*, Vol. 14 (2001) 31 - 35.

[34] D. Emadi, J. E. Gruzleski, J. M. Toguri, "The Effect of Na and Sr Modification on Surface Tension and Volumetric Shrinkage of A356 Alloy and Their Influence on Porosity Formation", *Metallurgical Transactions B*, Vol. 24B (1993) 1055 - 1063.

[35] D. Emadi, J. E. Gruzleski, "Combating Al-Si Porosity: The Strontium/Hydrogen Myth", *Modern Casting*, Vol. 85 (1995) 46 - 47.

[36] X. Bian, Z. Zhang, X. Liu, "Effect of Strontium Modification on Hydrogen Content and Porosity Shape of Al-Si Alloys", *Materials Science Forum*, Vol. 331 - 337 (2000) 361 - 366.

[37] C. M. Dinnis, A. K. Dahle, J. A. Taylor, "Eutectic Morphology and Porosity in Unmodified and Strontium-Modified Al-Si Alloys", *AFS Transactions*, Vol. 113 (2005) 99 - 106.

[38] L. Lu, K. Nogita, S. D. McDonald, A. K. Dahle, "Eutectic Solidification and its Role in Casting Porosity Formation", *JOM*, Vol. 56 (2004) 52 - 58.

[39] C. M. Dinnis, M. O. Otte, A. K. Dahle, J. A. Taylor, "The Influence of Strontium on Porosity Formation in Al-Si Alloys", *Metallurgical and Materials Transactions A*, Vol. 35A (2004) 3531 - 3541.

[40] P. D. Lee, S. Sridhar, "Direct observation of the effect of strontium on porosity formation during the solidification of aluminum-silicon alloys", *International Journal of Cast Metals Research*, Vol. 13 (2000) 185 - 198.

[41] L. Liu, A. M. Samuel, F. H. Samuel, H. W. Doty, S. Valtierra, "Role of Strontium Oxide on Porosity Formation in Al-Si Casting Alloys", *AFS Transactions*, Vol. 110 (2002) 449 - 462.

[42] S. M. Miresmaeili, S. G. Shabestari, S. M. A. Boutorabi, "The Effect of Sr-Modification Treatment on Porosity Formation of Reduced Pressure 319 Al Alloy Castings", *Canadian Metallurgical Quarterly*, Vol. 42 (2003) 245 - 252.

[43] A. M. Samuel, A. Pennors, C. Villeneuve, F. H. Samuel, H. W. Doty, S. Valtierra, "Effect of cooling rate and Sr-modification on porosity and Fe-intermetallics formation in Al-6.5% Si-3.5% Cu-Fe alloys", *International Journal of Cast Metals Research*, Vol. 13 (2000) 231 - 253.

[44] C. H. Caceres, M. B. Djurdjevic, T. J. Stockwell, J. H. Sokolowski, "The Effect of Cu Content on the Level of Microporosity in Al-Si-Cu-Mg Casting Alloys", *Scripta Materialia*, Vol. 40 (1999) 631 - 637.

[45] G. Boudreault, A. M. Samuel, F. H. Samuel, H. W. Doty, "Microstructural Observations on Porosity in A319.2 Alloy: Effect of Mold Type/Cooling Rate", *AFS Transactions*, Vol. 107 (1999) 207 - 216.

[46] A. M. Samuel, F. H. Samuel, C. Villeneuve, H. W. Doty, S. Valtierra, "Effect of Trace Elements on β-Al_5FeSi Characteristics, Porosity and Tensile Properties of Al-Si-Cu (319) Cast Alloys", *International Journal of Cast Metals Research*, Vol. 14 (2001) 97 - 120.

[47] J. A. Taylor, G. B. Schaffer, D. H. St.John, "The Role of Iron in the Formation of Porosity in Al-Si-Cu-Based Casting Alloys: Part I. Initial Experimental Observations", *Metallurgical and Materials Transactions A*, Vol. 30A (1999) 1643 - 1650.

[48] J. A. Taylor, G. B. Schaffer, D. H. St.John, "The Role of Iron in the Formation of Porosity in Al-Si-Cu-Based Casting Alloys: Part II. A Phase-Diagram Approach", *Metallurgical and Materials Transactions A*, Vol. 30A (1999) 1651 - 1655.

[49] J. R. Davis and Associates (Ed.) Aluminum and Aluminum Alloys, ASM International, Materials Park, OH, 1993, p. 784.

[50] K. Kurita, T. Donofrio, "New Heat Treatment System for Aluminum Automobile Components", *Industrial Heating*, Vol. 73 (2006) 51 - 55.

[51] R. D. Howard, "Aluminum Heat Treatment Processes, Applications and Equipment", *Industrial Heating*, Vol. 74 (2007) 61 - 65.

[52] J. Keist, "The Development of a Fluidized Bed Process for the Heat Treatment of Aluminum Alloys", *JOM*, Vol. 57 (2005) 34 - 39.

[53] S. K. Chaudhury, D. Apelian, "Fluidized Bed Heat Treatment of Cast Al-Si-Cu-Mg Alloys", *Metallurgical and Materials Transactions A*, Vol. 37A (2006) 2295 - 2311.

[54] S. K. Chaudhury, D. Apelian, "Effects of Rapid Heating on Aging Characteristics of T6 Tempered Al-Si-Mg Alloys Using Fluidized Bed", *Journal of Materials Science*, Vol. 41 (2006) 4684 - 4690.

[55] S. K. Chaudhury, D. Apelian, "Effects of Rapid Heating on Solutionizing Characteristics of Al-Si-Mg Alloys Using a Fluidized Bed", *Metallurgical and Materials Transactions A*, Vol. 37 (2006) 763 - 779.

[56] S. K. Chaudhury, D. Apelian, "Effects of Fluidised Bed Quenching on Heat Treating Characteristics of Cast Al-Si-Mg and Al-Si-Mg-Cu Alloys", *International Journal of Cast Metals Research*, Vol. 19 (2006) 361 - 371.

[57] I. J. Polmear, *LIGHT ALLOYS: Metallurgy of the light metals*, J. Wiley & Sons, New York, 1995, p. 362.

[58] *Heat Treating*, American Society for Metals, Materials Park, OH, 1981, p. 826.

[59] S. Shivkumar, C. Keller, D. Apelian, "Aging Behavior in Cast Al-Si-Mg Alloys", *AFS Transactions*, Vol. 98 (1990) 905 - 911.

[60] S. Shivkumar, S. Ricci Jr., D. Apelian, "Influence of Solution Parameters and Simplified Supersaturation Treatments on Tensile Properties of A356 Alloy", *AFS Transactions*, Vol. 98 (1990) 913 - 922.

[61] J. F. Hernandez-Paz, "Heat Treatment and Precipitation in A356 Aluminum Alloy", in: vol Ph.D. Thesis, McGill University, Montreal, QC, Canada, 2003, p. 112.

[62] F. Paray, "Heat Treatment and Mechanical Properties of Aluminum-Silicon Modified Alloys", in: Department of Mining and Metallurgical Engineering, vol Ph.D. Thesis, McGill University, Montreal, QC, Canada, 1992, p. 503.

[63] D. Apelian, G. K. Sigworth, "Fundamental Aspects of Heat Treatment of Cast Al-Si-Mg Alloys", *AFS Transactions*, Vol. 97 (1989) 727 - 742.

[64] Z. Li, A. M. Samuel, F. H. Samuel, C. Ravindran, S. Valtierra, H. W. Doty, "Factors Affecting Dissolution of $CuAl_2$ Phase in 319 Alloys", *AFS Transactions*, Vol. 111 (2003) 241 - 254.

[65] J. Gauthier, P. R. Louchez, F. H. Samuel, "Heat Treatment of 319.2 Aluminum Automotive Alloy, Part 1: Solution Heat Treatment", *Cast Metals*, Vol. 8 (1995) 91 - 106.

[66] J. Gauthier, F. H. Samuel, "Tensile Properties and Fracture Behavior of Solution-Heat-Treated 319.2 Al Automotive Alloy", *AFS Transactions*, Vol. 103 (1995) 849 - 857.

[67] J. H. Sokolowski, M. B. Djurdjevic, C. A. Kierkus, D. O. Northwood, "Improvement of 319 Aluminum Alloy Casting Durability by High Temperature Solution Treatment", *Journal of Materials Processing Technology*, Vol. 109 (2001) 174 - 180.

[68] O. Reiso, H. Overlie, N. Ryum, "Dissolution and Melting of Secondary Al_2Cu Phase Particles in an AlCu Alloy", *Metallurgical Transactions A*, Vol. 21A (1990) 1689 - 1695.

[69] O. Reiso, N. Ryum, N. Strid, "Melting of Secondary-Phase Particles in Al-Mg-Si Alloys", *Metallurgical Transactions A*, Vol. 24A (1990) 2629 - 2641.

[70] G. Wang, X. Bian, W. Wang, J. Zhang, "Influence of Cu and Minor Elements on Solution Treatment of Al-Si-Cu-Mg Cast Alloys", *Materials Letters*, Vol. 57 (2003) 4083 - 4087.

[71] R. Fuoco, E. R. Correa, "Incipient Melting During Solution Heat Treatment of Al-Si-Mg and Al-Si-Cu-Mg Alloys", *AFS Transactions*, Vol. 110 (2002) 417 - 433.

[72] F. H. Samuel, "Incipient Melting of $Al_5Mg_8Si_6Cu_2$ and Al_2Cu Intermetallics in Unmodified and Strontium-Modified Al-Si-Cu-Mg (319) Alloys during Solution Heat Treatment", *Journal of Materials Science*, Vol. 33 (1998) 2283 - 2297.

[73] A. M. Samuel, J. Gauthier, F. H. Samuel, "Microstructural Aspects of the Dissolution and Melting of Al_2Cu Phase in Al-Si Alloys during Solution Heat Treatment", *Metallurgical and Materials Transactions A*, Vol. 27A (1996) 1785 - 1798.

[74] P. S. Wang, S. L. Lee, J. C. Lin, M. T. Jahn, "Effects of Solution Temperature on Mechanical Properties of 319.0 Aluminum Casting Alloys Containing Trace Beryllium", *Journal of Materials Research*, Vol. 15 (2000) 2027 - 2035.

[75] M. H. Mulazimoglu, "Electrical Conductivity Studies of Cast Al-Si and Al-Si-Mg Alloys", in: Mining and Metallurgical Engineering, vol Ph.D. Thesis, McGill University, Montreal, Canada, 1988, p. 249.

[76] N. Crowell, S. Shivkumar, "Solution Treatment Effects in Cast Al-Si-Cu Alloys", *AFS Transactions*, Vol. 103 (1995) 721 - 726.

[77] D. Steele, D. Evans, P. Nolan, D. J. Lloyd, "Quantification of grain boundary precipitation and the influence of quench rate in 6XXX aluminum alloys", *Materials Characterization*, Vol. 58 (2007) 40 - 45.

[78] *Standard Practice for Heat Treatment of Aluminum-Alloy Castings from All Processes, ASTM Standard B917/B917M-2001*, ASTM, Philadelphia, PA, 2001.

[79] D. S. MacKenzie, "Design of Quench Systems for Aluminum Heat Treating Part I - Quenchant Selection", *Industrial Heating*, Vol. 73 (2006) 53 - 57.

[80] G. E. Totten, G. M. Webster, C. E. Bates, "An Overview of Aluminum Quenching with Polymer Quenchants", *Industrial Heating*, Vol. 65 (1998) 61 - 66.

[81] G. E. Byczynski, W. Kierkus, D. O. Northwood, D. Penrond, J. H. Sokolowski, W. A. Esseltine, J. Oswald, R. Thomas, "The Effect of Quench Rate on Mechanical Properties of 319 Aluminum Alloy Castings", *Materials Science Forum*, Vol. 217 - 222 (1996) 783 - 788.

[82] G. K. Sigworth, J. Howell, O. Rios, M. Kaufman, "Heat Treatment of Natural Aging Aluminum Casting Alloys", *AFS Transactions*, Vol. 114 (2006) 221 - 232.

[83] W. J. Poole, D. J. Lloyd, J. D. Embury, "The effect of natural ageing on the evolution of yield strength during artificial ageing for Al-Si-Mg-Cu alloys", *Materials Science and Engineering*, Vol. A234 - 236 (1997) 306 - 309.

[84] S. P. Ravindranathan, K. T. Kashyap, S. RaviKumar, C. Ramachandra, B. Chatterji, "Effect of Delayed Aging on Mechanical Properties of an Al-Cu-Mg Alloy", *Journal of Materials Engineering and Performance*, Vol. 9 (2000) 24 - 27.

[85] J. F. Hernandez-Paz, F. Paray, J. E. Gruzleski, D. Emadi, "Natural Aging and Heat Treatment of A356 Aluminum Alloy", *AFS Transactions*, Vol. 112 (2004) 155 - 164.

[86] S. Murali, K. T. Kashyap, K. S. Raman, K. S. S. Murthy, "Inhibition of Delayed Ageing by Trace Additions in Al-7Si-0.3Mg Cast Alloy", *Scripta Metallurgica et Materialia*, Vol. 29 (1993) 1421 - 1426.

[87] T. Gladman, "Precipitation Hardening in Metals", *Materials Science and Technology*, Vol. 15 (1999) 30 - 36.

[88] I. J. Polmear, "Role of Age Hardening in Modern Aluminum Alloys", in: *Proc. of the 3rd International Conference on Aluminum Alloys*, 22-26 June 1992, Trondheim, Norway, 1992, pp. 371 - 384.

[89] J. W. Martin, *Precipitation Hardening*, Butterworth-Heinemann, Oxford, England, 1998, p. 215.

[90] A. Guinier, "On the Birth of GP Zones", *Materials Science Forum*, Vol. 217-222 (1996) 3 - 6.

[91] D. A. Porter, K. E. Easterling, *Phase Transformations in Metals and Alloys*, Van Nostrand Reinhold (UK) Co. Ltd., Molly Millars Lane, Wokingham, Berkshire, England, 1981, p. 446.

[92] I. J. Polmear, "Atomic Processes Involved in Precipitate Nucleation in Aged Aluminum Alloys", *Materials Science Forum*, Vol. 363 - 365 (2001) 1 - 8.

[93] E. Ozawa, H. Kimura, "Behaviour of Excess Vacancies during the Nucleation of Precipitates in Aluminum-Silicon Alloys", *Materials Science and Engineering*, Vol. 8 (1971) 327 - 335.

[94] C. R. Brooks, *Heat Treatment, Structure and Properties of Non-Ferrous Alloys*, American Society for Metals, Metals Park, OH, 1982, p. 420.

[95] R. N. Lumley, I. J. Polmear, A. J. Morton, "Interrupted Aging and Secondary Precipitation in Aluminum Alloys", *Materials Science and Technology*, Vol. 19 (2003) 1483 - 1491.

[96] R. N. Lumley, J. Buha, I. J. Polmear, A. J. Morton, A. G. Crosky, "Secondary Precipitation in Aluminum Alloys & Its Role in Modern Heat Treatment", *Materials Science Forum*, Vol. 519521 (2006) 283 - 290.

[97] C. R. Hutchinson, S. P. Ringer, "Precipitation Processes in Al-Cu-Mg Alloys Microalloyed with Si", *Metallurgical and Materials Transactions A*, Vol. 31A (2003) 2721 - 2733.

[98] S. P. Ringer, K. Hono, I. J. Polmear, T. Sakurai, "Precipitation Processes during the Early Stages of Ageing in Al-Cu-Mg Alloys", *Applied Surface Science*, Vol. 94 (1996) 253 - 260.

[99] S. Abis, M. Massazza, P. Mengucci, G. Riontino, "Early Ageing Mechanisms in a High-Copper AlCuMg Alloy", *Scripta Materialia*, Vol. 45 (2001) 685 - 691.

[100] S. P. Ringer, K. Hono, T. Sakurai, I. J. Polmear, "Cluster Hardening in an Aged Al-Cu-Mg Alloy", *Scripta Materialia*, Vol. 36 (1997) 517 - 521.

[101] P. Ratchev, B. Verlinden, P. Van Houtte, "S' Phase Precipitation in Al-4wt%Mg-1wt%Cu Alloy", *Scripta Metallurgica et Materialia*, Vol. 30 (1994) 599 - 604.

[102] H. G. Kang, M. Kida, H. Miyahara, K. Ogi, "Age-Hardening Characteristics of Al-Si-Cu-Base Cast Alloys", *AFS Transactions*, Vol. 107 (1999) 507 - 515.

[103] R. K. Mishra, A. K. Sachdev, W. J. Baxter, "Strengthening Precipitates in Cast 339 Aluminum Alloy", *AFS Transactions*, Vol. 112 (2004) 179 - 191.

[104] G. Liu, G. J. Zhang, X. D. Ding, J. Sun, K. H. Chen, "Modeling the Strengthening Response to Aging Process of Heat-Treatable Aluminum Alloys Containing Plate/Disc or Rod/Needle-Shaped Precipitates", *Materials Science and Engineering A*, Vol. A344 (2003) 113 - 124.

[105] M. Murayama, K. Hono, "Pre-Precipitate Clusters and Precipitation Processes in Al-Mg-Si Alloys", *Acta Materialia*, Vol. 47 (1999) 1537 - 1548.

[106] K. Kido, K. Matsuda, T. Kawabata, T. Sato, S. Ikeno, "HRTEM Observation of Precipitates in Al-Mg-Si Alloy Containing Copper at Early Stage during Aging", *Materials Science Forum*, Vol. 396 - 402 (2002) 953 - 958.

[107] P. Donnadieu, F. Carsughi, A. Redjaimia, C. Diot, G. Lapasset, "Nanoscale Hardening Precipitation in AlMgSi Alloys: a Transmission Electron Microscopy and Small-Angle Neutron Scattering Study", *Journal of Applied Crystallography*, Vol. 31 (1998) 212 - 222.

[108] C. Cayron, P. A. Buffat, "Transmission Electron Microscopy Study of the Beta-Prime Phase (Al-Mg-Si Alloys) and QC Phase (Al-Cu-Mg-Si Alloys): Ordering Mechanism and Crystallographic Structure", *Acta Materialia*, Vol. 48 (2000) 2639 - 2653.

[109] M. Murayama, K. Hono, M. Saga, M. Kikuchi, "Atom Probe Studies on the Early Stages of Precipitation in Al-Mg-Si Alloys", *Materials Science and Engineering A*, Vol. A250 (1998) 127 - 132.

[110] G. A. Edwards, K. Stiller, G. L. Dunlop, M. J. Couper, "The Precipitation Sequence in Al-Mg-Si Alloys", *Acta Materialia*, Vol. 46 (1998) 3893 - 3904.

[111] A. K. Gupta, D. J. Lloyd, S. A. Court, "Precipitation Hardening in Al-Mg-Si Alloys with and without Excess Si", *Materials Science and Engineering A*, Vol. A316 (2001) 11 - 17.

[112] D. G. Eskin, "Hardening and Precipitation in the Al-Cu-Mg-Si Alloying System", *Materials Science Forum*, Vol. 396 - 402 (2002) 917 - 922.

[113] W. Reif, J. Dutkiewicz, R. Ciach, S. Yu, J. Krol, "Effect of Ageing on the Evolution of Precipitates in AlSiCuMg Alloys", *Materials Science and Engineering A*, Vol. A234 - 236 (1997) 165 - 168.

[114] S. Esmaeili, X. Wang, D. J. Lloyd, W. J. Poole, "On the Precipitation-Hardening Behaviour of the Al-Mg-Si-Cu Alloy AA6111", *Metallurgical and Materials Transactions A*, Vol. 34A (2003) 751 - 763.

[115] J. Y. Yao, G. A. Edwards, D. A. Graham, "Precipitation and Age-Hardening in Al-Si-Cu-Mg-Fe Casting Alloys", *Materials Science Forum*, Vol. 217 - 222 (1996) 777 - 782.

[116] R. M. Gomes, T. Sato, H. Tezuka, A. Kamio, "Precipitation Behavior of P/M Hypereutectic Al-Si-Cu-Mg Alloys Containing Fe and Ni", *Materials Transactions, JIM*, Vol. 39 (1998) 357 - 364.

[117] S. C. Weakley-Bollin, W. Donlon, C. Wolverton, J. W. Jones, J. E. Allison, "Modeling the Age-Hardening Behavior of Al-Si-Cu Alloys", *Metallurgical and Materials Transactions A*, Vol. 35A (2004) 2407 - 2418.

[118] M. L. Purtee, "Aging Effects of an Aluminum-Based 319 Alloy", *Foundry Management & Technology*, Vol. 126 (1998) 40 - 43.

[119] D. Gloria, F. Hernandez, S. Valtierra, M. A. Cisneros, "Dimensional Changes during Heat Treating of an Automotive 319 Alloy", in: *Proc. of the 20th ASM Heat Treating Society Conference*, 9-12 Oct. 2000, ASM International, St. Louis, MO, 2000, pp. 674 - 679.

[120] H. Mancha-Molinar, H. F. Lopez, A. Silva, K. Still, "Role of T7 Heat Treating on the Dimensional Stability of Automotive A319 Al Alloys", in: *Proc. Conf. Advances in Lightweight Automotive Castings and Wrought Aluminum Alloys*, SAE International, Detroit, MI, 2004, pp. 103 - 113.

[121] J. Gauthier, P. R. Louchez, F. H. Samuel, "Heat Treatment of 319.2 Aluminum Automotive Alloy. Part 2, Ageing Behaviour", *Cast Metals*, Vol. 8 (1995) 107 - 114.

[122] R. DasGupta, S. DasGupta, C. Brown, Factors Affecting Tensile Properties of Castings, in: Proc. Conf. Advances in Lightweight Automotive Castings and Wrought Aluminum Alloys, SAE International, Detroit, Mi, 2004, pp. 95 - 100.

[123] Z. Li, A. M. Samuel, F. H. Samuel, C. Ravindran, S. Valtierra, H. W. Doty, "Parameters Controlling the Performance of AA319-Type Alloys, Part I. Tensile Properties", *Materials Science and Engineering A*, Vol. A367 (2004) 96 - 110.

[124] Z. Li, A. M. Samuel, F. H. Samuel, C. Ravindran, S. Valtierra, H. W. Doty, "Parameters Controlling the Performance of AA319-Type Alloys, Part II. Impact Properties and Fractography", *Materials Science and Engineering A*, Vol. A367 (2004) 111 - 122.

[125] C. H. Caceres, I. L. Svensson, J. A. Taylor, "Strength-Ductility Behaviour of Al-Si-Cu-Mg Casting Alloys in T6 Temper", *International Journal of Cast Metals Research*, Vol. 15 (2003) 531 - 543.

[126] P. Ouellet, F. H. Samuel, "Effect of Mg on the Ageing Behaviour of Al-Si-Cu 319 Type Aluminum Casting Alloys", *Journal of Materials Science*, Vol. 34 (1999) 4671 - 4697.

[127] P. Sepehrband, R. Mahmudi, F. Khomamizadeh, "Effect of Zr Addition on the Aging Behavior of A319 Aluminum Cast Alloy", *Scripta Materialia*, Vol. 52 (2005) 253 - 257.

[128] G. Wang, X. Bian, J. Qiao, J. Zhang, "Effect of Be on Aging Behavior of an Al-Si-Cu-Mg Cast Alloy", *Journal of Materials Engineering and Performance*, Vol. 13 (2003) 99 - 102.

[129] R. N. Lumley, A. J. Morton, G. O'Donnell, I. J. Polmear, "New Aluminum Alloy Heat Treatment Improves Properties, Reduces Process Costs", *Industrial Heating*, Vol. 71 (2004) 31 - 34.

[130] R. N. Lumley, I. J. Polmear, A. J. Morton, "Control of Secondary Precipitation to Improve the Performance of Aluminum Alloys", *Materials Science Forum*, Vol. 396 - 402 (2002) 893 - 898.

[131] R. N. Lumley, I. J. Polmear, A. J. Morton, "Novel Ageing Treatments to Enhance Mechanical Properties of Aluminum Alloys", in: *J.T. Staley Honorary Symposium on Aluminum Alloys 'Materials Solutions 2001'*, Indiana, IN, ASM International, Materials Park, OH, 2001, pp. 248 - 254.

[132] R. N. Lumley, I. J. Polmear, A. J. Morton, "The Utilisation of Secondary Ageing to Improve the Mechanical Properties of Aluminum Alloys", in: A. Dahle (Ed.) *1st International Light Metals Technology Conference 2003*, Brisbane, Australia, 2003, pp. 377 - 382.

[133] M. Tash, F. H. Samuel, F. Mucciardi, H. W. Doty, "Effect of Metallurgical Parameters on the Hardness and Microstructural Characterization of As-Cast and Heat-treared 356 and 319 Aluminum Alloys", *Materials Science and Engineering A*, Vol. 443 (2007) 185 - 201.

[134] G. Liu, G. J. Zhang, R. H. Wang, W. Hu, J. Sun, K. H. Chen, "Heat Treatment-Modulated Coupling Effect of Multi-Scale Second-Phase Particles on the Ductile Fracture of Aged Aluminum Alloys", *Acta Materialia*, Vol. 55 (2007) 273 - 284.

[135] M. Warmuzek, *Aluminum-Silicon Casting Alloys Atlas of Microfractographs*, ASM International, Materials Park, OH, 2004, p. 124.

[136] M. A. Moustafa, F. H. Samuel, H. W. Doty, S. Valtierra, "Effect of Mg and Cu additions on the microstructural characteristics and tensile properties of Sr-modified Al-Si eutectic alloys", *International Journal of Cast Metals Research*, Vol. 34 (2002) 235 - 253.

[137] J. G. Kaufman, *Introduction to Aluminum Alloys and Tempers*, ASM International, Materials Park, OH, USA, 2000, p. 258.

[138] D. E. Newbury, D. C. Joy, *Advanced Scanning Electron Microscopy and X-Ray Microanalysis*, Plenum Press, New York, USA, 1986.

[139] R. Gauvin, A Review of Transmission Electron Microscopy for the Characterization of Materials, in: R. A. Lessard, H. Franke (Eds.), Materials Characterization and Optical Probes Techniques, vol CR69, 1997, pp. 200 - 229.

[140] K. Branch, *Fundamentals and Applications of Scanning Electron Microscopy*, Kyoritsu Publishing, Tokyo, Japan, 2000.

[141] L. E. Murr, *Electron and Ion Microscopy and Microanalysis: Principles and Applications*, Marcel Dekker Press, New York, NY, USA, 1991, p. 837.

[142] W. F. Miao, D. E. Laughlin, "Effects of Cu content and Preaging on Precipitation Characteristics in Aluminum Alloy 6022", *Metallurgical and Materials Transactions A*, Vol. 31A (2000) 361 - 371.

[143] P. Ratchev, B. Verlinden, P. DeSmet, P. Van Houtte, "Artificial Aging of Al-Mg-Cu Alloys", *Materials Transactions, JIM*, Vol. 40 (1999) 34 - 41.

[144] H. Toda, K. Minami, M. Kobayashi, K. Uesugi, A. Takeuchi, T. Kobayashi, "Observation of Precipitates in Aluminum Alloys by Sub-NEcrometer Resolution Tomography Using Fresnel Zone Plate", *Materials Science Forum*, Vol. 519 - 521 (2006) 1361 - 1367.

[145] A. Deschamps, M. Dumont, L. Lae, F. Bley, "Use of Small-Angle X-Ray Scattering for the Characterisation of Precipitates in Aluminum Alloys", *Materials Science Forum*, Vol. 519 - 521 (2006) 1349 - 1355.

[146] G. Al-Marahaleh, "Effect of Heat Treatment on the Distribution and Volume Fraction of Mg_2Si in Structural Aluminum Alloy 6063", *Metal Science and Heat Treatment*, Vol. 48 (2006) 17 - 21.

[147] G. Harlow, "Particle Statistics in Aluminum", *International Journal of Reliability, Quality and Safety Engineering*, Vol. 13 (2006) 379 - 395.